



HAL
open science

Supercritical fluids synthesis, characterization and test of HDS catalysts : Assessment of criticality of metals contained in HDS catalysts

Cyril Quilfen

► **To cite this version:**

Cyril Quilfen. Supercritical fluids synthesis, characterization and test of HDS catalysts : Assessment of criticality of metals contained in HDS catalysts. Material chemistry. Université de Bordeaux, 2016. English. NNT : 2016BORD0405 . tel-01583028

HAL Id: tel-01583028

<https://theses.hal.science/tel-01583028>

Submitted on 6 Sep 2017

HAL is a multi-disciplinary open access archive for the deposit and dissemination of scientific research documents, whether they are published or not. The documents may come from teaching and research institutions in France or abroad, or from public or private research centers.

L'archive ouverte pluridisciplinaire **HAL**, est destinée au dépôt et à la diffusion de documents scientifiques de niveau recherche, publiés ou non, émanant des établissements d'enseignement et de recherche français ou étrangers, des laboratoires publics ou privés.

THÈSE PRÉSENTÉE
POUR OBTENIR LE GRADE DE
DOCTEUR DE
L'UNIVERSITÉ DE BORDEAUX

ÉCOLE DOCTORALE DES SCIENCES CHIMIQUES
SPÉCIALITÉ Physico-chimie de la matière condensée

Par Cyril QUILFEN

**Supercritical fluids synthesis, characterization and tests of
HDS catalysts**
Assessment of criticality of metals contained in HDS catalysts

Sous la direction de : Cyril AYMONIER, Armin RELLER et Denis UZIO

Soutenue le 15 décembre 2016

Membres du jury :

M. MAGLIONE, Mario	Directeur de Recherche CNRS - ICMCB, Univ. Bordeaux	Président
Mme LAMONIER, Carole	Professeur des Universités - UCCS, Univ. Lille	Rapporteur
Mme MARTÍNEZ SÁNCHEZ, Cristina	Directeur de Recherche CSIC - ITQ, Valencia	Rapporteur
M. AYMONIER, Cyril	Directeur de Recherche CNRS - ICMCB, Univ. Bordeaux	Examineur
M. ETOURNEAU, Jean	Professeur Émérite - ICMCB, Univ. Bordeaux	Examineur
M. LOUBET, Philippe	Maître de Conférence - ISM, Univ. Bordeaux	Examineur
M. RELLER, Armin	Professeur des Universités - Univ. Augsburg	Examineur
M. UZIO, Denis	Ingénieur de Recherche – IFPEN	Examineur

Acknowledgments

This PhD work has been done in collaboration between three entities, the Supercritical Fluids group located at the Institute of Condensed Matter Chemistry of Bordeaux (ICMCB – CNRS - France), the University of Augsburg (Germany) and the French Institute of Petroleum (IFPEN – France). I would like to thank all people who have been involved in this project and all entities who welcomed me on their premises. They have allowed me to perform my work in good conditions and in a well working atmosphere. I would particularly thank the University of Bordeaux which has provided the grant to realize this PhD work.

I would then thank M. Mario Maglione, director of the ICMCB, for welcoming me in its laboratory and for having accepted to preside the assessment committee of my PhD defence. Moreover, I would thank M. Jean Etourneau who was at the initiative of this collaboration between the University of Augsburg and the ICMCB. I also thank him for having been one of the members of my assessment committee.

I would like then express my sincere gratitude to the two people who have taken the time to review my manuscript Ms. Carole Lamonier, professor at the University of Lille and researcher at the UCCS Lille, France, and Ms. Cristina Martínez-Sánchez, CSIC research director at the ITQ in Valencia, Spain. My acknowledgments go also to M. Philippe Loubet, associate professor at Bordeaux INP, who has accepted to be one member of my assessment committee.

My greatest thanks go to the people who have supervised my work during these three years, M. Cyril Aymonier, CNRS research director at the ICMCB, M. Denis Uzio, research engineer at the IFPEN, and M. Armin Reller, professor at the University of Augsburg. Thank you very much for the scientific help you provided me during these three years. I learned a lot on several areas including chemistry, characterisations, catalysis and criticality and you give me numerous advices to perform an interesting work. Thank you a lot for that.

I would then acknowledge all people who permits to well conduct this work in many ways. At ICMCB, I would thank Eric Lebraud for having performed XRD measurements, Alexandre Fargues for its help to implement a sulfidation process, Christine Labrugère for XPS measurements, Laetitia Etienne for ICP analysis, Sonia Buffière and Marion Gayot for TEM measurements. I would also thank Thierry Tassaing for *in situ* Raman analysis and Odile Babot for BET measurements from ISM.

The multidisciplinary of this PhD work also makes me thank people who work in others labs than ICMCB. I would like to thank Anne Boffo who has performed catalytic tests and allowed characterizations of my samples by microprobe analysis at the IFPEN. I would also acknowledge Renate Diessenbacher from the University of Augsburg and Claudia Loch from the Fraunhofer Institute who contributed to the good progress of my stays in Germany.

As a PhD project, does not involve only scientist people, I would also thank people who help me so much regarding administrative aspects. For that, I would thank people from “Gestion” service, Carole Malburet from the “Mission” service, Stéphane Toulin from the Library service and all people working at the infrastructure of the ICMCB (Sandrine, Jacques, Alain, Bernard, Edgar...).

Then, I would like to thank all the people with that I was able to meet during these three years. First of all, I would thank all my colleagues from the Supercritical Fluids group, I have spent a really

good time with you. Among them, I would thank, Blanca, Bruno, Lucile, Angela, Oana, Sam, Samantha, Céline, Mathieu, Prassanth, Maria, Aimery, Gilles, Sushitra, Fan, Arnaud... Then, I would also thank people with whom I crossed most time, the Picon team (Baptiste, Romain, Marie, Thomas, Mathias) but also Guillaume and Cédric. I hope that we will keep in touch and I wish you the best for your future.

Finally, I would like to thank my friends from Lyon and from “les Vosges”, with whom I have also spent some nice week-ends and nice travels (Guadeloupe, HK) with them. I would also thank my parents, my family and Léa who supported me during these three years.

Content

Summary in French.....11

General Introduction.....23

Chapter I:

Assessment of the criticality of metals contained in hydrodesulfurization catalysts.....29

Chapter II:

Bibliographic study.....51

Chapter III:

Experimental set-ups and characterization techniques.....93

Chapter IV:

Monitoring of the preparation of HDS catalyst precursors by *in situ* Raman spectroscopy.....117

Chapter V:

Understanding of the process of precursor catalyst preparation through a parametric study.....147

Chapter VI:

Catalytic evaluation.....193

General Conclusion.....215

Appendices.....221

Synthèse en milieux supercritiques, caractérisation et tests de catalyseurs d'hydrodésulfuration (HDS). *Evaluation de la criticité des éléments contenus dans les catalyseurs HDS.*

Introduction

De nos jours, plus de 7 milliards de personnes vivent sur terre et la population est en continuelle augmentation. Cette population a des besoins et la constante évolution de notre industrie permet de répondre à certains, un des besoins majeurs étant celui de l'énergie. Durant le siècle précédent, le pétrole a largement contribué au développement de notre industrie moderne et va continuer à être la principale source d'énergie pour répondre à cette demande croissante.

Afin de minimiser notre empreinte écologique, le protocole de Kyoto proposé en 1998 vise à réduire les gaz à effet de serre émis dans l'atmosphère, provenant principalement des industries et des véhicules. L'utilisation de coupes pétrolières « propres » est donc nécessaire. Pour cela, les législations concernant la teneur en hétéroatomes présents dans les coupes pétrolières sont de plus en plus drastiques. Par exemple, en Europe, la teneur maximale en soufre dans l'essence et le diesel est limitée à 10 ppm. Afin de respecter ces législations, les raffineries ont besoin de posséder des unités d'hydrotraitement de plus en plus performantes.

Dans une raffinerie, les unités d'hydrotraitement sont présentes tout au long du raffinage du pétrole et permettent d'enlever les hétéroatomes des coupes pétrolières. Afin d'atteindre une teneur de 10 ppm en soufre, une amélioration des unités d'hydrodésulfuration est nécessaire et cela passe par une amélioration de l'activité catalytique des catalyseurs permettant d'éliminer le soufre des coupes pétrolières.

Depuis de nombreuses années, ces catalyseurs n'ont cessé d'être optimisés et améliorés afin d'accroître leurs performances. Pour cela, de nouvelles méthodes de synthèse ont été développées afin d'augmenter la dispersion et l'accessibilité de la phase active. Dans ce travail, nous proposons l'étude d'un nouveau procédé pour préparer des catalyseurs HDS couplant une imprégnation à sec classique avec l'utilisation des fluides supercritiques et plus particulièrement du dioxyde de carbone supercritique (scCO₂). Ce travail a été organisé autour de quatre grands axes qui vont être résumés dans les parties suivantes.

Evaluation de la criticité des éléments contenus dans les catalyseurs HDS

Le premier axe étudié, un concept encore peu employé en science des matériaux, est l'étude de la criticité des éléments contenus dans ces catalyseurs. En effet, la diminution des ressources en métaux est une réalité moins connue que celle concernant la diminution des énergies fossiles mais tout aussi importante. Dans ce travail nous nous sommes basés sur l'évaluation de la criticité du molybdène, du cobalt et du soufre, les trois principaux éléments présents dans la phase active d'un catalyseur HDS. L'aluminium, présent dans le support, n'a pas été étudié dû à son abondance dans la croûte terrestre. Pour cela, l'utilisation de différents indicateurs tels que les réserves, les ressources, la production, l'utilisation, la substitution, le recyclage et le commerce de ces éléments ont été pris en compte pour estimer leur criticité.

Concernant le molybdène, 80% des réserves sont localisées dans des pays développés ou en voie de développement que sont les Etats-Unis, la Chine et le Chili, ce qui implique qu'un manque d'approvisionnement dû à des instabilités géopolitiques est peu probable. De plus, plusieurs compagnies sont impliquées dans l'extraction et la mise en forme du molybdène ce qui permet d'avoir une concurrence et une régulation du prix du molybdène. Par contre, l'utilisation du molybdène dans les aciers techniques servant à la construction ou à des applications pour le développement des énergies vertes peut rapidement augmenter. Les propriétés uniques apportées par le molybdène font que sa substitution par un autre élément est difficile. Le molybdène n'est donc pas considéré comme critique pour l'Union Européenne (U.E.) mais peut le devenir rapidement avec l'émergence de nouveaux besoins pour les pays en voie de développement.

La criticité du cobalt a ensuite été évaluée par l'utilisation des mêmes indicateurs que pour le molybdène. Il a été montré tout d'abord que les réserves de cobalt sont inégalement réparties dans la croûte terrestre. En effet, la majeure partie des réserves sont localisées en République Démocratique du Congo (RDC) (Figure 1).

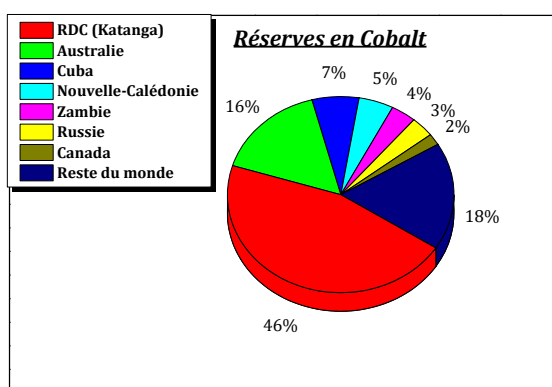


Figure 1: Réserves en Cobalt.

Ce pays est un des pays les plus pauvres et a subi de nombreuses guerres qui en fait une région géopolitiquement instable. Cette instabilité pourrait engendrer des risques en approvisionnement du cobalt pour l'U.E. Cette raison augmente donc la criticité de cet élément. De plus, cet élément est principalement extrait en tant que coproduit du nickel ou du cuivre, ce qui engendre des difficultés pour augmenter sa production. Le cobalt est principalement utilisé dans les batteries, et du fait de l'augmentation du nombre des voitures électriques et des appareils portables électroniques, on peut prévoir une augmentation de son utilisation. Le cobalt est aussi utilisé dans les turbines d'éoliennes, les panneaux solaires et les technologies « gas to liquid » et « coal to liquid ». Comme pour le molybdène, la substitution du cobalt par un autre élément entraîne, la plupart du temps, une diminution des performances recherchées. Grâce à l'étude de ces différents indicateurs, nous pouvons mettre en avant le fait que le cobalt est un élément critique pour l'industrie européenne.

Cette étude préliminaire dans l'évaluation de la criticité des principaux éléments contenus dans les catalyseurs HDS nous a permis d'avoir une vision plus large et une meilleure connaissance de ces éléments. Ces éléments, de haute importance pour le développement de notre industrie, sont donc à utiliser avec le plus grand soin. Cela passe donc par le développement de nouvelles méthodes de préparation de ce type de catalyseurs afin d'augmenter le nombre de sites actifs participant à la réaction HDS.

Etat de l'art concernant les catalyseurs d'hydrodésulfuration

Les législations concernant la teneur en soufre dans les coupes pétrolières devenant de plus en plus drastiques (Figure 2), une amélioration constante des catalyseurs HDS est donc nécessaire.

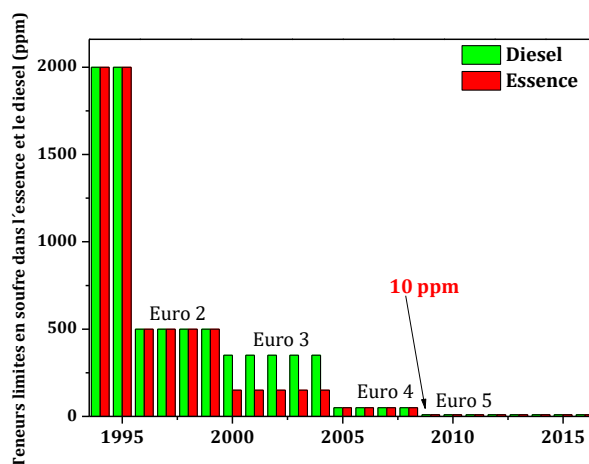


Figure 2: Evolution des teneurs en soufre dans l'essence et le diesel pour l'U.E.

Le soufre est responsable d'une importante pollution s'il n'est pas éliminé avant la combustion des fuels. En effet, la recombinaison des oxydes de soufre dans la haute atmosphère va générer des pluies acides. De plus, le soufre est un poison pour un grand nombre de catalyseurs présent le long du processus de raffinage. Un besoin en coupes pétrolières « propres » est donc nécessaire et cela passe par l'élimination des composés soufrés les plus réfractaires tels que le dibenzothiophène (DBT) et les DBT alkylés.

Les catalyseurs HDS conventionnels sont basés sur des feuillets de disulfure de molybdène (MoS_2) décorés à leurs coins par des atomes de cobalt (phase CoMoS) et dispersés sur un support de type alumine. Ces catalyseurs sont préparés par une imprégnation à sec des précurseurs métalliques sur le support. Cette étape est suivie par une étape de maturation pendant laquelle les espèces métalliques diffusent à l'intérieur des pores du support. Une fois la migration des espèces réalisée, un séchage du catalyseur est effectué afin d'éliminer le solvant restant. La plupart du temps, cette étape est suivie d'un étape de calcination où les ions associés aux espèces métalliques sont éliminés et une phase dispersée d'oxydes est observée. La dernière étape consiste en l'activation du catalyseur dans laquelle la phase oxyde est transformée en phase sulfure. A la fin de cette activation, la phase dite CoMoS dispersée sur le support est alors obtenue. Afin d'augmenter l'activité du catalyseur, une phase bien dispersée de nanocristallites de CoMoS est recommandée. Les sites catalytiques sont reliés à la morphologie et la taille des feuillets de MoS_2 . Dans un constant souci d'amélioration de l'activité catalytique, de nombreuses méthodes de synthèse alternatives ont été étudiées. Par exemple, nous pouvons citer l'utilisation de composés de type hétéropolyanions permettant l'augmentation de la promotion de la phase active par le cobalt et /ou d'éviter la formation de composés résistant à la sulfuration. L'utilisation de complexes organiques, aidant à la dispersion de la phase active, à la solvatisation des espèces et d'autres, a aussi été reportée dans de nombreuses études.

Un autre axe permettant d'augmenter l'activité catalytique est l'utilisation de nouvelles méthodes de synthèse comme le dépôt par voie chimique, l'utilisation des micro-ondes ou encore l'utilisation des fluides supercritiques.

Nous proposons dans ce travail, l'utilisation du dioxyde de carbone supercritique (scCO_2). Le scCO_2 possède, en effet, d'intéressantes propriétés pouvant apporter des bénéfices en terme d'augmentation de la dispersion de la phase métallique, mais aussi l'obtention d'un catalyseur en un temps de synthèse réduit et un gain d'énergie. Comparé à d'autres groupes de recherches, nous avons utilisé une méthode différente pour préparer ces matériaux catalytiques. En effet, à la place de l'utilisation de composés toxiques et/ou coûteux, tels que les carbonyles et les composés organométalliques, nous avons décidé d'utiliser des précurseurs conventionnels, l'heptamolybdate d'ammonium, l'acide phosphomolybdique et les nitrates de cobalt. Afin d'éviter un long temps de synthèse, nous avons décidé d'imprégner les espèces métalliques par une imprégnation à sec conventionnelle suivie d'un traitement sous CO_2 supercritique. En jouant sur le solvant d'imprégnation, nous avons pu modifier les espèces chimiques obtenues sur le support après la réaction. Les principaux solvants testés ont été l'eau, le méthanol, l'éthanol et le propan-1-ol. Les affinités du scCO_2 avec les différents solvants d'imprégnation permettent de faire varier le mécanisme réactionnel de précipitation des espèces métalliques. Pour préparer ces catalyseurs, un procédé utilisant le scCO_2 a donc été développé et est présenté Figure 3.

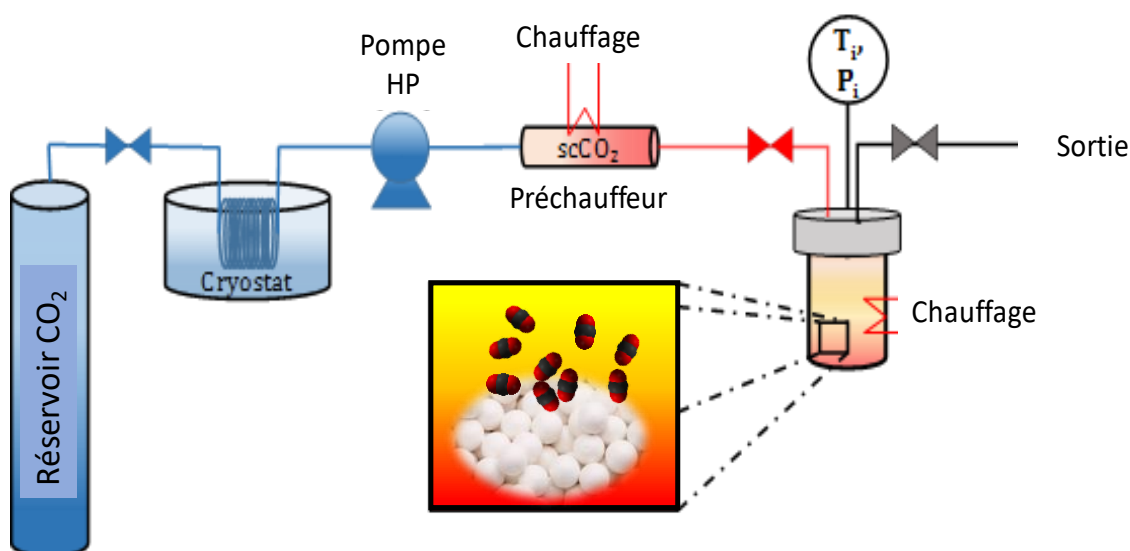


Figure 3: Procédé scCO_2 utilisé pour la préparation de catalyseurs HDS

Afin d'étudier et de comprendre ce procédé de synthèse, une étude *in situ* a été tout d'abord réalisée en suivant la préparation des catalyseurs par le biais de la spectroscopie Raman.

Etude *in situ* Raman de la préparation de catalyseurs HDS en milieu scCO_2

Nous avons suivi la préparation de catalyseurs HDS en milieu scCO_2 par l'enregistrement de spectres Raman à la surface des billes de support et en fonction de la température. Afin de comparer l'effet de l'atmosphère employée, les mesures ont été faites sous scCO_2 ainsi que sous air. De plus, l'étude de deux solvants (l'eau et l'éthanol) ainsi que l'étude de deux précurseurs du molybdène (heptamolybdate d'ammonium (HMA) et acide phosphomolybdique (HPA)), nous ont permis de choisir le meilleur système à employer lors de la préparation des matériaux catalytiques.

Nous avons observé que l'utilisation du HMA avec l'eau conduit à la formation d'espèces cristallisées de type polymolybdates lors d'un traitement sous scCO_2 alors qu'une phase amorphe

est obtenue lors d'un traitement sous air. La même tendance a été observée lors de l'ajout du promoteur de cobalt dans la solution d'imprégnation. De plus dans ce cas, nous avons observé la formation de molybdate de cobalt cristallisé (β -CoMoO₄), espèce résistante à la sulfuration, à relativement basse température. Il a donc été montré que l'utilisation de l'eau et du HMA pour la dispersion des espèces oxydes sur le support ne semblait pas être la meilleure option.

Nous avons donc décidé de nous diriger sur l'utilisation d'un autre système, le système HPA/éthanol. En effet, l'utilisation du HPA permet d'éviter la présence de contre-ions qui pourraient être néfastes dans la suite de la préparation du catalyseur. Il est, de plus, soluble dans l'éthanol ce qui n'est pas le cas du HMA. La Figure 4 montre l'évolution des spectres Raman pour ce système en fonction de la température sous atmosphère de scCO₂.

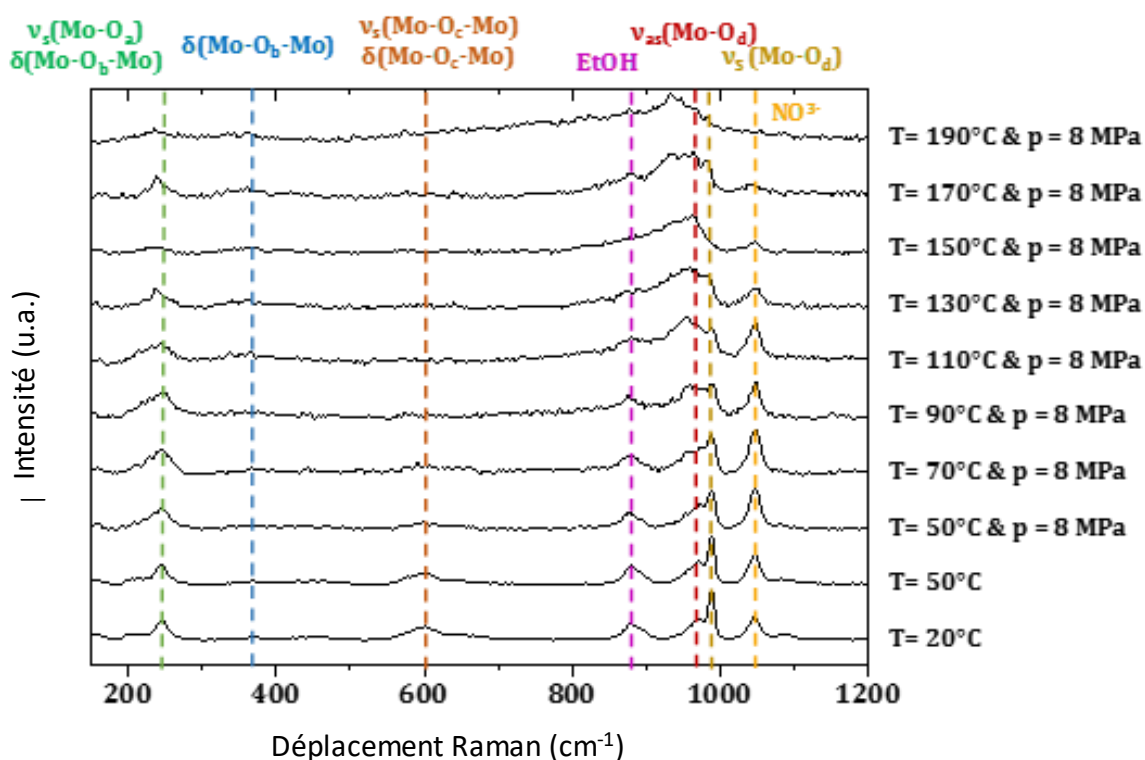


Figure 4: Evolution des spectres Raman pour le système HPA-éthanol en fonction de la température.

Ces expériences nous ont permis de mettre en exergue certaines hétérogénéités des espèces en fonction de la zone de la bille de support analysée et de déterminer quelle est la température de travail recommandée pour éviter la formation de certaines espèces chimiques. Le système utilisant l'éthanol a montré de meilleurs résultats concernant la dispersion des espèces chimiques et la distribution en taille des cristallites, c'est pourquoi nous avons choisi de principalement étudier ce système.

Influence des paramètres de synthèse sur les phases oxo métallique et sulfurée

Afin de comprendre et d'optimiser la synthèse de catalyseurs HDS, nous avons étudié plusieurs paramètres expérimentaux qui sont résumés Figure 5.

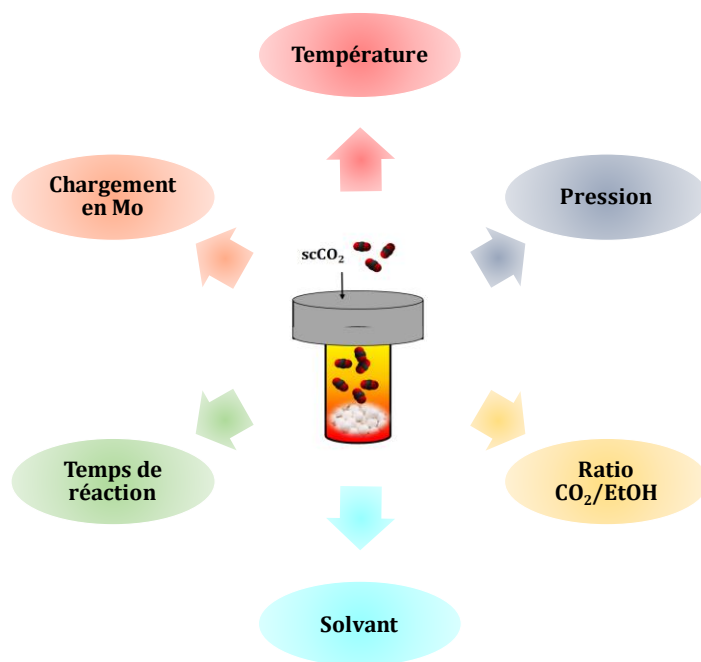


Figure 5 : Différents paramètres expérimentaux étudiés

Pour chaque paramètre, plusieurs conditions ont été testées et les matériaux obtenus ont été caractérisés par différentes techniques d'analyse (Raman, DRX, ICP, SPX, microsonde et MET) avant et après sulfuration.

Grâce à cette étude, nous avons pu comparer notre procédé avec un procédé de synthèse conventionnel et déterminer les avantages de l'utilisation du procédé $scCO_2$. Premièrement, l'utilisation de l'éthanol comme solvant d'imprégnation permet d'éviter la formation d'espèces liées à la dissolution d'une partie du support et de réduire le temps de diffusion des espèces dans les pores du catalyseur. Deuxièmement, une précipitation des espèces en utilisant le $scCO_2$ permet de travailler à des températures modérées (entre 50 et 150°C), ce qui est un gain d'énergie non négligeable pour une future industrialisation comparé à une synthèse standard. Cette précipitation prenant place quasiment directement après injection du $scCO_2$ et permet un gain de temps considérable. Ce procédé utilisant le $scCO_2$ apparaît donc comme prometteur pour la préparation d'une large gamme de matériaux. Il a été déterminé les principaux effets de chaque paramètre sur les espèces obtenues sur le support après réaction.

La température a un effet important sur les espèces obtenues. En effet, pour des températures supérieures à 150°C, il a été montré la formation de molybdates de cobalt, précédemment observée lors des expériences *in situ* Raman réalisées. Cette formation de $CoMoO_4$ a été assignée à la formation d'un précurseur de type $Co_x(OH)_y(NO_3)_z(CO_3)_m.nH_2O$ qui se combine avec les

polymolybdates. À basses températures, la présence de petites cristallites de HPA a été trouvée. La Figure 6 montre les différents diffractogrammes obtenus pour des échantillons synthétisés à différentes températures et l'évolution des différentes espèces cristallisées formées.

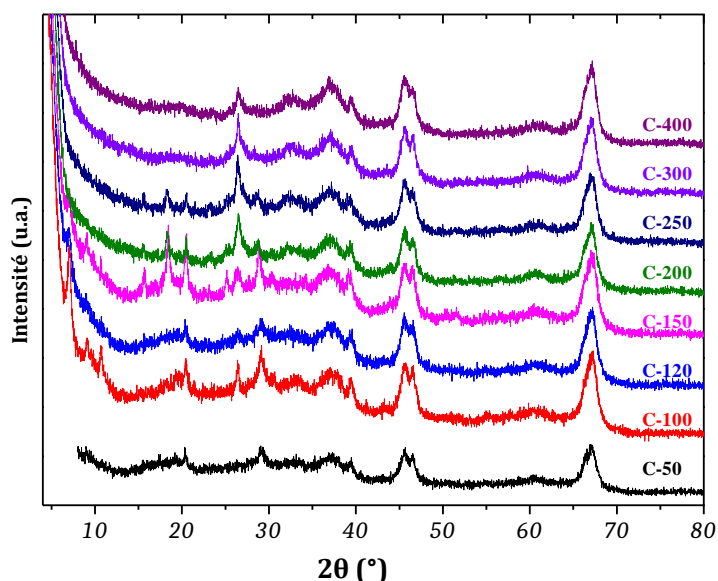


Figure 6: Diffractogrammes RX des échantillons obtenus à différentes températures.

Le second effet étudié est celui de la pression en CO_2 . Il a été montré que cette dernière a un effet sur la taille des cristallites obtenues. En effet, une synthèse à haute pression (~25 MPa) permet d'obtenir de plus petites particules qu'à basse pression (~5MPa). Cela peut être attribué à la différence d'expansion du solvant par le scCO_2 . Un travail à haute pression permet donc de faire « gonfler » plus rapidement le solvant d'imprégnation et de générer un plus grand nombre de nuclei que pour une synthèse à basse pression.

Le troisième effet étudié est le ratio entre le solvant d'imprégnation et le scCO_2 . Il a été montré que le ratio CO_2/EtOH a un effet non négligeable sur la taille des particules obtenues. En effet, une synthèse à faible ratio CO_2/EtOH donne des cristallites de taille plus importante que pour une synthèse à grand ratio CO_2/EtOH . Cela aussi a été attribué au coefficient d'expansion de l'éthanol par le scCO_2 . De plus, il a été montré une dépolymérisation d'une partie du HPA lors d'une synthèse à faible ratio CO_2/EtOH . Cette dépolymérisation a été attribuée à la formation d'eau et la non stabilité du HPA en présence d'eau. Cette eau provenant de la déshydratation de l'éthanol par le HPA (catalyseur pour la déshydratation des alcools). Mais même si de plus larges particules ont été obtenues dans le cas d'une synthèse à faible ratio CO_2/EtOH , cet effet n'a pas été observé sur la taille des feuillets de MoS_2 formés après activation du catalyseur. La Figure 7 présente un cliché MET d'un catalyseur activé. On peut y observer les feuillets de MoS_2 dispersés sur le support d'alumine.

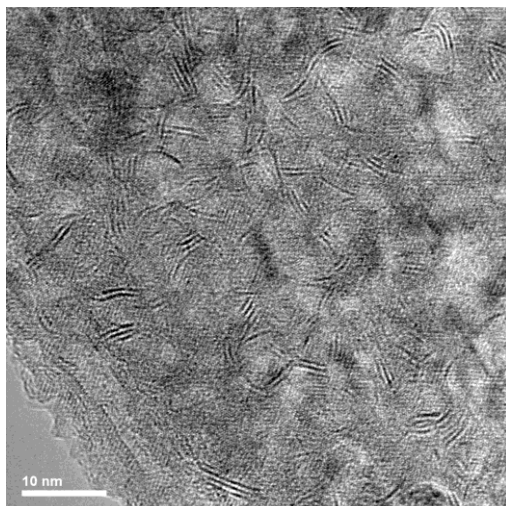


Figure 7: Exemple de cliché MET obtenu pour un catalyseur activé.

Le quatrième effet étudié est le solvant d'imprégnation. Pour cela trois alcools ont été testés, le méthanol, l'éthanol et le propan-1-ol. Cette étude a mené à des résultats intéressants concernant le type d'espèces présent sur le support après la réaction. En effet, après avoir analysé chaque échantillon par spectroscopie Raman sur les surfaces des billes d'alumine coupées en deux, il a été montré que le HPA est conservé sur toute la surface dans le cas du méthanol. Tandis que dans les autres cas, la présence d'un mélange de HPA et de polymolybdates a été observé. Ces différences d'espèces ont été attribuées à la différence de déshydratation des alcools. En effet, il est plus facile de déshydrater le propan-1-ol que l'éthanol et que le méthanol. Plus d'eau résultant de cette déshydratation va donc être formée dans le cas du propan-1-ol et la présence de plus d'espèces de type polymolybdates est donc observée, le HPA n'étant pas stable en présence d'eau. Il est donc possible de faire varier les espèces en changeant le solvant d'imprégnation.

Le cinquième effet étudié est le temps de réaction. Cela a permis de mettre en avant le fait qu'il est possible d'obtenir des espèces bien dispersées sur le support en un temps très court correspondant à uniquement l'injection de $scCO_2$. Ce paramètre est donc important et permet un gain de temps considérable comparé à une synthèse conventionnelle.

Après avoir caractérisé les échantillons obtenus en faisant varier ces différents paramètres, ces derniers ont été testés en catalyse.

Evaluation catalytique des matériaux préparés en scCO₂

Cette partie est dédiée à l'évaluation catalytique des matériaux préparés. Pour cela, trois réactions catalytiques ont été étudiées : l'hydrogénation du toluène, permettant de faire un premier criblage des catalyseurs et de déterminer quels sont les plus actifs, suivie de l'hydrodésulfuration du DBT et l'hydrodésulfuration du 4,6-dimethyldibenthiothiophène (4,6-DMDBT).

Il a été montré que la formation de molybdates de cobalt cristallisés était néfaste pour l'activité catalytique et que les meilleurs résultats sont obtenus pour une température de synthèse de 100-120°C. Cette observation a été faite pour les trois réactions étudiées. La Figure 8 montre les résultats obtenus pour les échantillons synthétisés à différentes températures dans le cas de l'hydrogénation du toluène et pour une référence synthétisée sous air.

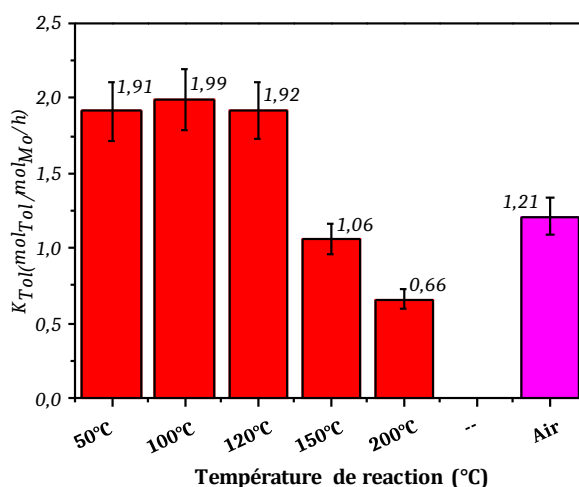


Figure 8 : Hydrogénation du toluène pour les échantillons synthétisés à différentes températures.

L'étude du ratio CO₂/EtOH a montré que les meilleurs résultats catalytiques sont obtenus pour une synthèse à haut ratio. Cela a été attribué à la formation de plus petites cristallites dans le cas d'une synthèse à haut ratio.

Concernant le solvant d'imprégnation, le méthanol a donné de meilleurs résultats que les deux autres alcools testés. Le solvant d'imprégnation a donc un effet non négligeable sur l'activité catalytique résultante.

Un des principaux avantages de l'utilisation de ce procédé est le fait de pouvoir obtenir un catalyseur actif en un temps de synthèse réduit. Il a en effet été montré que le temps de synthèse n'a quasiment aucune influence sur l'activité catalytique obtenue.

Ce procédé a donc montré qu'il était possible d'obtenir des catalyseurs actifs en HDS et donnant de meilleures performances qu'une synthèse conventionnelle.

Conclusion

Ce travail de thèse était organisé autour de quatre grands objectifs. L'évaluation de la criticité des éléments contenus dans les catalyseurs HDS est le premier objectif étudié. Cela a permis d'avoir une meilleure connaissance des éléments employés et ce type d'étude va devenir de plus en plus nécessaire lors du développement de nouveaux matériaux. Il a été montré que le molybdène et le cobalt ne sont pas critiques pour la préparation de catalyseurs HDS mais peuvent le devenir rapidement dû à leur utilisation dans bon nombre de nouvelles technologies « vertes ».

Le second objectif était l'étude de la préparation de catalyseurs HDS en milieu $scCO_2$. Pour cela, des expériences *in situ* Raman nous ont permis de mettre en avant les meilleurs paramètres de synthèse à utiliser pour la préparation de matériaux. L'utilisation de l'éthanol en tant que solvant d'imprégnation par rapport à l'eau et le HPA en tant que précurseur du molybdène, ont donc été choisis.

Le troisième objectif concernait l'étude, le développement et l'optimisation du procédé utilisant le $scCO_2$ pour la préparation de catalyseurs HDS. Pour cela, plusieurs paramètres expérimentaux ont été étudiés par le suivi des phases oxométallique et sulfurée des matériaux obtenus. Il a été montré que les meilleurs échantillons ont été ceux synthétisés en utilisant le méthanol, un haut ratio $CO_2/EtOH$ et une température modérée (100-120°C).

Le dernier objectif de ce travail a été dédié à l'évaluation catalytique des matériaux synthétisés à partir de trois réactions différentes : l'hydrogénation du toluène, l'hydrodésulfuration du DBT et du 4,6-DMDBT.

Ce travail nous a donc permis de mettre en place un procédé de préparation de catalyseurs HDS. Ce procédé est novateur et permet un gain de temps et d'énergie comparé à une synthèse conventionnelle. De plus, l'adaptabilité de ce procédé à la synthèse d'un grand nombre de matériaux différents en fait un procédé de choix et, de surcroit, industrialisable pour la préparation de matériaux supportés.

General Introduction

Nowadays, more than 7 billion people are living on Earth and the population is growing and will continue in the future. Moreover, our modern industry is in constant development and has needs, particularly in terms of energy. Oil has widely contributed to the development of modern industry during the last century and continues to largely respond of energy needs even if several options are possible today.

Renewable energies are one of the best options for the future to respond to this demand. Unfortunately, these green energies are not enough developed to satisfy our standard of living and oil will still be a major part of our energy in the next decades. Using oil implies to clean oil in order to minimize our ecological footprint. For that developed countries have decided to reduce greenhouse gases by the implementation of the Kyoto Protocol of 1998. Pollution for road vehicles are a major part of emissions and the use of a “clean “oil is therefore necessary.

The diminution of low sulfur content available crude oil as well as the use, especially in Europe, of gasoline vehicles enforce the use of dense fuels containing a large part of undesirable heteroatoms (S, N, O and metals). This use of denser fuels is along with environmental regulations concerning greenhouse emissions during its combustion. Regulations concerning sulfur content present in crude oil are more and more drastic. For example, in Europe, sulfur content in diesel and gasoline is limited to 10 ppm and in USA to 15 ppm. In order to meet these stringent regulations, refining process has to be performant and especially in hydrotreatment units.

Hydrotreatment units are present along refining process and are necessary to remove heteroatoms naturally present in crude oil. However, to reach a 10 ppm content of sulfur an improvement of the hydrodesulfurization (HDS) process turns out to be mandatory. This enhancement passes through an improvement of the catalytic activity. For many years, catalysts present in HDS have been studied and upgraded. Now, to reach regulations concerning sulfur content, new synthesis methods are implemented and developed to enhance the performance of HDS catalysts in terms of phase utilization and dispersion of active metals. In this work, we propose the study of a new process to prepare HDS catalysts coupling a common dry impregnation with the use of supercritical fluids, especially supercritical carbon dioxide (scCO₂). This process provides an interesting alternative using a so called “green solvent”.

This PhD is thus related to the preparation, characterization and tests of HDS catalysts prepared in supercritical fluids as well as the assessment of the criticality of metals contained in these catalysts. This work has been done in collaboration between the Institute of Condensed Matter Chemistry of Bordeaux (ICMCB – France), the University of Augsburg (Germany) and the French Institute of Petroleum (IFPEN).

This PhD work is organized around four key objectives:

- Assessment of the criticality of metals contained in HDS catalysts,
- *In situ* investigations of the chemistry during the preparation of HDS catalysts,
- Materials synthesis of HDS catalyst precursors via the scCO₂ process,
- Catalytic evaluation of prepared materials.

The first chapter of this PhD is dedicated to the assessment of the criticality of metals contained in HDS catalysts, namely molybdenum and cobalt. The depletion of metal resources is, indeed, less commonly known than the diminution of fossil fuels. The evaluation of the origin, reserves, uses, processing and so on of metals is more and more a topical issue. The assessment of

criticality of molybdenum and cobalt has thus been studied. This survey allows to have a wider vision about elements we have employed during this work. Elements studied are described using indicators permitting to assess criticality. A similar approach has been used to study the sulfur.

The second chapter of this work deals with the bibliography survey concerning the hydrotreatment process as well as the use of supercritical fluids and especially carbon dioxide for the synthesis of HDS catalysts. Firstly, an overview of the hydrotreatment is presented with regulations of sulfur content present in crude oil and most refractory sulfur compounds. The presentation of the active CoMoS phase, where molybdenum disulfide layers are promoted at their edges by cobalt atoms, is made along with the commonly employed synthesis to prepare these catalysts. Structural models of the active phase and new synthesis methods to obtain higher active catalysts are also introduced in this section. Secondly, application of supercritical carbon dioxide to synthesize HDS catalytic materials along with properties brought by supercritical fluids are highlighted in this bibliographic study.

The third chapter presents the process proposed in this PhD for the synthesis of HDS catalysts as well as that one employed to monitor chemical reactions occurring during their preparation, especially an original set-up to perform *in situ* Raman investigations. It also puts forward characterization techniques employed to quantify and identify species present onto the surface of our support after synthesis and after activation by sulfidation of these catalysts. In order to estimate catalytic performances brought by a synthesis using a supercritical process, experimental parameters assigned to catalytic tests performed are also exposed in this chapter.

In order to better understand our supercritical fluid based process, we have investigated chemical reactions occurring during synthesis and results are presented in this fourth chapter. For that, the monitoring of the synthesis through *in situ* Raman measurements allows us to select the most interesting metallic precursor (between ammonium heptamolybdate and phosphomolybdic acid) as well as solvent (between water and alcohol) to perform impregnation for the preparation of these HDS catalysts. Experiments using $scCO_2$ have then be compared to a commonly employed synthesis to put forward advantages and drawbacks brought by the use of a supercritical media to perform HDS catalyst synthesis. The chapter four of this PhD is dedicated to results obtained with the *in situ* studies.

After having chosen the best conditions for our process, the fifth chapter presents effects induced by varying several experimental parameters. Diverse parameters studied have been highlighted, such as the temperature and pressure of reaction, the ratio between carbon dioxide and solvent of impregnation as well as the solvent of impregnation to only cite those which may have impacts on the dispersion and particles sizes of species present onto the surface of the support before sulfidation. Moreover, the reaction time has also been studied, the time being indeed very important for the use of a process at industrial scale. A focus on this parameter has thus been made. All materials prepared were characterized in their oxometallic and sulfided phases. The influences of these experimental parameters on the obtained materials were then estimated via the characterization of their phases before activation (oxometallic phase) and after activation (sulfided phase).

The last chapter of this PhD work is dedicated to the evaluation of catalytic performances of materials prepared via $scCO_2$ process. For that purpose, three main catalytic tests have been performed through a collaboration with the French Institute of Petroleum (IFPEN). The first test performed, allowing the evaluation of the hydrogenation activity of catalysts, was in toluene

hydrogenation. Catalytic materials, which have given the best performances, have then been tested in hydrodesulfurization of dibenzothiophene, a model molecule for the study of HDS catalysts. A third catalytic test has been performed on several samples, the hydrodesulfurization of 4,6-dimethyldibenzothiophene (4,6-DMDBT), one of the most refractory compound containing sulfur and present in crude oil.

This work has been made possible by a funding granted by the University of Bordeaux (doctoral contract n° 2013/FD/28) and in part by funding from IFPEN. The collaboration between three entities, namely ICMCB, IFPEN and the University of Augsburg, has allowed to work in a wide subject covering assessments of criticalities of metals used in HDS catalysts, monitoring of chemical reactions occurring during a synthesis with supercritical fluids via *in situ* measurements as well as synthesis, characterization and catalytic tests of materials prepared using an unconventional process.

Chapter I: Assessment of the criticality of metals contained in hydrodesulfurization catalysts

The image displays a periodic table of elements, with the transition metals highlighted in yellow. The elements S, Mo, and Co are highlighted with red boxes. Below the main table are two smaller, semi-transparent versions of the periodic table.

Group	1	2	3	4	5	6	7	8	9	10	11	12	13	14	15	16	17	18
Period 1	H																	He
Period 2	Li	Be											B	C	N	O	F	Ne
Period 3	Na	Mg											Al	Si	P	S	Cl	Ar
Period 4	K	Ca	Sc	Ti	V	Cr	Mn	Fe	Co	Ni	Cu	Zn	Ga	Ge	As	Se	Br	Kr
Period 5	Rb	Sr	Y	Zr	Nb	Mo	Tc	Ru	Rh	Pd	Ag	Cd	In	Sn	Sb	Te	I	Xe
Period 6	Cs	Ba	La	Hf	Ta	W	Re	Os	Ir	Pt	Au	Hg	Tl	Pb	Bi	Po	At	Rn
Period 7	Fr	Ra	Ac	Rf	Db	Sg	Bh	Hs	Mt	Ds	Rg	Cn	Nh	Fl	Mc	Lv	Ts	Og

Legend for transition metals:

- Alkali Metal
- Alkaline Earth
- Transition Metal
- D-block
- s-block
- p-block
- d-block
- f-block
- lanthanide
- actinide

I. INTRODUCTION.....	31
II. MOLYBDENUM CRITICALITY	32
II.1. INTRODUCTION.....	32
II.2. RESERVES AND RESOURCES OF MOLYBDENUM.....	32
II.3. PRODUCTION OF MOLYBDENUM.....	33
<i>II.3.1. Evolution of the molybdenum production.....</i>	<i>33</i>
<i>II.3.2. Main producing countries of molybdenum.....</i>	<i>34</i>
<i>II.3.3. Types of mines where molybdenum is recovered</i>	<i>34</i>
<i>II.3.4. Main mining and refining companies of molybdenum</i>	<i>35</i>
<i>II.3.5. Ecology and health impact of molybdenum mining and production</i>	<i>35</i>
II.4. USES OF MOLYBDENUM	36
II.5. SUBSTITUTABILITY OF MOLYBDENUM.....	37
II.6. RECYCLABILITY OF MOLYBDENUM	37
II.7. TRADE OF MOLYBDENUM [45].....	38
II.8. CONCLUSION ABOUT MOLYBDENUM CRITICALITY	38
III. COBALT CRITICALITY.....	39
III.1. INTRODUCTION.....	39
III.2. RESERVES AND RESOURCES OF COBALT	39
III.3. PRODUCTION OF COBALT	40
<i>III.3.1. Evolution of the cobalt production.....</i>	<i>40</i>
<i>III.3.2. Main producing countries of cobalt.....</i>	<i>41</i>
<i>III.3.3. Mining and processing of cobalt.....</i>	<i>41</i>
<i>III.3.4. Main mining and refining companies of cobalt</i>	<i>42</i>
<i>III.3.5. Ecology and health impact of cobalt mining and production</i>	<i>42</i>
III.4. USES OF COBALT	42
III.5. SUBSTITUTABILITY OF COBALT	43
III.6. RECYCLABILITY OF COBALT	43
III.7. TRADE OF COBALT.....	44
III.8. CONCLUSION ABOUT COBALT CRITICALITY.....	44
IV. CONCLUSION	45
V. BIBLIOGRAPHY.....	46

I. Introduction

Nowadays, environmental regulations are more and more drastic concerning the sulfur content. For example, in European Union (E.U.) and Japan it is necessary to meet 10 ppm of sulfur in gas-oil and gasoline [1,2]. To remove sulfur from gas-oil and gasoline and meet these regulations, efficient hydrodesulfurization (HDS) catalysts are required. Commonly at industrial scale, HDS catalysts are based on molybdenum disulfide layers decorated at their edges by cobalt atoms [3] and formed the so called “CoMoS phase”. Elements contained in these catalysts are metals and these resources are limited and a lack of supply could generate massive troubles in the economy which use them. For that, the study of the criticality of those elements is growing of interest, especially in European Union where the number of metals mined in this area is limited.

For that, a concept has been developed these past years in order to estimate if an element or material can be crucial for our industry and thus for our everyday life. Hereafter, is presented the definition of the concept of criticality according to the E.U. [4].

Determining criticality and choosing appropriate indicators are something which are not an exact science and different methodologies can be used. One of the most difficult part of assessing criticality is the availability of data, the lack of communication of some companies concerning their production of metals and the importance of each indicator compared to the others. In their report [4], European Union as defined the concept of criticality as following: “*to qualify as critical, a raw material must face high risks with regard to access to it (i.e. high supply risks or high environmental risks) and be of high economic importance.*”. In Table I.1 are presented some indicators [5–8] which permits to assess criticality. The first part of this chapter deals with the criticality of molybdenum and the second one is dedicated to the criticality of cobalt. In each part, an introduction of the element, reserves and resources of this element, its production, uses and recycling are studied. A similar study was carried out for the sulfur and the results can be find in Appendix 1.

Table I.1: Indicators assessing the criticality of an element.

Indicators	
Availability of the element	Country concentration
Depletion time	Commodity price
By product dependency	Companies involved in mining
Recovery of the element (exploration & production costs, technologies ...)	Economic importance in emerging technologies
Country risks (geopolitical status)	Recyclability
Environmental risk	Substitutability

II. Molybdenum criticality

II.1. Introduction

Molybdenum is a chemical element which has the atomic number 42, an atomic weight of 95.96 g.mol⁻¹ and for symbol Mo. It lies in the periodic table's second transition series, in Group VIB between chromium and tungsten. It is a silvery-white metal with one of the highest melting temperature (2623°C). Molybdenum has also a very low thermal expansion and, when alloyed in steels, it greatly increases their strength and resistance to corrosion. Its chemical behaviour is similar to its neighbour, the tungsten. It is the 54th most abundant element in the Earth's crust but it is rather present in oxide forms with various valence states. Molybdenum does not occur naturally as a free metal on Earth and most common minerals containing molybdenum are molybdenite (MoS₂), wulfenite (PbMoO₄) and powellite (CaMoO₄). The metal is produced via the direct mining of molybdenite [5,9,10]. Molybdenum has an extraordinary versatility, as it has oxidation states from -II to VI, numbers of coordination from 4 to 8 and varied stereochemistry. It has also the ability to form compounds with organic or inorganic ligands and to form bi- and polynuclear compounds [10]. Molybdenum is present in living organisms with a role as heteroatom at the active site of certain enzymes but it is toxic in high amounts [11,12].

II.2. Reserves and resources of molybdenum

Molybdenum does not occurs as a free metal and can occur in various minerals but only molybdenite (MoS₂) is suitable for industrial production of marketable products [13]. Molybdenite can occur as the sole mineralization in an ore body, but it is often associated with the sulfide minerals of other metals, notably copper. In viable ore bodies, the Mo content ranges between 0.01 wt.% and 0.25 wt.%. From the USGS data [14–16], the world reserves of Mo are about 11 million tonnes (Mt) with most of the reserves located in China (4.3 Mt), in the United States (2.7 Mt) and in Chile (1.8 Mt). While the identified world resources of molybdenum are about 5.4 Mt in the United States, and in the rest of the world, about 14 million tonnes. Molybdenum occurs as the principal metal sulfide in large low-grade porphyry molybdenum deposits and as an associated metal sulfide in low-grade porphyry copper deposits [16]. Figure I.1 depicts the reserves of Mo per country:

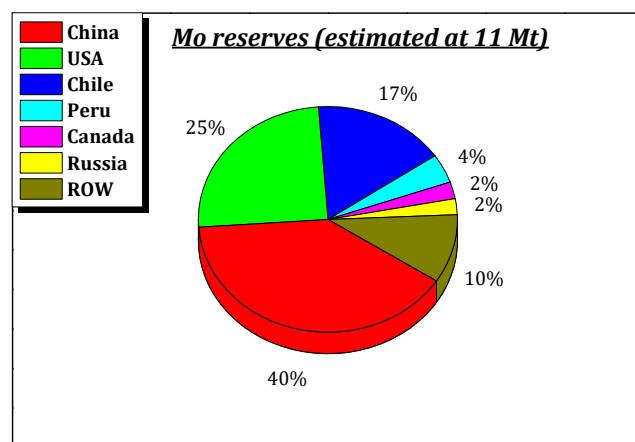


Figure I.1: Molybdenum reserves per countries.

As it can be observed from Figure I.1, reserves of molybdenum are unequally distributed over the Earth's crust. Indeed, China, United States and Chile possess around 80 % of the world reserves of Mo but resources of molybdenum are adequate to supply world needs for a foreseeable future and countries which hold the largest reserves have a little risk of geopolitical supply constraint and have a reasonable standard of living [17].

II.3. Production of molybdenum

II.3.1. Evolution of the molybdenum production

Depending upon the minerals contained in the ore body and their quality, molybdenum mines are grouped in three classes:

- Primary mines, where the recovery of molybdenite is the sole objective,
- By-product mines, where the recovery of copper-bearing ores is the primary objective and the molybdenite recovery provides additional economic value,
- Co-product mines, where the commercial viability of the mine requires that both molybdenite and copper-bearing minerals be recovered.

The production of molybdenum has still increased during the last century [18,19] and these past years [20–23] as presented in Figure I.2.

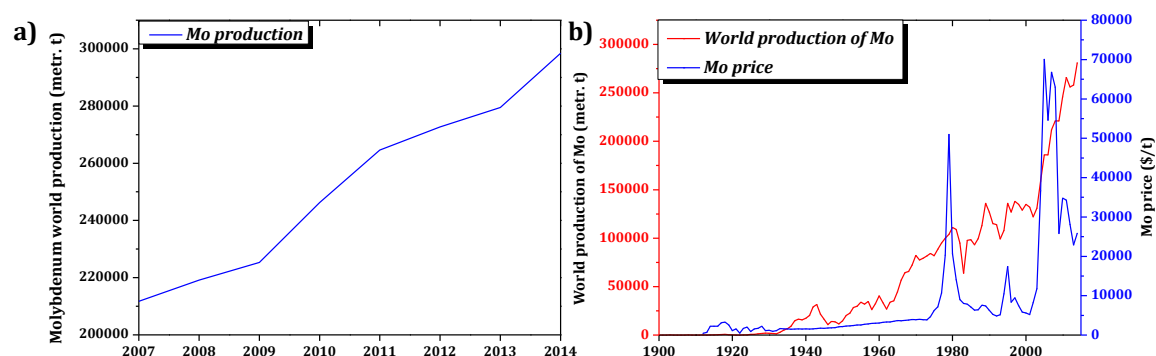


Figure I.2: Evolution of the molybdenum production over the last 7 years (a) and evolution of the molybdenum production and price over the last century (b).

The increase of molybdenum over the last century can be assessed right to the development of engineering steels and technical alloys, which represents a large part of the use of molybdenum [24,25]. From 2007 to 2014, an increase of molybdenum production is observed and can be linked to the development of emerging countries which have a need of engineering steels and technical alloys. Concerning the molybdenum price, two important increases are observed since 1970. The first one in 1978-1979 is due to the high demand owing to generally strong economic conditions and the Iranian Revolution, leading to the second oil shock [26], caused copper companies to start operating or building by-product Mo recovery circuits. The year after, the price was decreased due to the diminution of molybdenum demand owing to recession and overproduction. Between 2003 and 2007, the molybdenum mine production moved strongly upwards in response to greater demand from the iron and steel industry until 2008-2009 were the global financial crisis led to a decrease of prices and were many new mining projects were slowed or suspended [27,28].

II.3.2. Main producing countries of molybdenum

In 2014, the production of molybdenum was estimated around 300 000 tonnes [23] with 80 wt.% of the molybdenum produced from three countries: China, United States and Chile (see Figure I.3). These countries are also those who own the largest reserves of molybdenum. China produced in 2014 more than 40 wt.% of the molybdenum used worldwide. This monopoly of the production can lead to lack of supply chain due to the growing situation of China and the use of large part of molybdenum for its own economic development. One risk of supply could come from the political instability of China [23].

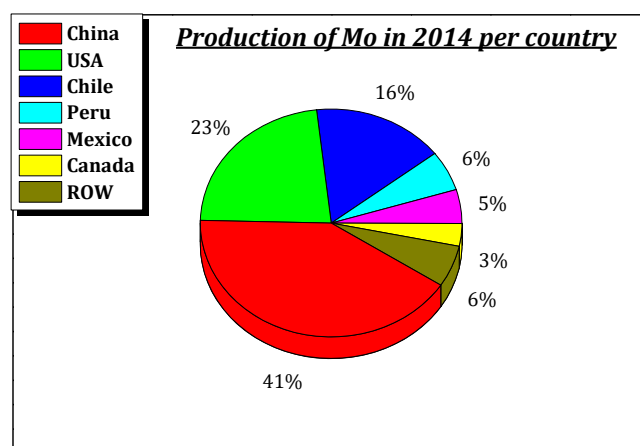


Figure I.3: Production of molybdenum in 2014 (Mo produced: 298 645 t).

II.3.3. Types of mines where molybdenum is recovered

The type of mines where the molybdenum is recovered can impact the supply of molybdenum. Indeed, if the molybdenum is mined as by product, its supply is very dependant of the main metal mined, the copper in the case of the molybdenum. Figure I.4 represents the different mines of molybdenum per type of mines (mining of Mo only or Mo mined as by product of copper).

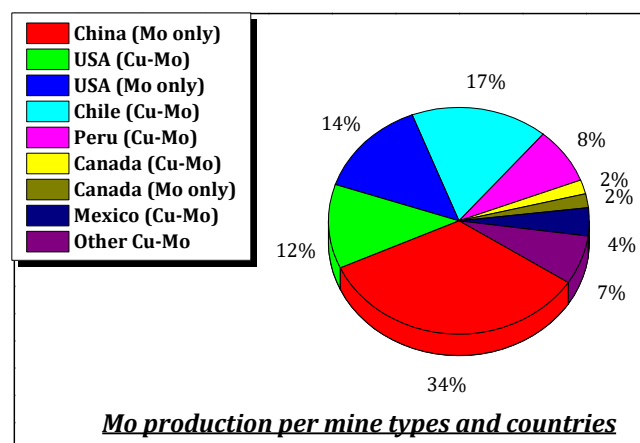


Figure I.4: Production of Mo by country and mine type in 2012 (adapted from [29]).

Around 50 wt.% of the molybdenum produced in 2012 have been mined in a Mo mine with two third of the production in China. The rest of the molybdenum produced was as by product of the copper mining. If China is excluded of the production, means that around 75 wt.% of the

molybdenum production is dependant of the copper production. Its production is therefore highly related to the copper production and price.

II.3.4. Main mining and refining companies of molybdenum

Only several companies are involved in the mining of molybdenum around the world. The largest production is attributed to the U.S. company Freeport McMoran which accounted for 15 wt.% of the world production of Mo in 2011 [30].

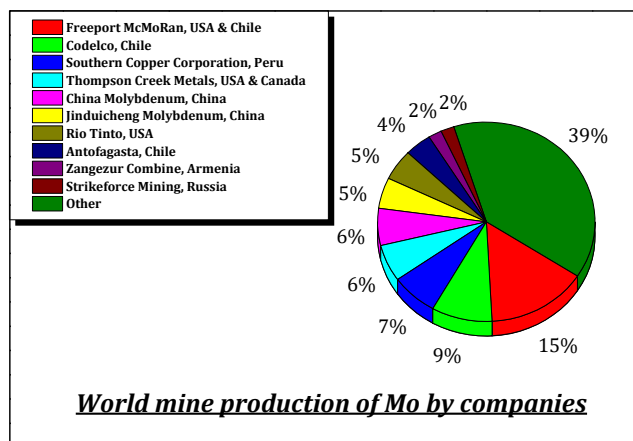


Figure I.5: World mine production of Mo by companies in 2011 (adapted from [29]).

The second largest production is attributed to the Chilean company Codelco which accounted for 9 wt.% of the Mo production in 2011 [31]. The third one is attributed to the Mexican company Grupo Mexico SA de CV which has produced 7 wt.% of the molybdenum in 2011 [32].

The fact that production of Mo is own by several mining companies decreases the risk of supply of molybdenum. Furthermore, it allows to introduce competition and affect the price of molybdenum.

II.3.5. Ecology and health impact of molybdenum mining and production

Molybdenum is an element which is essential for all species [33]. But as for many elements, too high concentrations of molybdenum can impact the human health and environment. No harmful effects have been reported from workers in the mining and processing industries [5]. The major source of pollution is a pollution by heavy metals and fine particulates. During mining, solid or liquid wastes contaminated are dumped or leaked into waterways [34] and during crushing fine particulate matters are dispersed into atmosphere [35] as during transportation and smelting where gaseous pollutants are also released into the atmosphere [36]. Furthermore, the creation of an intensive economy in China, in order to produce at low costs, means that questions about environmental protection are not always taken in account. In China, where working conditions are still not properly regulated, a large number of accidents is observed during mining. These accidents can be due to several reasons. Most common accidents occurring in the mining industry are gaseous explosions due to mechanical errors or malfunctioning equipments and accidents due to blasting (fly-rocks, premature blast or misfires) [37].

II.4. Uses of molybdenum

Molybdenum is used in various applications [38,39] but its main use is in engineering and stainless steels with more than 60 wt.% of the molybdenum produced in 2015. Figure I.6 is representing the different applications of new molybdenum.

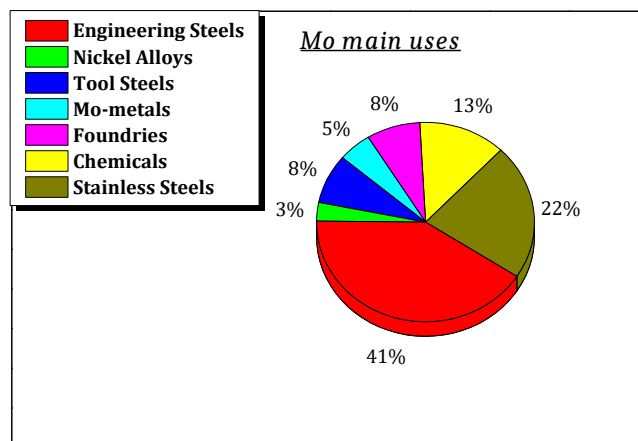


Figure I.6: Molybdenum main uses in 2015 (adapted from [38]).

New molybdenum, which come from mined ore and not from recycled metal counts for almost two third of the Mo used in constructional steels, cast iron and tools and high-speed steels. Another 20 wt.% of the new Mo produced is used for stainless steels. The remaining 20 wt.% is mainly used as superalloys, chemicals and as metal.

The interest of using molybdenum is important due to its many interesting properties. When it is used [40]:

- In stainless steels, Mo improves the corrosion resistance. It permits to use stainless steels in chemical processes, in marine applications, in architectures, in buildings and constructions, in water distributions. When added to the stainless steels, Mo increases the elevated temperature resistance allowing its use for heat exchangers and automotive exhaust systems,
- In grade alloy steels and irons, Mo improves hardenability, reduces temper embrittlement, resists hydrogen attack and sulfide stress cracking, increases elevated temperature strength and improves weldability. These properties of alloy steels and irons when Mo is added permit their uses in a large part of engineered products (automotive, aircraft and aerospace, drilling, mining, processing, chemical and petrochemical processing ...),
- In grade superalloys, molybdenum is a very important alloying element for corrosion resistance and high temperature nickel-based alloys. The uses of these high performance alloys are chemical processing, pharmaceutical, oil & gas, petrochemical and pollution control, heat treating, mineral processing and waste incineration applications,
- In alloys, Mo is used for its same properties as previously and their applications are high temperature applications,
- In chemistry, molybdenum is extraordinarily versatile which gives it unique properties and that is why it is used in many different applications:

- *Catalysts*: MoS₂ is well known to be the most commercial used catalyst for removing sulfur from crude oil. Bi-Mo oxides are used for selective propene oxidation; Fe-Mo oxides can be employed for methanol oxidation and for the synthesis of formaldehyde. The uses of heteropolyanions based on molybdenum are numerous and various [41,42]. Several other applications of Mo based catalysts can be found as epoxidation or acrolein oxidation [40],
- *Pigments*: molybdates-based pigments are used for their stable orange color formation and their corrosion resistance,
- *Corrosion inhibitors*: molybdates are used to inhibit corrosion in water-based systems, in automobile engine anti-freezes and in paints,
- *Smoke suppressants*: ammonium octamolybdate is used with PVC to suppress the formation of smoke in confined spaces (aircrafts, hospitals...),
- *Lubricants*: due to its layered structure MoS₂ is an effective lubricant,
- *Chemicals in agriculture*: molybdates are used in fertilizer formulations because Mo has such properties necessary for several enzymes.

II.5. Substitutability of molybdenum

Due to the unique properties of molybdenum, it is difficult to substitute it in major applications, as an alloying element in steels and cast irons. Potential substitutes will lead to a lack of performance. Potential substitutes include [5,16]:

- In alloy steels, chromium, vanadium, niobium and boron could be substitution elements,
- In tool steels, Mo can be substituted by tungsten,
- In refractory materials for high temperature applications, graphite, tungsten and tantalum can substitute molybdenum,
- In pigments for molybdenum orange, chrome-orange, cadmium-red and organic-pigments can be some substitutes of Mo,
- In catalysts, especially in HDS catalysts, Mo can be substitute by tungsten or nickel phosphide.

The difficulty of having the same versatility and properties as molybdenum made him an important element for our current modern technologies. The substitutability of molybdenum is thus at a high level in terms of criticality.

II.6. Recyclability of molybdenum

The amount of molybdenum which is recycled is difficult to quantify. Steels and other alloys containing molybdenum are frequently recycled and may account for as much as 30 wt.% of demand [5]. Data found about recycling were different depending on the sources. From the USGS [43], the old scrap ratio (OSR) of molybdenum was of 67 % while from the UNEP [44], the OSR has been estimated at 33 %. Its End Of Life Recycling Rate (EOL-RR) has been estimated at 30 % and its recycling rate (RR) at 33 % [43].

II.7. Trade of molybdenum [45]

The principal uses for molybdenum are expected to continue to be stainless steels and iron casts, chemicals and catalysts. Molybdenum is vital for the energy industry and it plays a major role in the development of green energy. Indeed, it is used for high-strength steels for automobiles to reduce weight and improve fuel economy and safety. The molybdenum plays also a critical role in catalysts which reduce sulfur in crude oil [2,46], and the catalysts market will increase more and more for the production of ultra-low sulfur diesel (ULSD). Furthermore, the demand for molybdenum alloys will increase in order to meet the stringent regulations about carbon dioxide emissions regulations. Molybdenum alloys are also necessary to the green energy developments (reduction of carbon footprint, wind turbines, high temperature engines...)

Emerging countries, such as China and India will increase the molybdenum demand for steels and cast irons for the development of oil and gas production, motor components, power plants, alternative and renewable energies. Roskill Information Services Ltd [29] reported that global demand for molybdenum was expected to increase at an average of 4.6 % in the next years.

II.8. Conclusion about molybdenum criticality

As it has been presented through this study, molybdenum is necessary for many applications and its demand will increase in the next years due to its uses in greener applications and alloys. Developing countries as China or India will need more and more molybdenum to continue their growth. Most of the molybdenum reserves are located in three developed or in development countries and are adequate to supply world needs for a foreseeable future. Furthermore, several companies are involved in mining and processing of this element which permits to have a concurrence and a regulation of price is possible. Molybdenum is used for its specific properties which made it difficult to substitute with another element. We can afford to say that molybdenum is not a critical element but it could become one really quickly with the emergence of new needs for the developing countries. The use of molybdenum in HDS catalysts represents a small part of the produced molybdenum. However, due to environmental regulations, the use of Mo in these catalysts is expected to increase. However, reserves of it are adequate for a foreseeable future.

III. Cobalt criticality

III.1. Introduction

Cobalt is a lustrous grey metal which has for symbol Co, an atomic number of 27 and an atomic weight of 58.93 g.mol⁻¹. This is an element of the transition metals group and it is located between iron and nickel on the fourth line and the ninth column of the Periodic Table of the elements [47]. Cobalt is one of the 27 elements essential to man. Indeed, it is the central atom of the Vitamin B12 (also called cobalamin) which is vital for humans. Cobalt is an element with unique properties, this is why it has many applications [48]:

- It has a high melting point (1493°C) and retains its strength up to high temperatures. It is therefore used for applications requiring significant constraints (cutting tools, superalloys, high speed steels...),
- It is a ferromagnetic element as nickel and iron. This property is also valid at high temperature because the Curie's temperature of cobalt is 1121°C. It is therefore used in magnets,
- Cobalt produces intense blue colours when mixed with silica or alumina (e.g. cobalt blue (CoAl₂O₄)). Cobalt is used for millenaries to produce pigments in ceramics and enamels,
- Its multivalence gives it an enhancement of its catalytic action. It is used in a large range of chemicals (catalysts, paints, adhesives...).

Cobalt possesses a close packed hexagonal crystal structure at room temperature; this structure changes at 421°C to a centred cubic form. For cobalt, its commonest valency is Co²⁺ but in some complexes, a mixed valencies can be observed (e.g. in Co₃O₄, Co²⁺ and Co³⁺). All these properties of cobalt made it a useful element in a wide range of sectors.

III.2. Reserves and resources of cobalt

Cobalt is present in the Earth's crust in a concentration of around 0.002 wt.% [5,49,50] but it is usually found at low concentrations. From the USGS, reserves of Co are estimated to 7 500 000 tonnes and identified world resources are about 15 million tonnes. The majority of these resources are in nickel-bearing laterite deposits while most of the rest occurring in nickel-copper sulfide deposits in Australia, Canada and Russia, and in the sedimentary copper deposits of Congo and Zambia (Copperbelt) [14]. Australian's researchers quantify recoverable reserves-resources of Co at 15.9 million tonnes [51]. Main reserves are located in Democratic Republic of Congo (DRC) in the province of Katanga (copper-belt) and in Australia [14,51,52]. Figure I.7 represents a chart pie listing the main reserves of cobalt.

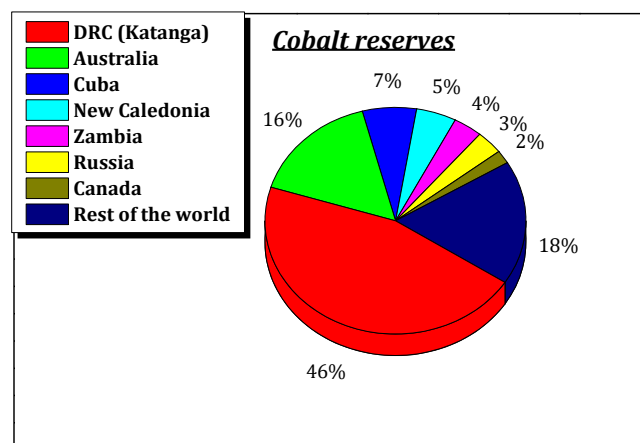


Figure I.7: Cobalt reserves per country.

DRC, Australia and Cuba hold almost $\frac{3}{4}$ of the estimated reserves, with DRC which holds almost the half of worldwide reserves. Europa does not possess any important reserves of cobalt which is a real problem.

III.3. Production of cobalt

III.3.1. Evolution of the cobalt production

The production of cobalt has still increased during these past years. According to the World Mining Data [53], the annual production of cobalt was around 130 000 t in 2014 and 64 000 t in 2007, which means that cobalt production has doubled over the last seven years.

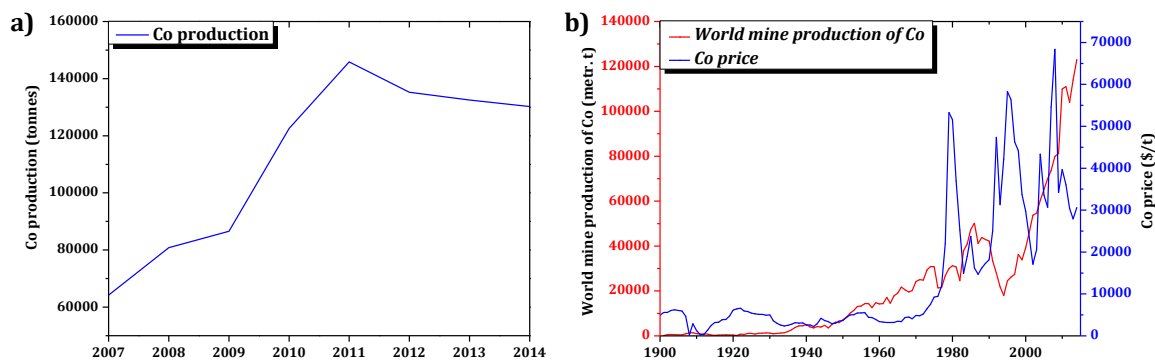


Figure I.8: Evolution of the cobalt production over the last 7 years (a) and evolution of the cobalt production and price over the last century (b).

This increase since the 19th century is due to its unique properties and its applications in a wide range of products, principally as the major part of the cathode in a Li-ion battery. Production of batteries is more and more important mainly due to the development of electric and hybrid cars [54]. But also due to the fact that the emerging countries are reaching a higher and higher level of life and their demands are turning increasingly to new technologies which contain batteries and thus cobalt (smartphones, tablets, laptops, netbooks...) [55].

Another increase of consumption of cobalt comes from its use in almost every form of clean energy production technology. Indeed, refining catalysts and particularly hydrotreatment catalysts contain cobalt and molybdenum [56] but also catalyst necessary to process gas to liquid (GTL) and coal to

liquid (CTL) technologies. We found also cobalt in super magnets in wind turbines and it is used in solar panels and fuel cells.

III.3.2. Main producing countries of cobalt

In 2014, almost two third of the cobalt production came from DRC which could be problematic in the supply chain due to the geopolitical instability of this geographic area. Other producers of cobalt are Canada, China, Zambia and Australia. These five countries provide more than 75 wt.% of the cobalt used [53].

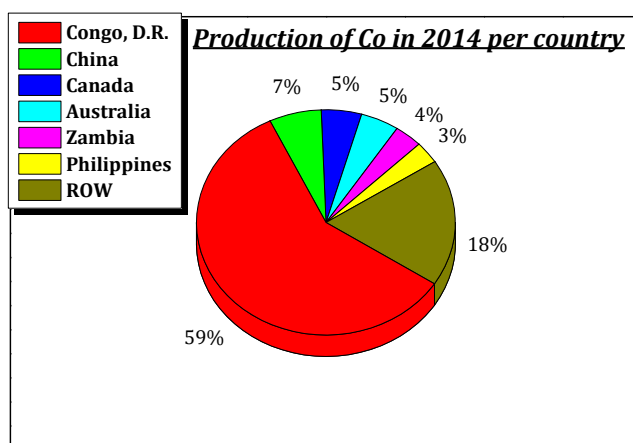


Figure I.9: Production of cobalt in 2014 (Co produced: 130 222 t)

The production is largely dominated by the country which holds the largest reserves of cobalt. But this is not the case for cobalt's refining. Indeed, DRC does not possess all facilities to refine all the cobalt production. The refining is mainly done abroad, principally in Finland and China [57]. One of the main drawback is the fact that DRC is one of the poorest country of the world and possesses a permanent geopolitical instability which could lead easily to a lack of supply of cobalt. As DRC is the main producer and the country which holds the main reserves of cobalt, it is necessary to know the geopolitical aspect of this country and the environmental impact of the cobalt mining to estimate risks in the supply chain. In fifteen years, DRC has known two wars and more than five million people were killed between 1996 and 2002. These wars influenced the cobalt's price. We observed indeed an increase of price at the moment of these wars (see Figure I.8) [58–60]. Moreover, some institutions have reported child labour in mining operations. 50 000 of 100 000-140 000 people involved in mining in Katanga area are under 18 years old [58–60]. A lot of artisanal mining is observed in this area which means no safety, a hard labour in dangerous conditions and no work regulations. Moreover, some mines are controlled by armed groups. Democratic Republic of Congo is also one of the poorest country of the world, ranked 186 on 187 on the HDI (Human Development Index) by the United Nations while its owns large mineral resources [17]. The life expectancy in the DRC is 48.7 years and the mean years of schooling for adult people is 3.5 years. The GNI (Gross National Income) of the DRC is around US\$ 319 compared to France where the GNI is around US\$ 30277 [17].

III.3.3. Mining and processing of cobalt

Due to the fact that cobalt is found at low concentration, it is principally produced as by-product [49–51] of nickel or copper mining. Indeed, 57 wt.% of the cobalt produced comes as by product from the nickel extraction and 37 wt.% as by product from the copper extraction. Only 6 wt.% of Co produced comes from primary arsenide ores (in Morocco and Canada) [51]. Cobalt can arise

from different ore types [61] and thus the technique employed to obtain cobalt products is different [61,62].

III.3.4. Main mining and refining companies of cobalt

Several companies are involved in the mining and the processing of cobalt ores. These companies are principally implanted in the copper-belt where reserves are the largest. Main companies involved in mining and processing of cobalt are listed hereafter:

- *Glencore Xsatra*, a swiss group, one of the world's largest mining company. From their annual report, this company has extracted 18 000 t of Co in 2011, which means 16 wt.% of the worldwide Co produced in 2011,
- *ENRC* (Eurasian Natural Resources Corporation) is a U.K. listed, Kazakhstan focused company. In 2011, this company has produced 11 400 t of Co representing 10 wt.% of the world production,
- *Freeport McMoran* is an U.S. company involved in mining. In 2011, this company has produced 6 400 t of Co representing 6 wt.% of the world production.

Several other companies are involved in the extraction of cobalt but do not communicate about their production data. The company *Glencore Xsatra* possess facilities to mining cobalt in the principal countries which have the most important reserves of cobalt. The fact that a company produces 1/6 of the annual cobalt production could entail difficulties of supply.

III.3.5. Ecology and health impact of cobalt mining and production

Mining and processing of metals are activities which demand the use of large quantities of chemicals and need a lot of energy. These operations, producing toxic gases which could be released in the atmosphere, create environmental and public health issues. Artisanal mining, metal smelting and processing of metals are considered as one of the world's worst pollution [63]. Due to mining industry, African Copperbelt belongs to the top ten of the most polluted areas worldwide. Soil, air and food are contaminated by dust particles of metals and by chemicals. People who are living close to mines and smelters possess high level of toxic metals (As, Cr, Co, Cu, Se, Sn and U) in their organisms [64].

III.4. Uses of cobalt

Cobalt has been used from at least 2600 B.C. for its blue color. It was incorporated in pottery and glass [65]. Nowadays cobalt is used in a wide range of applications [66] from chemicals [67] to metallurgical applications [68] via magnetic alloys [69] and hardmetals [70]. Figure I.10 represents the main applications of cobalt. A large part is dedicated to Li-ion batteries, as major part of the cathode, which is a growing sector [54]. Cobalt is also used for environmental and energy renewable applications. It is used in fuel cell technologies, in oil desulphurization and for new technologies as gas-to-liquid or coal-to-liquid processes. Cobalt is present in solar panels and wind turbine generators for its high performances properties in superalloys and magnets. These are the second and third main uses of this element.

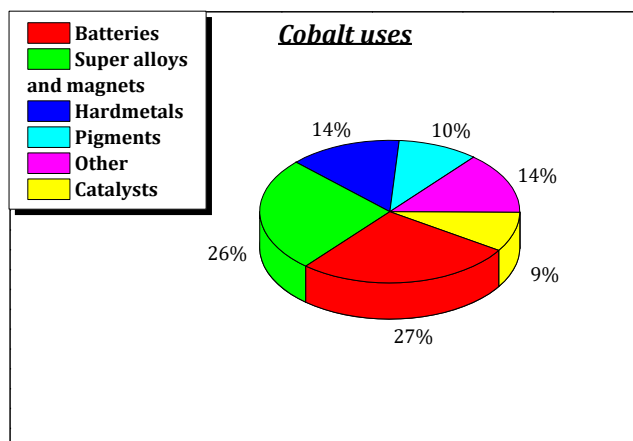


Figure I.10: Main uses of cobalt (adapted from [5])

Cobalt is also a very important element for strategic and industrial purposes as it is used in turbine blades, jet engines but also in mining, drilling equipments and cemented carbides [54].

III.5. Substitutability of cobalt

Due to unique properties of Co, for example its hardness and wear resistance when it is present in alloys, cobalt is an element which is difficult to replace. Most of the time some substitutes will lead to a loss of performance. Hereafter are presented some possible substitutes of cobalt in different applications [16]:

- In magnets, cobalt can be replaced by barium or strontium ferrites, Nd-Fe-B or nickel iron alloys,
- In paints, cobalt can be replaced by cerium, iron, platinum, manganese or vanadium,
- In diamond tools, it can be substituted by adding iron and copper to it,
- In curing unsaturated resins, copper iron manganese can be used as a substitute of cobalt,
- In wear resistant materials, ceramics, cermets, nickel or iron cobalt nickel alloys can be some substitutes of Co,
- In the case of Li-ion batteries, instead of using Co as major part of the cathode, Fe-P, manganese, Ni-Co-Al or Ni-Co-Mn can be used,
- In petroleum catalyst (e.g. HDS catalyst), cobalt can be replaced by nickel.

III.6. Recyclability of cobalt

Nowadays, new sources of metals appear and come from “urban mines”. Indeed, we have used in a century, a large scale of metals [5]. Most of the time, these metals are not enough recycled and lost in the environment. Another major problem is the presence of these metals in too small quantities in products. Technical issues to recover these tiny quantities of metals are a difficult but necessary challenge. In the case of cobalt, its recycling content is of 32 %, its end of life recycling rate is of 68 % and its old scrap ratio is of 50 % [43,44].

These percentages show that cobalt has reached a high level of recycling. This is mainly due to its high price and its unpredictable supply. The desire to reduce environmental impact of cobalt-laden batteries in landfills has also played a great role to this high level of recycling [5].

III.7. Trade of cobalt

In recent years, global cobalt production has been higher than consumption, resulting to a decrease of the price due to a market surplus [54]. China was the world's leading producer of refined cobalt, and much of its production was from cobalt-rich ore and partially refined cobalt imported from DRC. Significant stocks of Co have been accumulated in China which made it one of the leading supplier of cobalt.

III.8. Conclusion about cobalt criticality

We have shown, through the study of several indicators of criticality, that cobalt is a very unique and necessary metal for the development of new greener technologies. Its major use in batteries implies a large demand for cobalt in a foreseeing future. Mainly associated to the growth of electrical and hybrid vehicles and the need of new devices for emerging countries. Cobalt is also part of all green technologies such as wind turbines, solar panels, GTL and CTL technologies. As its substitution leads to a loss a performance, we can therefore affirm that demand for cobalt will increase during the next decades. The importance of cobalt in HDS catalysts is well known and its demand for this use will increase in the next years. A careful use of cobalt is thus necessary and new synthesis methods to produce more active HDS catalysts without loss of cobalt are studied. However, in HDS catalysts, cobalt can be replaced by nickel to obtain a catalyst with similar performances.

The major part of cobalt reserves is located in a poor and instable country, the Democratic Republic of Congo, which can lead to a lack of supply. Moreover, cobalt is mainly recovered as a by-product. This makes it very dependent of copper and nickel prices and creates difficulties to expand its production.

A high rate of recycling is mandatory for our future to avoid lack of supply and limit environmental issues. Its particularly necessary to recycle cobalt for Europa which does not possess any reserves of this element.

Cobalt is therefore an element on which we should keep an eye on it and work on new recycling techniques and other substitution elements to avoid the paralysation of new technologies sector.

IV. Conclusion

Through this chapter, reserves, resources, production, uses, substitutability, recyclability and trade of metals contained in HDS catalysts have been presented. Molybdenum and cobalt are used in a wide range of applications and reserves of these elements are inequitably distributed in the Earth's crust. In both cases, several countries own important reserves of these elements.

In the case of molybdenum, China, USA and Chile hold more than 80 wt.% of reserves but these countries are considered as developed or in developing which limits a lack of supply due to geopolitical instabilities. Furthermore, several companies are involved in the mining and processing of molybdenum which permits a concurrence and a regulation of price. The unique properties of molybdenum made difficult its substitution by another element. We can afford to say that molybdenum is not a critical element but it could become one really quickly with the emergence of new needs for the developing countries.

For cobalt, we found that its properties made it a very unique element used in a large range of applications and especially greener ones. For example, its use in batteries implies a large demand of it with the growth of demand in electrical vehicles but also in new devise for emerging countries. Cobalt is also part of all green technologies such as wind turbines, solar panels, GTL and CTL technologies. As its substitution leads to a loss of performance, the demand for Co will increase during the next decades. Moreover, major part of cobalt reserves is located in a poor and instable country, the Democratic Republic of Congo. The fact that around 50 wt.% of cobalt reserves are located in this country, could lead to a lack of supply. Moreover, cobalt is mainly recovered as a by product which makes it very dependent of copper and nickel prices and involves difficulties to expand production. Cobalt can thus be considered as critical for European Union and a close observation of it is necessary. Moreover, efforts about recycling must quickly committed.

This study allowed us to have a wider vision and a better knowledge about elements employed for the preparation of HDS catalysts. Furthermore, to avoid the loss of metals in the form of bulk in HDS catalysts, new synthesis methods, as the process proposed in this work, are investigated. These methods are developed to increase the dispersion of metals and avoid the presence of bulk compounds, where metal atoms contained inside the bulk are not catalytically active.

A similar study has been carried out in the case of the element sulfur and results are presented in Appendix 1. The abundance of the aluminium (3rd most abundant element on earth) made that it was not studied regarding criticality in this study.

V. Bibliography

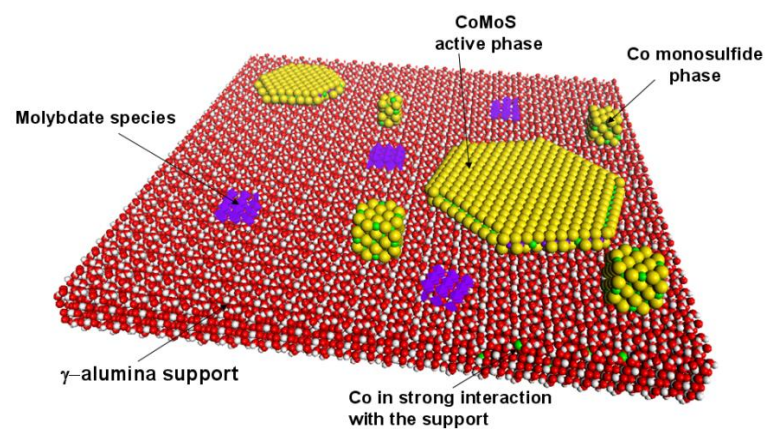
- [1] The European Parliament, the Council of the European Union, Directive 2009/30/EC of the European Parliament and of the Council of 23 April 2009, 2009.
- [2] Ministry of Economy Trade and Industry (METI), Law on the quality control of gasoline and other fuels (Fuel Quality Control Law), 2014.
- [3] H. Topsøe, B.S. Clausen, F.E. Massoth, *Catalysis*, Springer Berlin Heidelberg, Berlin, Heidelberg, 1996.
- [4] E.C.E. and Industry, Critical raw materials for the EU Report of the Ad-hoc Working Group on defining critical raw materials, 2010.
- [5] B. Achzet, A. Reller, C. Rennie, M. Ashfield, J. Simmons, *Materials critical to the energy industry. An introduction*, 2011.
- [6] R. Mills, Congo and Cobalt Critical, (2012). <http://aheadoftheherd.com/Newsletter/2012/Congo-and-Cobalt-Critical.htm>.
- [7] B. Achzet, C. Helbig, How to evaluate raw material supply risks - an overview, *Resour. Policy*. 38 (2013) 435–447.
- [8] T.E. Graedel, R. Barr, C. Chandler, T. Chase, J. Choi, L. Christoffersen, E. Friedlander, C. Henly, C. Jun, N.T. Nassar, D. Schechner, S. Warren, M. Yang, C. Zhu, Methodology of metal criticality determination, *Environ. Sci. Technol.* 46 (2012) 1063–1070.
- [9] American Elements, Molybdenum (Mo), (2016). <https://www.americanelements.com/mo.html>.
- [10] IMOA, Molybdenum Properties, (2012) 2012. <http://www.imoa.info/molybdenum/molybdenum-properties.php>.
- [11] R.R. Mendel, Metabolism of Molybdenum, in: *Met. Cell*, Banci, Luc, Springer Berlin Heidelberg, 2013.
- [12] J. Lener, B. Bibr, Effects of molybdenum on the organism (a review)., *J. Hyg. Epidemiol. Microbiol. Immunol.* 28 (1984) 405–419.
- [13] D.R. Lide, *Handbook of Chemistry and Physics*, CRC Press, 1993.
- [14] U.S. Department of the Interior, U.S. Geological Survey, *Mineral Commodity Summaries 2013*, 2013.
- [15] U.S. Department of the Interior, U.S. Geological Survey, *Mineral Commodity Summaries 2015*, 2015.
- [16] U.S. Department of the Interior, U.S. Geological Survey, *Mineral Commodity Summaries 2016*, 2016.
- [17] United Nations Development Programme, *Human Development Index and its components*, (2014). <http://hdr.undp.org/en/statistics/hdi>.

-
- [18] T.D. Kelly, G.R. Matos, Molybdenum statistics _ Historical statistics for mineral and material commodities in the United States: U.S. Geological Survey Data Series 140, (2005). <http://pubs.usgs.gov/ds/2005/140/> (accessed January 1, 2015).
- [19] U.S. Geological Survey, Molybdenum Statistics, 2012.
- [20] C. Reichl, G. Schatz, G. Zsak, World Mining Data 2013, 2013.
- [21] C. Reichl, M. Schatz, G. Zsak, World Mining Data 2014, 2014.
- [22] C. Reichl, M. Schatz, G. Zsak, World Mining Data 2015, 2015.
- [23] C. Reichl, M. Schatz, G. Zsak, World Mining Data 2016, 2016.
- [24] H. Imgrund, N. Kinsman, Molybdenum -an extraordinary metal in high demand, 2007. www.imoa.info (accessed June 13, 2016).
- [25] IMO, Molybdenum uses, (2012). <http://www.imoa.info/molybdenum-uses/molybdenum-uses.php> (accessed January 1, 2014).
- [26] Y. Yeboah, The Pennsylvania State University, The Second Shock: The Great Panic, (2014). <https://www.e-education.psu.edu/egee120/node/292> (accessed January 1, 2015).
- [27] U.S. Geological Survey, U.S. Department of the Interior, Metal Prices in the United States Through 2010, 2012.
- [28] InfoMine, Historical Molybdenum Prices and Price Chart, (2015). <http://www.infomine.com/investment/metal-prices/molybdenum-oxide/all/> (accessed January 1, 2015).
- [29] J. Chegwiddden, Roskill Consulting Group Ltd, Evaluating current and future supply of molybdenum, 2012.
- [30] Freeport McMoran, Freeport McMoran annual report, 2011.
- [31] Codelco, Codelco Annual report, 2011.
- [32] Grupo de Mexico SA de CV, Grupo Mexico SA de CV Annual report, 2011.
- [33] J.R. Turnlund, W.R. Keyes, G.L. Peiffer, G. Chiang, Molybdenum absorption, excretion, and retention studied with stable isotopes in young men during depletion and repletion, *Am. J. Clin. Nutr.* 61 (1995) 1102–1109.
- [34] Friends of Nature, Institute of Public and Environmental Affairs, Green Beagle, The IT industry has a critical duty to prevent heavy metal pollution, 2010.
- [35] G.L. Liao, D.X. Liao, Q.M. Li, Heavy metals contamination characteristics in soil of different mining activity zones, *Trans. Nonferrous Met. Soc. China (English Ed.)* 18 (2008) 207–211.
- [36] P. Mayfair, Metals Smelters and Processing, SuperGreenMe. (2009). <http://www.supergreenme.com/go-green-environment-eco:Metals-Smelters-and-Processing-> (accessed January 1, 2015).

-
- [37] P. Dozolme, Common Mining Accidents, (2016). <http://mining.about.com/od/Accidents/a/Common-Mining-Accidents.htm> (accessed January 1, 2015).
- [38] International Molybdenum Association, Uses of new Molybdenum, (2015). <http://www.imoa.info/molybdenum-uses/molybdenum-uses.php> (accessed June 16, 2016).
- [39] T.D. Kelly, G.R. Matos, End Uses of Molybdenum, 2005.
- [40] IMOA, Uses of new Molybdenum, (2012). <http://www.imoa.info/molybdenum-uses/molybdenum-uses.php> (accessed June 16, 2016).
- [41] I. V Kozhevnikov, Advances in catalysis by heteropolyacids, *Russ. Chem. Rev.* 56 (1987) 1417–1443.
- [42] I. V Kozhevnikov, Catalysis by heteropoly acids and multicomponent polyoxometalates in liquid-phase reactions, *Chem. Rev.* 98 (1998) 171–198. doi:10.1021/cr960400y.
- [43] U.S. Department of the Interior, U.S. Geological Survey, Flow studies for recycling metal commodities in the United States, 2004.
- [44] T.E. Graedel, J. Allwood, J.-P. Birat, B.K. Reck, S.F. Sibley, G. Sonnemann, M. Buchert, C. Hagelüken, Recycling Rates of Metals - A Status Report, A report of the Working Group on the global metal flows to the International Resource Panel, 2011. doi:ISBN 978-92-807-3161-3.
- [45] U.S. Geological Survey, U.S. Department of the Interior, D.E. Polyak, Molybdenum [Advance Release], in: 2011 Miner. Yearb., 2012.
- [46] Union Européenne, Journal Officiel de l'Union Européenne, L76, 22 mars 2003, Directive 2003/70/CE, (2003) L76/10-L76/19.
- [47] American Elements, Cobalt (Co), (n.d.). <https://www.americanelements.com/co.html>.
- [48] Cobalt Development Institute, About Cobalt, (n.d.).
- [49] Cobalt Development Institute, Cobalt Supply & Demand, 2012.
- [50] R.L. Rudnick, S. Gao, Treatise on Geochemistry, Elsevier, 2014. doi:10.1016/B978-0-08-095975-7.00301-6.
- [51] G.M. Mudd, Z. Weng, S.M. Jowitt, I.D. Turnbull, T.E. Graedel, Quantifying the recoverable resources of by-product metals: The case of cobalt, *Ore Geol. Rev.* 55 (2013) 87–98.
- [52] Cobalt Development Institute, A Short History of Cobalt, 2006.
- [53] C. Reichl, M. Schatz, G. Zsak, WORLD-MINING-DATA, 2013.
- [54] Global Cobalt Corporation, Cobalt, Vancouver, n.d.
- [55] Formation Capital Corporation, C o b a l t . . . The essential element, 2010.

-
- [56] P. Grange, Catalytic Hydrodesulfurization, *Catal. Rev.* 21 (1980) 135–181.
- [57] J. Bedder, Cobalt production in the DRC Major changes, minor implications ?, 2013.
- [58] SwedWatch, Powering the Mobile World. Cobalt production for batteries in the DR Congo and Zambia, 2007.
- [59] Business for Social Responsibility, Conflict Minerals and the Democratic Republic of Congo, 2010. http://www.bsr.org/reports/BSR_Conflict_Minerals_and_the_DRC.pdf.
- [60] Global Witness, Digging in Corruption: Fraud, Abuse and Exploitation in Katanga's Copper and Cobalt Mines, 2006. http://www.globalwitness.org/media_library_get.php/278/1256196433/kat-doc-engl-lowres.pdf.
- [61] C.-H. Wu, Low Energy-Consumption Industrial Production of Ultra-Fine Spherical Cobalt Powders, in: A.Z. Ahmed (Ed.), *Energy Conserv.*, 2012.
- [62] British Geological Survey, Cobalt, 2009. www.MIneralsUK.com.
- [63] The Blacksmith Institute, Green Cross, The world's worst pollution problems: the top ten of the toxic twenty, (2008).
- [64] C.L.N. Banza, T.S. Nawrot, V. Haufroid, S. Decrée, T. De Putter, E. Smolders, B.I. Kabyla, O.N. Luboya, A.N. Ilunga, A.M. Mutombo, B. Nemery, High human exposure to cobalt and other metals in Katanga, a mining area of the Democratic Republic of Congo, *Environ. Res.* 109 (2009) 745–752.
- [65] Cobalt Development Institute, History, Cobalt Facts, 2006. http://www.thecdi.com/cdi/images/documents/facts/COBALT_FACTS-History.pdf (accessed July 27, 2016).
- [66] Cobalt Development Institute, Main uses, Cobalt Facts, 2006. http://www.thecdi.com/cdi/images/documents/facts/COBALT_FACTS-Properties_and_Main_Uses.pdf (accessed July 27, 2016).
- [67] Cobalt Development Institute, Chemicals, Cobalt Facts, 2006. http://www.thecdi.com/cdi/images/documents/facts/COBALT_FACTS-Chemicals2015.pdf.
- [68] Cobalt Development Institute, Metallurgical Uses, Cobalt Facts, 2006. http://www.thecdi.com/cdi/images/documents/facts/COBALT_FACTS-Metallurgical_uses.pdf (accessed July 27, 2016).
- [69] Cobalt Development Institute, Magnetic Alloys, Cobalt Facts, 2006. http://www.thecdi.com/cdi/images/documents/facts/COBALT_FACTS-Magnetic_Alloys.pdf (accessed July 27, 2016).
- [70] Cobalt Development Institute, Cemented Carbides, Cobalt Facts, 2006. http://www.thecdi.com/cdi/images/documents/facts/COBALT_FACTS-Cemented_Carbides.pdf.

Chapter II: Bibliographic study



I. INTRODUCTION.....	53
II. AN OVERVIEW OF THE HYDROTREATMENT PROCESSES.....	55
II.1. OIL REFINING PROCESS.....	55
<i>II.1.1. Overview of the refining process.....</i>	<i>55</i>
<i>II.1.2. Hydrodesulfurization.....</i>	<i>56</i>
II.2. HYDRODESULFURIZATION CATALYSTS	62
<i>II.2.1. Common catalysts used in HDS.....</i>	<i>62</i>
<i>II.2.2. Active phase in HDS catalysts</i>	<i>62</i>
<i>II.2.3. Typical synthesis of a HDS catalyst</i>	<i>67</i>
<i>II.2.4. Alternatives methods for the synthesis of HDS catalysts.....</i>	<i>71</i>
II.3. CONCLUSION ABOUT HDS CATALYSIS	74
III. SUPERCRITICAL FLUIDS ROUTE FOR THE SYNTHESIS OF HDS CATALYSTS.....	75
III.1. INTRODUCTION TO SCFs	75
III.2. CASE OF SUPERCRITICAL CARBON DIOXIDE (SCCO ₂).....	75
III.3. PREPARATION OF HDS CATALYSTS USING SCF	76
III.4. CONCLUSION	78
IV. CONCLUSION AND OBJECTIVES OF THE PHD.....	79
V. BIBLIOGRAPHY.....	81

I. Introduction

Nowadays, environmental regulations concerning emission gases are more and more stringent, especially concerning the sulfur content in petroleum-based fuels. When sulfur is not removed from fossil fuels, its presence can be detrimental on many levels. First, it can poison catalysts present in the refining process which implies a renewal of catalyst more frequently. But the most damaging effect of its presence takes place during its combustion where it is released into the atmosphere. Sulfur oxides formed will react in the high atmosphere to be transformed into sulfuric acid and generate acid rains, which are an environmental disaster. Regulations about sulfur content are thus drastic in developed countries and increasingly stricter in developing countries, as depicted in Figure II.1 for sulfur content in diesel fuel.

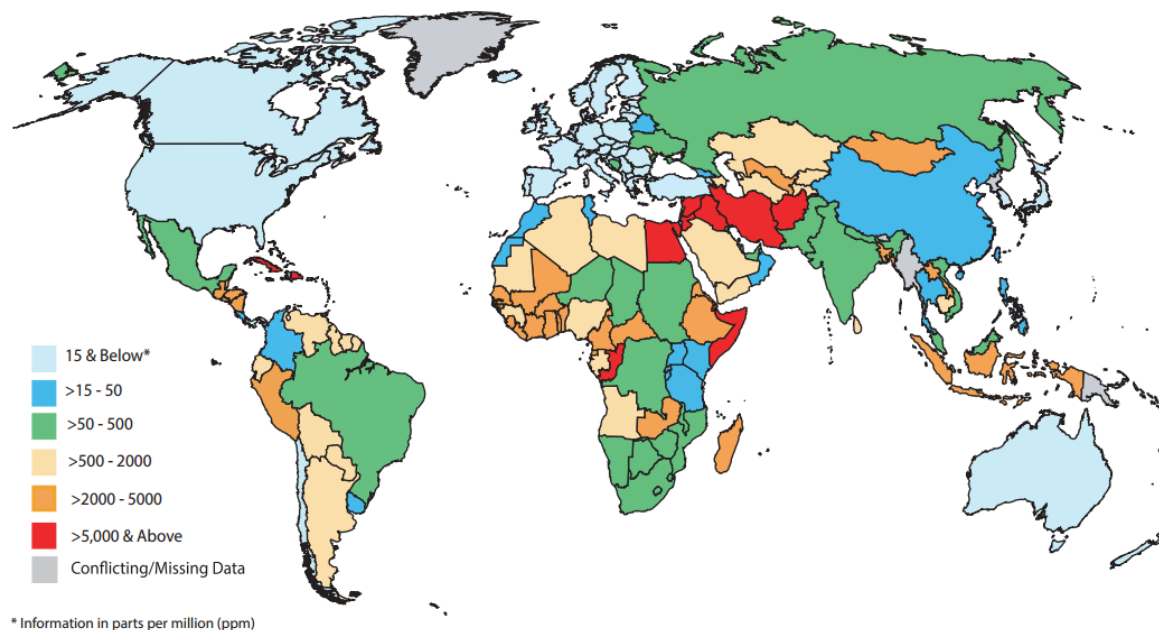


Figure II.1 : Diesel fuel sulfur levels : global status in June 2015 (adapted from [1]).

In most of the developed countries, regulations on the sulfur content in petroleum-based fuels is fixed at 15ppm or less. For developing countries, these regulations authorize a higher content. For example, in China the regulation allows a sulfur content between 15 ppm and 50 ppm. While other countries such as Egypt allows a sulfur content of 5000 ppm or above. During these past twenty years, regulations above sulfur content have evolved significantly as depicted in Figure II.2. This represents the evolution of sulfur content in diesel and gasoline for European Union during the last twenty years.

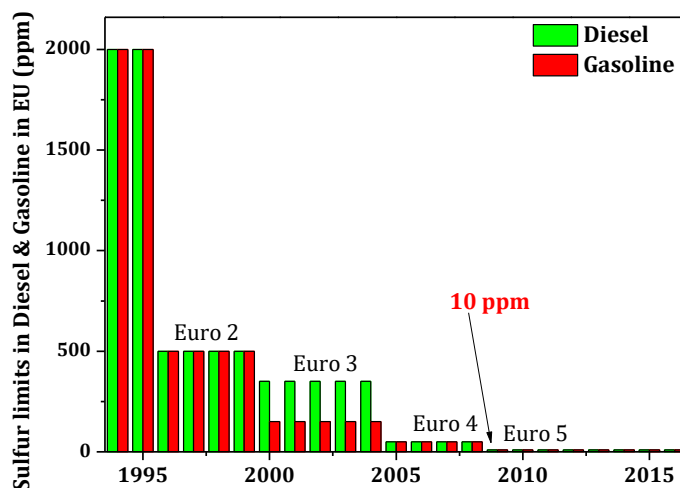


Figure II.2: Evolution of sulfur limits in diesel and gasoline for the European Union.

In order to meet the increasing demand for clean fuels, catalysts need to be more efficient to remove more than 99.9% of sulfur contained in feedstocks and reach 10 ppm of sulfur content. For that, hydrodesulfurization (HDS) catalysts need to be very performant and consequently new synthesis methods are necessary.

This chapter deals, first with the presentation of the hydrotreatment process. HDS process, sulfur compounds present in crude oil, reactions of hydrodesulfurization (HDS), catalysts employed as well as their preparation are presented in this part.

As most of the time, new synthesis method means the use of an unconventional process, the second part is dedicated to the presentation of supercritical fluids and especially the use of supercritical carbon dioxide (scCO₂) for the synthesis of HDS catalysts.

The last part of this chapter is dedicated to the presentation of the objectives of this PhD. They concern the investigations of chemical reactions occurring during the preparation of HDS catalyst precursors, the synthesis of catalytic materials using supercritical fluids as well as the catalytic performances of synthesized catalysts.

II. An overview of the hydrotreatment processes

II.1. Oil refining process

II.1.1. Overview of the refining process

During the last century, oil has widely participated in the development of our modern society and by the fact of it requires processing before use, the oil refining has become a major part of our industry. Crude oil is composed of a wide range of products, mostly hydrocarbons, which formed a complex mixture. Refining crude oil is so far necessary to obtain a large range of useful products. They will be employed for many purposes such as transportations (gasolines, kerosene, diesel), heating (LPG, fuels oils), feedstocks for the petrochemical industry (naphtha, LPG), special manufacturing routes (lubricating oils, greases, bitumen) and for special products (solvents, wax, coke) [2]. Depending of their origins, crude oils possess different fractions of these products and a different content of undesirable heteroatoms (nitrogen, sulfur, oxygen and metals). These fractions can be classified as follows [3]:

- Light distillates: Liquefied petroleum gas (LPG), gasoline, naphtha,
- Middle distillates: kerosene, jet fuel, diesel,
- Heavy distillates,
- Residuum: heavy fuel oil, lubricating oils, wax, asphalt,

To separate the various oil fractions, a refinery has a wide range of different units, which are represented in Figure II.3. All major processes are shown in the flow scheme diagram but may differ according to the location of the refinery. An European market has indeed not the same needs of products than an U.S. market [4]. Three main steps are necessary to obtain valuable and useful products. The separation process being the first one where products are separated mainly by distillation. The second one is the hydrotreatment process where the different heteroatoms present in crude oil are removed from it. These treatment units are present at each stage of the refining process and are denominated as hydrotreater in the flow scheme diagram. The third one is the conversion process where separated products are converted into useful compounds.

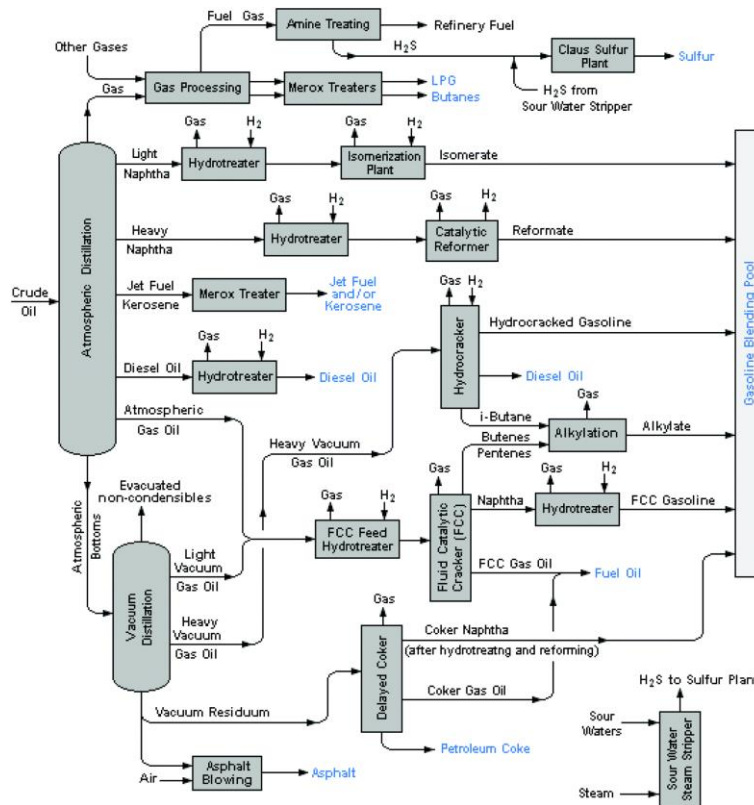


Figure II.3: Flow scheme diagram of a U.S. refinery (from [5]).

Hydrotreatment units are a main part of a refining process and are necessary to remove sulfur, nitrogen, oxygen and metals from the feedstocks. The sulfur being the heteroatom with the highest content in crude oil, the next part is dedicated to the removing of sulfur by hydrodesulfurization.

II.1.2. Hydrodesulfurization

II.1.2.a. Sulfur content depending of the crude oil's origin

Sulfur can be present at different content in crude oil depending of the origin of the latter. Figure II.4 is an example of selected crude oils from different worldwide locations with their densities and sulfur contents.

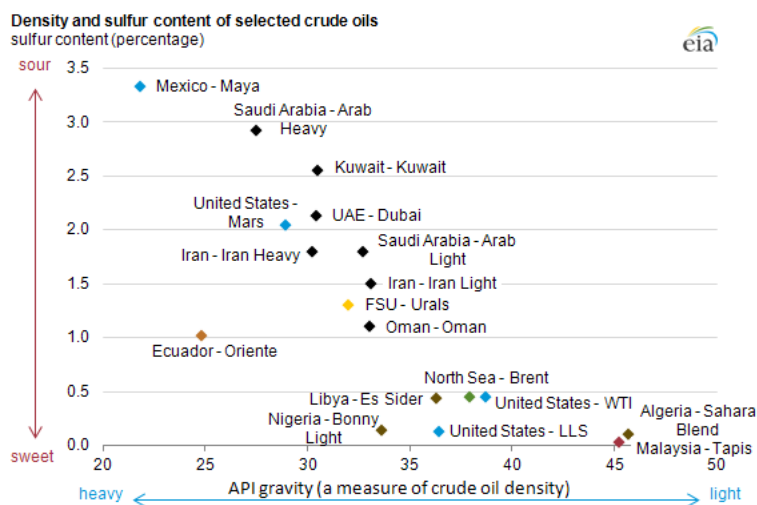


Figure II.4: Density and sulfur content of different crude oils [6].

These differences in sulfur content lead to a difference of complexity in refining. A crude oil which possesses a high content of sulfur will be more difficult to treat and refine than a low sulfur content crude oil. This sulfur content is an important factor in pricing crude oil. Low sulfur crude oil (< 1 wt.%) is the most desirable, but also the most expensive, while high sulfur crude oil (> 1.5 wt.%) is cheaper but will be more difficult to refine.

II.1.2.b. Sulfur compounds present in oil ranges

It has been shown that the sulfur content is linked to the origin of crude oil, but it is also dependent on the oil range to treat in a refinery. After the separation by distillation, different ranges of oil are obtained and do not possess the same sulfur compounds. On average, sulfur content increases with the molecular weight of products. In the case of light naphtha, sulfur compounds are mainly thiols, thioethers and disulfides. Whereas in heavy naphtha, diesel oil and light FCC naphtha, sulfur compounds contain thiophenes, dibenzothiophenes (DBT) and alkylbenzothiophene. Fractions possessing the heaviest density (coker naphtha and gas oil, FCC gas oil) mainly contain alkylbenzothiophene, DBT and alkyl dibenzothiophene [7]. Figure II.5 shows sulfur compounds in the finished products of gasoline, jet fuel and diesel representative of commercial transportation fuels in U.S. These are the most refractory compounds in each range of transportation fuels. Alkylbenzothiophene and alkyl dibenzothiophene compounds are more difficult to remove mainly due to the steric hindrance of carbon groups around the sulfur atoms [8,9].

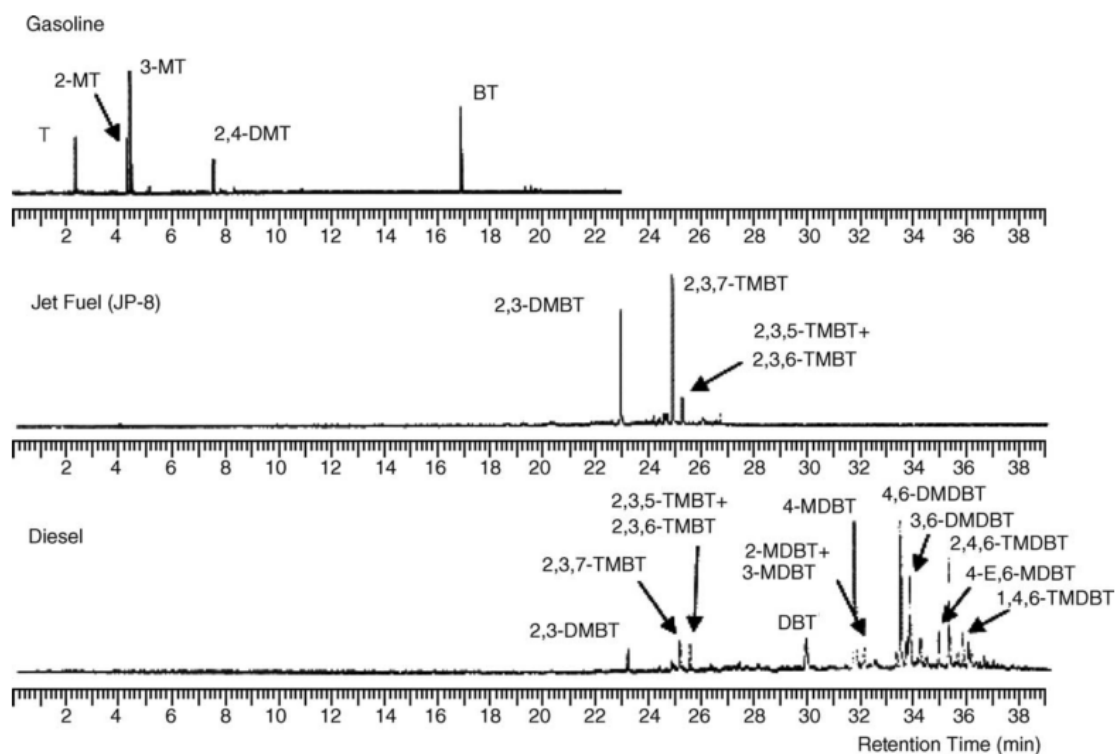


Figure II.5: Sulfur compounds present in commercial gasoline, jet fuel and diesel oil identified by GC-FPD analysis coupled with GC-MS (from [10]).

The most refractory compounds are 4-substituted and 4,6-disubstituted dibenzothiophenes (respectively 4-MDBT and 4,6-DMDBT). These sulfur heterocycles may be called β -DBTs by the fact that 4 and 6 positions are β to the sulfur atom [10]. Figure II.6 represents different sulfur compounds present in oil with their reactivity, feedstock range and their increase in size and difficulty to be removed in HDS.

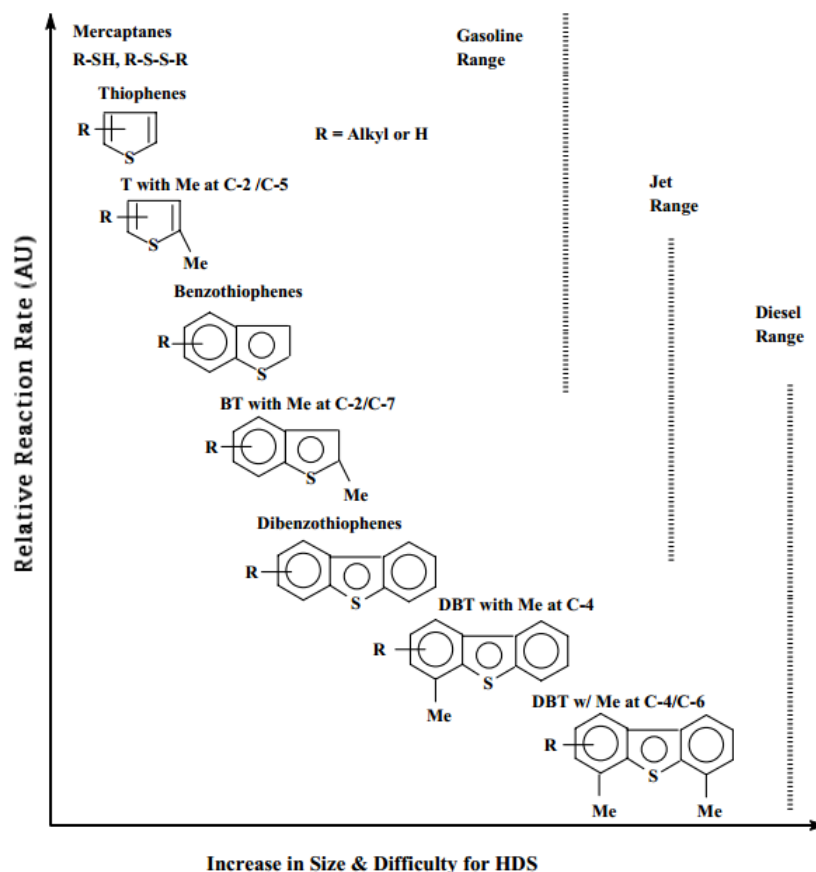


Figure II.6: Organosulfur compounds present in crude oil and their increase in size and difficulty to be removed (from [11]).

II.1.2.c. Hydrodesulfurization mechanisms

The molecular size and the structure of the sulfur-containing compounds strongly affect their reactivity in HDS as shown in Figure II.6. The order in desulfurization rates has been reported as following [12]:



Higher dibenzothiophene, such as benzonaphthothiophene, hydrogenation of one of the aromatic rings accompanies HDS. Hydrogenated compounds are indeed easily desulfurized than thiophenic compounds [13,14].

When a substituent group is adjacent to the S atom, it generally retards HDS. While methyl groups distant from the S atom generally increase HDS activity due to an increase of the electron density on the S atom, those methyl groups adjacent to the S atom decrease reactivity due to steric effect. This is one of the main reasons why 4,6-DMDBT are ten times less reactive than DBT [15].

For thiophene HDS, two pathways have been proposed, as presented in Figure II.7. Reaction pathways for the HDS of thiophene occur via a hydrogenation (HYD) or a direct desulfurization (DDS) routes. Owens et al. [16], Hargreaves et al. [17] and McCarthy et al. [18] have proposed that the HDS of thiophene occurs mainly via the direct desulfurization (DDS) pathway when working at atmospheric pressure (a and b in Figure II.7). Startsev et al. [19] have suggested that HDS of

thiophene leads directly to butene (f in Figure II.7) and that reaction intermediates are retained on the same surface sites during the reaction.

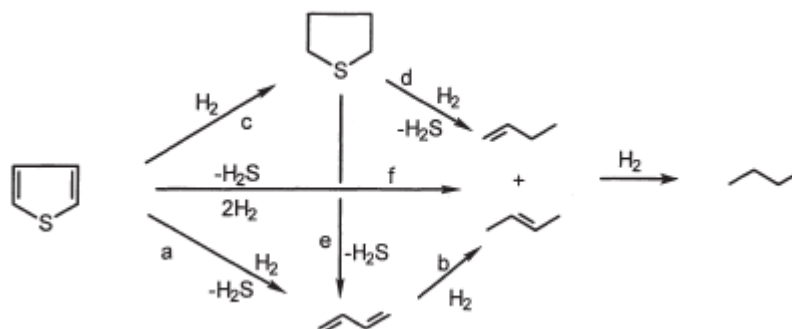


Figure II.7: Reaction pathways for the HDS of thiophene (from [20]).

Blake et al. [21] have studied the HDS of tetrahydrothiophene over MoS₂ catalyst at low pressure and found the presence of thiophene and butadiene compounds suggesting the existence of two reaction pathways (via e, b and via -c, a, b in Figure II.7)

For higher analogues of thiophenes (e.g. benzothiophene, ...), studied at elevated pressures, hydrogenated S-intermediates are present, suggesting parallel paths [22–24] and even prehydrogenation may be necessary before C-S bond cleavage occurs [17,25–29]. Schulz et al., have found that tetrahydrothiophene is a major intermediate in the HDS of thiophene at high pressures suggesting the presence of two parallel paths for the HDS of thiophene [29].

As environmental regulations require an elimination of more than 99.99% of sulfur present in crude oil, the removal of refractive sulfur compounds is mandatory. The removing of these sulfur compounds is known as deep-HDS and applied for DBT and alkylated-DBT.

For the HDS of DBT, two reaction pathways are also in parallel [30]. The formation of biphenyl (BP) compounds from DBT, by direct S-elimination, is the major pathway for this reaction, called direct desulfurization pathway (DDS). The second reaction pathway goes through the hydrogenation of DBT to hexahydrodibenzothiophene, followed by HDS to cyclohexylbenzene (minor pathway). This reaction pathway is called hydrogenation pathway. Figure II.8 presents the two reaction pathways for the HDS of DBT.

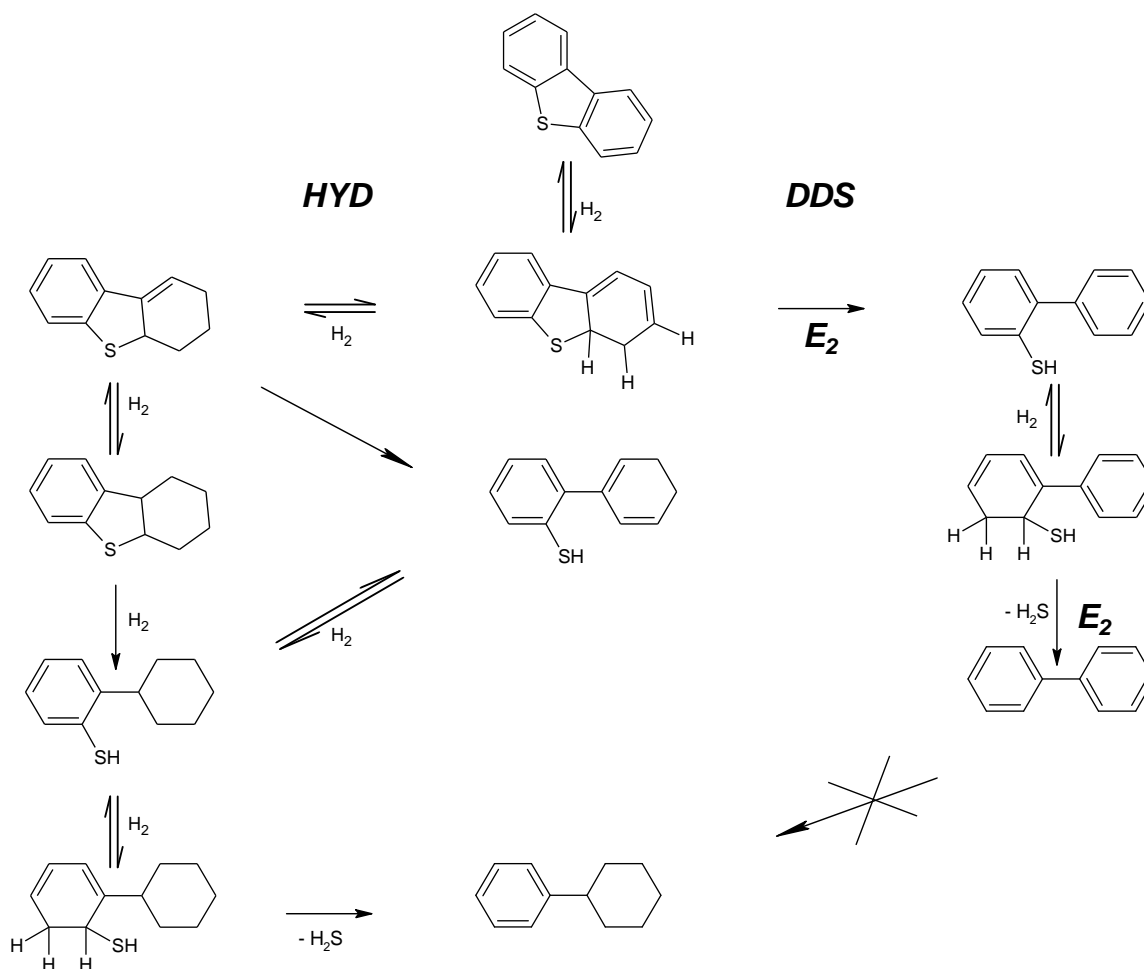


Figure II.8: Reaction pathways for the HDS of DBT (adapted from [31]).

Bataille et al. [31] reported that, under conventional HDS conditions [32], the DDS pathway contributed to 80% of the overall HDS of DBT. To obtain a C-S bond cleavage ending with two phenyl rings, a hydrogenation of one of the double bonds in the proximity of the S atom is necessary. A dehydrogenated product is obtained and the C-S bond can be open by an elimination process. To cleave the second C-S bond leading to biphenyl product, the same mechanism probably occurs.

For the HYD pathway, the first step is the hydrogenation of a bond in one of the ring leading to dihydrodibenzothiole (DHDBT) compounds as intermediate. The second cleavage of the C-S in the HYD route does not require the second aromatic ring to be fully hydrogenated and may occur through a DDS-type process leading to the production of cyclohexylbenzene (CHB) instead of dicyclohexyls-type compounds.

The hydrogenation pathway becomes more important for large sulfur compounds. It has been shown for benzonaphthothiole that HDS via prehydrogenation of one of the naphthalene rings was comparable in rate to the DDS route [33]. The localization of the electron density determines the reaction pathways. If the electron density is localized on the S-atom, the HDS via a DDS pathway is favoured. Whereas, if the electron density is more delocalized, hydrogenation precedes the C-S bond rupture.

For alkyl-substituted DBT, the position of the methyl groups induces a steric hindrance and makes these sulfur-containing compounds less reactive in HDS. A model molecule for the study of deep-HDS is the 4,6-dimethyldibenzothiophene (4,6-DMDBT).

As for the HDS of DBT, HDS of 4,6-DMDBT occurs via two reaction pathways. The hydrogenation (HYD) pathway with the formation of methylcyclohexyltoluene (MCHT) through a hexahydrodimethyldibenzothiophene (6H-DMDBT) intermediate. Whereas, through the DDS pathway, the product formed is 3,3'-dimethylbiphenyl (3,3'-DMBP). Figure II.9 represents the HDS of 4,6-DMDBT with the two pathways.

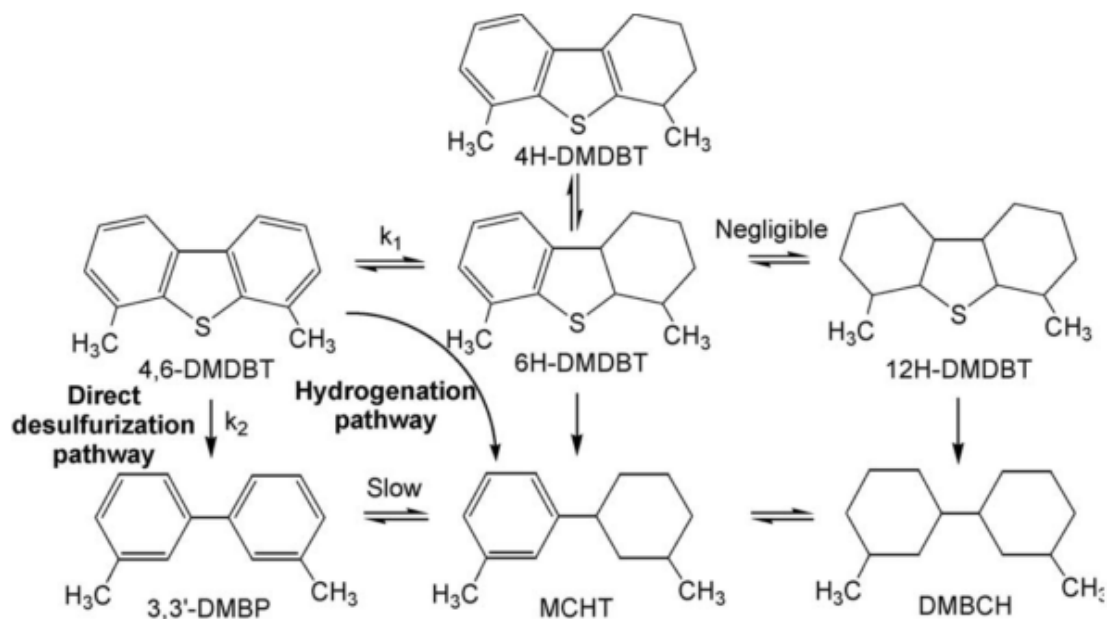


Figure II.9: Reaction pathways for the HDS of 4,6-DMDBT (from [34]).

The HYD pathway is the main route for the HDS of 4,6-DMDBT due to the steric hindrance induced by the methyl groups located in β -positions of the S-atom [8,35]. The nature of the steric hindrance has been and continues to be under debate. In one side is that steric hindrance retards the adsorption of 4,6-DMDBT on the catalyst surface, suggesting an end-on adsorption mode involving interactions between the sulfur atom and the active sites [35–37]. In other side, steric hindrance slows down the surface C-S bond scission, suggesting a side-on adsorption mode involving the π -electrons of the aromatic ring [31,38–40]. It has also been reported that the steric hindrance could reduce the rate of oxidative addition of the C-S bond on catalytic sites [41] or could retard the adsorption of dehydrogenated intermediates [31].

II.2. Hydrodesulfurization catalysts

II.2.1. Common catalysts used in HDS

The origin of hydrotreating processes goes back to the 1930s when German researchers from BASF developed catalysts for cracking and hydrogenation processes [42]. It was known that under catalytic conditions required for industrial hydrotreating, it was particles of MoS_2 (or WS_2) promoted by either cobalt or nickel and dispersed on a support material which were responsible for the removal of sulfur [43,44]. Industrial applications of such catalysts were already reported in 1943 [45].

Usually, catalysts contained 1-4 wt.% of Co (Ni) and 8-16 wt.% of Mo (W) and typical supports are alumina, silica-alumina, silica or zeolites, having surface areas of $100\text{-}300\text{ m}^2\cdot\text{g}^{-1}$. Catalysts based on CoMo have shown to be excellent for HDS but less active for HDN and hydrogenation of aromatics, whereas catalysts based on NiMo are more active in HDN and hydrogenation [46].

These last decades, numerous efforts have been done to understand the promoting effect of cobalt (or nickel) on the HDS activity of MoS_2 and to obtain a complete description of the active sites where the catalytic reaction takes place. These last decades, several structural models have been proposed and some of them are presented hereafter.

II.2.2. Active phase in HDS catalysts

II.2.2.a. Unpromoted catalysts: case of MoS_2

The active phase of the catalyst is generated by sulfidation of the oxide catalyst precursor [47,48] and consists of molybdenum disulfide layers. Typically, from one to five layers are stacked together and bonded by van der Waals (VdW) forces. These layers possess a hexagonal geometry and each MoS_2 particle consists of a layer of molybdenum atoms between two layers of sulfur atoms as presented in Figure II.10.

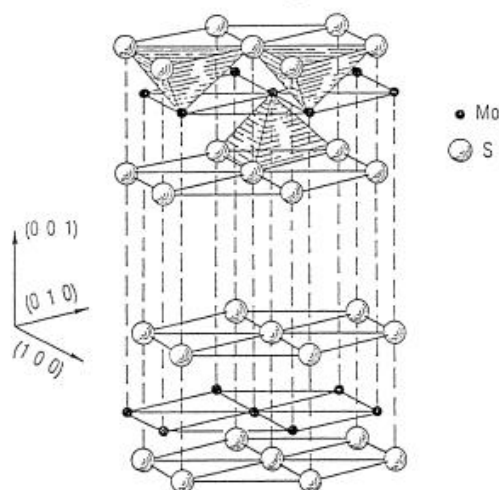


Figure II.10: MoS_2 hexagonal structure (from [49]).

Each molybdenum atom is surrounded by six sulfur atoms coordinated in a trigonal prismatic structure [50]. Two different types of planes can be distinguished in a MoS_2 particle: a basal-plane and an edge-plane where the active sites are located. The importance of “edges and corners” sites

was first reported by Voorhoeve et al. [51] and Farragher et al. [52] and the importance of sulfur vacancies as catalytic sites is now well accepted [53,54]. As the sulfur atoms present in the basal plane are more difficult to be removed than these present at edges and corners, sulfur vacancies occur at these sites and thus the catalytic reaction. This variation of catalytic activity against to the position of Mo atoms, has permit to Kasztelan et al. [50] the development of a geometrical model based on a single layer. When the size of the single layer MoS_2 increases, the ratio between Mo atoms present in basal and edge planes is modified. The crystallite size of MoS_2 particles is therefore important to have the higher catalytic sites. Figure II.11 shows that the proportion of edge sites is related to the morphology of the MoS_2 particle and that the evolution of the slab size modifies the number of edge Mo atoms and this evolution is dependent on the morphology of the slabs.

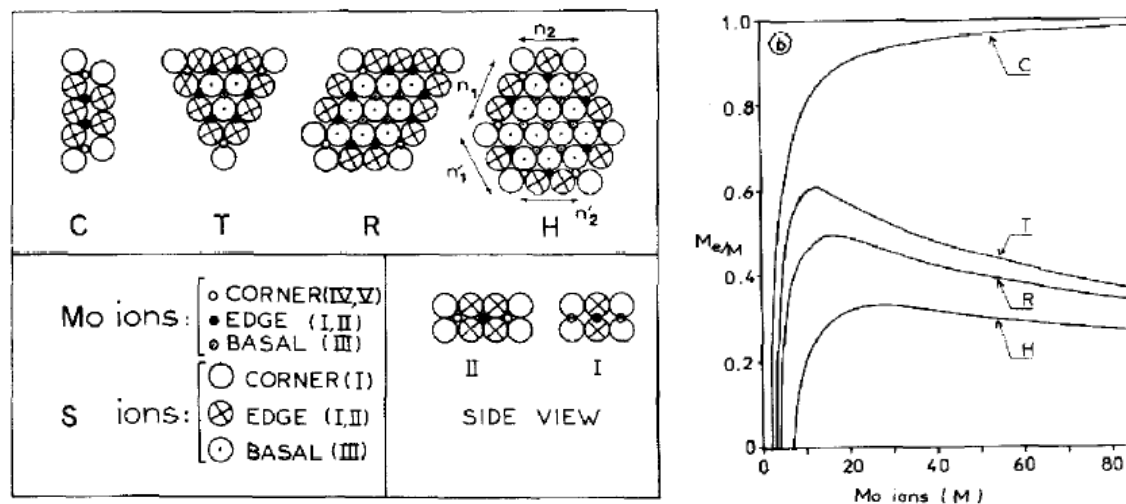


Figure II.11: Top view of the different symmetrical MoS_2 single slab with the specification of the different types of ions (left) and evolution of the number of edge Mo atoms versus the slab size M for the different symmetrical MoS_2 single slab (right). C: chain, T: triangle, R: rhombohedron and H: hexagon. From [50].

Later, Daage and Chianelli [54] have proposed a model for a bulk catalyst containing multi-layers of MoS_2 . This model is called “rim-edge model”. In this model (Figure II.12), two different types of catalytic sites can be found: edge sites located in all layers and rim sites located at the top and at the down of particles.

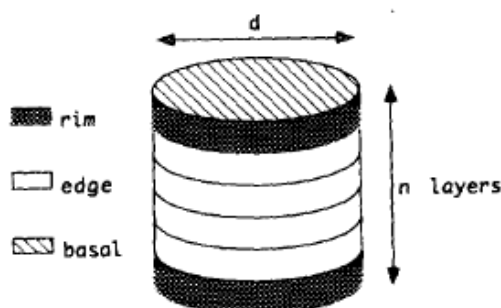


Figure II.12: Rim-edge model of a MoS_2 particle [54].

The relative concentration of each site depends on the morphology of MoS_2 and more precisely upon the stacking height of the layers. According to Daage and coworkers, the hydrodesulfurization (HDS) of dibenzothiophene (DBT) occurs via the sulfur hydrogenolysis (DDS) on both sites (edge-

and rim-sites) whereas the HDS of DBT via hydrogenation occurs only on rim sites. The selectivity of DDS/HYD can be tuned by varying the stacking of MoS₂ layers.

With the development of Density Functional Theory (DFT) calculations, a description of an unpromoted catalyst has been made. These particles possess two types of edges, metallic edges (denoted Mo-edge) and sulfided edges (denoted S-edge), as presented in Figure II.13.

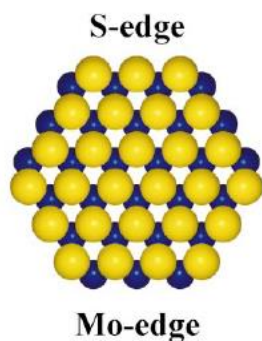


Figure II.13: Ball model of a hypothetical bulk truncated MoS₂ hexagon exposing both Mo- and S-edges. Mo: blue; S: yellow. Adapted from [55].

The stability of these different edge types and so the morphology of the particles depends on the experimental conditions. Indeed, it has been shown by Schweiger et al. [56], that the sulfidation conditions can give different morphologies to the particles. Under high sulfiding conditions, particles have a triangular morphology and all edges are metallic whereas under more reductive conditions, particles have a truncated triangular morphology and edges are composed of Mo-edges (majority) and S-edges [57]. These results have been confirmed by Lauritsen et al. [57], by combining DFT calculations with scanning tunnelling microscopy (STM). These two different structures are represented in Figure II.14.

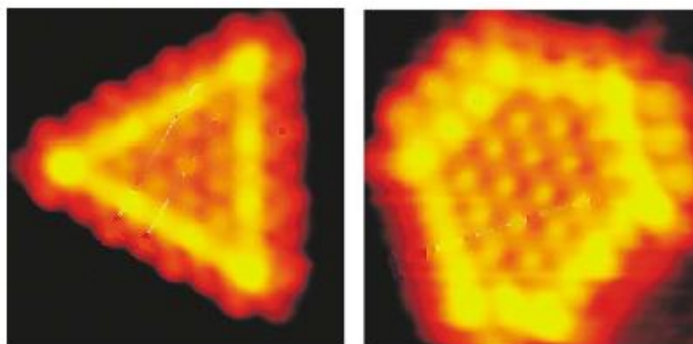


Figure II.14: Atom-resolved STM images of a triangular single-layer MoS₂ nanocluster synthesized under high sulfiding conditions (left) and under sulfo-reductive conditions (right). Adapted from [57].

Morphology and size of particles can be tuned by varying experimental parameters. As they are responsible for the number of active sites, the catalytic activity is thus strongly dependent on the experimental conditions employed for catalyst synthesis and activation.

The active phase of a HDS catalyst, composed of MoS₂ promoted by Co (or Ni), has been extensively studied these past decades and several structural models have been proposed and are presented in the following part.

II.2.2.b. Structural models of sulfided promoted HDS catalysts

Most accepted structural models have been developed in order to determine the location of the promoter in MoS₂ layers as well as its catalytic importance. These models are presented in Figure II.15

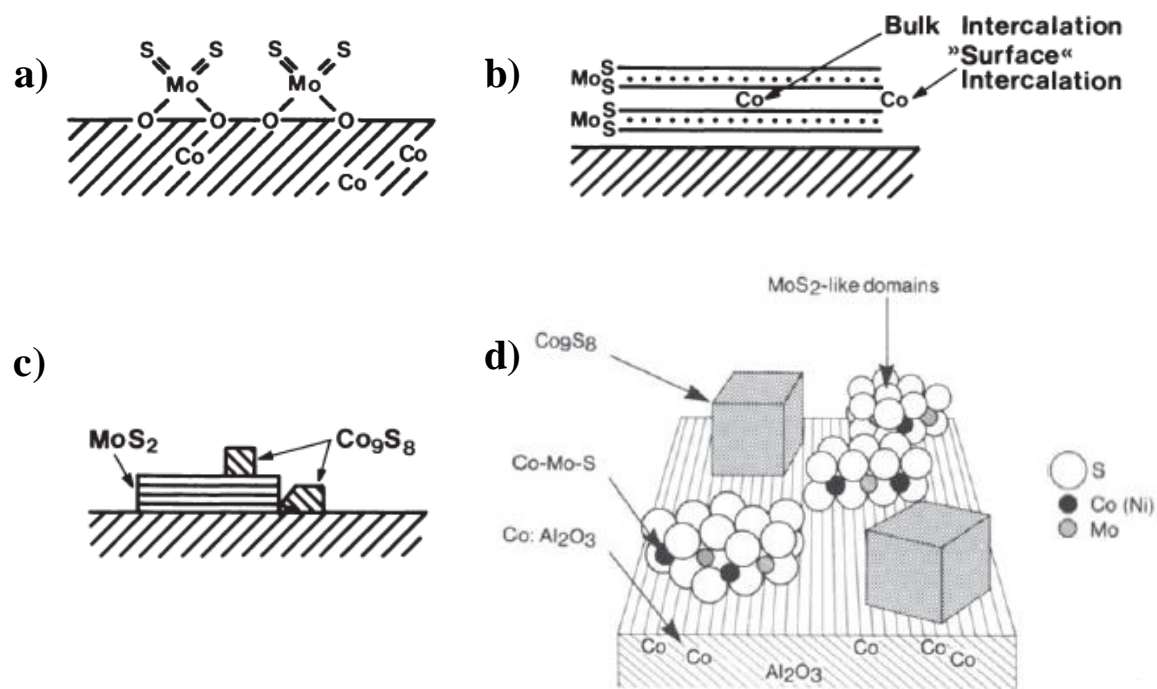


Figure II.15 : Most important structural models ; a) monolayer model [58], b) intercalation model [51,52,59], c) contact synergy model [60] and d) Co-Mo-S model [61].

Schuit et al. have detailed the first model of the structure of CoMo/Al₂O₃ catalyst, known as monolayer model [58,62–64] (Figure II.15.a). In this model, molybdenum species are assumed to be bonded to the surface of alumina in the calcined state to form a monolayer. Surface OH groups of alumina interact with Mo to form oxygen bridges [65]. On the top of the monolayer, O²⁻ ions compensate the incorporation of Mo⁶⁺ ions. Cobalt was assumed to be in tetrahedral positions in the surface of alumina by replacing Al³⁺ ions. It has been suggested that the insertion of cobalt in replacement of aluminium cations in the surface layer adjacent to the monolayer increase the stability of the latter, leading to the promotional effect of cobalt. Upon sulfiding O²⁻ ions are replaced by S²⁻ ions in the layer located on the top of the monolayer. Due to the larger size of S²⁻ ions, a maximum of one atom of sulfur per two atoms of oxygen may be incorporated. Under conditions of catalysis, the presence of hydrogen leads to the removal of some of S²⁻ ions, resulting to the reduction of adjacent molybdenum ions to Mo³⁺. These sites were believed to be catalytically active in HDS.

Another model proposed and developed by Voorhoeve and Stuiver [51,59] is known as intercalation model (Figure II.15.b). They proposed that the catalyst consists of MoS₂ slabs on the surface of alumina. Each one containing Mo atoms sandwiched between two hexagonal, close-packed planes of sulfur atoms and promoter's atoms occupy octahedral positions between the slabs. Later, it has been shown by Farragher and Cossee [52,66] that the intercalation of Co in ideal crystals of MoS₂ is energetically not possible [67] and a modified model known as "pseudo-intercalation" has been

proposed. In this model, it is assumed that Co atoms are located on the edge surfaces of the lattice of MoS_2 . These models assume the presence of three dimensional structures of MoS_2 to intercalate promoter's atom.

The model, known as contact synergy model (Figure II.15.c), which has been proposed by Delmon et al. [68–71] assumes that Mo is present as MoS_2 . In this model, the existence of two distinct phases on the surface of the catalyst has been proposed. When Co_9S_8 is present close to the MoS_2 slabs, the activity of the catalyst increases. This contact leads to a spill-over of hydrogen from Co_9S_8 to MoS_2 [60,72]. Hydrogen would thus promote the creation of vacancies on the surface of MoS_2 and will increase the number of active sites for hydrotreatment reactions.

The advances in characterization of catalysts and the use of *in situ* characterization techniques enable Topsøe and coworkers to provide a detailed structural description of CoMo catalysts [73–79] and known as Co-Mo-S model (Figure II.15.d). It has been shown that the CoMoS phase consists in MoS_2 structures with the promoter atoms located at the edges in five-fold coordinated sites (tetragonal pyramidal-like geometry) at the $(10\bar{1}0)$ edges planes of MoS_2 . As depicted in Figure II.15.d, different species are also present on the surface of the support, as Co_9S_8 and Co in the alumina lattice.

Depending on the conditions of preparation of the catalyst, single and multiple slab Co-Mo-S structures have been observed. The single-slab structure, called Type-I Co-Mo-S, where the phase interacts strongly with the support through probably Mo-O-Al linkages located at the edges. The multiple slab structure, called Type-II Co-Mo-S [80–82], where interactions with the support are weak. It has been shown by Topsøe et al. [81] that the sulfidation temperature are in part responsible of the presence of Type-I and Type-II structures. Type-II structures are formed at higher sulfidation temperature than Type-I.

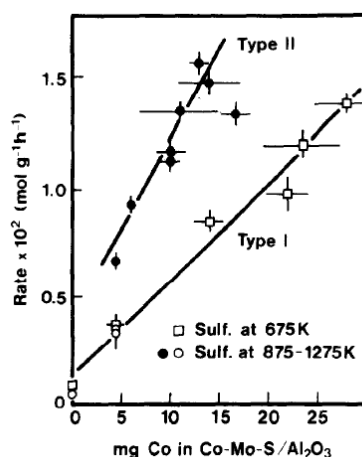


Figure II.16: HDS activity as function of Co content and sulfidation temperature [81].

Figure II.16 shows the difference of activity in the HDS of thiophene using a CoMo/Al₂O₃ catalyst as function of the Co content and the sulfidation temperature.

The Co-Mo-S model is the most favoured model compared to the others due to its basis using *in situ* characterizations and one of its advantage is the possibility to link quantitatively the promotion to the measured amount of Co atoms in the Co-Mo-S phase.

II.2.3. Typical synthesis of a HDS catalyst

As mentioned previously, HDS catalysts are based on molybdenum sulfide promoted by cobalt and dispersed onto a support, generally alumina. The different steps in the preparation of a HDS catalyst are presented in Figure II.17 and can be divided into three major steps: the impregnation and diffusion of metallic precursors into the pores of the support, the thermal treatment to precipitate species and to remove undesirables counter ions and the activation of catalyst by sulfidation.

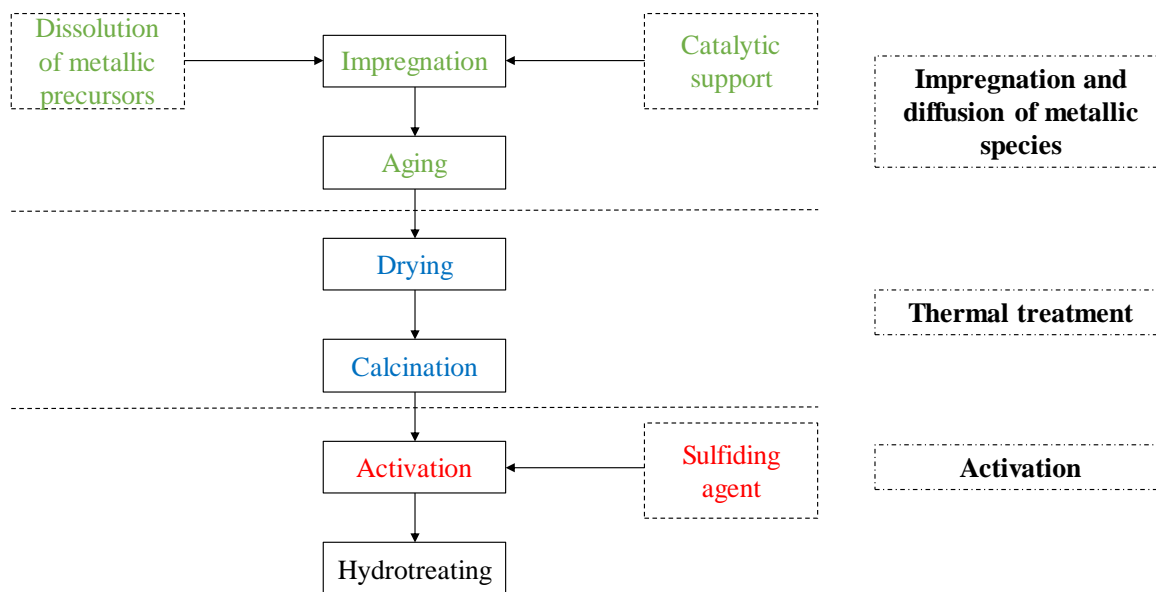
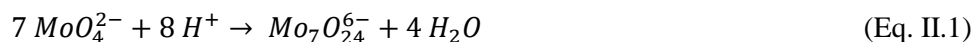


Figure II.17: Steps involved in the preparation of HDS catalysts.

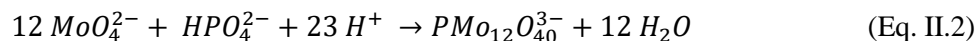
Each step involved in the preparation of HDS catalysts has its limitations and will influence the resulting activity of the catalyst. This part is presented from common molybdenum precursors to the activation of the catalyst and includes all intermediate steps.

A commonly employed molybdenum precursor for the synthesis of a CoMo/Al₂O₃ precursor catalyst is the ammonium heptamolybdate (NH₄)₆Mo₇O₂₄ [83–85]. When dissolved in aqueous solution, oxo-molybdenum species are influenced by the pH [86,87]. At basic pH, monomeric species [MoO₄²⁻] are the majority, whereas at acidic pH, polymeric species are present. Various polymolybdates are thus possible by tuning the pH of the impregnation solution. When a heteroatom, as phosphorus or silicon atom, is added to a molybdenum solution, the formation of polyoxometalate (or polyanion) compounds is observed. They are a specific class of compounds where the chemistry involved lies between coordination chemistry and solid state chemistry. These polyanions consist of an assembly of oxygen polyhedra obtained by sharing one or more oxo- (or hydroxo-) ligands. These polyhedrals are joined by their corners, edges or faces. Heteropolyanions (HPA) contain at least two different metals and can possess numerous different structure, the most widely studied being the heteropolyanion with a Keggin structure. The use of HPA in catalysis has increased these past years [88] due to the ability of these compounds to act as acid catalysts as well as redox catalysts. Another advantage of the use of heteropoly-compounds is the possibility of cobalt atoms to be close to the molybdenum atoms directly from the starting compound. This proximity has already shown interesting results in improving catalyst performances [89]. These advantages make HPA compounds appropriate starting materials for heterogeneous catalysts [90–95].

Isopolyanions are formed by condensation of oxoanions (MO_4^{n-}) which occurs by acidification of the solution, as presented in Eq. II.1.



When another oxoanion is present in solution (for example PO_4^{3-}), the transition metal atoms join together around this oxoanion and after polycondensation form an heteropolyanion according to Eq. II.2.



Several types of heteropolyanion structure can be obtained and most studied HPA structures are detailed hereafter.:

- HPA with a Keggin structure, case of phosphomolybdic acid

Polyoxometalates were first reported by Berzelius in 1826 [96] but the first determination of the structure has been done by Keggin in 1934 [97]. This HPA consists of the arrangement of MoO_6 octahedra around a central PO_4 tetrahedron. Several arrangements are possible having the same $\text{P/Mo} = 1/12$ ratio and various isomers formed by the rotation of 60° of a Mo_3O_{13} group can be isolated (see Figure II.18 (left)). A representation of the structure of a α -isomer HPA is shown in Figure II.18 (right) with the different oxygens.

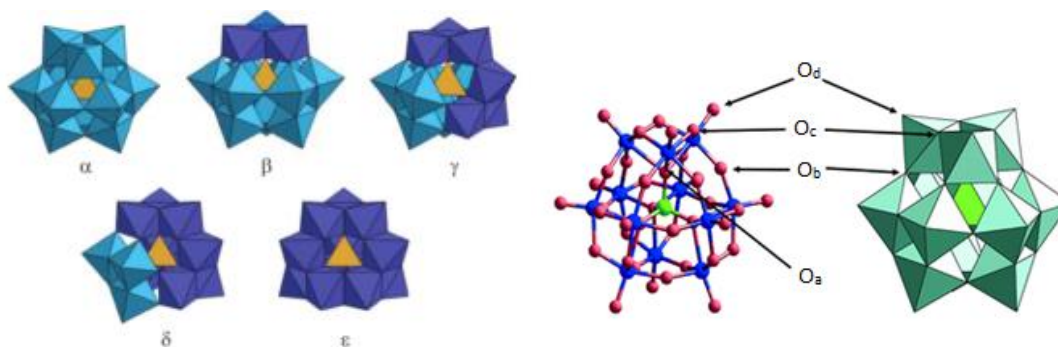


Figure II.18: Left: representations of the different rotational isomers of the Keggin structure (from [98]). Right: representation of the $\text{H}_3\text{PMo}_{12}\text{O}_{40}$ heteropolyanion with a Keggin structure adapted from [99].

The 12 MoO_6 octahedra are connected by shared edges to form trimetallic Mo_3O_{13} groups. In blue are Mo atoms, in green is the P atom and in red are the O atoms. Oxygen atoms present in the Keggin structure are not equivalent and four different types can be identified:

- 12 oxygen atoms, denoted O_d , which are linked to a single Mo atom,
- 12 oxygen atoms, denoted O_c , which are connecting to two MoO_6 octahedra inside a trimetallic M_3O_{13} group,
- 12 oxygen atoms, denoted O_b , which are connecting two trimetallic groups,
- 4 oxygen atoms, denoted O_a , which are common to PO_4 tetrahedron and to the three octahedral of a single trimetallic group.

Lacunary structures, where one or more Mo sites are vacant, can also be isolated. These vacancies could be filled by one or more transition metals to form substituted heteropolyanions with a Keggin structure [91,100,101].

- HPA with an Anderson structure

This structure, which was first proposed by Anderson in 1937 [102], consists of six MO_6 octahedra around a central XO_6 heteroatom octahedron in a single plane. A representation of an Anderson-type HPA structure is shown in Figure II.19. This formation of this type of HPA is often observed during the preparation of HDS catalyst from ammonium heptamolybdate, where molybdenum oxoanions react with released aluminium ions to form $\text{AlMo}_6\text{O}_{24}\text{H}_6^{3-}$ (AlMo_6) [103,104]



Figure II.19: Representation of an Anderson-type HPA (adapted from [98]).

Several other types of heteropolyanion structures can be found, such as Wells-Dawson and Strandberg structures [98,105], but are less employed for the preparation HDS catalysts and will not be described in this part.

- Deposition and diffusion of metallic precursors by impregnation and ageing

Typically, in a laboratory scale, metal precursors employed are AHM and HPA. Before their impregnation into the support, they are dissolved into water to form the so called “solution of impregnation”. Water is generally used due to its low cost, availability and to the fact that no unwanted elements are remaining after drying. This solution of impregnation is then impregnate in a support [106,107]. Two mains types of impregnation are usually employed. The first type of impregnation is an impregnation in excess (or equilibrium impregnation) where the volume of solution for the impregnation is much larger than the total porous volume of the support used. In this case, species diffuse into the pores of the support to reach a thermodynamic equilibrium. The content of metal species deposit onto the support is related to the properties of the support and to the concentration of species into the solution of impregnation, a controlled of the content of metallic species is therefore unpredictable. This technique implies a large quantity of solvent to be removed, which is a supplement cost for its use in industrial scale.

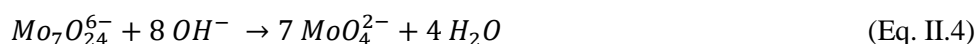
The second type of impregnation is an incipient wetness impregnation (or dry impregnation). In this case, the volume to be impregnate is equal to the porous volume of the support. This second technique allows the use of the total metal precursors introduced in the impregnation solution. However, the final loading of metal on the support will depend of the solubility of the precursors in the solvent. Sometimes, several dry impregnations can be made to increase the final loading of metals. This method is the most frequently used industrially due to its control over the deposited content, the saving of solvent and the easily removing of solvent by drying compared to an impregnation in excess.

During impregnation, several physico-chemical phenomena occur: diffusion into the pores of the support, acid-base reactions between metallic species and the surface of the support, adsorption of species, partial dissolution of the support and so on [108].

For example, in the preparation of alumina-supported HDS catalyst with ammonium heptamolybdate, the change of molybdenum species occurs during the deposition onto the support as a function of the molybdenum content. $\text{Mo}_7\text{O}_{24}^{6-}$ isopolyanions are stable in acidic medium whereas MoO_4^{2-} is stable at low pH. When in contact with the support, acid-base reactions take place due to the OH surface groups present on the surface of the alumina as presented in Eq. II.3.

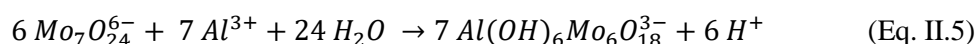


The pH of the solution will rise to the Zero Charge Point (ZCP) of the support (for alumina around 8-9). This effect is called “buffer effect”. For low molybdenum content (typically less than 2 $\text{Mo}\cdot\text{nm}^{-2}$), stable species in acidic medium ($\text{Mo}_7\text{O}_{24}^{6-}$) will be decomposed into monomolybdate species (MoO_4^{2-}), stable in basic medium, according to Eq. II.4.



If the content of molybdenum present in solution is higher, the “buffer effect” does not longer take place and the pH tends to be acidic. Stable species in acidic medium $\text{Mo}_7\text{O}_{24}^{6-}$ are not decomposed and interact electrostatically with the support surface.

If the Mo content is higher, another effect appears. Indeed, the impregnation solution becomes more acidic and a dissolution of the alumina is observed. This dissolution leads to a release of aluminium ions which can react with the isopolyanions species to form an Anderson-type heteropolyanion [103,104] according to Eq. II.5.



This Anderson-type heteropolyanion can precipitate with NH_4^+ ions present in the solution to form a precipitate ($(\text{NH}_4)_3\text{AlMo}_6(\text{OH})_6\text{O}_{18}$) with a low solubility resulting of large crystallites on the surface of the support after drying. All these species have different features in Raman spectroscopy and can be therefore characterized as it will be described in the Chapter IV.

When the support is impregnated, it is placed in a solvent saturated atmosphere and let to age for a defined time. During this phase, migration of species into the pores of the support is observed. This diffusion of species can be observed using Raman spectroscopy in order to determine the time necessary to obtain a good distribution of species into the pores and the whole surface of the support [109,110]. The maturation time is related to the interactions between anions species and the support. For example, if the pH of the solution is larger than the PZC of the support, the interactions between anions and the support will be diminished and diffusion will be fast. However, weak interaction between the metal and the support could lead to agglomeration of metal oxides during drying. Many parameters have to take in account to obtain a well dispersed oxides onto the support.

- Thermal treatment

After a period of maturation, the impregnated support is dried. During this step, the evaporation of the solvent is leading to the precipitation of species when the saturation limits are reached. In addition to physico-chemical phenomena, thermal phenomena are also involved during this step. Experimental conditions of the thermal treatment are therefore determinant for a good dispersion of species. If typically, the solvent is removed by evaporation, it is also possible to remove it by using another fluid (e.g. supercritical fluid).

The second thermal treatment is the calcination step. However, this step is not necessary and catalyst can be directly activated from its dried state. During the calcination, counter ions present

(NO_3^- and NH_4^+) on the surface will be removed and converted into their oxide forms and molybdenum and cobalt species are converted into their respective oxides MoO_3 and Co_3O_4 . Several other species can be found at the surface of the support after calcination, such as species in strong interaction with the support (CoAl_2O_4) or a crystalline phase of CoMoO_4 . These compounds having a negative effect on catalytic activity. The presence of aluminium molybdate ($\text{Al}_2(\text{MoO}_4)_3$) after calcination under dry air is due to the formation of AlMo_6 during the impregnation and aging steps. This latter specie can be reformed if the aluminium molybdate is rehydrated and had to be avoided during the preparation of catalysts because this oxide phase leads to species resistant to sulfidation (large clusters of MoO_3 and/or unsupported $\text{Al}_2(\text{MoO}_4)_3$).

- Activation by sulfidation

To be active in HDS, previously oxide catalyst precursor formed has to be activated. For that, the dried or calcined catalyst is placed under a sulfide reducing atmosphere at temperatures around 300-500°C. During this step, oxygen atoms are replaced by sulfur atoms and molybdenum goes from a +VI oxidation state to a +IV oxidation state.

Sulfidation can either be done in gas phase (using $\text{H}_2\text{S}/\text{H}_2$ mixtures) or in liquid phase (using liquid feedstock/ H_2) and sulfidation can be done *in situ* (catalyst introduced in the HDS unit under its oxide form and sulfided before the reaction) or *ex situ* (sulfidation is carried out before the introduction of the catalyst into the HDS unit).

HDS catalysts must be more and more active and having a long-life time. Commonly employed method to prepare catalysts presented before have limitations. Although this method is simple to perform at industrial scale, it is sometimes difficult to obtain a well-dispersed phase of small MoS_2 crystallites onto the support. The presence of undesirable species or large clusters entrains a loss of metals and reduces the promotion of the active phase resulting in a low activity. Moreover, looking at all steps to perform for the preparation of HDS catalysts, a long time is necessary as well as the use of high temperatures. The conventional method is consumer of time and energy. In an effort to tackle these various limitations, numerous alternative methods have been proposed and most relevant are presented hereafter.

II.2.4. Alternatives methods for the synthesis of HDS catalysts

Alternatives methods can be related to each step of the preparation of HDS catalysts, from the metallic precursors to the addition of an agent to enhance sulfidation, with the possibility to play on various conditions: metallic precursors, addition of additives, catalyst preparation methods or the type of support.

- Uses of modified heteropoly-compounds as precursors

One of the common method for the preparation of a wide range of heteropolyanions (HPAs) is the method described by Tsigdinos [111]. Spojakina and coworkers [112] were the first to show that catalyst prepared from a nickel salt of Keggin-type HPA supported on alumina can lead to an active catalyst in thiophene hydrodesulfurization as well as a catalyst prepared by using conventional precursors and having the same metal content. They found that after impregnation onto a titania support, the HPA structure was conserved whereas on alumina, the formation of the Anderson HPA $\text{AlMo}_6\text{O}_{24}\text{H}_6^{3-}$ was observed for high Mo content [113].

Griboval et al., have prepared several cobalt salts of phosphomolybdenum and silicomolybdenum acids and have compared them to a conventional HDS catalyst having the same metal content and containing or not phosphorus [114–117]. Two types of cobalt salts have been prepared: $\text{Co}_{3/2}\text{PMo}_{12}\text{O}_{40}$ and $\text{Co}_{7/2}\text{PMo}_{12}\text{O}_{40}$. In both cases, cobalt acts as counterion to the HPA ion and reduced ion. This method allows the introduction of metals and phosphorus in the same time and to avoid the presence of nitrate and ammonium counterions which can have a negative effect on the dispersion of species (formation of AlMo_6 precipitate). They show that during impregnation the structure of the reduced HPA salt is conserved whereas the structure of the unreduced salt is broken down. This difference is due to the stability of the salts in a different range of pH. The unreduced salt is only stable in acidic medium, whereas the reduced salt is stable up to a pH of 7. To compare these catalysts, they used two reference preparations: one based on ammonium heptamolybdate (AHM) and cobalt nitrate and the other one based on molybdenum oxide, cobalt carbonate and phosphoric acid. Results in thiophene conversion show that the reduced catalyst has the higher activity in thiophene conversion. The strong interaction between the promoter and the HPA may improve the decoration of MoS_2 slabs by Co atoms. An improvement in thiophene conversion has also been done by using a HPA with cobalt replacing one Mo atom in the structure ($\text{PCoMo}_{11}\text{O}_{40}\text{H}^{6-}$) [115].

One of the main drawback of using Keggin-type heteropolyanion is that they have a limited Co/Mo ratio. In order to increase this Co/Mo ratio and to avoid the presence of counterions (NH_4^+ , NO_3^-), several Anderson-type HPAs have been synthesized and tested in HDS [118–120]. Lamonier et al. [120,121], have shown that for a catalyst based on $\text{Co}_3(\text{Co}_2\text{Mo}_{10}\text{O}_{38}\text{H}_4)$ on alumina compared to a reference catalyst containing the same amount of metals, the thiophene conversion is increased by 50%. Also on this point, this increase of conversion is reported to be due to the close contact of the promoter and the molybdenum and the absence of negative counterions.

The use of heteropolyanions for the synthesis of HDS catalysts has shown their efficiency in improving the activity. The most used HPAs being the Keggin-type, it has been shown that the most active is those containing a cobalt atom in the structure. As the ratio Co/Mo is low when using this type of HPA, the development for the synthesis of new HPAs compounds with different structure (Anderson, Strandberg) has permitted the introduction of a higher cobalt content. The increase of efficiency of these catalysts has been attributed to the proximity of cobalt and molybdenum atoms in the oxide precursor, leading to an easier decoration of MoS_2 slabs by Co atoms. Moreover, the absence of counterions, such as NH_4^+ or NO_3^- , permits also a better dispersion of the oxide onto the surface of alumina.

- The use of organic additives

The addition of organic additives modifies the physico-chemical properties of the catalyst during its preparation. Additive agents can be introduced at all stages of the preparation of the catalyst:

- During the synthesis of the support, where the additives permit to control the growth of alumina particles,
- On the support, in order to modify the interactions between the metallic precursors and the hydroxyl groups of the support. They improve the dispersion of species and can avoid the precipitation of negative species (such as AlMo_6),
- With metallic precursors to act as a complexing and/or solvating agent. It helps to the dispersion of metals by increasing the solubility of species or the formation of different species,

- After the drying or calcination steps, to redistribute and modify species present on the surface of the support.

For example, glycol-type additives have shown to be able to redistribute Anderson-type HPA AlMo_6 [122,123]. Glycol acts via its solvating role where redissolution/redispersion phenomena are enhanced. During the activation of the catalyst, the number of promoted sites is improved compared to a catalyst prepared without additives. These higher numbers of active sites lead to an increase of the activity of the catalyst.

Additives can be introduced during all steps of the preparation of the catalyst to modify its physico-chemical properties. Two types of additives can be differentiated:

- Complexing additives, such as nitrilotriacetic acid (NTA) [124–127], ethylenediaminetetraacetic acid (EDTA) [128–131], organo-sulfided compounds and so on, play a key role during the sulfidation step by mainly increasing the promotion of the active phase,
- Non-complexing additives, such as diethylene glycol monobutyl ether (DEGBE) [132], diethylene glycol (DEG) [133] or triethylene glycol (TEG) [134–137] and so on, play a major role in changes of the precursor by dispersion, formation of new species. However, it only affects slightly the sulfidation step.

Introduction of organic additives permits the reduction of the interaction between the hydroxyl groups present on the surface of the support and the precursors. They can dissolve the unwanted compounds, such as AlMo_6 , and stabilise the surface of the support. They can also enhance the promotion of molybdenum by cobalt and disperse crystalline undesirable species such as CoMoO_4 or large MoO_3 clusters. Most of the time, the addition of organic additives leads to an increase of the activity of the HDS catalysts.

- The development of new catalyst preparation methods

Several other methods less conventional can be employed in order to increase the activity of HDS catalysts. Moon and coworkers [138–141] have used a sonochemical method to disperse MoS_2 crystallites, followed by a selective deposition of cobalt on the resulting crystallites. The obtained catalyst has shown two to three times higher activity than a conventional catalyst in DBT HDS and 4,6-DMDBT HDS. This technique to enhance dispersion has been employed by several other groups [142–144].

Okamoto et al. [145–149], have used a chemical vapor deposition (CVD) method to prepare HDS catalysts. For that, they first sulfided the oxide Mo precursor and then deposit cobalt on it by using CVD. To finish, the catalyst is resulfided to form the active phase. Thanks to this technique, they observed a better promotion of MoS_2 by Co atoms.

Another method for the preparation of the catalyst is the microwave hydrothermal method. Zhao et al. [150], have deposited WO_3 on alumina support by using this technique. It has been shown that this technique gives a high dispersion of tungsten and weak interaction between tungsten and alumina. This high dispersion is attributed to the rapid nucleation and inhibited growth of tungsten species. They also attributed this to the enhancement of the mobility of ions induced by microwave hydrothermal conditions. Moreover, the preparation time with this method is reduced to 15 min.

The use of ultrasonic spray pyrolysis for the synthesis of HDS catalysts has also been reported by Suslick et al.[151,152]. For that, they used a colloidal silica as template and ammonium thiomolybdate as Mo precursor. The solution is then ultrasonically nebulized into micro-droplets into a furnace where is flowed a gas. After evaporation of the solvent and decomposition of the precursors, a composite $\text{MoS}_2/\text{SiO}_2$ is obtained. The SiO_2 network can then be removed by acid treatment.

Moreover, the use of supercritical fluids has been reported by few research groups for the synthesis of HDS catalysts and their results are presented hereafter.

II.3. Conclusion about HDS catalysis

This part is a description of HDS chemistry. An overview of hydrotreating, reactions of HDS, catalyst commonly used in HDS and new alternative methods for the preparation of $\text{CoMoS}/\text{Al}_2\text{O}_3$ catalysts have been described.

Hydrotreatment processes are present in many stages of the refining process and are necessary to remove heteroatoms naturally present in crude oil. The use of crude oil having a high sulfur content as well as the more and more stringent regulations regarding sulfur content, imply a need of more and more active catalysts. These catalysts must allow the removal of refractory sulfur containing compounds such as DBT and 4,6-DMDBT.

Optimization of the dispersion of the oxometallic phase onto the support and the avoidance of species which are detrimental for the catalytic activity are key parameters to obtain an efficient HDS catalyst. Moreover, synthesis of HDS catalyst using conventional method requires a long-time and a non-negligible need of energy to perform thermal treatment. The use of new synthesis methods appears thus interesting to try to overcome these limitations.

The use of alternative method can also bring interesting features. For example, the use of supercritical carbon dioxide (scCO_2) for the synthesis of this kind of catalyst appears to be an interesting unconventional method. Indeed, the use of carbon dioxide under temperature and pressure allows the possibility of tuning many experimental parameters.

The next part is thus dedicated to the use of supercritical fluids for the preparation of catalytic materials.

III. Supercritical fluids route for the synthesis of HDS catalysts

This part deals with the few reported use of supercritical fluids to synthesize supported HDS catalysts. In a first part, an introduction about supercritical fluids (SCFs) is given and in a second part, some studies about the synthesis of materials and especially HDS catalysts are presented.

III.1. Introduction to SCFs

Each fluid being above its critical temperature (T_c) and its critical pressure (p_c) is said to be “supercritical”. This domain offers the possibility of a continuous change from the liquid phase to the gas phase, which presents physico-chemical properties (density, viscosity and diffusivity) intermediate between the gas and the liquid phases. Table II.1 shows the comparison of the physical properties of liquids, gas and SCFs.

Table II.1: Comparison of physical properties of liquids, gas and supercritical fluids (from [153] with data from [154]).

physical quantity	gas (ambient)	supercritical fluid (T_c, P_c)	liquid (ambient)
density ρ (kg m^{-3})	0.6–2	200–500	600–1600
dynamic viscosity η (mPa s)	0.01–0.3	0.01–0.03	0.2–3
kinematic viscosity ν^a ($10^6 \text{ m}^2 \text{ s}^{-1}$)	5–500	0.02–0.1	0.1–5
diffusion coefficient D ($10^6 \text{ m}^2 \text{ s}^{-1}$)	10–40	0.07	0.0002–0.002

^a Kinematic viscosity was estimated from dynamic viscosity and density, $\nu = \eta/\rho$.

These properties can be tuned by varying temperature and pressure and made supercritical fluids interesting candidates for materials synthesis, recycling, extraction and so on [155]. A supercritical fluid can act as solvent, anti-solvent and reagent depending on the process used [156].

III.2. Case of supercritical carbon dioxide (scCO₂)

Supercritical carbon dioxide (scCO₂) is a good candidate to be used as supercritical fluid. Supercritical CO₂ is, indeed, non-polluting, abundant, inexpensive, non-flammable and has easy reachable critical coordinates ($T_c = 31^\circ\text{C}$; $p_c = 7.38 \text{ MPa}$). That is why, it is used in a wide range of applications and different processes. The phase diagram of carbon dioxide is presented in Figure II.20.

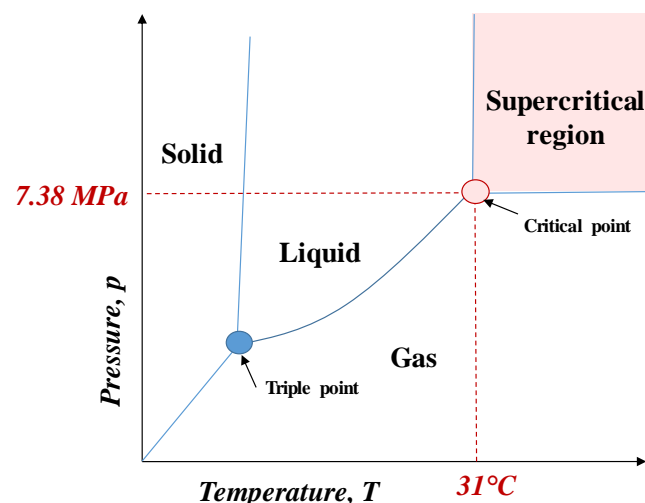
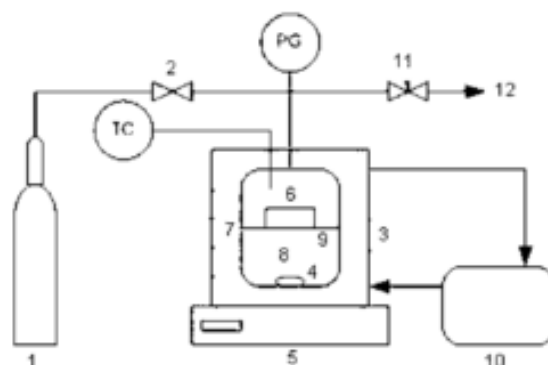


Figure II.20: Phase diagram of carbon dioxide.

As for other SCFs, mass transfer rates are considerably faster than in a liquid solvent. It permits to scCO_2 to easily penetrate inside porous structures. The scCO_2 solubilizes non-polar molecules but can also solubilize polar compounds to a certain extent since scCO_2 has a large quadrupole moment. The addition of co-solvent (such as ethanol, methanol and so on) permits to increase the solvating power of scCO_2 for polar solutes. In the next part, a summary of the different processes using scCO_2 to prepare HDS catalysts is proposed.

III.3. Preparation of HDS catalysts using SCF

Only few studies exist on the preparation of HDS catalysts using supercritical carbon dioxide. Alibouri et al. [157,158] have prepared NiMo catalysts supported on Al-HMS (Al-hexagonal mesoporous silica) using the supercritical deposition method. For that, they first prepared the Al-HMS support and then used molybdenum hexacarbonyl ($\text{Mo}(\text{CO})_6$) and nickel nitrate ($\text{Ni}(\text{NO}_3)_2 \cdot 6\text{H}_2\text{O}$) as metal precursors. $\text{Mo}(\text{CO})_6$ has been chosen for its solubility in scCO_2 , but as the promoter source precursor $\text{Ni}(\text{NO}_3)_2 \cdot 6\text{H}_2\text{O}$ was insoluble in scCO_2 , they have chosen to add methanol as co-solvent. To perform the impregnation of the support with metal precursors, they used the experimental set-up represented in Figure II.21.

Figure II.21: Experimental set-up for scCO_2 deposition: (1) CO_2 tank, (2) valve, (3) bath, (4) magnetic stirrer, (6) basket, (7) vessel, (8) solution, (9) screen, (10) circulating heater and cooler, (11) needle valve, (12) vent, from [157].

The support was placed in the basket (6) and the solution of methanol and metal precursors was placed in the high pressure vessel. The vessel was cooled at 10°C and charged with 6.5 MPa of CO₂. The temperature of the vessel was then increased to 80°C leading to an increase of the pressure. The operating conditions (80°C, 27.6 MPa) were maintained for a period of 24 h before depressurization and cooling. Then, they compared their catalyst prepared using supercritical fluid chemical deposition (SFCD) with a catalyst prepared by a conventional method.

They first observed that the structure of the support was remained using SFCD method compared to the conventional method. Secondly, they found a better dispersion of Ni and Mo for the catalyst synthesized by SFCD, using XRD measurements and oxygen chemisorptions. TPR measurements have shown a lower temperature of reducibility for the catalyst synthesized using SFCD compared to the conventional one.

Their catalysts were tested in HDS of DBT. They found a higher conversion in DBT at 330°C for the catalyst synthesized in scCO₂ compared to the conventional catalyst and a commercial catalyst despite of the higher activation energy of the catalyst synthesized with the SFCD method. Table II.2 presents the reaction rate constants for HDS of DBT, activation energies and frequency factors of these three tested catalysts.

Table II.2: Reaction rate constants (mol/g_{cat}.min.10⁵) for HDS of DBT (top) and activation energy and frequency factor (down).

catalyst	270 °C	290 °C	310 °C	330 °C
NiMo/Al-HMS (SDM)	0.58	0.80	1.40	3.65
NiMo/Al-HMS (CIM)	0.53	0.66	1.21	2.20
NiMo/Al ₂ O ₃ (commercial)	0.58	0.66	1.35	2.42

catalyst	k ₀ (mol/g cat. min)	E/R (°C)
NiMo/Al-HMS (SDM)	3.72 × 10 ⁷	9852
NiMo/Al-HMS (CIM)	9.74 × 10 ⁵	7902
NiMo/Al ₂ O ₃ (commercial)	1.64 × 10 ⁶	8158

Last interesting result they obtained, was a lower CHB/BP selectivity for the catalyst prepared in SCF compared to others, which means that DDS route was favoured. The preference for the DDS route is important to have a less consumption of hydrogen.

Alibouri and coworkers have also prepared CoMo on Al-HMS catalysts [159] by using the supercritical deposition method and found similarly results in terms of dispersion and enhancement of the activity.

By using Al₂O₃ as support, they also prepared HDS catalysts by supercritical deposition method [158]. They used the same set-up, characterizations and testing and conclude same results about dispersion and enhancement of the activity in HDS of DBT.

In conclusion of the work of Alibouri et al., the supercritical deposition method is an interesting technique to improve the dispersion of species onto the surface of the support, which is mandatory in catalysis. However, due to the toxicity of molybdenum hexacarbonyl and the long time of the synthesis (24 h) made this process complexly to be implemented at an industrial scale.

Motos et al. (in the frame of a collaboration ICMCB/IFPEN) [160] have prepared nickel phosphide supported on silica HDS catalysts by using a scCO₂ assisted process. For that, they dissolved in distilled water, the required amounts of metals and performed a dry impregnation of the silica

support. After a period of ageing, the impregnated support was placed in a high pressure vessel and scCO_2 was injected into it. The injection of scCO_2 (60°C, 8.0 MPa) permits to favour dispersion and leads to a flash drying of the catalyst. An increase of the reactor temperature permits (300-400°C, 25.0 MPa) the thermal decomposition of precursors under scCO_2 atmosphere. Figure II.22 presents the catalyst preparation and the experimental set-up used for the preparation of these nickel phosphide supported on silica catalysts.

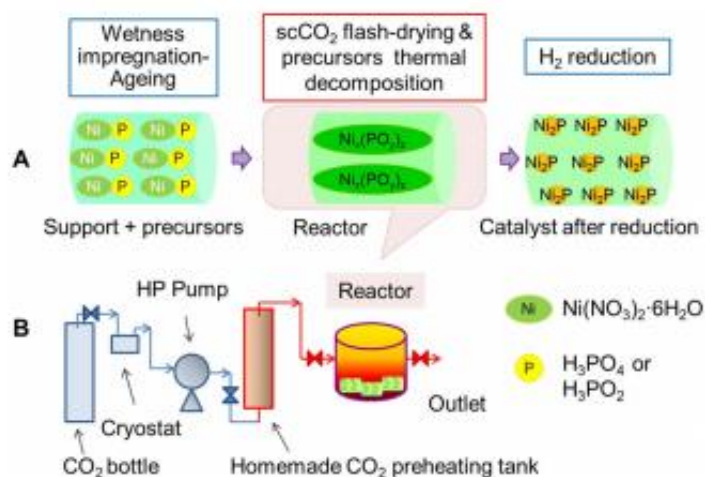


Figure II.22: A) Flow scheme of the catalyst preparation. B) Set-up of the experiment for the fast injection of scCO_2 (from [160]).

The fast injection of scCO_2 induces the precipitation of species into the silica pores by removing water (“flash precipitation”). This flash precipitation is due to the low solubility of scCO_2 in water and the low dielectric constant of scCO_2 compared to water ($\epsilon < 1.8$ for scCO_2 and $\epsilon < 78.5$ for water at ambient conditions). The obtained dry catalyst has then been reduced using H_2 prior to its testing in HDS of 4,6-DMDBT.

They found that the first-order rate constant k_{HDS} was much higher (10 times) by using a catalyst prepared in scCO_2 than for a catalyst prepared by a conventional technique. This higher first-order rate constant for the scCO_2 catalyst is due to the smaller Ni_2P particles with higher reducibility compared to the catalyst prepared with a conventional technique.

In conclusion of the study performed by Motos et al., using scCO_2 to prepare supported HDS catalysts is a very promising method and this method can be extended to a large range of materials. Moreover, using “flash precipitation” post impregnation method allows to work with conventional metal precursors and therefore avoid the use of harmful and expensive metal precursors, such as organo-complexes or metal carbonyls. This work was at the origin of this PhD project.

III.4. Conclusion

The use of supercritical carbon to prepare materials has been extensively studied. However, the synthesis of HDS catalysts using scCO_2 has received little attention. It appears thus interesting to use this abundant, inexpensive and with low critical coordinates molecule. The few investigations made in the synthesis of HDS catalysts with scCO_2 have shown promising results in terms of enhancement of the catalytic activity compared to catalysts prepared via conventional method. The ambition of this PhD project is to bring new features on the widely studied topic that is HDS.

IV. Conclusion and objectives of the PhD

Through this chapter, we have presented the environmental context of the presence of sulfur in crude oil and regulations linked to that. Regulations being more and more drastic to minimize our ecological footprint and low sulfur content crude oils being more and more rare, the development of more efficient catalysts is required. Sulfur is responsible of environmental issues such as acid rains but also a poison for catalysts during the refining of oil. Nowadays, every refinery possesses hydrotreatment processes to reduce amounts of undesirable heteroatoms naturally present in crude oil.

The need of cleaner fuels to meet these environmental regulations implies the removing of 99.9% of sulfur and especially the removing of the most refractory sulfur containing compounds, which are dibenzothiophene and alkylated dibenzothiophene.

Conventional catalysts are based on MoS₂ layers decorated at their edges with cobalt (or nickel) atoms and dispersed onto an alumina-type support. These catalysts are typically prepared by dry impregnation of metallic precursors followed by a maturation step. Once metallic species have migrated into pores of the support, a drying of the catalyst is performed to evaporate the remaining solvent. A calcination step can also occur where the counter ions associated to the metallic precursors are removed. After this stage an oxide phase dispersed onto the support is obtained. To have an activated catalyst, oxide precursor is sulfided in order to replace oxygen atoms by sulfur atoms and form the active phase CoMoS of the catalyst. A well-dispersed phase of nanocrystallites of CoMoS are therefore recommended to increase the activity of the catalyst as catalytic sites are related to the morphology and sizes of MoS₂ slabs. In worries of increasing the catalytic activity, numerous alternative methods have been studied. The use of new starting metallic precursors to enhance the promotion of the active phase or avoid compounds which are refractory to the sulfidation. For that, new heteropolycompounds have been synthesized having different promoter/metal ratios and structures. The addition of complexing and non-complexing additives has also widely studied as well as their effect on the redispersion of the oxometallic phase, their solvating roles and so on.

The use of new synthesis methods has also been presented with for example the synthesis of HDS catalysts by chemical vapor deposition, microwave hydrothermal or ultrasonic spray pyrolysis. For that, in this work, we proposed the use of a new process to synthesize HDS catalyst precursor using supercritical carbon dioxide.

The last part was dedicated to the presentation of supercritical fluids and their possibility of use to prepare HDS catalysts. Supercritical carbon dioxide possesses interesting properties which can bring benefits in the enhancement of the dispersion of the oxometallic phase but particularly to reduce synthesis time and energy required.

In this work, we use a different method to deposit Mo and Co particles onto an alumina support. Indeed, instead of using harmful or expensive compounds, such as metal carbonyls or metal complexes, we have chosen to use more conventional precursors: ammonium heptamolybdate, phosphomolybdic acid and cobalt nitrate. In order to avoid a long time of synthesis, we prefer the traditional incipient wetness impregnation followed by a supercritical carbon dioxide treatment. Playing on the co-solvent used (water, methanol, ethanol or n-propanol) and thus its affinity with scCO₂, it is possible to vary the reaction mechanism. If the impregnation solvent is water and when the scCO₂ is injected on the impregnated support, the water will be removed from the pores of the

support by the scCO₂ and will induce a “flash precipitation” of the metal precursors. Whereas, by using an alcohol as impregnating solvent, scCO₂ will expand the alcohol. A scCO₂ expanded fluid is then obtained and when the pressure of scCO₂ increases, the volume of the expanded fluid increases too, leading to the supersaturation of the impregnation solution and therefore to the precipitation of metal species.

This PhD project is so structured around four main objectives:

- Assessment of the criticality of metals contained in HDS catalysts,
- Investigations of chemical reactions occurring during the precipitation of oxometallic species,
- Understanding of the process of preparation of HDS catalysts using scCO₂,
- Catalytic performances of the synthesized catalysts.

The study and estimation of the criticality of metals contained in HDS catalysts, molybdenum and cobalt is the first objective. This survey was realized in collaboration with the University of Augsburg and the Fraunhofer Institute, both located in Germany. This permits to have a broader vision of the use of these metals. Results of this study can be found in the first chapter of this work.

The understanding of the chemistry which occurs during preparation of HDS catalyst precursors when using scCO₂ and the comparison with a conventional thermal treatment is the second objective. For that, the monitoring of the chemical reaction with *in situ* Raman experiments has been employed. Indeed, fast response of Raman spectroscopy allowed us to determine the most appropriate experimental parameters to use in the future synthesis of HDS catalyst precursors.

The third objective concerns the synthesis of HDS catalyst precursors in a reactor using scCO₂ to precipitate molybdenum and cobalt species onto the alumina support. During this work, several parameters were tested to investigate the effect of each one on the resulting HDS catalysts. Characterizations of oxometallic phases of HDS catalyst precursors permit to link experimental parameters employed with structural and chemical forms obtained. After sulfidation, catalysts were characterized and confronted with characterizations of the oxometallic phase.

The evaluation of the catalytic performances of synthesized samples is the last objective of this PhD project. For that, catalytic tests have been performed in the site of IFP Energies Nouvelles located in Solaize. Three model reactions were investigated: the hydrogenation of toluene to have a first screening of the catalytic performances. Then, for catalysts with the best activities, the HDS of dibenzothiophene and the HDS of 4,6-dimethyldibenzothiophene have been tested.

V. Bibliography

- [1] UNEP, Diesel Fuel Sulphur Levels: Global Status June 2015, 2015. http://www.unep.org/Transport/New/PCFV/pdf/Maps_Matrices/world/sulphur/MapWorldSulphur_June2015.pdf (accessed 09/14/2016).
- [2] W.W. Irion, O.S. Neuwirth, Oil Refining, in: Ullmann's Encycl. Ind. Chem., Wiley-VCH Verlag GmbH & Co. KGaA, Weinheim, Germany, 2000.
- [3] W.L. Leffler, Petroleum refining for the nontechnical person, 2nd Edition, PennWell Books, 1985.
- [4] M.S. Talmadge, R.M. Baldwin, M.J. Bidy, R.L. McCormick, G.T. Beckham, G.A. Ferguson, S. Czernik, K.A. Magrini-Bair, T.D. Foust, P.D. Metelski, C. Hetrick, M.R. Nimlos, A perspective on oxygenated species in the refinery integration of pyrolysis oil, *Green Chem.* 16 (2014) 407–453.
- [5] UOP, Refining Flow Scheme, <http://www.uop.com/refining-flowscheme> (accessed 07/13/2016).
- [6] Density and sulphur content of different crude oil, (2013). <http://www.eia.gov/todayinenergy/detail.cfm?id=7110>.
- [7] H. Schulz, W. Böhringer, F. Ousmanov, P. Waller, Refractory sulfur compounds in gas oils, *Fuel Process. Technol.* 61 (1999) 5–41.
- [8] M. Houalla, D.H. Broderick, A. V. Sapre, N.K. Nag, V.H.J. de Beer, B.C. Gates, H. Kwart, Hydrodesulfurization of methyl-substituted dibenzothiophenes catalyzed by sulfided Co-Mo/Al₂O₃, *J. Catal.* 61 (1980) 523–527.
- [9] D.H. Broderick, B.C. Gates, M. Houalla, N.K. Nag, A. V. Sapre, Hydrodesulfurization of dibenzothiophene catalyzed by sulfided CoO-MoO₃- γ -Al₂O₃: the reaction network, *AIChE J.* 24 (1980) 1015–1021.
- [10] C. Song, X. Ma, New design approaches to ultra-clean diesel fuels by deep desulfurization and deep dearomatization, *Appl. Catal. B Environ.* 41 (2003) 207–238.
- [11] X. Ma, L. Sun, C. Song, A new approach to deep desulfurization of gasoline, diesel fuel and jet fuel by selective adsorption for ultra-clean fuels and for fuel cell applications, *Catal. Today.* 77 (2002) 107–116.
- [12] N. Nag, Hydrodesulfurization of polycyclic aromatics catalyzed by sulfided CoO-MoO₃/ γ -Al₂O₃: The relative reactivities, *J. Catal.* 57 (1979) 509–512.
- [13] O. Weisser, S. Landa, Sulfide catalysts, their properties and applications, Pergamon, New York, 1973.
- [14] D.R. Kilanowski, H. Teeuwen, V.H.J. Debeer, B.C. Gates, G.C.A. Schuit, H. Kwart, Hydrodesulfurization of thiophene, benzothiophene, dibenzothiophene, and related compounds catalyzed by sulfided CoO-MoO₃- γ -Al₂O₃ - Low-pressure reactivity studies, *J. Catal.* 55 (1978) 129–137.

-
- [15] M. Houalla, D. Broderick, V.H.J. Debeer, B.C. Gates, H. Kwart, Hydrodesulfurization of dibenzothiophene and related compounds catalyzed by sulfided $\text{CoO-MoO}_3\text{-}\gamma\text{-Al}_2\text{O}_3$ - Effects of reactant structure on reactivity, *Abstr. Pap. Am. Chem. Soc.* 22 (1977) 941.
- [16] P.J. Owens, C.H. Amberg, Thiophene desulfurization by a microreactor technique, in: *Solide surfaces*, (1961) pp. 182–198.
- [17] A.E. Hargreaves, J.R.H. Ross, Investigation of the mechanism of the hydrodesulfurization of thiophene over sulfided $\text{Co-Mo-Al}_2\text{O}_3$ Catalysts .2. Effect of promotion by cobalt on the C-S bond cleavage and double-bond hydrogenation-dehydrogenation activities of tetrahydrothiophene and related compounds, *J. Catal.* 56 (1979) 363–376.
- [18] K. McCarty, G.L. Schrader, Deuterodesulfurization of thiophene: An investigation of the reaction mechanism, *J. Catal.* 103 (1987) 261–269
- [19] A.N. Startsev, V.A. Burmistrov, Y.I. Yermakov, Sulphide catalysts on silica as a support, *Appl. Catal.* 45 (1988) 191–207.
- [20] H. Topsøe, B.S. Clausen, F.E. Massoth, Hydrotreating catalysis, in: J.R. Anderson, M. Boudart (Eds.), *Catalysis*, Springer Berlin Heidelberg, Berlin, Heidelberg, 1996: pp. 1–269.
- [21] M.R. Blake, M. Eyre, R.B. Moyes, P.B. Wells, Catalysis by sulfides .2. Tetrahydrothiophene hydrodesulfurization catalyzed by powdered molybdenum-disulfide, *Bull. Des Soc. Chim. Belges.* 90 (1981) 1293–1299.
- [22] F. Daly, Hydrodesulfurization of benzothiophene over $\text{CoO-MoO}_3\text{-Al}_2\text{O}_3$ catalyst, *J. Catal.* 51 (1978) 221–228.
- [23] J. Devanneaux, J. Maurin, Hydrogenolysis and hydrogenation of thiophenic compounds on a $\text{Co-Mo-Al}_2\text{O}_3$ catalyst, *J. Catal.* 69 (1981) 202–205.
- [24] J. Devanneaux, J. Maurin, Hydrogenation and hydrogenolysis of thiophenic compounds: Correction and comments, *J. Catal.* 80 (1983) 491.
- [25] F. Ruetter, E. V Ludena, Molecular-orbital calculations of the hydrodesulfurization of thiophene Over a Mo-Co catalyst, *J. Catal.* 67 (1981).
- [26] J. Kraus, M. Zdrzil, Tetrahydrothiophene as intermediate in hydrodesulfurization of thiophene, *React. Kinet. Catal. Lett.* 6 (1977) 475–480.
- [27] P. Geneste, P. Amblard, M. Bonnet, P. Graffin, Hydrodesulfurization of oxidized sulfur-compounds in benzothiophene, methylbenzothiophene, and dibenzothiophene series over $\text{CoO-MoO}_3\text{-Al}_2\text{O}_3$ catalyst, *J. Catal.* 61 (1980) 115–127.
- [28] M. Zdrzil, The chemistry of the hydrodesulphurization process (Review), *Appl. Catal.* 4 (1982) 107–125.
- [29] H. Schulz, D. V Do, Fast and slow steps of hydrodesulfurization, *Bull. Des Soc. Chim. Belges.* 93 (1984) 645–651.

-
- [30] V. Vanrysselberghe, G.F. Froment, Hydrodesulfurization of dibenzothiophene on a CoMo/Al₂O₃ catalyst: reaction network and kinetics, *Ind. Eng. Chem. Res.* 35 (1996) 3311–3318.
- [31] F. Bataille, J.-L. Lemberon, P. Michaud, G. Pérot, M. Vrinat, M. Lemaire, E. Schulz, M. Breysse, S. Kasztelan, Alkyldibenzothiophenes hydrodesulfurization-promoter effect, reactivity, and reaction mechanism, *J. Catal.* 191 (2000) 409–422.
- [32] P. Michaud, J.L. Lemberon, G. Perot, Hydrodesulfurization of dibenzothiophene and 4,6-dimethyldibenzothiophene: Effect of an acid component on the activity of a sulfided NiMo on alumina catalyst, *Appl. Catal. A-General.* 169 (1998) 343–353.
- [33] A. V Sapre, D.H. Broderick, D. Fraenkel, B.C. Gates, N.K. Nag, Hydrodesulfurization of benzo[b]naphtho[2,3-d]thiophene catalyzed by sulfided CoO-MoO₃-γ-Al₂O₃ - the reaction network, *Aiche J.* 26 (1980) 690–694.
- [34] S.T. Oyama, T. Gott, H. Zhao, Y.-K. Lee, Transition metal phosphide hydroprocessing catalysts: A review, *Catal. Today.* 143 (2009) 94–107.
- [35] M. Houalla, N.K. Nag, A. V Sapre, D.H. Broderick, B.C. Gates, Hydrodesulfurization of dibenzothiophene catalyzed by sulfided CoO-MoO₃-Al₂O₃: The reaction network, *AIChE J.* 24 (1978) 1015–1021.
- [36] M. Houalla, D.H. Broderick, A. V Sapre, N.K. Nag, V.H.J.D. Beer, B.C. Gates, H. Kwart, Hydrodesulfurization of methyl-substituted dibenzothiophenes catalyzed by sulfided Co-Mo-γ-Al₂O₃, *J. Catal.* 61 (1980) 523–527.
- [37] X. Ma, K. Sakanishi, T. Isoda, I. Mochida, Comparison of sulfided CoMo/Al₂O₃ and NiMo/Al₂O₃ catalysts in deep hydrodesulfurization of gas oil fractions, *Abstr. Pap. Am. Chem. Soc.* 208 (1994) 83.
- [38] T. Kabe, A. Ishihara, Q. Zhang, Deep desulfurization of light oil .2. Hydrodesulfurization of dibenzothiophene, 4-methyldibenzothiophene and 4,6-dimethyldibenzothiophene, *Appl. Catal. A-General.* 97 (1993) L1--L9.
- [39] V. Meille, E. Schulz, M. Lemaire, M. Vrinat, Hydrodesulfurization of alkyldibenzothiophenes over a NiMo/Al₂O₃ catalyst: kinetics and mechanism, *J. Catal.* 170 (1997) 29–36.
- [40] J. Mijoin, G. Perot, F. Bataille, J.L. Lemberon, M. Breysse, S. Kasztelan, Mechanistic considerations on the involvement of dihydrointermediates in the hydrodesulfurization of dibenzothiophene-type compounds over molybdenum sulfide catalysts, *Catal. Letters.* 71 (2001) 139–145.
- [41] D.D. Whitehurst, T. Isoda, I. Mochida, Present state of the art and future challenges in the hydrodesulfurization of polyaromatic sulfur compounds, *Adv. Catal. Vol 42.* 42 (1998) 345–471.
- [42] A.C. Smith, L.W. Moore, *Chem. Met. Eng.* 48 (1941) 77.

-
- [43] R. Prins, V.H.J. de Beer, G.A. Somorjai, Structure and Function of the Catalyst and the Promoter in Co Mo - Hydrodesulfurization Catalysts, *Catal. Rev. Sci. Eng.* 31 (1989) 1–41.
- [44] T. Pecoraro, Hydrodesulfurization catalysis by transition metal sulfides, *J. Catal.* 67 (1981) 430–445.
- [45] A.C. Byrns, W.E. Bradley, M.W. Lee, Catalytic desulfurization of gasolines by cobalt molybdate process, *Ind. Eng. Chem.* 35 (1943) 1160–1167.
- [46] H. Topsøe, B.S. Clausen, F.E. Massoth, *Catalysis*, Springer Berlin Heidelberg, Berlin, Heidelberg, 1996.
- [47] J. Grimblot, Genesis, Architecture and nature of sites of Co(Ni)–MoS₂ supported hydroprocessing catalysts, *Catal. Today.* 41 (1998) 111–128.
- [48] E. Payen, Genesis of the hydrodesulfurization active phase: A Raman and X-ray absorption spectroscopic study., *Abstr. Pap. Am. Chem. Soc.* 226 (2003), Amer Chem Soc.
- [49] M.R. Hilton, P.D. Fleischauer, {TEM} lattice imaging of the nanostructure of early-growth sputter-deposited {MoS₂} solid lubricant films, *J. Mater. Res.* 5 (1990) 406–421.
- [50] S. Kasztelan, H. Toulhoat, J. Grimblot, J.P. Bonnelle, D. Lille, A geometrical model of the active phase of hydrotreating catalysts, *Appl. Catal.* 13 (1984) 127–159.
- [51] R.J.H. Voorhoeve, J.C.M. Stuiver, Kinetics of hydrogenation on supported and bulk nickel-tungsten sulfide catalysts, *J. Catal.* 23 (1971) 228–235.
- [52] A.L. Farragher, P. Cossee, *Proc 5th Int Cong Catal*, in: J.W. Hightower (Ed.), Amsterdam, 1973: p. 1301.
- [53] K.-I. Tanaka, *Catalysis Controlled by the Constitution of Active Sites*, in: H.P. D.D. Eley, P.B. Weisz (Eds.), Academic Press, 1985: pp. 99–158.
- [54] M. Daage, Structure-function relations in molybdenum sulfide catalysts: The “Rim-Edge” Model, *J. Catal.* 149 (1994) 414–427.
- [55] J.. Lauritsen, S. Helveg, E. Lægsgaard, I. Stensgaard, B.. Clausen, H. Topsøe, F. Besenbacher, Atomic-scale structure of Co–Mo–S nanoclusters in hydrotreating catalysts, *J. Catal.* 197 (2001) 1–5.
- [56] H. Schweiger, P. Raybaud, G. Kresse, H. Toulhoat, Shape and edge sites modifications of MoS₂ catalytic nanoparticles induced by working conditions: A theoretical study, *J. Catal.* 207 (2002) 76–87.
- [57] J.V. Lauritsen, M.V. Bollinger, E. Lægsgaard, K.W. Jacobsen, J.K. Nørskov, B.S. Clausen, H. Topsøe, F. Besenbacher, Atomic-scale insight into structure and morphology changes of MoS₂ nanoclusters in hydrotreating catalysts, *J. Catal.* 221 (2004) 510–522.
- [58] G.C.A. Schuit, B.C. Gates, *Chemistry and engineering of catalytic Hydrodesulfurization*, *AICHE J.* 19 (1973) 417–438.

-
- [59] R.J.H. Voorhoeve, Electron spin resonance study of active centers in nickel-tungsten sulfide hydrogenation catalysts, *J. Catal.* 23 (1971) 236–242.
- [60] B. Delmon, New hypothesis explaining synergy between 2 Phases in heterogeneous catalysis - case of hydrodesulfurization catalysts, *Bull. Des Soc. Chim. Belges.* 88 (1979) 979–987.
- [61] H. Topsøe, B.S. Clausen, Importance of Co-Mo-S type structures in hydrodesulfurization, *Catal. Rev.* 26 (1984) 395–420.
- [62] J.M.J.G. Lipsch, G.C.A. Schuit, The CoO-MoO₃-Al₂O₃ catalyst, *J. Catal.* 15 (1969) 179–189.
- [63] J.M.J.G. Lipsch, G.C.A. Schuit, The CoO-MoO₃-Al₂O₃ catalyst, *J. Catal.* 15 (1969) 174–178.
- [64] J.M.J.G. Lipsch, G.C.A. Schuit, The CoO-MoO₃-Al₂O₃ catalyst, *J. Catal.* 15 (1969) 163–173.
- [65] M. Dufaux, M. Che, C. Naccache, *CR Acad Sci Ser C.* 268 (1969) 2255.
- [66] A.L. Farragher, No Title, in: *Symp Role Solid State Chem. Catal. ACS Meet., New Orleans, 1977.*
- [67] R. Huisman, R. de Jonge, C. Haas, F. Jellinek, Trigonal-prismatic coordination in solid compounds of transition metals, *J. Solid State Chem.* 3 (1971) 56–66.
- [68] P. Grange, Catalytic Hydrodesulfurization, *Catal. Rev.* 21 (1980) 135–181.
- [69] P. Grange, B. Delmon, Role of cobalt and molybdenum sulfides in hydrodesulfurization Catalysts - Review, *J. Less-Common Met.* 36 (1974) 353–360.
- [70] G. Hagenbach, P. Courty, B. Delmon, Physicochemical investigations and catalytic activity measurements on crystallized molybdenum sulfide-cobalt sulfide mixed catalysts, *J. Catal.* 31 (1973) 264–273.
- [71] B. Delmon, No Title, in: H.F. Barry, P. Mitchell (Eds.), *3rd Conf Chem. Uses molybdenum, 1979: p. 73.*
- [72] D. Pirotte, J.M. Zabala, P. Grange, B. Delmon, The remote-control of the active-sites of hydrodesulfurization catalysts comparison of experimental results with the model, *Bull. Des Soc. Chim. Belges.* 90 (1981) 1239–1248.
- [73] H. Topsøe, B.S. Clausen, R. Candia, C. Wivel, S. Morup, In situ Mossbauer emission-spectroscopy studies of unsupported and supported sulfided co-mo hydrodesulfurization catalysts - evidence for and nature of a Co-Mo-S phase, *J. Catal.* 68 (1981) 433–452.
- [74] C. Wivel, R. Candia, B.S. Clausen, S. Morup, H. Topsøe, On the catalytic significance of a Co-Mo-S phase in Co-Mo-Al₂O₃ Hydrodesulfurization catalysts - Combined In situ Mossbauer emission-spectroscopy and activity studies, *J. Catal.* 68 (1981) 453–463.

-
- [75] I. Alstrup, I. Chorkendorff, R. Candia, B.S. Clausen, H. Topsøe, A combined X-Ray photoelectron and Mössbauer emission spectroscopy study of the state of cobalt in sulfided, supported, and unsupported CoMo catalysts, *J. Catal.* 77 (1982) 397–409.
- [76] L.S. Byskov, M. Bollinger, J.K. Norskov, B.S. Clausen, H. Topsøe, Molecular aspects of the H₂ activation on MoS₂ based catalysts the role of dynamic surface arrangements, *J. Mol. Catal. A-Chemical*. 163 (2000) 117–122.
- [77] N.-Y. Topsøe, H. Topsøe, Characterization of the structures and active sites in sulfided CoMo-Al₂O₃ and NiMo-Al₂O₃ catalysts by NO chemisorption, *J. Catal.* 84 (1983) 386–401.
- [78] D. Pirotte, J.M. Zabala, P. Grange, B. Delmon, The Remote Control of the Active Sites of Hydrodesulphurization Catalysts Comparison of Experimental Results with the Model, *Bull. Des Sociétés Chim. Belges*. 90 (1981) 1239–1248. doi:10.1002/bscb.19810901208.
- [79] B.S. Clausen, B. Lengeler, R. Candia, J. Als-Nielsen, H. Topsøe, EXAFS studies of calcined and sulfided Co-Mo HDS catalysts, *Bull. Des Sociétés Chim. Belges*. 90 (1981) 1249–1259.
- [80] H. Topsøe, B.S. Clausen, N.-Y. Topsøe, P. Zeuthen, Progress in the design of hydrotreating catalysts based on fundamental molecular insight, in: M.A.-H. D.L. Trimm S. Akashah, A. Bishara (Eds.), *Catal. Pet. Refin. 1989 Proceedings Conf. Catal. Pet. Refin.*, Elsevier, 1989: pp. 77–102.
- [81] H. Topsøe, B.S. Clausen, Active sites and support effects in hydrodesulfurization catalysts, *Appl. Catal.* 25 (1986) 273–293.
- [82] R. Candia, O. Sørensen, Jør. Villadsen, N.-Y. Topsøe, B.S. Clausen, H. Topsøe, Effect of sulfiding temperature on activity and structures of Co-Mo/Al₂O₃ catalysts. ii, *Bull. Des Sociétés Chim. Belges*. 93 (1984) 763–774.
- [83] L. Lizama, T. Klimova, Highly active deep HDS catalysts prepared using Mo and W heteropolyacids supported on SBA-15, *Appl. Catal. B-Environmental*. 82 (2008) 139–150.
- [84] O. V Klimov, A. V Pashigreva, M.A. Fedotov, D.I. Kochubey, Y.A. Chesalov, G.A. Bukhtiyarova, A.S. Noskov, Co-Mo catalysts for ultra-deep HDS of diesel fuels prepared via synthesis of bimetallic surface compounds, *J. Mol. Catal. A-Chemical*. 322 (2010) 80–89.
- [85] H. Li, M. Li, Y. Chu, F. Liu, H. Nie, Effect of different preparation methods of MoO₃/Al₂O₃ catalysts on the existing states of Mo species and hydrodesulfurization activity, *Fuel*. 116 (2014) 168–174.
- [86] K.H. Tytko, O. Glemser, Isopolymolybdates and isotungstates, *Adv. Inorg. Chem. Radiochem.* (1976) 19.
- [87] S. Kasztelan, J. Grimblot, J.P. Bonnelle, E. Payen, H. Toulhoat, Y. Jacquin, Preparation of Co-Mo- δ -Al₂O₃ and Ni-Mo- δ -Al₂O₃ catalysts by pH regulation of molybdenum solution. Characterization of supported species and hydrogenation activities, *Appl. Catal.* 7 (1983) 91–112.

-
- [88] I. V Kozhevnikov, *Advances in Catalysis by Heteropolyacids*, *Russ. Chem. Rev.* 56 (1987) 1417–1443.
- [89] J.A.R. Van Veen, P.A.J.M. Hendriks, R.R. Andrea, E.J.G.M. Romers, A.E. Wilson, *Chemistry of phosphomolybdate adsorption on alumina surfaces. 2. The molybdate/phosphated alumina and phosphomolybdate/alumina systems*, *J. Phys. Chem.* 94 (1990) 5282–5285.
- [90] M. Sun, J. Zhang, P. Putaj, V. Caps, F. Lefebvre, J. Pelletier, J.-M. Basset, *Catalytic oxidation of light alkanes (C1-C4) by heteropoly compounds.*, *Chem. Rev.* 114 (2014) 981–1019.
- [91] A. Griboval, P. Blanchard, E. Payen, M. Fournier, J.L. Dubois, J.R. Bernard, *On the use of PCo(Ni)Mo-11 heteropolyanions for the preparation of alumina supported HDS catalysts, Hydrotreatment Hydrocracking Oil Fractions.* 127 (1999) Technol Inst.
- [92] Y. Kim, H. Kim, J. Lee, K. Sim, Y. Han, H. Paik, *A modified Wacker catalysis using heteropolyacid: Interaction of heteropolyanion with Cu(II) in cyclohexene oxidation*, *Appl. Catal. A-General.* 155 (1997) 15–26.
- [93] M. Misono, *Catalysis of heteropoly compounds (polyoxometalates)*, 2013.
- [94] T. Komaya, M. Misono, *Activity Patterns of H₃PMo₁₂O₄₀ and Its alkali salts for oxidation reactions*, *Chem. Lett.* (1983) 1177–1180.
- [95] R. Włodarczyk, M. Chojak, K. Miecniowski, A. Kolary, P.J. Kulesza, R. Marassi, *Electroreduction of oxygen at polyoxometallate-modified glassy carbon-supported Pt nanoparticles*, *J. Power Sources.* 159 (2006) 802–809.
- [96] J.J. Berzelius, *Berzelius, J. J. Poggendorffs Ann. Phys. Chem.* 1826, 6, 369, *Poggendorffs Ann. Phys. Chem.* 6 (1826) 369.
- [97] J.F. Keggin, *No Title*, *Proc. R. Soc. London, Ser. A.* 144 (1934) 75–100.
- [98] X. López, J.J. Carbó, C. Bo, J.M. Poblet, *Structure, properties and reactivity of polyoxometalates: a theoretical perspective.*, *Chem. Soc. Rev.* 41 (2012) 7537–71.
- [99] J.M. Poblet, X. Lopez, C. Bo, *Ab initio and DFT modelling of complex materials: towards the understanding of electronic and magnetic properties of polyoxometalates*, *Chem. Soc. Rev.* 32 (2003) 297.
- [100] M.T. Pope, *Heteropoly and Isopoly Oxometalates*, Springer Berlin Heidelberg, Berlin, 1983.
- [101] R. Palchevaa, A. Spojakina, G. Tyuliev, K. Jiratova, L. Petrov, *The effect of nickel on the component state and HDS activity of alumina-supported heteropolytungstates*, *Kinet. Catal.* 48 (2007) 847–852.
- [102] J.S. Anderson, *Constitution of the Poly-acids*, *Nature.* 140 (1937) 850–850.

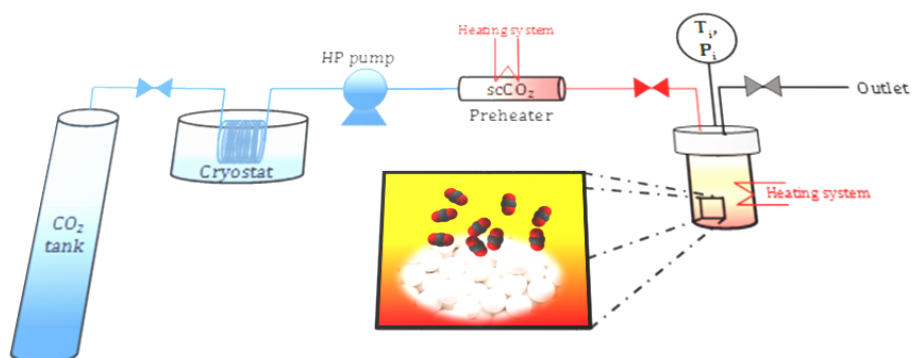
-
- [103] X. Carrier, J.F. Lambert, M. Che, ligand-promoted alumina dissolution in the preparation of MoO/ γ Al₂O₃ catalysts : evidence for the formation and deposition of an Anderson-type alumino heteropolymolybdate, *J. Am. Chem. Soc.* 119 (1997) 10137–10146.
- [104] L. Le Bihan, P. Blanchard, M. Fournier, E. Payen, V. Cedex, Raman spectroscopic evidence for the existence of 6-molybdoaluminate entities on an Mo / Al O oxidic precursor, *J. Chem. Soc., Faraday Trans.* 94 (1998) 937–940.
- [105] R. Strandberg, No Title, *Acta Chem. Scand.* 28 (1974) 217.
- [106] A.N. Startsev, The Mechanism of HDS Catalysis, *Catal. Rev. Eng.* 37 (1995) 353–423.
- [107] M. Zdražil, Recent advances in catalysis over sulphides, *Catal. Today.* 3 (1988) 269–365.
- [108] J. A. R. van Veen, P.A.J.M. Hendriks, R.R. Andréa, E.J.G.M. Romers, A.E. Wilson, Phosphomolybdate adsorption on alumina surfaces. 2. the molybdate/phosphated alumina and phosphomolybdate/alumina systems, *J. Phys. Chem.* 94 (1990) 5282–5285.
- [109] J.A. Bergwerff, L.G.A. van de Water, T. Visser, P. de Peinder, B.R.G. Leliveld, K.P. de Jong, B.M. Weckhuysen, Spatially resolved Raman and UV-visible-NIR spectroscopy on the preparation of supported catalyst bodies: Controlling the formation of H₂PMo_{0.11}CoO₄₀⁵⁻ inside Al₂O₃ pellets during impregnation, *Chem. Eur. J.* 11 (2005) 4592–4601.
- [110] J.A. Bergwerff, Spatially Resolved Spectroscopy on the Preparation of CoMo/Al₂O₃ hydrodesulphurization catalysts, 2007.
- [111] Tsigdino.GA, C.J. Hallada, Synthesis and electrochemical properties of heteropolymolybdates, *J. Less-Common Met.* 36 (1974) 79–93.
- [112] A.A. Spojakina, B. Gigov, D.M. Shopov, Synthesis and properties of hydrodesulfurization catalysts .4. thiophene hydrodesulfurization on molybdenum catalysts containing heteropoly compounds, *React. Kinet. Catal. Lett.* 19 (1982) 11–14.
- [113] A.A. Spojakina, S. Damyanova, V. Sharkova, T. Yureva, in: *Proc. 6th Int. Symp. Heterog. Catal. Part I*, Sofia, 1987: p. 503.
- [114] A. Griboval, P. Blanchard, E. Payen, M. Fournier, J.L. Dubois, Alumina supported HDS catalysts prepared by impregnation with new heteropolycompounds. Comparison with catalysts prepared by conventional Co–Mo–P coimpregnation, *Catal. Today.* 45 (1998) 277–283.
- [115] A. Griboval, R. Blanchard, E. Payen, M. Fournier, J.L. Dubois, J.R. Bernard, Characterization and catalytic performances of hydrotreatment catalysts prepared with silicium heteropolymolybdates: comparison with phosphorus doped catalysts, *Appl. Catal. A-General.* 217 (2001) 173–183.
- [116] A. Griboval, P. Blanchard, E. Payen, M. Fournier, J.L. Dubois, Alumina supported HDS catalysts prepared by impregnation with new heteropolycompounds, *Hydrotreatment Hydrocracking Oil Fractions.* 106 (1997) Royal Flemish Soc Engineers, Technol Inst.

-
- [117] A. Griboval, P. Blanchard, E. Payen, M. Fournier, J.L. Dubois, Preparation of hydrodesulfurization catalysts by impregnation of alumina with new heteropolycompounds, *Chem. Lett.* (1997) 1259–1260.
- [118] C. Martin, *Catalyseurs d'hydrodésulfurisation préparés à partir d'hétéropolyanions de type Anderson*, Université des Sciences et Technologies de Lille, 2003.
- [119] C. Martin, C. Lamonier, E. Payen, V. Harlé, New starting CoMo heteropolyoxomolybdates for the preparation of HDS catalysts, *Catal. Today* 48 (2003) 42–43.
- [120] C. Lamonier, C. Martin, J. Mazurelle, V. Harlé, D. Guillaume, E. Payen, Molybdocobaltate cobalt salts: new starting materials for hydrotreating catalysts, *Appl. Catal. B Environ.* 70 (2007) 548–556.
- [121] J. Mazurelle, C. Lamonier, C. Lancelot, E. Payen, C. Pichon, D. Guillaume, Use of the cobalt salt of the heteropolyanion $[\text{Co}_2\text{Mo}_{10}\text{O}_{38}\text{H}_4]^{6-}$ for the preparation of CoMo HDS catalysts supported on Al_2O_3 , TiO_2 and ZrO_2 , *Catal. Today* 130 (2008) 41–49.
- [122] V. Costa, K. Marchand, M. Digne, C. Geantet, New insights into the role of glycol-based additives in the improvement of hydrotreatment catalyst performances, *Catal. Today* 130 (2008) 69–74.
- [123] V. Costa, B. Guichard, M. Digne, C. Legens, P. Lecour, K. Marchand, P. Raybaud, E. Krebs, C. Geantet, A rational interpretation of improved catalytic performances of additive-impregnated dried CoMo hydrotreating catalysts: a combined theoretical and experimental study, *Catal. Sci. Technol.* 3 (2013) 140–151.
- [124] M.S. Thompson, Preparation of high activity silica-supported hydrotreating catalysts and catalysts thus prepared, 1986. <https://www.google.com/patents/EP0181035A2?cl=en>.
- [125] M.A. Lelias, J. van Gestel, F. Mauge, J.A.R. van Veen, Effect of NTA addition on the formation, structure and activity of the active phase of cobalt-molybdenum sulfide hydrotreating catalysts, *Catal. Today* 130 (2008) 109–116.
- [126] M.A. Lelias, P.J. Kooyman, L. Mariey, L. Oliviero, A. Travert, J. van Gestel, J.A.R. van Veen, F. Mauge, Effect of NTA addition on the structure and activity of the active phase of cobalt-molybdenum sulfide hydrotreating catalysts, *J. Catal.* 267 (2009) 14–23.
- [127] Y. Ohta, T. Shimizu, T. Honma, M. Yamada, Effect of chelating agents on HDS and aromatic hydrogenation over CoMo- and NiW/ Al_2O_3 , *Hydrotreatment Hydrocracking Oil Fractions*. 127 (1999) Technol Inst.
- [128] M. Parvari, P. Moradi, The Influence of boria and EDTA on the hydrodesulfurization activity on CoMoS supported catalysts, *Int. J. Chem. React. Eng.* 9 (2011) S7.
- [129] M.S. Rana, J. Ramirez, A. Gutierrez-Alejandre, J. Ancheyta, L. Cedeno, S.K. Maity, Support effects in CoMo hydrodesulfurization catalysts prepared with EDTA as a chelating agent, *J. Catal.* 246 (2007) 100–108.
- [130] M.A. Lelias, E. Le Guludec, L. Mariey, J. van Gestel, A. Travert, L. Oliviero, F. Mauge, Effect of EDTA addition on the structure and activity of the active phase of cobalt-molybdenum sulfide hydrotreatment catalysts, *Catal. Today* 150 (2010) 179–185.

-
- [131] V. Sundaramurthy, A.K. Dalai, J. Adjaye, Effect of EDTA on hydrotreating activity of CoMo/ γ -Al₂O₃ catalyst, *Catal. Letters*. 102 (2005) 299–306.
- [132] P. Mazoyer, C. Geantet, F. Diehl, C. Pichon, T.S. Nguyen, M. Lacroix, In situ EXAFS study of the sulfidation of a hydrotreating catalyst doped with a non chelating organic additive, *Oil Gas Sci. Technol. D Ifp Energies Nouv.* 60 (2005) 791–799.
- [133] Y. Muhammad, C. Li, Dibenzothiophene hydrodesulfurization using in situ generated hydrogen over Pd promoted alumina-based catalysts, *Fuel Process. Technol.* 92 (2011) 624–630.
- [134] S. Takao, U. Kikko, U. Yuji, Y. Eiji, Y. Toshio, Y. Hideharu, A. Satoshi, K. Tetsuro, Catalysts for hydrotreating hydrocarbon oils and methods of preparing the same, EP0601722, 1998.
- [135] Y. Urugami, E. Yamaguchi, H. Yokozuka, K. Uekusa, hydrotreating catalysts: composition, preparation and uses, WO96/41848, 1996.
- [136] T.S. Nguyen, S. Loridant, L. Chantal, T. Cholley, C. Geantet, Effect of glycol on the formation of active species and sulfidation mechanism of CoMoP/Al₂O₃ hydrotreating catalysts, *Appl. Catal. B-Environmental*. 107 (2011) 59–67.
- [137] D. Nicosia, R. Prins, The effect of glycol on phosphate-doped CoMo/Al₂O₃ hydrotreating catalysts, *J. Catal.* 229 (2005) 424–438.
- [138] J.J. Lee, H. Kim, J.H. Koh, A. Jo, S.H. Moon, Performance of CoMoS/Al₂O₃ prepared by sonochemical and chemical vapor deposition methods in the hydrodesulfurization of dibenzothiophene and 4,6-dimethyldibenzothiophene, *Appl. Catal. B-Environmental*. 58 (2005) 89–95.
- [139] J.J. Lee, H. Kim, J.H. Koh, A. Jo, S.H. Moon, Performance of fluorine-added CoMoS/Al₂O₃ prepared by sonochemical and chemical vapor deposition methods in the hydrodesulfurization of dibenzothiophene and 4,6-dimethyldibenzothiophene, *Appl. Catal. B-Environmental*. 61 (2005) 274–280.
- [140] A. Cho, J.H. Koh, S. Il Lee, S.H. Moon, Activity and thermal stability of sonochemically synthesized MoS₂ and Ni-promoted MoS₂ Catalysts, *Catal. Today*. 149 (2010) 47–51.
- [141] A. Cho, J.J. Lee, J.H. Koh, A. Wang, S.H. Moon, Performance of NiMoS/Al₂O₃ prepared by sonochemical and chemical vapor deposition methods in the hydrodesulfurization of dibenzothiophene and 4,6-dimethyldibenzothiophene, *Green Chem.* 9 (2007) 620–625.
- [142] N.A. Dhas, A. Ekhtiarzadeh, K.S. Suslick, Sonochemical preparation of supported hydrodesulfurization catalysts, *J. Am. Chem. Soc.* 123 (2001) 8310–8316.
- [143] E. Gusta, V. Sundaramurthy, A.K. Dalai, J. Adjaye, Hydrotreating of heavy gas oil derived from athabasca bitumen over Co-Mo/ γ -Al₂O₃ catalyst prepared by sonochemical method, *Top. Catal.* 37 (2006) Chem Inst Canada, Catalysis Div.
- [144] I. Uzcanga, I. Bezverkhyy, P. Afanasiev, C. Scott, M. Vrinat, Sonochemical preparation of MoS₂ in aqueous solution: Replication of the cavitation bubbles in an inorganic material morphology, *Chem. Mater.* 17 (2005) 3575–3577.

-
- [145] Usman, T. Yamamoto, T. Kubota, Y. Okamoto, Effect of phosphorus addition on the active sites of a Co-Mo/Al₂O₃ catalyst for the hydrodesulfurization of thiophene, *Appl. Catal. A-General*. 328 (2007) 219–225.
- [146] Y. Okamoto, A novel preparation-characterization technique of hydrodesulfurization catalysts for cleaner fuels, *Catal. Today*. 132 (2008) 9–17.
- [147] T. Kubota, H. Okamoto, Y. Okamoto, Hydrodesulfurization activity of highly dispersed Co sulfide clusters prepared in zeolite cages, *Catal. Letters*. 67 (2000) 171–174.
- [148] Y. Okamoto, K. Ochiai, M. Kawano, T. Kubota, Evaluation of the maximum potential activity of Co-Mo/Al₂O₃ catalysts for hydrodesulfurization, *J. Catal.* 222 (2004) 143–151.
- [149] Y. Okamoto, A. Kato, Usman, K. Sato, I. Hiromitsu, T. Kubota, Intrinsic catalytic activity of SiO₂-supported Co-Mo and Co-W sulfide catalysts for the hydrodesulfurization of thiophene, *J. Catal.* 233 (2005) 16–25.
- [150] H. Wang, Y. Wu, Z. Liu, L. He, Z. Yao, W. Zhao, Deposition of WO₃ on Al₂O₃ via a microwave hydrothermal method to prepare highly dispersed W/Al₂O₃ hydrodesulfurization catalyst, *Fuel*. 136 (2014) 185–193.
- [151] S.E. Skrabalak, K.S. Suslick, Hydrodesulfurization with MoS₂ synthesized by ultrasonic spray pyrolysis, *Abstr. Pap. Am. Chem. Soc.* 231 (2006) Amer Chem Soc.
- [152] S.E. Skrabalak, K.S. Suslick, Porous MoS₂ synthesized by ultrasonic spray pyrolysis, *J. Am. Chem. Soc.* 127 (2005) 9990–9991.
- [153] A. Baiker, Supercritical fluids in heterogeneous catalysis., *Chem. Rev.* 99 (1999) 453–474.
- [154] L.T. Taylor, *Supercritical fluid extraction*, Wiley-VCH Verlag GmbH & Co. KGaA, 1996.
- [155] A. Loppinet-Serani, C. Aymonier, F. Cansell, Supercritical water for environmental technologies, *J. Chem. Technol. Biotechnol.* 85 (2010) 583–589.
- [156] E. Reverchon, R. Adami, Nanomaterials and supercritical fluids, *J. Supercrit. Fluids*. 37 (2006) 1–22.
- [157] M. Alibouri, S.M. Ghoreishi, H.R. Aghabozorg, Hydrodesulfurization activity of NiMo/Al-HMS nanocatalyst synthesized by supercritical impregnation, *Ind. Eng. Chem. Res.* 48 (2009) 4283–4292.
- [158] M. Alibouri, S.M. Ghoreishi, H.R. Aghabozorg, Effect of supercritical deposition synthesis on dibenzothiophene hydrodesulfurization Over NiMo/Al₂O₃ Nanocatalyst, *AIChE J.* 55 (2009) 2665–2674.
- [159] M. Alibouri, S.M. Ghoreishi, H.R. Aghabozorg, Hydrodesulfurization of dibenzothiophene using CoMo/Al-HMS nanocatalyst synthesized by supercritical deposition, *J. Supercrit. Fluids*. 49 (2009) 239–248.
- [160] B. Motos-Pérez, D. Uzio, C. Aymonier, Preparation of nickel phosphide hydrodesulfurization catalysts assisted by supercritical carbon dioxide, *ChemCatChem*. 7 (2015) 3441–3444.

Chapter III: Experimental set-ups and characterization techniques



I. INTRODUCTION.....	95
II. EXPERIMENTAL SET-UP FOR THE SYNTHESIS OF OXIDE CATALYST PRECURSORS	95
II.1. MATERIALS.....	95
II.2. SCHEME OF THE SET-UP USED TO SYNTHESIZE OXIDE CATALYST PRECURSORS	98
II.3. TYPICAL PROTOCOL OF SYNTHESIS OF CATALYST PRECURSORS	98
III. CHARACTERIZATION TECHNIQUES	99
III.1. OXOMETALLIC PHASE CHARACTERIZATIONS	99
<i>III.1.1. Raman analyses</i>	<i>99</i>
<i>III.1.2. Elementary analysis</i>	<i>100</i>
<i>III.1.3. X-Ray Diffraction</i>	<i>100</i>
<i>III.1.4. μ-probe analyses</i>	<i>101</i>
III.2. SULFIDED PHASE CHARACTERIZATION	101
<i>III.2.1. Activation of the catalyst precursor</i>	<i>101</i>
<i>III.2.2. X-Ray Photoelectron Spectrometry</i>	<i>102</i>
<i>III.2.3. High Resolution Transmission Electron Microscopy (HR-TEM)</i>	<i>107</i>
IV. CATALYTIC TESTS	108
IV.1. TOLUENE HYDROGENATION AT CONSTANT SULFUR CONTENT IN HIGH THROUGHPUT UNIT.....	108
IV.2. HYDRODESULFURIZATION OF DBT AND 4,6-DMDBT IN A FIXED BED REACTOR.....	110
<i>IV.2.1. Hydrodesulfurization of DBT.....</i>	<i>110</i>
<i>IV.2.2. Hydrodesulfurization of 4,6-DMDBT.....</i>	<i>112</i>
<i>IV.2.3. Evaluation of catalysts.....</i>	<i>113</i>
V. CONCLUSION	114
VI. BIBLIOGRAPHY.....	115

I. Introduction

This chapter is dedicated to experimental set-ups and characterization techniques employed during this work. The first part presents the set-up used for the synthesis of catalyst precursors in a “batch” reactor, the different starting metallic materials, the main properties of solvents, as well as the progress of an experiment. The second part introduces the different characterization techniques used to describe the oxometallic and sulfided phases of synthesized catalyst precursors. The presentation of the *in situ* Raman set-up employed to the monitoring of the catalyst precursor preparation is also described in this part. The process employed to sulfide catalysts is presented in the section related to the characterization of the sulfided phase. A third part is related to the different catalytic tests performed to evaluate the performances of our catalysts, namely the hydrogenation of toluene, the hydrodesulfurization of dibenzothiophene and the hydrodesulfurization of 4,6-dimethyldibenzothiophene.

II. Experimental set-up for the synthesis of oxide catalyst precursors

In this part, the starting materials and the properties of solvents employed to synthesize catalyst precursors are first described. Then, the experimental set-up and the progress of an experiment are presented.

II.1. Materials

Starting materials were purchased from Sigma-Aldrich and Alfa Aesar and used without further purification. The molybdenum sources were the ammonium heptamolybdate ($(\text{NH}_4)_6\text{Mo}_7\text{O}_{24}\cdot 4\text{H}_2\text{O}$, CAS: 12054-85-2, MW: 1235.86 g.mol⁻¹, ACS reagent) and the phosphomolybdic acid ($\text{H}_3\text{PMo}_{12}\text{O}_{40}\cdot x\text{H}_2\text{O}$, CAS: 51429-74-4, MW: 1825,25 g.mol⁻¹ (anhydrous basis), ACS reagent). To determine the content of crystallization molecules of water, a thermogravimetric analysis has been performed and results can be found in Appendices. The cobalt source was the cobalt (II) nitrate hexahydrate ($\text{Co}(\text{NO}_3)_2\cdot 6\text{H}_2\text{O}$, CAS: 10026-22-9, MW: 291,03 g.mol⁻¹, ACS reagent, $\geq 98\%$). Distilled water employed was deionized in our laboratory. Alcohols used were methanol (CH_3OH), absolute ethanol ($\text{CH}_3\text{CH}_2\text{OH}$, 99,8%) and propan-1-ol ($\text{CH}_3\text{CH}_2\text{CH}_2\text{OH}$). The support used was a delta alumina ($\delta\text{-Al}_2\text{O}_3$) provided by IFPEN (70315, $V_p = 1 \text{ mL}\cdot\text{g}^{-1}$, $S = 120 \text{ m}^2\cdot\text{g}^{-1}$). The gas employed was carbon dioxide (CO_2) purchased from Air Liquide. Table III.1 summarizes the different reagents used in this study, whereas Table III.2 summarizes the main properties of the solvents used to perform this work.

Table III.1: Metallic precursors used in this work.

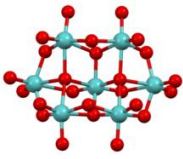
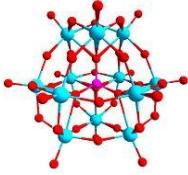
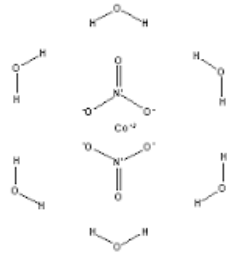
Metallic precursors		
Ammonium heptamolybdate tetrahydrate	Phosphomolybdic acid hydrate	Cobalt (II) nitrate hexahydrate
 <p>● Mo ● O</p>	 <p>● Mo ● O ● P</p>	
<ul style="list-style-type: none"> • Soluble in water • Insoluble in alcohols 	<ul style="list-style-type: none"> • Soluble in water • Soluble in alcohols 	<ul style="list-style-type: none"> • Soluble in water • Soluble in alcohols

Table III.2: Main properties of the solvents used in this work (data from NIST).

Compound	Formula	T _c (°C)	p _c (MPa)	ρ _c (g.mL ⁻¹)	Molar mass (g.mol ⁻¹)
<i>Water</i>	H ₂ O	374	22.1	0.32	18
<i>Methanol</i>	CH ₃ OH	239.5	8.1	0.28	32
<i>Ethanol</i>	CH ₃ CH ₂ OH	240.8	6.3	0.28	46
<i>n-Propanol</i>	CH ₃ CH ₂ CH ₂ OH	263.8	5.2	0.27	60
<i>Carbon dioxide</i>	CO ₂	31	7.38	0.47	44

Figure III.1 represents critical coordinates of all solvent as well as these of mixtures CO₂/alcohols employed during this work.

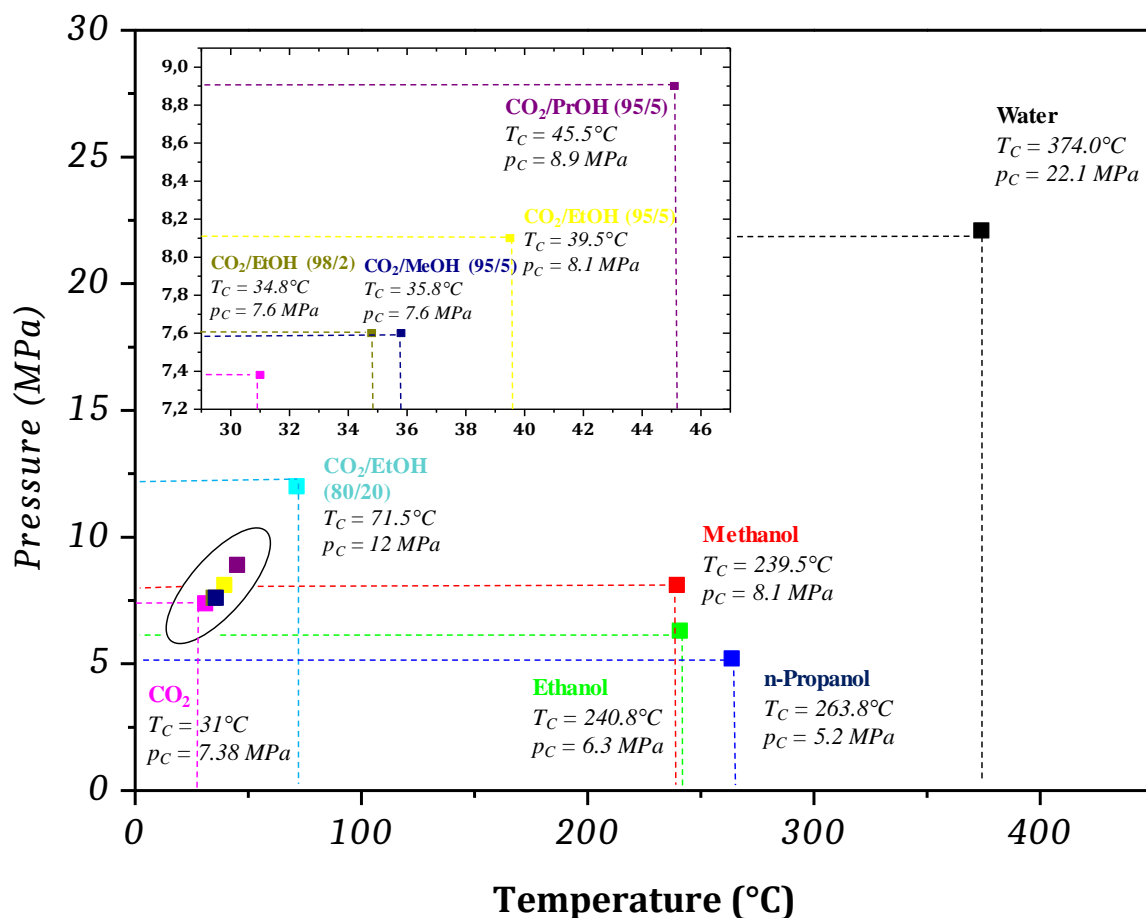


Figure III.1: Critical coordinates of solvents and mixtures employed during this work.

Depending on the molar ratio of CO₂/ethanol employed, changes of critical coordinates are observed. This is also valid for the alcohol used to perform the impregnation of metallic precursors. The next part presents the set-up for the preparation of the oxometallic phase of HDS catalysts.

II.2. Scheme of the set-up used to synthesize oxide catalyst precursors

The scheme of the set-up employed to prepare oxide catalyst precursors is represented in Figure III.2.

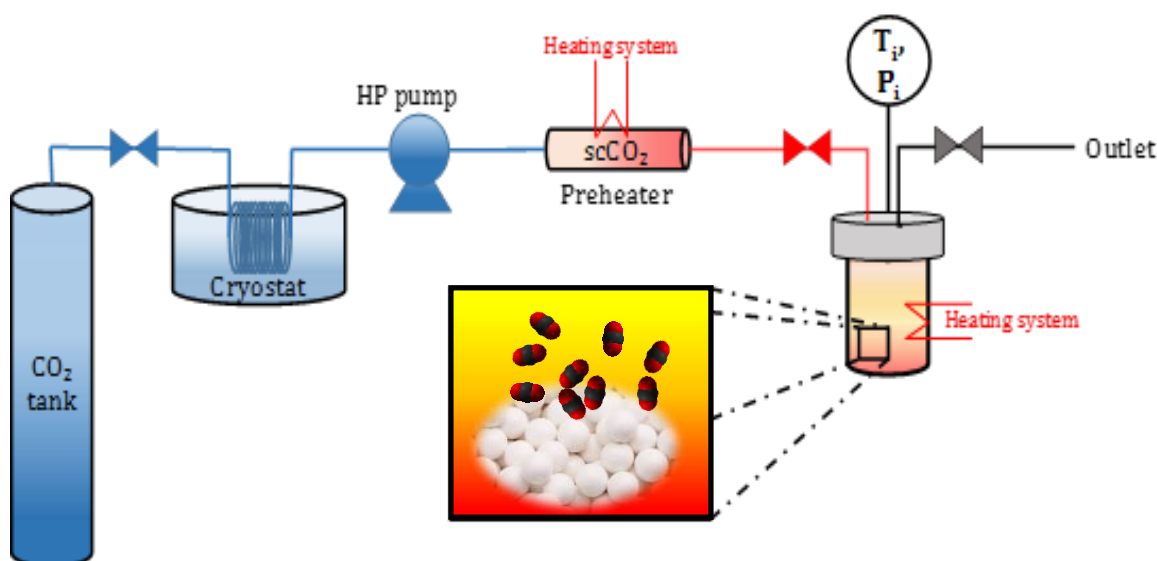


Figure III.2: Scheme of the process used to prepare oxide catalyst precursors.

This process includes a carbon dioxide bottle coupled with a cryostat in order to be able to pump CO₂ in its liquid form. For that and to increase the pressure in the reactor, a high pressure pump is present before the preheater. The preheater enables us to put carbon dioxide in supercritical conditions. Then, a batch reactor of 50 mL is present and contains the impregnated support. This reactor can be operated at high pressure (up to 40 MPa) and high temperature (up to 400°C). Pressure and temperature controllers permit to know the conditions present inside the batch reactor.

II.3. Typical protocol of synthesis of catalyst precursors

During this work, we have focused our investigations on CoMo supported alumina catalyst precursors. First, the desired amounts of Mo and Co are dissolved in an appropriate volume of solvent in order to perform an incipient wetness impregnation. Amounts of Mo and Co have been determined to reach a loading of 10 wt.% Mo, common loading for HDS catalysts [1], and a molar ratio Co/(Co + Mo) of 0,4, optimum ratio for the decoration of MoS₂ by Co atoms [2,3]. After a conventional dry impregnation, impregnated supports are placed in a closed vessel with a saturated atmosphere of solvent and aged for a defined period of time (mainly 1h). After this maturation step, the solid is loaded in the batch reactor and the reactor is sealed. The preheater is filled with cooled CO₂ in order to reach a pressure of 20 MPa and the temperature is set at 120°C. The CO₂ is then supercritical. When the pressure and the temperature are stabilized, the reactor temperature is set to 50°C and the temperature is maintained for 10 min. After stabilization of the reactor temperature, the valve located between the reactor and the preheater is opened. This permits to reach a pressure of about 8 MPa inside the reactor. Then, the temperature of the reaction is brought with the temperature controller to the desired temperature. The ramp rate of the temperature is kept at 5°C/min. When the desired temperature is reached, the pressure is adjusted to 22 MPa and these conditions are kept for the desired time (typically 1 hour). At the end of the experiment, the reactor is slowly depressurized until to reach a pressure of about 8 MPa and the heating is stopped. A supercritical drying with CO₂ is then performed for 30 minutes. Then, the pressure is released and the reactor is opened to recover a dried solid.

III. Characterization techniques

In this part, characterization techniques employed to study oxide and sulfided phases of the catalyst are introduced. Figure III.3 depicts characterization techniques employed during this work to determine the structure and composition of our synthesized catalysts before (oxometallic phase) and after sulfidation (sulfided phase) as well as catalytic tests performed.

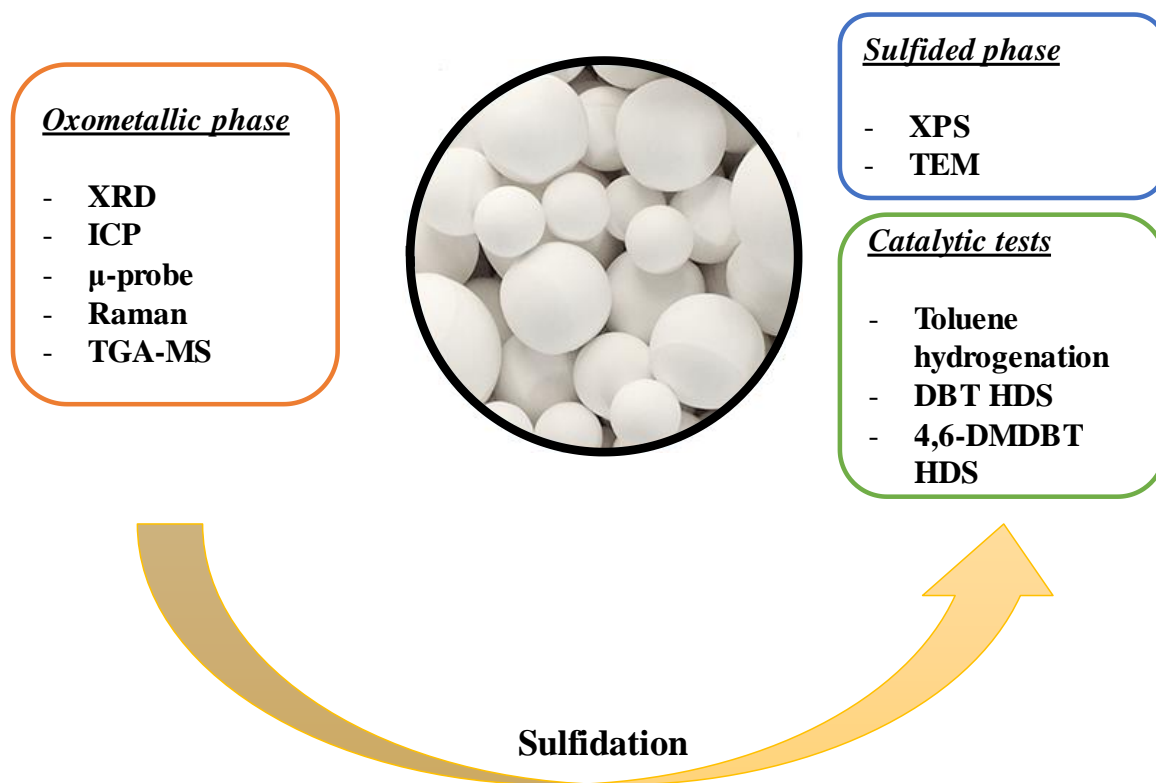


Figure III.3: Characterization techniques for the investigations of composition and structure of synthesized catalysts

III.1. Oxometallic phase characterizations

Several characterization techniques were employed to determine composition and structure of the oxometallic phase in synthesized samples.

III.1.1. Raman analyses

One of the most employed technique during this work was Raman spectroscopy. This technique allowed us to investigate the chemistry occurring during the preparation of catalysts and to determine species present onto the core and the surface of the alumina pellets. More information about this technique is given in *Appendix III: Raman characterization*.

III.1.1.a. Equipments

Two types of apparatus have been used during this project:

- A DXR Raman microscope from Thermo Scientific with a 532 nm wavelength excitation laser operating at 1-8 mW output power. The focus is made with a confocal microscope with a x10 objective. The resolution was 2 cm^{-1} over a spectra range from 50 to 3500 cm^{-1} .

- A XploRA spectrometer from Horiba Scientific with a 532 nm wavelength excitation laser operating at 1-10 mW output power. The focus is made with a confocal microscope with a x10 objective. The resolution was 2 cm^{-1} over a spectra range from 50 to 3500 cm^{-1} .

III.1.1.b. Experimental set-up for the *in-situ* Raman study during the preparation of oxometallic catalyst precursor

In situ Raman Spectroscopy (RS) is a powerful tool to study the evolution of species during the preparation of catalysts [4]. In our case, we have used this technique under working conditions, in temperature and pressure.

A home-made process coupled with a Raman spectrometer has been developed to study the evolution of species during the preparation of oxometallic catalyst precursors. The scheme of the home-made set-up employed is represented in Figure III.4.

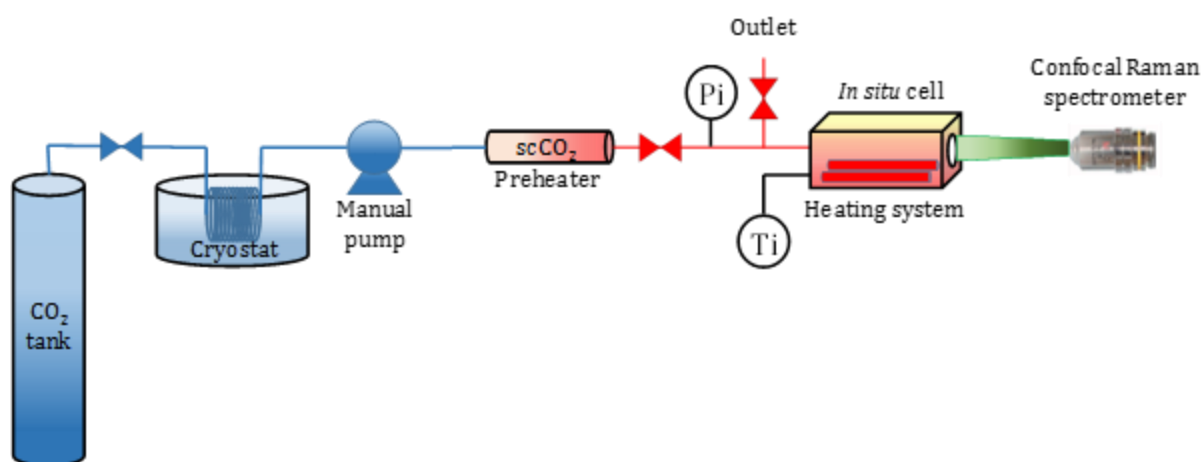


Figure III.4: Scheme of the set-up used to perform *in situ* Raman experiments

The impregnated sample is placed in the cell equipped with a sapphire window. The *in situ* cell is equipped with a heating system and a temperature controller. A pressure controller is placed upstream of the cell. A preheater allows us to reach the supercritical conditions of CO_2 in order to inject it under these conditions in the *in situ* cell. As the CO_2 has to be cold to be pumped, a cryostat has been placed between the CO_2 tank and the manual pump. The manual pump and the heating system allowed us to monitor our chemical reaction from room temperature up to around 300°C and from atmospheric pressure up to 10 MPa. Spectra were recorded each $10\text{-}20^\circ\text{C}$ after the stabilization of the temperature in the *in situ* cell.

III.1.2. Elementary analysis

In order to determine the content in molybdenum, cobalt and phosphorus in our samples, Inductively Coupled Plasma equipped with an Optical Emission Spectrometer (ICP-OES) has been used. Analyses were carried out by Laetitia Etienne (ICMCB-CNRS) using a Varian 720-ES apparatus. Prior to analysis, samples were mixed in nitric acid, hydrogen peroxide and distilled water and dissolved using a micro wave equipment to obtain a clear solution of our metals and support.

III.1.3. X-Ray Diffraction

X-Ray Diffraction measurements were made using a PANalytical X'Pert MPD Bragg-Brentano θ - θ geometry diffractometer equipped with a secondary monochromator over an angular range of 2θ

= 4-80°. The $\text{CuK}_{\alpha 1\alpha 2}$ ($\lambda_1 = 1.54060 \text{ \AA}$, $\lambda_2 = 1.54441 \text{ \AA}$) radiations are generated at 40 kV and 40 mA. These XRD measurements were carried out by Eric Lebraud (ICMCB).

The XRD pattern of the support used in this work ($\delta\text{-Al}_2\text{O}_3$) is presented in Figure III.5 with its associated reference pattern (JCPDS # 046-1215). Peaks corresponding to the support will not be attributed in the following chapters and only supported species will be attributed.

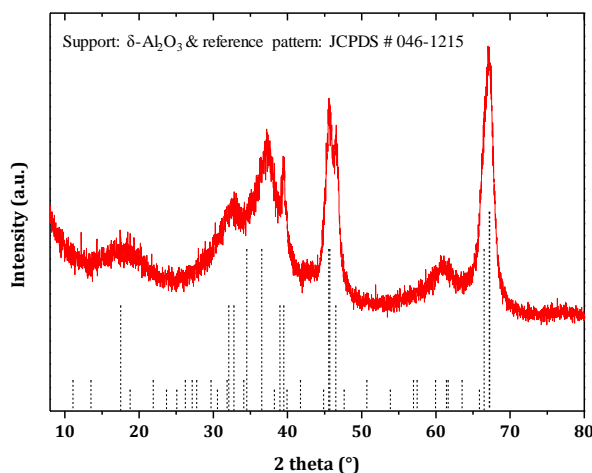


Figure III.5: XRD pattern of the support used in this study ($\delta\text{-Al}_2\text{O}_3$) (red line) and reference pattern associated to $\delta\text{-Al}_2\text{O}_3$ (JCPDS #046-1215) (black line)

III.1.4. μ -probe analyses

To verify the dispersion of elements onto the surface of our support, microprobe analyses were carried out at IFPEN Solaize using a JEOL 8100 Electron Probe Micro Analyzer. In this technique, a material is irradiated by an electron beam and the characteristic X-Ray generated by the material is measured. For each sample, alumina beads were placed into a polymeric resin before to be cut in half. Analyses were carried out on the surface of the cut beads. Measurements were done with a step of 30 μm along the diameter of alumina beads. For each sample, measurements were done on several beads and results presented are an average of all measurements.

III.2. Sulfided phase characterization

After characterization of the oxometallic phase of catalysts, they were sulfided and characterized using two analysis techniques: X-Ray Photoelectron Spectroscopy (XPS) and High Resolution Transmission Electron Microscopy (HR-TEM).

III.2.1. Activation of the catalyst precursor

In order to be active, a HDS catalyst has to be under its sulfided form. For that, we have implemented a sulfidation line in our laboratory. A scheme of the sulfidation cell is represented in Figure III.6. Each catalyst precursor has been sulfided for two hours at 350°C with a heating ramp rate of 5°C.min⁻¹ and under a $\text{H}_2/\text{H}_2\text{S}$ (85/15, v/v) flow of 2 L.h⁻¹.g_{catalyseur}⁻¹. This flow of $\text{H}_2/\text{H}_2\text{S}$ was kept after sulfidation until the temperature decreased to 200°C and then a flow of Ar was passed through the sulfided catalyst until the room temperature has been reached. This permits to remove unreacted physisorbed H_2S on the surface of the catalyst. After the sulfidation step, sulfided catalysts were kept under inert atmosphere to avoid any reoxidation before characterization of the sulfided phase.

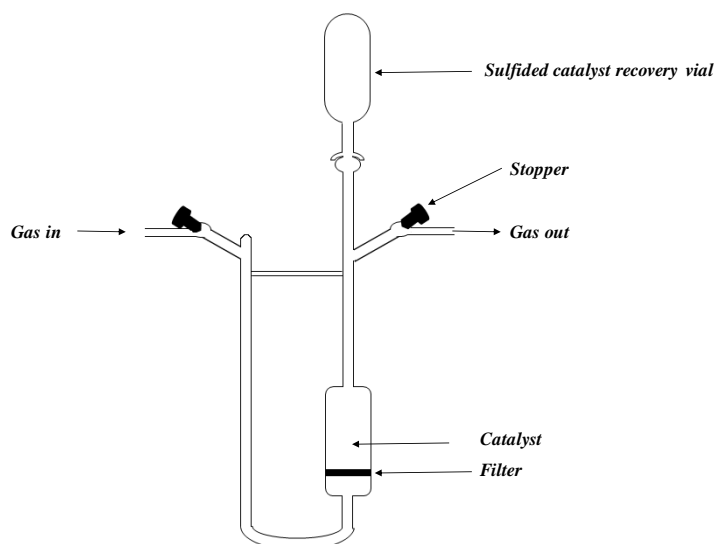


Figure III.6: Sulfidation cell employed for the activation of catalyst

III.2.2. X-Ray Photoelectron Spectrometry

XPS is a powerful technique to detect elements present on the surface of the catalysts and their oxidation states. The protocol of an analysis and the different equations permitting the quantification of each specie depending of its oxidation state is detailed in this part.

- Protocol of analysis

To prevent the reoxidation of our sulfided catalysts, samples were prepared under argon atmosphere by using a glove box. A carbon tape was placed on the XPS support to fix an indium foil on it. Then, samples were deposited on the indium foil after being crushed and aluminium tape was placed on a part of each sample to remove parasitic charges. Samples were then placed into a transport box to keep an inert atmosphere. Prior to analysis, transport box is opened and the XPS support is placed rapidly in the analysis chamber. During the preparation and prior to analysis, samples are in contact with air for a maximum time of 10 seconds. Analyses were carried out in collaboration with Christine Labrugère (Placamat).

The XPS spectra were recorded on a Thermo Scientific K-alpha instrument with Al monochromator source (1486.6 eV) and a hemi-spherical analyzer operating at fixed pass energy of 40 eV. The measurements were made at ambient temperature in steps of 0.05 eV for cobalt, 0.1 eV for molybdenum, sulfur, aluminium and carbon contamination, and at a pressure lower than $1 \cdot 10^{-6}$ Pa in the sample analysis chamber. For each sample, analyses were carried out in two different points.

Binding energies (BE) of the various elements have been referenced to the C 1s level of the carbon contamination at 284.6 eV. The curves were integrated applying a Shirley type baseline. The collected spectra were analyzed by using CasaXPS software. The effective atomic concentration $[i]$ of the atom i was obtained from the measurement of the corresponding total peak area A_i and the use of appropriate sensitivity factor S_i furnished by the constructor. To approach the effective atomic surface concentrations, all the atoms (except carbon contamination) detected on the surface were considered.

For each atom, the obtained signal was decomposed into different contributions relative to various chemical species. The calculation of the respective contribution of each peak area permits to determine the relative concentration of each chemical for each element. Figure III.7 represents a survey spectra recorded for a sulfided CoMo catalyst and the different contributions of each element present on the surface of the sample.

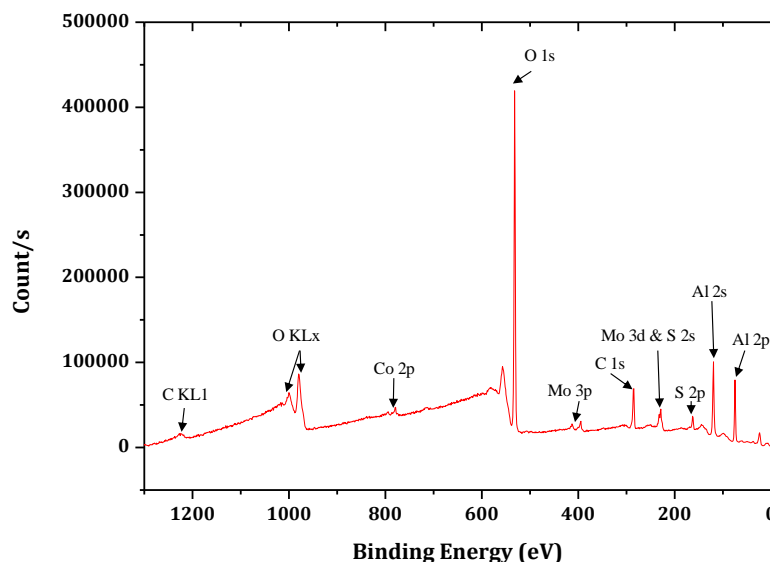


Figure III.7: Example of a XPS survey spectra obtained for a CoMoS/Al₂O₃ catalyst.

XPS analyses allowed the determination of the chemical composition of atoms contained in activated catalysts. XPS spectrum of molybdenum oxide supported on alumina is first presented and has been used as reference for the assignments of species and the determination of constraints in position, intensity and full width at half maximum.

- Mo 3d spectra of the oxide phase

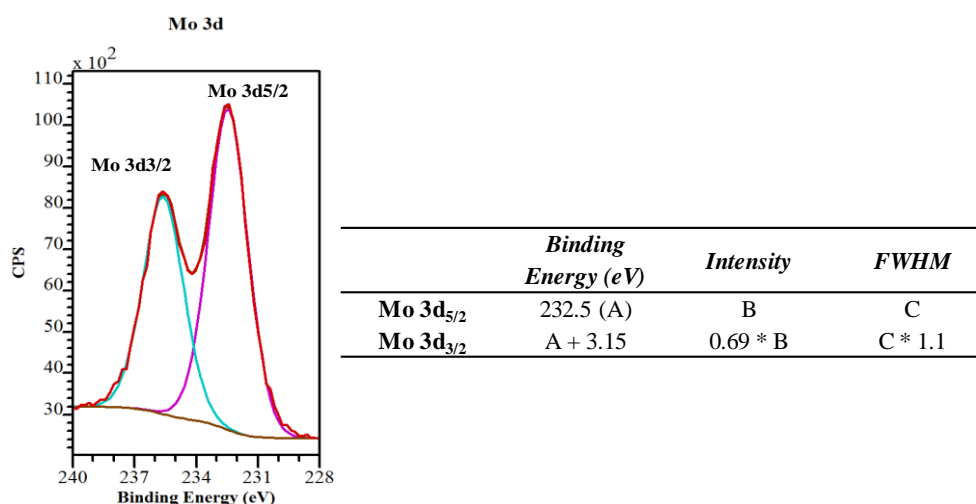


Figure III.8: XPS spectra of Mo oxide phase supported on alumina

Constraints in terms of binding energy (BE), intensity and FWHM are presented in the previous table. For the FWHM, a ratio between Mo 3d_{5/2} and Al 2p of 1.1 has been used as reference. In the case of the sulfided samples, binding energy corresponding to the Mo^{VI} 3d_{5/2} has a shift of 1eV

compared to its binding energy in oxide catalyst. The shift binding energy has already been reported and explained by the fact that environment around molybdenum is less oxidic due to the sulfidation in molybdenum sulfide [5].

- Mo 3d spectra of the sulfided phase

Figure II.9 represents the Mo 3d XPS spectra of a sulfided catalyst with the different deconvolutions performed to determine the concentration of each phase.

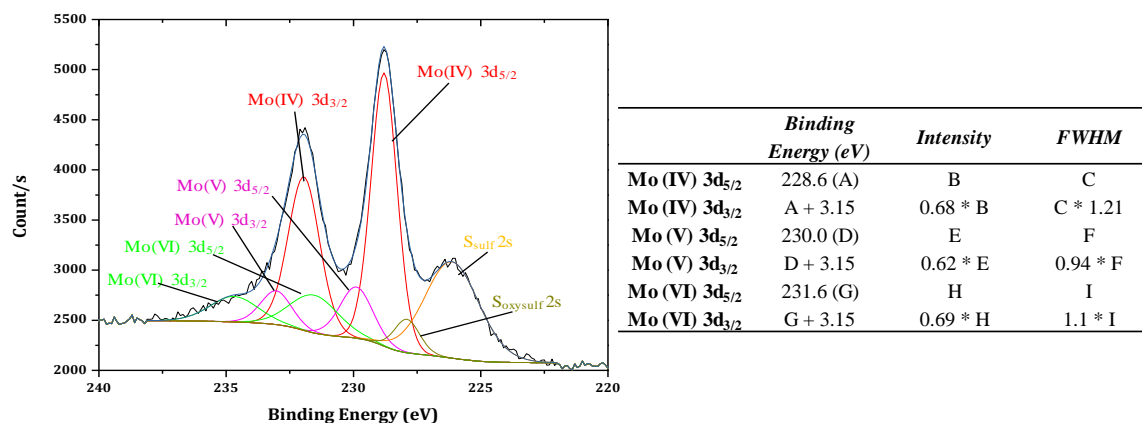


Figure III.9: Mo 3d XPS spectra of a sulfided HDS catalysts

Constraints in terms of binding energies, FWHM and intensities used to describe the XPS spectra of Mo 3d in a sulfided catalyst are presented in Figure III.9 (left).

- Co 2p spectra of the oxide phase

For Co 2p spectra, it can be decomposed in two main contributions and their associated satellite peaks. Co 2p_{3/2} and Co 2p_{1/2} contributions have been found in our reference compound at 781.5 eV and 797.3 eV respectively. The decomposition of Co 2p spectra is difficult due to the presence of multiple satellite peaks. For the attribution of each contribution and constraints associated, we referred to the literature about XPS study in the case of HDS catalyst characterizations [3,6]. Parameters used to attribute each contributions of cobalt in its oxide environment are presented in Table III.3.

Table III.3: Constraints in terms of BE, FWHM and intensities for the deconvolution of Co 2p XPS spectra

	<i>Binding Energy (eV)</i>	<i>Intensity</i>	<i>FWHM</i>
Co (II) 2p_{3/2}	781.5 (A)	B	C
Co (II) 2p_{1/2}	A + 15.8	B * 0.42	C * 1.02
Sat. 1	A + 2.1	B * 0.27	C * 0.92
Sat. 2	A + 5.1	B * 0.94	C * 1.97
Sat. 3	A + 9.9	B * 0.01	C * 0.49
Sat. 4	A + 17.5	B * 0.14	C * 1.08
Sat. 5	A + 21.7	B * 0.47	C * 1.62
Sat. 6	A + 25.2	B * 0.04	C * 0.99
Sat. 7	A - 4.3	B * 0.12	C * 1.46

- Co 2p spectra of the sulfided phase

Figure III.10 represents the Co 2p XPS spectra of the sulfided phase of HDS catalyst with their assigned species.

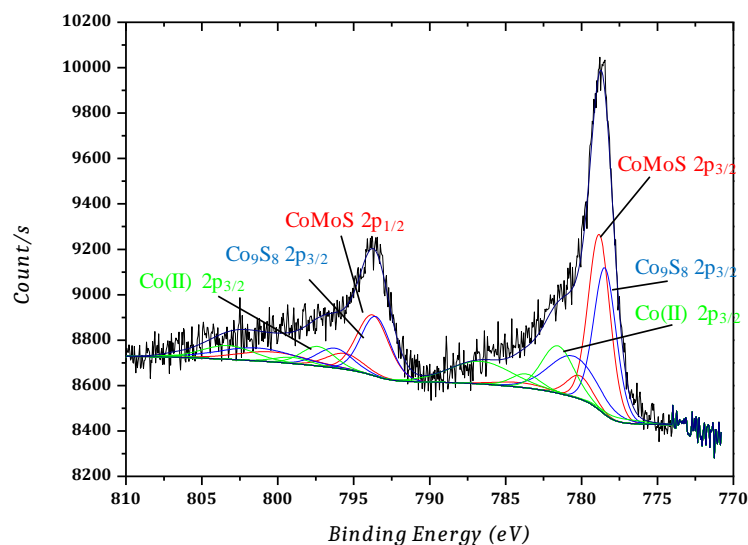


Figure III.10: Co 2p XPS spectra of a sulfided HDS catalysts

Three different species are present in the Co 2p XPS spectra of a sulfided HDS catalyst. The active phase labelled as CoMoS phase, a sulfided phase of cobalt Co_9S_8 (Co-S) and a phase of Co^{2+} resulting of the unsulfided cobalt present onto alumina. To estimate concentration of each phase, XPS spectra must be deconvolute using appropriate constraints. These constraints have been determined by performing XPS measurements on oxide phase of HDS catalyst for Co^{2+} atoms and are from literature [3,6–8]. Constraints applied in terms of BE, FWHM and intensities for Co_9S_8 species are presented in Table III.4 whereas Table III.5 presents constraints related to the CoMoS species.

Table III.4: Constraints in terms of BE, FWHM and intensities for the deconvolution of Co-S species in Co 2p XPS spectra

	<i>Binding Energy (eV)</i>	<i>Intensity</i>	<i>FWHM</i>
Co-S 2p_{3/2}	777.7 (A)	B	C
Co-S 2p_{1/2}	A + 15.1	B * 0.53	C * 1.3
Sat. 1	A + 2.1	B * 0.6	C * 2.15
Sat. 2	A + 17.8	B * 0.21	C * 1.56
Sat. 3	A + 22.9	B * 0.3	C * 3.4

Table III.5: Constraints in terms of BE, FWHM and intensities for the deconvolution of CoMoS species in Co 2p XPS spectra

	<i>Binding Energy (eV)</i>	<i>Intensity</i>	<i>FWHM</i>
CoMoS 2p_{3/2}	778.5 (A)	B	C
CoMoS 2p_{1/2}	A + 14.91	B * 0.5	C * 1.45
Sat. 1	A + 1.31	B * 0.15	C * 1.13
Sat. 2	A + 5.15	B * 0.06	C * 2.26
Sat. 3	A + 16.77	B * 0.15	C * 1.66
Sat. 4	A + 21.5	B * 0.18	C * 3.17

- S2p spectra of the sulfided catalyst

The last element studied in XPS was the sulfur. An example of a XPS spectra of S2p is presented in Figure III.11.

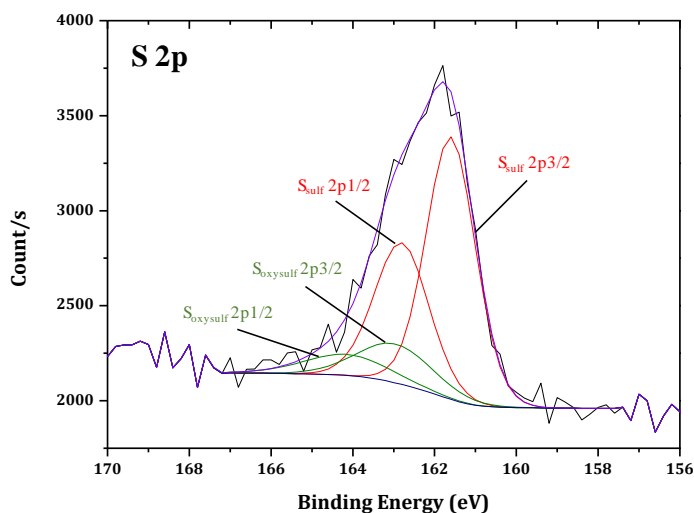


Figure III.11: S 2p XPS spectra of a sulfided HDS catalyst

From the deconvolution of XPS spectra, it is possible to determine and quantify the different species present on the surface of the catalyst. To obtain a good characterization of species, the concentration of molybdenum species, molybdenum disulfide (MoS_2), oxysulfide molybdenum (Mo(V)) and molybdenum oxide (Mo(VI)) have to be determined. As well as, the concentrations of cobalt species, cobalt sulfide (Co_9S_8), the catalytic active phase (CoMoS), cobalt oxide and the concentration of sulfides and sulfates species must be known.

Once, these deconvolutions are done, an area for each specie (A_i) is determined and the relative concentration of the compounds present on the surface of the support can be exposed. For example, in the case of cobalt atoms, the relative concentration of the CoMoS is determined using Eq. III.1.

$$\text{CoMoS}(\%) = \left(\frac{A_{\text{CoMoS}}}{A_{\text{CoMoS}} + A_{\text{Co(II)}} + A_{\text{Co}_9\text{S}_8}} \right) * 100 \quad \text{Eq. III.1}$$

The effective weight amount of CoMoS phase [CoMoS] present in the catalyst can be determined in multiplying the percentage of CoMoS phase by the total concentration of cobalt ([Co]) present in the catalyst.

$$[\text{CoMoS}] = \text{CoMoS}(\%) * [\text{Co}] / 100 \quad \text{Eq. III.2}$$

The sulfidation rate of molybdenum is given by using the Eq. III.3.

$$\text{SRMo}(\%) = \left(\frac{\text{Concentration of MoS}_2}{\text{Total concentration of Mo}} \right) * 100 \quad \text{Eq. III.3}$$

The promotion rate of the catalyst is determined by using the Eq. III.4 and represents the percentage of cobalt decorating edges of molybdenum disulfide.

$$\text{PRCo}(\%) = \left(\frac{\text{Concentration of CoMoS}}{\text{Total concentration of Co}} \right) * 100 \quad \text{Eq. III.4}$$

All these calculations allow the comparison of catalysts and permit to highlight relationships between characterization and catalytic tests.

The second technique used to characterize sulfided catalysts was the transmission electron microscopy.

III.2.3. High Resolution Transmission Electron Microscopy (HR-TEM)

HR-TEM permits to evaluate the size, the distribution and the morphology of phases present in sulfided catalysts, such as the molybdenum disulfide phase when it is well crystallized or the Co_9S_8 phase when it is present in the catalyst.

High Resolution Transmission Electron Microscopy (HR-TEM) analyses were performed, in collaboration with Sonia Buffière and Marion Gayot (Placamat), by using a microscope JEOL 2200FS equipped with an electron beam working at 200kV. Analyses were performed in bright field mode. Prior to analysis, samples were prepared by putting several drops of dispersed sulfided catalyst in ethanol onto a copper grid coated with carbon. After analysis, 200 particles consisting of layers of MoS_2 were counted in size and in stacking to perform statistics and link catalytic results with characterization results. An example of TEM pictures obtained for a $\text{CoMoS}/\text{Al}_2\text{O}_3$ catalyst is presented in Figure III.12.

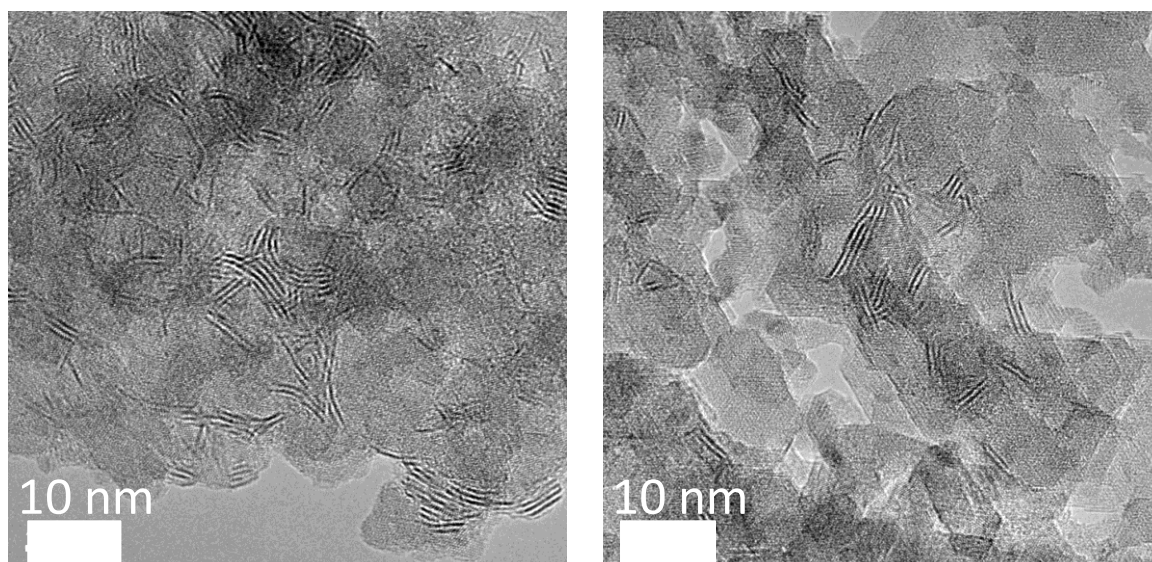


Figure III.12: TEM pictures of a $\text{CoMoS}/\text{Al}_2\text{O}_3$ catalyst

After characterizations of catalysts in their oxometallic and sulfided phases, their catalytic performances were evaluated using three different tests. These catalytic tests are presented in the following part.

IV. Catalytic tests

All catalytic tests have been performed in units located at IFPEN Solaize on three main reactions. The first one is the toluene hydrogenation. This test permits to obtain a reaction rate constant of toluene hydrogenation and allows a first comparison of catalysts. The second and third ones are hydrodesulfurization of model molecules which were the dibenzothiophene (DBT) and the 4,6-dimethyldibenzothiophene (4,6-DMDBT), respectively.

IV.1. Toluene hydrogenation at constant sulfur content in High Throughput Unit

These tests have been carried out in a high throughput unit which can test up to 16 catalysts at the same time. The goal of this test is the evaluation of the activity of sulfided catalysts, determined by the reaction of toluene hydrogenation and the isomerization of cyclohexane, in presence of H_2S and under hydrogen pressure. The feedstock used for the test consists of:

- 5.88 wt% of dimethyldisulfide (DMDS) (4 wt% S),
- 20 wt% of toluene,
- 74.12 wt% of cyclohexane.

This feedstock has a density of 0.795 g.cm^{-3} . The catalytic testing is performed in a gas phase, in a fixed bed reactor, and is divided in two steps. The first step is the *in situ* activation of the catalyst and the second step is the test of the catalyst. Figure III.13 represents the progress of a test.

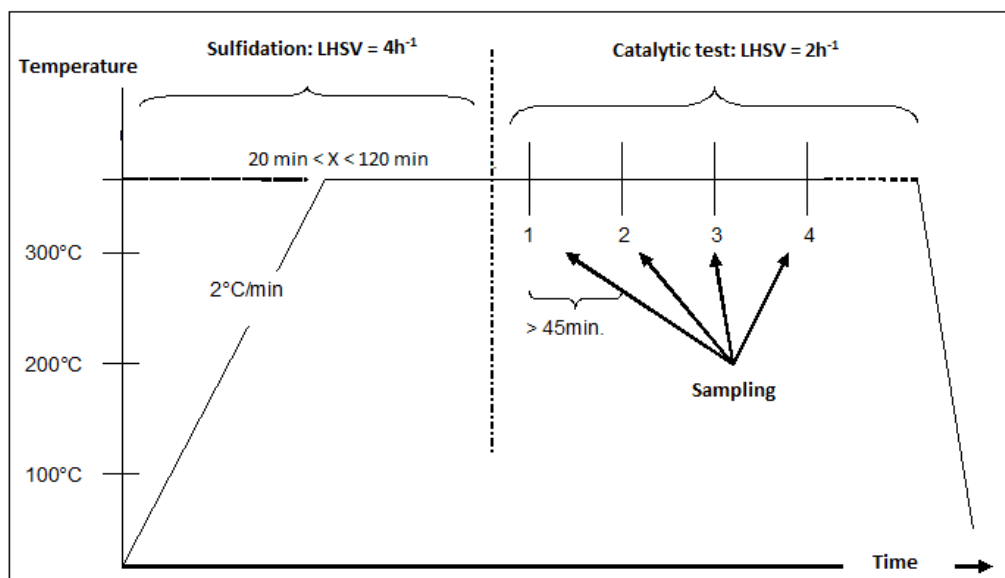


Figure III.13: Schematic representation of the progress of a test

During the sulfidation step, the pressure is 6 MPa, the Liquid Hourly Space Velocity (LHSV) is of 4 h^{-1} , the ratio $H_2/\text{feedstock}$ is $450 \text{ l}_N/\text{l}$ and the temperature is 350°C with a ramp rate of $2^\circ\text{C}\cdot\text{min}^{-1}$ to reach this temperature. The sulfidation time is 1h. After this step, the test phase is performed with the same operating conditions excepted for the LHSV which is decreased at 2 h^{-1} . The test is performed for 375 min and a sampling is done during along the test. Products are analyzed by Gas Chromatography. Table III.6 represents sulfidation and test conditions and Table III.7 summarizes the partial pressures (P_P) of reactants considering the ratio H_2/HC .

Table III.6: Experimental conditions for the hydrogenation of toluene

	<i>Sulfidation</i>	<i>Test</i>
<i>Pressure</i>	6 MPa	6 MPa
<i>LHSV</i>	4 h ⁻¹	2 h ⁻¹
<i>Ratio H₂/HC</i>	450 nL/l	450 nL/l
<i>Ramp rate</i>	2°C/min	X
<i>Temperature</i>	350°C	350°C
<i>Time</i>	60 min	375 min

Table III.7: Partial pressures of reactants for a total pressure of 6 MPa and a ratio H₂/HC of 450 nL/l

<i>Total pressure of 6 MPa</i>	
<i>p_{pH2}</i>	3.68 MPa
<i>p_{pH2S}</i>	0.215 MPa
<i>p_{pCH4}</i>	0.215 MPa
<i>p_{pToluene}</i>	0.37 MPa
<i>p_{pCC6}</i>	1.52 MPa

During the test, several products are formed and their quantification permits to obtain the activity of hydrogenation and the rate of cyclohexane isomerization. The latter provides information about the acidity of the catalyst. Below are shown simplified mechanisms of these reactions as well as the equations allowing the comparison of catalysts.

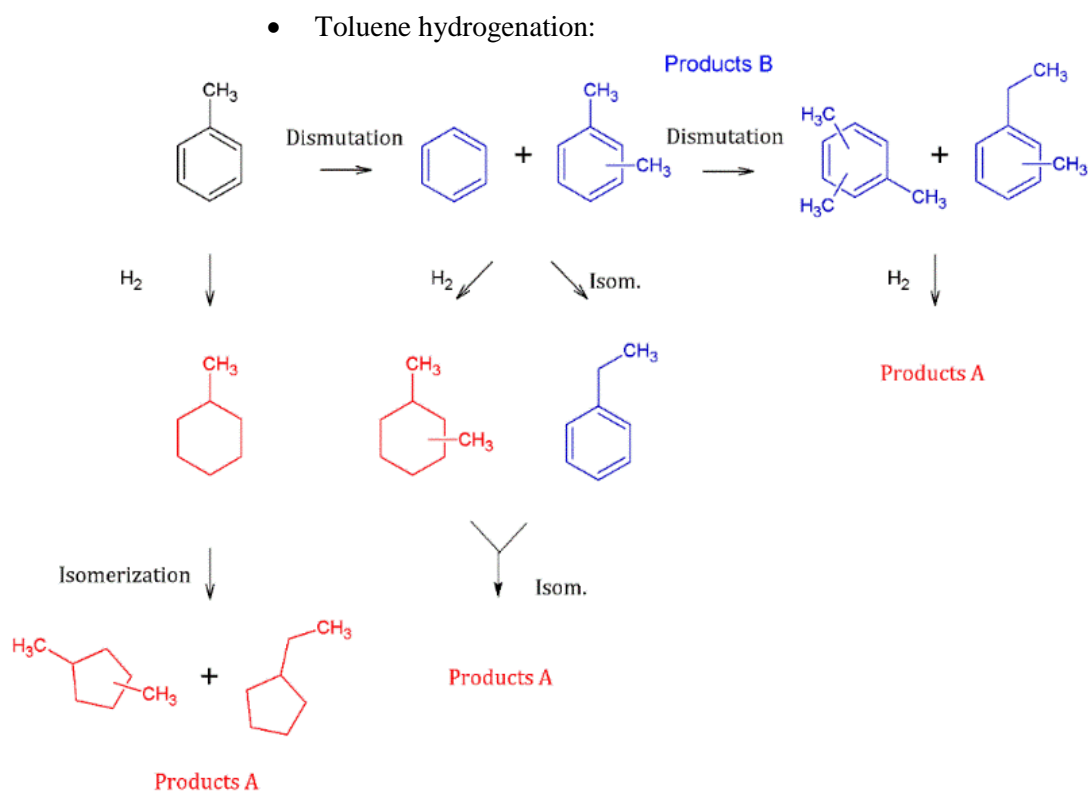


Figure III.14: Reaction pathway of toluene hydrogenation

Figure III.14 shows the hydrogenation pathways of toluene. In red are represented the products resulting of toluene hydrogenation and named products A. In blue are represented products resulting of dismutation of toluene and are not hydrogenated; they are named products B. Products A leading to hydrogenated compounds are not represented.

In the case of the toluene hydrogenation, a hydrogenation activity A can be calculated using Eq. III.6 and considering a first order reaction with respect to toluene.

$$X = \left(\frac{\Sigma \% \text{ mol of products A}}{\Sigma \% \text{ mol of products A} + \Sigma \% \text{ mol of products B (including unconverted toluene)}} \right) \quad \text{Eq. III.6}$$

To provide a basis for comparing global hydrogenation activity of different catalysts, a reaction rate constant K_{Tol} has been applied. This reaction rate constant is expressed in mole of toluene per mole of molybdenum per hour and its calculation is displayed in Eq. III.7.

$$K_{Tol} = \frac{\ln\left(\frac{100}{100-X}\right) * LHSV * d * [Tol] * M_{Mo}}{FPD * M_{Tol} * [Mo]} \quad \text{Eq. III.7}$$

With:

- $LHSV$ represents the Liquid Hourly Space Velocity, which is the ratio between the volume of catalyst and the volume of feedstock, in h^{-1} ,
- d represents the feedstock density in g.mL^{-1} ,
- $[Tol]$ represents the weight concentration of toluene in the feedstock, in wt%,
- M_{Mo} represents the molar mass of molybdenum, in g.mol^{-1} ,
- FPD represents the filled packed density, in g.mL^{-1} ,
- M_{Tol} represents the molar mass of toluene, in g.mol^{-1} ,
- $[Mo]$ represents the weight concentration of molybdenum in the catalyst, in wt%.

The different catalysts tested in toluene hydrogenation will be compared to their reaction rate constants, in order to avoid differences of molybdenum content and filled packed density.

Catalysts, which have given the most interesting results in toluene hydrogenation, have been testing in hydrodesulfurization of dibenzothiophene (DBT) and some in hydrodesulfurization of 4,6-dimethyldibenzothiophene (4,6-DMDBT). Experimental conditions of these tests are presented in the following part.

IV.2. Hydrodesulfurization of DBT and 4,6-DMDBT in a fixed bed reactor

These tests of HDS of DBT and 4,6-DMDBT have been performed in a fixed bed reactor in a unit located at IFPEN Solaize. Prior to the test, catalysts were sulfided *in situ*; experimental conditions of sulfidation and tests are commented in detail below.

IV.2.1. Hydrodesulfurization of DBT

In order to perform the sulfidation *in situ* of the catalyst, a feedstock composed of 5.88 wt% of dimethyldisulfide (DMDS) in ortho-xylene has been used. Then to perform the test, the feedstock used is presented in Table III.8. Experimental parameters concerning the sulfidation and testing steps are summarized in Table III.9. The volume of catalyst used for each test was of 0.5 mL.

Table III.8: Feedstock used for the HDS of DBT

<i>Product</i>	<i>Weight fraction (%)</i>
Dimethyldisulfide (DMDS)	1.2
Dibenzothiophene (DBT)	1.2 (2000 ppm S)
N-hexadecane (n-C16)	0.8
Ortho-xylene (o-xylene)	96.8

Table III.9: Experimental conditions of the HDS test of DBT

	<i>Sulfidation</i>	<i>Test</i>
<i>Pressure</i>		3 MPa
<i>LHSV</i>		32 h ⁻¹
<i>Ratio H₂/HC</i>	450 nL/l	562.5 nL/l
<i>HC flow</i>	8 mL.h ⁻¹	16 mL.h ⁻¹
<i>Temperature</i>	350°C	290-320°C
<i>Time</i>	3 h	

As detailed in the bibliography study, desulfurization of DBT occurs via two main pathways, the direct desulfurization route (DDS) and the hydrogenation route (HYD). The DDS leads to biphenyls (BP) whereas the HYD yields to tetra- and hexa- hydrodibenzothiophenes (THDBT and HHDBT) and then to cyclohexylbenzenes (CHB) and dicyclohexyls (DCH). The different products resulting of these pathways are summarized in Figure III.15.

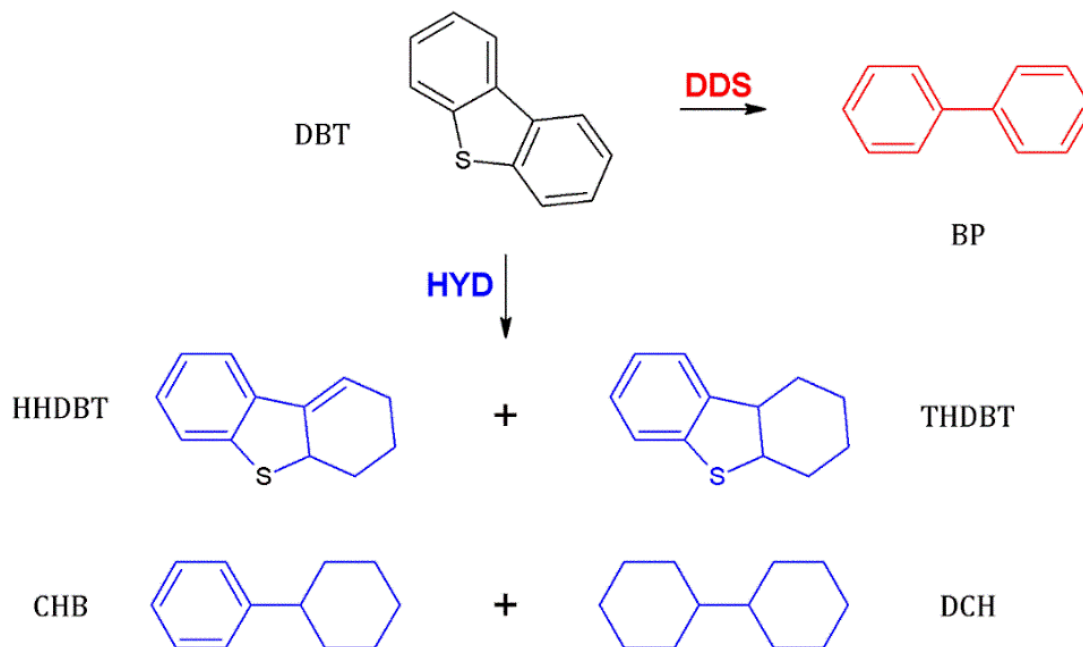


Figure III.15: Products of the DBT hydrodesulfurization

As results of testing, several information can be highlighted. The test being performed at different temperatures; it is therefore possible to obtain conversion of DBT at these temperatures as well as selectivities in products. From these conversions, it is possible to obtain the reaction rate constant

k of the pseudo-first-order reaction of DBT HDS. A selectivity DDS/HYD can also be determined by using reaction rate constants associated to DDS and HYD pathways. All equations permitting to obtain these values are presented in the section IV.2.3 of this chapter.

IV.2.2. Hydrodesulfurization of 4,6-DMDBT

This sulfur compound being more viscous than DBT, several problems have been encountered during the testing phase. The DBT has thus been chosen in priority to test all catalysts, only several catalysts have been tested using 4,6-DMDBT as sulfur compound

Feedstocks used to perform the *in situ* sulfidation and the test are described in Table III.10 as well as experimental parameters applied during this test are summarized in Table III.11.

Table III.10: Feedstocks used for the sulfidation and the testing in HDS of 4,6-DMDBT

Sulfidation		Test	
<i>Product</i>	<i>Weight fraction (%)</i>	<i>Product</i>	<i>Weight fraction (%)</i>
Cyclohexane (CC6)	74.12	Cyclohexane (CC6)	58.57
Dimethyldisulfide (DMDS)	5.88	Dimethyldisulfide (DMDS)	0.6
Ortho-xylene (o-xylene)	20.00	Ortho-xylene (o-xylene)	40
		Quinoleine	0.5
		4,6-dimethyldibenzothiophene (4,6-DMDBT)	0.33 (500 ppm S)

Table III.11: Experimental conditions of HDS of 4,6-DMDBT

	<i>Sulfidation</i>	<i>Test</i>
<i>Pressure</i>	3 MPa	3 MPa
<i>LHSV</i>	4h ⁻¹	4 h ⁻¹
<i>Ratio H₂/HC</i>	240 nL/l	240 nL/l
<i>HC flow</i>	16 mL.h ⁻¹	16 mL.h ⁻¹
<i>Temperature ramp rate</i>	1.7°C.min ⁻¹	
<i>Temperature</i>	350°C	300-320°C
<i>Time</i>	1 h	

As for the HDS of DBT, HDS of 4,6-DMDBT occurs via two main pathways: the hydrogenation route (HYD) and the direct desulfurization route (DDS). A schematic of these reaction pathways is presented in Figure III.16. For this simplified reaction pathway, products obtained via the HYD pathway are methylcyclohexanetoluene (MCHT) and dimethyldicyclohexane (DMDCH) whereas product obtained via the DDS pathway is dimethylbiphenyl (DMBP).

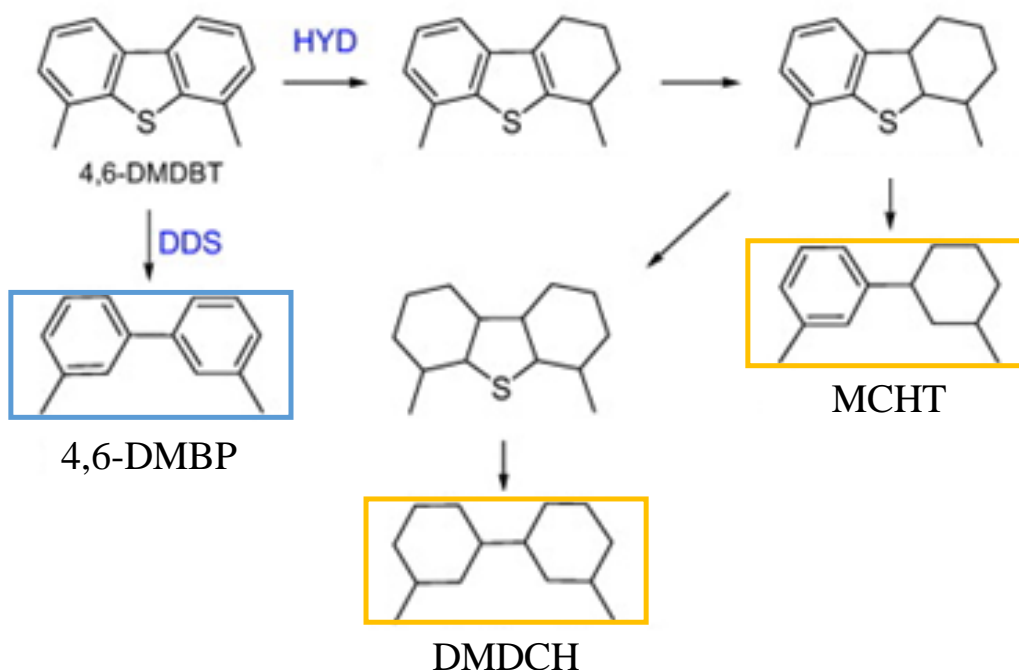


Figure III.16.:Schematic representation of the two pathways for the HDS of 4,6-DMDBT

IV.2.3. Evaluation of catalysts

First, the total conversion of 4,6-DMDBT can be calculated by using Eq. III.8. In addition, conversions of 4,6-DMDBT through both HYD and DDS pathways can be calculated using Eq. III.9 and Eq. III.10, respectively.

$$\%X_{4,6-DMDBT} = \frac{n_{\text{Products of 4,6-DMDBT conversion}}}{n_{4,6-DMDBT, \text{total}}} \times 100 \quad \text{Eq. III.8}$$

$$\%X_{HYD} = \frac{n_{HYD}}{n_{4,6-DMDBT, \text{total}}} \times 100 \quad \text{Eq. III.9}$$

$$\%X_{DDS} = \frac{n_{DDS}}{n_{4,6-DMDBT, \text{total}}} \times 100 \quad \text{Eq. III.10}$$

Where

$$n_{HYD} = n_{DMDCH} + n_{MCHT}$$

$$n_{DDS} = n_{DMBP}$$

And with n representing the number of moles of HYD or DDS products. Then, from these conversions, it is possible to calculate a reaction rate constant (k_{HDS}) and reaction rate constants associated to each pathway (k_{HYD} and k_{DDS}) using the Eq. III.11.

$$k_X = \frac{\ln\left(\frac{100}{100-X}\right) * LHSV * d * [DMDBT] * M_{Mo}}{FPD * M_{DMDBT} * [Mo]} \quad \text{Eq. III.11}$$

With:

- $LHSV$ represents the Liquid Hourly Space Velocity, which is the ratio between the volume of catalyst and the volume of feedstock, in h^{-1} ,
- d represents the feedstock density in g.mL^{-1} ,
- $[DMDBT]$ represents the weight concentration of DMDBT in the feedstock, in wt%,

- M_{Mo} represents the molar mass of molybdenum, in $\text{g}\cdot\text{mol}^{-1}$,
- FPD represents the filled packed density, in $\text{g}\cdot\text{mL}^{-1}$,
- M_{DMDBT} represents the molar mass of toluene, in $\text{g}\cdot\text{mol}^{-1}$
- $[Mo]$ represents the weight concentration of molybdenum in the catalyst, in wt%.

As experiments have been carried out at different temperatures, we can calculate an activation energy for the reaction for each catalyst. For that, we have calculated the different k for each temperature and then we have plotted the logarithm of each k as a function of $1/T$ in order to obtain a $\ln(k_0)$ and the activation energy by using the Arrhenius equation.

$$k = k_0 e^{\left(\frac{E_a}{RT}\right)} \quad \text{Eq. III.12}$$

These activation energies have been calculated for each rate constant (total, via HYD pathway and via DDS pathway).

V. Conclusion

Through this chapter, we have described all experimental parameters we used to perform synthesis of our HDS catalyst precursors in a batch reactor using scCO_2 to precipitate oxide species onto the surface of alumina. All characterization techniques employed have also been highlighted with information that we can obtain from each analysis as well as explanations about treatments of data.

In situ Raman measurements allowed to monitor the reaction occurring during the treatment of the impregnated sample either via a classical thermal treatment or via thermal treatment under an atmosphere containing scCO_2 . Results of these experiments are presented in the chapter dealing with the understanding of chemistry occurring during the preparation of HDS catalyst precursors.

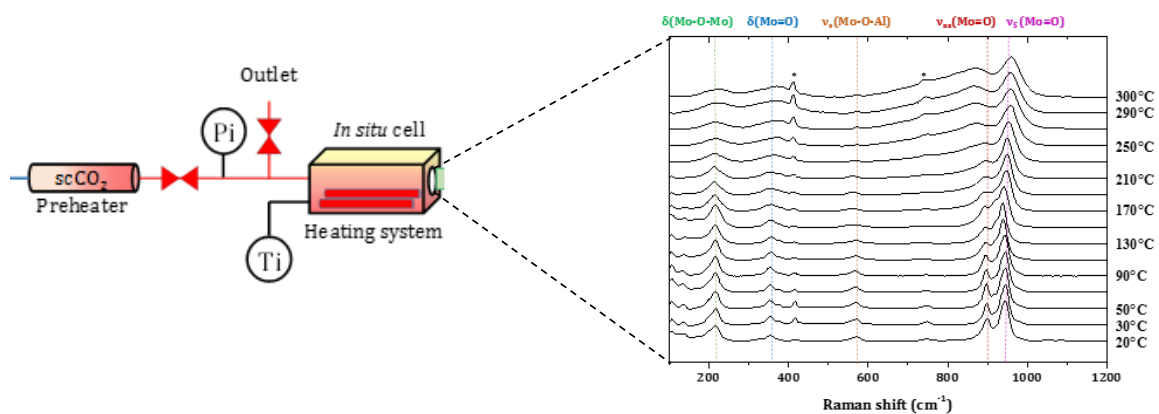
Experimental parameters of the synthesis of HDS catalyst precursors in a batch reactor have also been described with the different effects about which we have played on. Characterizations, allowing the determination of oxide phase present on the alumina surface after synthesis, have also been detailed.

Last part of this chapter was dedicated to the characterizations of sulfided catalysts using XPS and HR-TEM as well as the testing of catalysts. For that, three different catalytic tests were performed. Study of the hydrogenation of toluene, in order to obtain the hydrogenation ability of these catalysts, was the testing performed on all synthesized materials. Those which have given the best results have then been tested in HDS of DBT and/or 4,6-DMDBT.

VI. Bibliography

- [1] H. Topsøe, B.S. Clausen, F.E. Massoth, *Catalysis*, Springer Berlin Heidelberg, Berlin, Heidelberg, 1996.
- [2] H. Beuther, R.A. Flinn, J.B. McKinley, for better hydrodesulfurization activity of promoted molybdenum oxide–alumina catalysts, *Ind. Eng. Chem.* 51 (1959) 1349–1350.
- [3] A. Gandubert, C. Legens, D. Guillaume, S. Rebours, E. Payen, X-ray Photoelectron Spectroscopy surface quantification of sulfided CoMoP Catalysts – relation between activity and promoted sites – Part I: Influence of the Co/Mo Ratio, *Oil Gas Sci. Technol. - Rev. l'IFP.* 62 (2007) 79–89.
- [4] G. Mestl, In situ Raman spectroscopy - a valuable tool to understand operating catalysts, *J. Mol. Catal. A Chem.* 158 (2000) 45–65.
- [5] A. Galtayries, S. Wisniewski, J. Grimblot, Formation of thin oxide and sulphide films on polycrystalline molybdenum foils: characterization by XPS and surface potential variations, *J. Electron Spectros. Relat. Phenomena.* 87 (1997) 31–44.
- [6] A. D. Gandubert, E. Krebs, C. Legens, D. Costa, D. Guillaume, P. Raybaud, Optimal promoter edge decoration of CoMoS catalysts: A combined theoretical and experimental study, *Catal. Today.* 130 (2008) 149–159.
- [7] A.D. Gandubert, C. Legens, D. Guillaume, E. Payen, X-ray photoelectron spectroscopy surface quantification of sulfided CoMoP catalysts. Relation between activity and promoted sites. Part II: Influence of the sulfidation temperature, *Surf. Interface Anal.* 38 (2006) 206–209.
- [8] A.M. Venezia, X-ray photoelectron spectroscopy (XPS) for catalysts characterization, *Catal. Today.* 77 (2003) Italian Chem Soc, Gruppo Int Catalisi. doi:10.1016/S0920-5861(02)00380-2.

Chapter IV: Monitoring of the preparation of HDS catalyst precursors by *in situ* Raman spectroscopy



I. INTRODUCTION.....	119
II. REFERENCE RAMAN SPECTRA OF STARTING MATERIALS	120
III. <i>IN SITU</i> INVESTIGATION OF THE PREPARATION OF HDS CATALYST PRECURSORS USING AHM AS MO SOURCE.....	123
III.1. EVOLUTION OF SPECIES UNDER AIR DRYING	123
III.2. EVOLUTION OF SPECIES UNDER SCCO ₂ DRYING.....	126
III.3. CONCLUSION ABOUT EXPERIMENT UNDER AIR AND UNDER SCCO ₂	130
IV. <i>IN SITU</i> INVESTIGATION OF THE PREPARATION OF HDS CATALYST PRECURSORS USING PHOSPHOMOLYBDIC ACID (HPA)	132
IV.1. EVOLUTION OF SPECIES AFTER AGEING	132
IV.2. <i>IN SITU</i> INVESTIGATION OF IMPREGNATION OF ALUMINA WITH HPA.....	134
IV.2.1. <i>Evolution of species under air drying</i>	134
IV.2.2. <i>Evolution of Mo species under scCO₂ drying</i>	135
IV.3. CONCLUSION ABOUT THE USE OF HPA AS MO SOURCE	138
V. CONCLUSION	140
VI. BIBLIOGRAPHY.....	142

I. Introduction

This part is dedicated to the understanding of the chemistry occurring in our process during the preparation of HDS catalyst precursors and more particularly the oxometallic phase of these catalysts before sulfidation. The main studied parameter is the use of supercritical carbon dioxide (scCO₂) to favor the precipitation and diffusion of the metallic precursors. In order to compare the use of scCO₂ against a conventional drying step, experiments were conducted under both atmosphere: scCO₂ and air.

We have chosen to use *in situ* Raman spectroscopy to monitor the catalyst precursor preparation which takes place on the surface of the support. This characterization technique provides fundamental molecular-level information about the catalyst surface structure [1]. Another advantage of this technique is its ease of use, because no preparation or pretreatment of the sample are required. However, one of the main limitation of this characterization technique is the small intensity of the Raman signal, which can be easily masked by the fluorescence of the sample [2]. Fluorescence being several order of magnitude more intense than the Raman signal. All the procedures employed to monitor the preparation of HDS catalyst precursors are detailed in the experimental part of this work (see Chapter III).

This *in situ* Raman study will allow us to optimize our preparation conditions for the future syntheses of the catalyst precursor. The first studied parameter was the molybdenum source. For that, two commonly used molybdenum sources have been tested: ammonium heptamolybdate (AHM) and phosphomolybdic acid (HPA). These experiments were performed with and without the cobalt promoter (cobalt nitrate) in order to see its influence on the resulting oxide species. The second investigated parameter was the solvent of impregnation. We have tested two solvents: water and ethanol. Finally, *in situ* experiments were carried out in air or in scCO₂.

First of all, reagents employed in this work (support: δ -Al₂O₃, ammonium heptamolybdate (AHM), phosphomolybdic acid (HPA) and cobalt nitrate) were characterized by Raman spectroscopy and their vibrational bands were assigned. Results are presented in the following part.

II. Reference Raman spectra of starting materials

The selected support in this work was a δ -alumina (δ -Al₂O₃) provided by IFPEN and its Raman spectrum is shown in Figure IV.1. A fluorescence of this material is observed, especially at high wavenumber. This fluorescence could hinder Raman signals of the species present on the surface and generates difficulties in the assignments of species. This strong fluorescence background can be attributed to the presence of defect sites and/or due to a laser-induced electronic excitation of surface -OH groups [3,4]. However, a work with a high-energy laser and at low wavenumbers regions is going to permit to reduce fluorescence and to observe weak Raman bands related to oxometallic species.

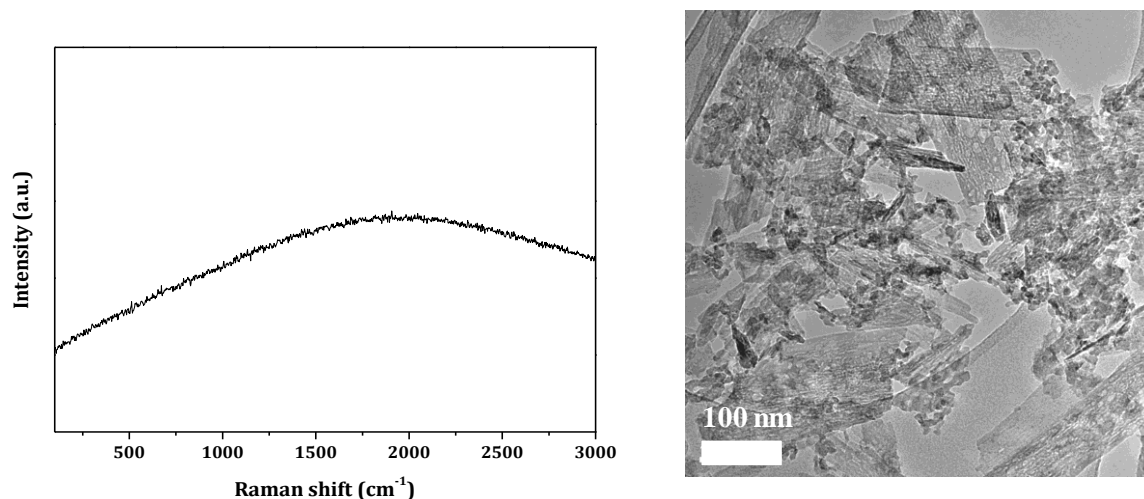


Figure IV.1: Raman spectra and TEM picture of δ -Al₂O₃ provided by IFPEN.

The alumina support is composed of a mixture of mesoporous platelets having different sizes.

- *Raman spectrum of ammonium heptamolybdate*

The first molybdenum source selected to prepare the catalyst precursors was the ammonium heptamolybdate tetrahydrate (NH₄)₆Mo₇O₂₄·4H₂O. Figure IV.2 represents the Raman spectra of a (NH₄)₆Mo₇O₂₄·4H₂O solid powder.

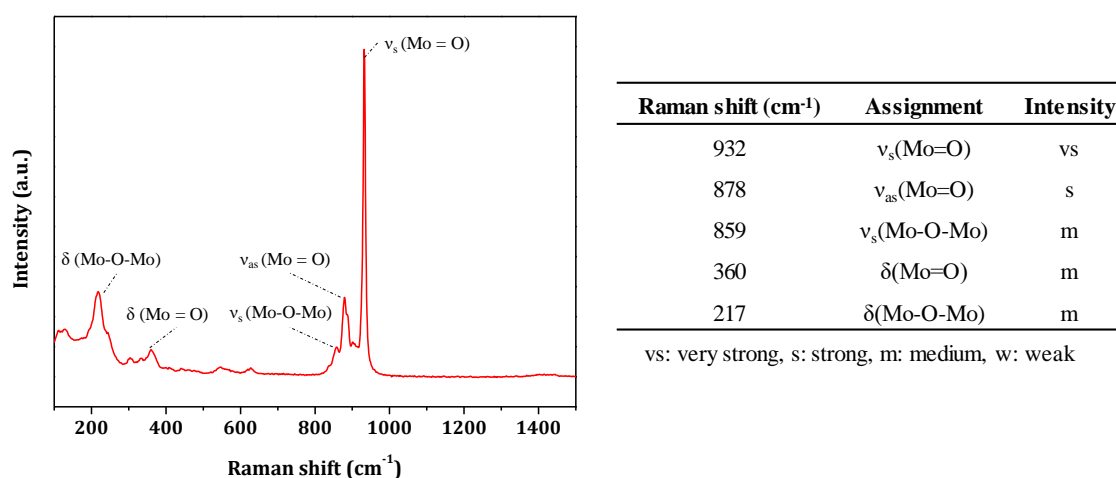


Figure IV.2: Raman spectra of ammonium heptamolybdate (left) and band assignments (right).

This compound possesses several bands and most intense ones can be assigned to the stretching and bending modes of Mo=O bonds or Mo-O-Mo bonds [5–9].

Suggested by Lindqvist [10], the structure of the polyanion has been confirmed by other groups [11] and consists of seven MoO₆ octahedra condensed by edges sharing three prominent zones of faces parallel to the axes [100], [001] and [101].

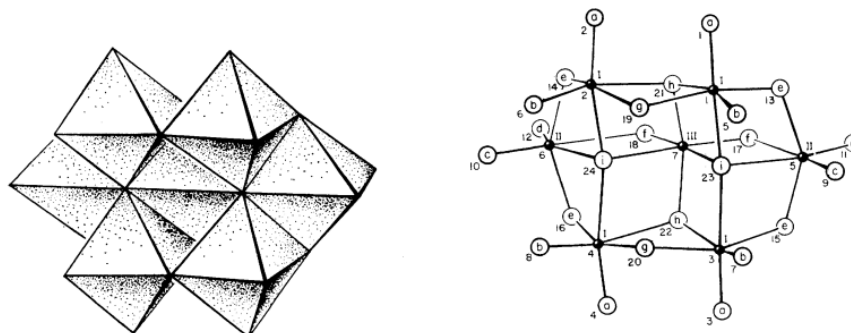


Figure IV.3: Left : MoO₆ groups as condensed polyhedra ; Right : bonding between atoms and atom numbering system (see [11] for further information)

The octahedral coordinated clusters are characterized by Raman bands attributed to the symmetric (890-1000 cm⁻¹ region) and asymmetric (830-970 cm⁻¹ region) stretching modes of the terminal Mo=O bonds [8]. Bands around 310-370 cm⁻¹ region are attributed to the bending mode of the Mo=O terminal bond, and the band around 850-870 cm⁻¹ region and 210-220 cm⁻¹ region are attributed to the symmetric stretching and bending modes of Mo-O-Mo bonds, respectively [5]. A representation of the polymolybdate ion Mo₇O₂₄⁶⁻ can be found in Figure IV.3.

- *Raman spectrum of phosphomolybdic acid*

Phosphomolybdic acid, H₃PMo₁₂O₄₀.xH₂O, is a heteropolyanion with a Keggin structure [12]. It consists of arrangements of MoO₆ octahedra around a central PO₄ tetrahedron. A representation of the heteropolyanion is shown in Figure IV.4.

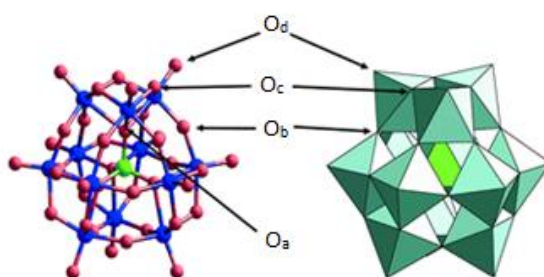


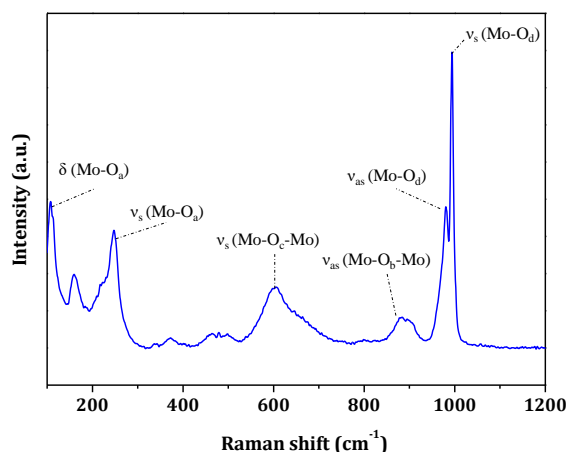
Figure IV.4: Representation of H₃PMo₁₂O₄₀ heteropolyanion with a Keggin structure (adapted from [13])

The 12 MoO₆ octahedra are connected by shared edges to form trimetallic Mo₃O₁₃ groups. In blue are Mo atoms, in green is the P atom and in red are the O atoms. Oxygen atoms present in the Keggin structure are not equivalent and four different types can be identified:

- 12 oxygen atoms, denoted O_d, which are linked to a single Mo atom,

- 12 oxygen atoms, denoted O_c, which are connected to two MoO₆ octahedra inside a trimetallic M₃O₁₃ group,
- 12 oxygen atoms, denoted O_b, which are connected to two trimetallic groups,
- 4 oxygen atoms, denoted O_a, which are common to PO₄ tetrahedron and to the three octahedral of a single trimetallic group.

The difference of oxygen atoms has an influence on the vibration bands positions in the Raman spectra of the heteropolyanion. Figure IV.5 represents the Raman spectra of the phosphomolybdic acid.



Observed(cm ⁻¹)	Assignment	Observed(cm ⁻¹)	Assignment
986 (vs)	v _s (Mo-O _d)	255 (w)	δ(O _c -Mo-O _c), δ(O _b -Mo-O _b)
971 (sh)	v _{as} (Mo-O _d)	246 (s)	v _s (Mo-O _a), δ(Mo-O _b -Mo)
964 (m)	v _{as} (Mo-O _d)	215 (w)	δ(Mo-O _b -Mo)
894 (w)	v _{as} (Mo-O _b -Mo)	203 (w)	δ(Mo-O-Mo), δ(O-Mo-O)
603 (m)	v _s (Mo-O _c -Mo), δ(Mo-O _c -Mo)	169 (w)	δ(Mo-O-Mo), δ(O-Mo-O)
465 (vw)	δ(Mo-O _b -Mo)	154 (w)	δ(Mo-O-Mo), δ(O-Mo-O)
451 (vw)	δ(Mo-O _b -Mo)	109 (s)	δ(Mo-O-Mo), δ(O-Mo-O)
370 (vw)	δ(Mo-O _b -Mo)	84	δ(Mo-O-Mo), δ(O-Mo-O)

vs: very strong, s: strong, m: medium, w: weak

Figure IV.5: Raman spectra of H₃PMo₁₂O₄₀.xH₂O (top) and band assignments (bottom).

Many vibration bands are observed on the Raman spectra of this heteropolyanion due to the different types of oxygen [14–16]. These vibration bands can be assigned to different bonds and vibrational modes and are presented in Figure IV.5. For the symmetric and asymmetric stretching modes of Mo-O_d, the region is located around 960-1000 cm⁻¹. For the Mo-O_b-Mo bonds, vibrational modes are located between 850-890 cm⁻¹ and for the Mo-O_c-Mo bonds, vibrational modes are between 600-800 cm⁻¹. Except for the Mo-O_d bonds, other bonds possess also bending modes of vibrations.

- *Raman spectra of cobalt nitrate hexahydrate (Co(NO₃)₂.6H₂O)*

The cobalt precursor does not possess many vibration bands and the most intense is due to the symmetric and asymmetric stretching modes of nitrates species NO₃⁻. Figure IV.6 represents the Raman spectra and assignments of bands of the solid compound of cobalt nitrate hexahydrate.

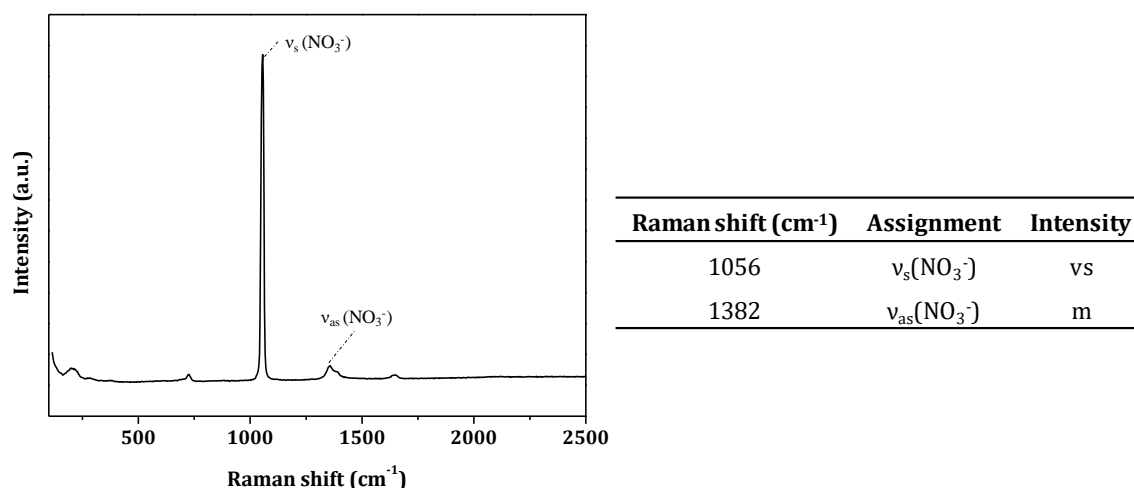


Figure IV.6: Raman spectra of cobalt nitrate hexahydrate (left) and assignments of vibrational bands (right).

III. *In situ* investigation of the preparation of HDS catalyst precursors using AHM as Mo source

In this part, we studied the preparation of the HDS catalyst precursor (catalyst before its activation by sulfidation) by using ammonium heptamolybdate (AHM) as Mo source. The solvent of impregnation used was distilled water due to the insolubility of AHM in alcohols. The preparation has been carried out with and without the cobalt promoter. In order to investigate the effect of *scCO*₂ on the HDS catalyst precursor preparation, the evolution of species was also studied under air, the common atmosphere for the drying of a HDS catalyst, for comparison. Figure IV.7 represents the different *in situ* experiments conducted with AHM as Mo source.

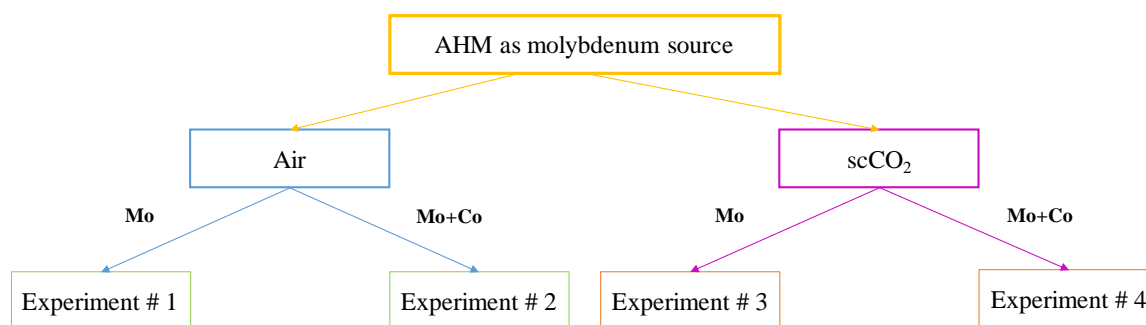


Figure IV.7: Experiments carried out using AHM as Mo source.

III.1. Evolution of species under air drying

The support has been impregnated with AHM to obtain a coverage of approximately 6 at (Mo).nm⁻² corresponding to a Mo loading of 10 wt.%, which means a high coverage and has been aged for a period of 24 h. Then, the experiment has been performed by increasing the temperature and Raman spectra have been recorded each 20°C after 10 min stabilization of the temperature. A temperature around 300°C has been reached at the end of the experiment and maintained for 15 min. Figure IV.8 shows the evolution of Raman spectra with the temperature.

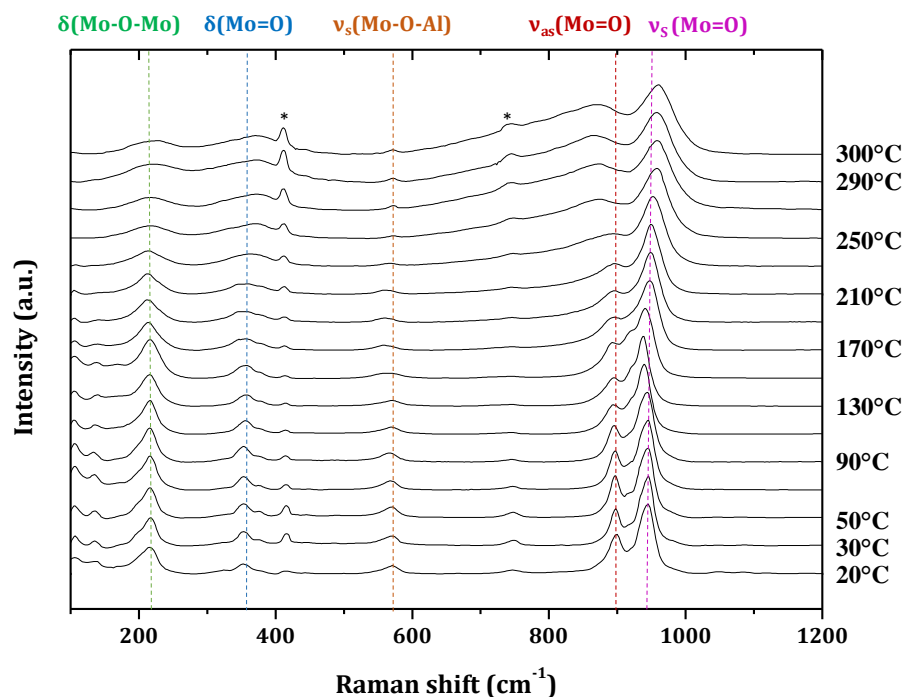


Figure IV.8: Raman spectra showing the evolution of the Mo species under air when increasing temperature (* represents Raman bands of the cell).

At room temperature, the Raman spectrum exhibits bands at 945 and 900 cm^{-1} , respectively assigned to the symmetric ($\nu_s(\text{Mo}=\text{O})$) and asymmetric ($\nu_{as}(\text{Mo}=\text{O})$) stretching mode of terminal Mo=O bond of dioxo cores of supported oxomolybdate species [17,18]. Bands at 571, 352 and 216 cm^{-1} are also observed. The band at 352 cm^{-1} is assigned to the deformation modes of the terminal Mo=O groups ($\delta(\text{Mo}=\text{O})$) whereas the band at 216 cm^{-1} is associated with the deformation modes of the bridging Mo-O-Mo bonds ($\delta(\text{Mo-O-Mo})$) [19,20]. The band located at 571 cm^{-1} is characteristic of a Al-O-Mo stretching mode [21]. All these bands are the fingerprint of an Anderson heteropolyanion ($\text{Al}(\text{OH})_6\text{Mo}_6\text{O}_{18}^{3-}$), denoted AlMo_6 [22].

The formation of this Anderson heteropolyanion has already been reported by Carrier et al. [22] and is due to the partial dissolution of alumina favored by the acidity of the solution of impregnation ($\text{pH} = 5\text{-}6$). Indeed, for high Mo coverage (greater than 2 at $\text{Mo}\cdot\text{nm}^{-2}$), all basic sites of alumina are neutralized by the solution and the buffer effect of the support is no longer predominant. The release from the support of several Al^{3+} ions is observed (and these ions react with the heptamolybdate ions to form an Anderson heteropolyanion AlMo_6 (see Chapter II for detailed information)) [23,24]. The release of Al^{3+} ions occurs during the maturation stage. Bergwerff et al. [25] have observed the formation of this Anderson heteropolyanion at the exterior of the catalyst bodies after a period of 30 min of maturation. AlMo_6 entities react with NH_4^+ ions to form a precipitate $(\text{NH}_4)_3[\text{Al}(\text{OH})_6\text{Mo}_6\text{O}_{18}]$ with a low solubility.

When the temperature is increased, a shift of the band assigned to $\nu_s(\text{Mo}=\text{O})$ towards higher wavenumbers is observed to reach a value of 960 cm^{-1} . This shift can be assigned to the shortening of Mo-O bonds upon dehydration [26–28].

At 150°C, a shift of the band located at 571 cm^{-1} , assigned to Al-O-Mo stretching mode, towards lower wavenumbers is also observed with the increase of the temperature. During dehydration, the net charge of the hydroxyl groups from $\text{Al}(\text{OH})_6$ octahedron is diminished, which weakens the Al-

O vibration [26]. At higher temperatures, the decrease of this band intensity suggests a partial decomposition of AlMo_6 entities starting for temperatures around 170-180°C. This observation is in agreement with the temperature of decomposition of AlMo_6 entities [26,29].

At a temperature of 300°C, bands are broader than at the beginning of the experiment and are located at 960, 871, 370 and 227 cm^{-1} . These bands can be assigned to well dispersed polymeric molybdate species [30,31].

This *in situ* investigation following of the molybdenum species during drying of the catalyst under air takes only in account the exterior surface of alumina pellets. Molybdenum species present in the core of the extrudate may be different. This heterogeneity of species as a function of the position on the pellet has been described by Bergwerff et al [24].

After a period of maturation of 24h, the presence of AlMo_6 compounds onto the surface of the alumina's pellet has been observed. These entities have then been decomposed during drying. A broadening of Raman bands has suggested a dispersion of molybdenum species with the formation of polymolybdates at the end of the experiment. These species may be reformed upon transfer in the wet air [32].

The second experiment was performed in the same way with the exception that cobalt was added to the impregnation solution. For that, alumina has been impregnated with a solution of AHM as Mo source and cobalt nitrate as Co promoter in order to obtain a Mo coverage of approximately 6 at $(\text{Mo})\cdot\text{nm}^{-2}$ and a molar ratio $\text{Co}/(\text{Co}+\text{Mo})$ of 0.3. Raman spectra recorded along the synthesis are presented in Figure IV.9.

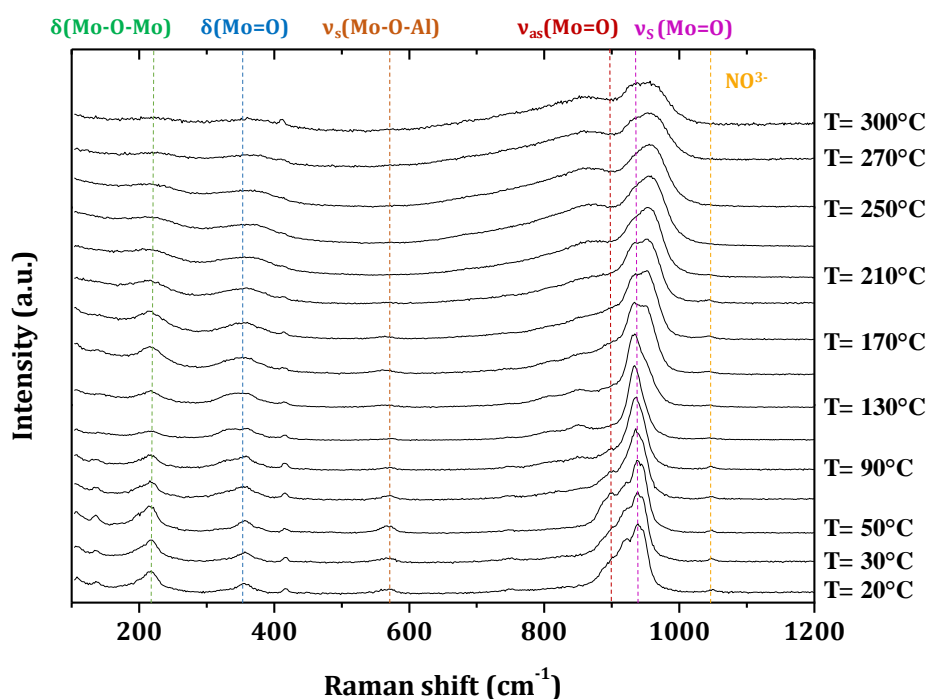


Figure IV.9: Raman spectra showing the evolution of species under air when increasing temperature.

In this case, we observe that Raman bands of the spectrum recorded at room temperature are similar to those observed in the previous experiment. The only exception is a lower intensity for the band located at 900 cm^{-1} and assigned to the asymmetric stretching mode of $\text{Mo}=\text{O}$. However, other bands have been assigned to the presence of the Anderson heteropolyanion AlMo_6 . The band

assigned to the symmetric stretching mode of the Mo=O bonds is located at 940 cm^{-1} . Whereas, the band corresponding to the stretching mode of Al-O-Mo is observed at 570 cm^{-1} .

When the temperature has reached 300°C , the symmetric stretching band of Mo=O has been shifted towards higher wavenumbers to reach 957 cm^{-1} . This shift suggests, as in the previous experiment, the presence of polymeric molybdate species. A decrease of the band located at 570 cm^{-1} suggests a decomposition of AlMo_6 entities with the temperature. Furthermore, the broadening of Raman bands suggests that polymeric molybdate species are well-dispersed onto the surface of alumina. However, a heterogeneity of species may be present depending of pellets analyzed [32].

Both experiments have shown similar results. The presence on the surface of the pellet of AlMo_6 entities has been observed regardless to the presence of promoter in the impregnation solution. An increase of the temperature has led to the decomposition of these species and to an increase of the dispersion of molybdenum. Final species have been attributed to polymeric molybdates. XRD characterization was performed on samples and no diffraction peaks attributed to molybdenum species have been observed, suggesting the presence of an amorphous phase and/or the presence of very small crystallites amorphous to XRD. Results obtained from *in situ* investigations following the drying of alumina pellets impregnated with AHM are in agreement with literature [21,25,32,33].

III.2. Evolution of species under scCO_2 drying

In these experiments, same procedures have been used than previously with the exception that catalysts were dried under scCO_2 .

First, alumina support has been impregnated with 10 wt.% of Mo and catalyst has been aged for 24 h. After maturation, the catalyst was placed in the *in situ* cell to perform the experiment (experimental parameters are detailed in Chapter III). The temperature was then increased up to 50°C and after 10 minutes of stabilization, scCO_2 was injected (up to 8 MPa) into the cell. Experiment was performed under the scCO_2 atmosphere and Raman spectra were recorded each 10-15 minutes. Figure IV.10 represents the evolution of recorded Raman spectra with the increase of the temperature under scCO_2 .

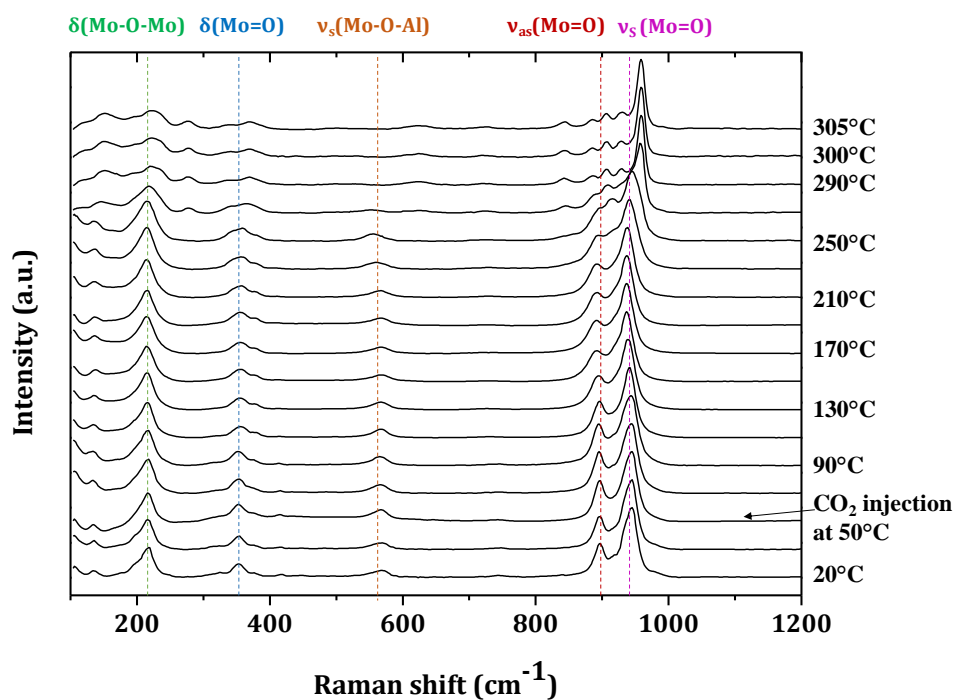


Figure IV.10: Raman spectra showing the evolution of the Mo species under scCO₂ when increasing temperature.

Unsurprisingly, molybdenum species present at room temperature are identical to those obtained in the case of the experiment under air, which means AlMo₆ species. These species have been formed during the maturation stage. The injection of scCO₂ at 50°C induces no change on the surface species present on the support. However, the resulting species recorded at 305°C, have been impacted by the scCO₂ atmosphere. Figure IV.11 represents the Raman spectrum recorded at 305°C.

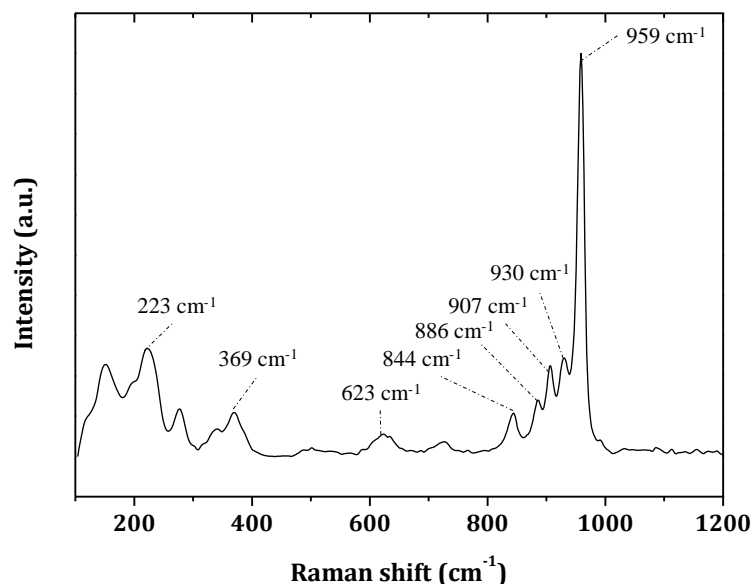


Figure IV.11: Raman spectrum recorded at 305°C.

Bands are narrower than in the case of the previous experiment which suggests poorly-dispersed polymeric molybdate species. The shift of the band corresponding to the symmetric stretching mode of Mo=O suggests, as previously, the presence of polymeric molybdate species (mixture of hepta-

and octamolybdates) [34–36]. This frequency shift indicates an increased degree of condensation of the molybdenum-oxygen species with shorter Mo-O bond length for the oxygen bridges [3].

To compare the evolution of the band assigned to $\nu_s(\text{Mo}=\text{O})$ in a case of a drying under air and under scCO_2 , its position has been plotted as a function of the temperature and presented in Figure IV.12. If starting and ending positions of the band are similar in the case of a drying under air and under scCO_2 , their evolution with the temperature are different.

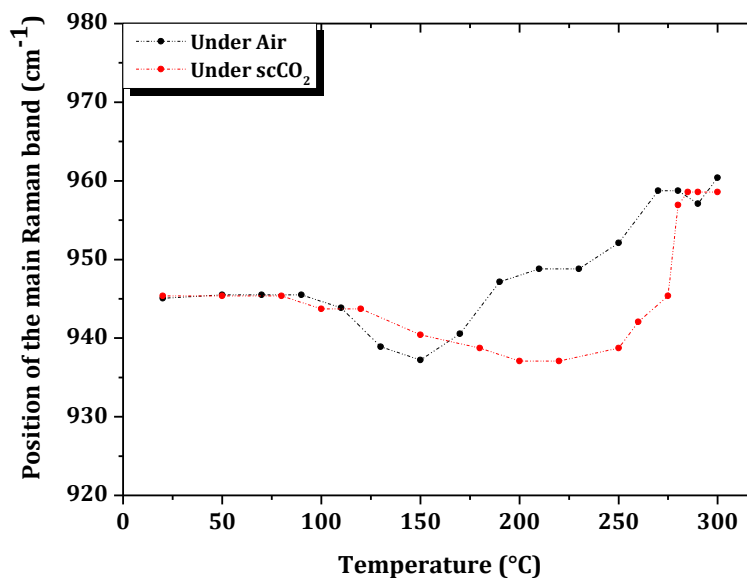


Figure IV.12: Evolution of the most intense Raman band as a function of the temperature.

First observation (not easily observable in previous Raman spectra) is a first shift of the main band towards lower wavenumbers before a second shift towards high wavenumbers. This let us think that from AlMo_6 entities present after maturation to polymolybdates species at the end of the experiment, an intermediate specie is formed and transformed.

The second observation is the manner in which evolves the band positions. In the case of an experiment under air, the minimum of position of the most intense band is found for a temperature of 150°C whereas for an experiment under scCO_2 , the position is found for a temperature of 200–250°C. Moreover, in the case of air, the position is slowly shifted towards higher wavenumbers (from 150°C to 275°C) whereas in the case of scCO_2 , the position is shifted rapidly towards higher wavenumbers (from 225°C to 275°C). The slow shift of the position of the main Raman band in the case of a drying under air may be explained by a slow decrease of the pH inside the pores of alumina due to removal of water. Whereas, in the case of a scCO_2 drying, a part of CO_2 is dissolved in water, decreasing the pH until the precipitation of polymolybdate species.

A second experiment under scCO_2 has been performed and consists of the addition of cobalt nitrate in the impregnation solution. For that, same loading of Mo and ratio promoter/molybdenum have been employed as well as identical experimental conditions. The evolution of Raman spectra is depicted in Figure IV.13.

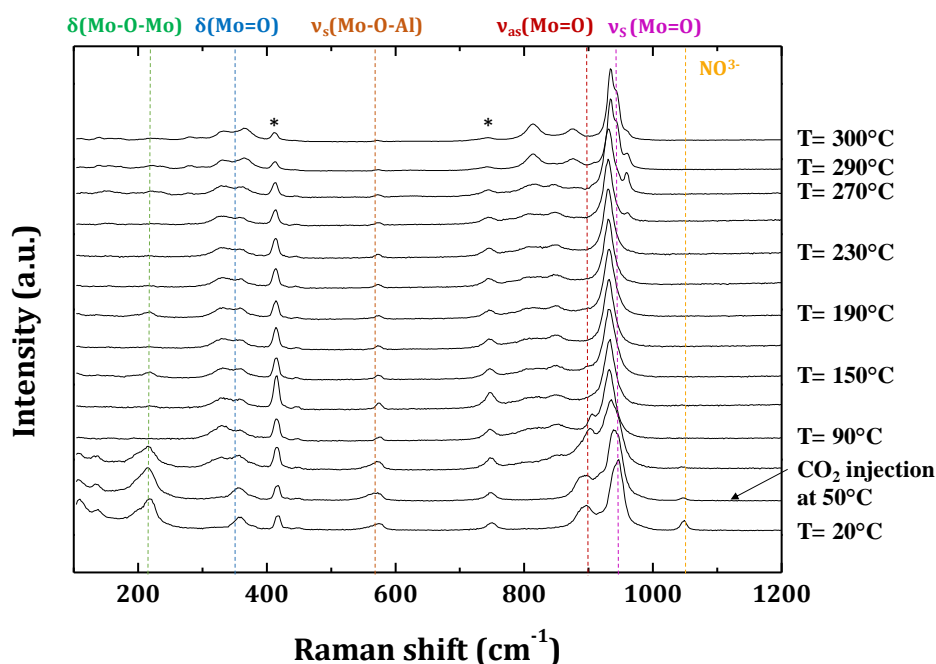


Figure IV.13: Raman spectra showing the evolution of Mo and Co species under scCO₂ when increasing temperature.

As for the previous experiment, species present at room temperature are assigned to an Anderson type heteropolyanion AlMo₆. When, the temperature is increased to around 90°C, the disappearance of bands assigned to the bending mode of Mo-O-Mo and Mo=O bonds and the appearance of bands at 330 and 854 cm⁻¹ are observed.

When the temperature reached 300°C, bands are narrower and located at 330, 364, 813, 876, 934 cm⁻¹ and a shoulder is observed at 945 cm⁻¹. The bands at 813 and 876 cm⁻¹ can be assigned to the Mo-O bond's stretching mode of two crystallographically inequivalent MoO₄ tetrahedra present in the β-CoMoO₄ structure [32,37–39]. Bands located at 330 and 364 cm⁻¹ are associated with the Mo-O bending mode of those inequivalent MoO₄ tetrahedra [39]. Moreover, the narrowing of the bands suggests poorly-dispersed species onto the surface of alumina at the end of the experiment.

The formation of a specie, in which the nature is not clearly established, is observed from a temperature of around 100°C. However, another research group has observed this Raman features and proposed the presence of a mixed CoMo oxyhydroxide [32]. This specie could be the precursor for the formation of cobalt molybdate entities at higher temperatures.

These samples synthesized under scCO₂ have then been characterized by XRD and their patterns are presented in Figure IV.14.

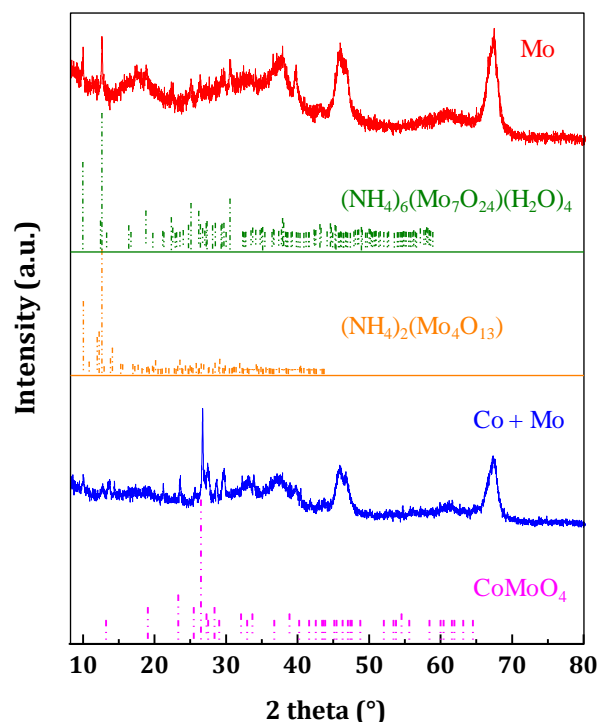


Figure IV.14: XRD patterns of samples synthesized under scCO_2 with Mo (red), Co + Mo (blue) and references patterns.

In both samples synthesized in scCO_2 , XRD peaks have been observed. In the case of the experiment performed with Mo, crystallized species have been attributed to two different polymeric molybdate species: $(\text{NH}_4)\text{Mo}_7\text{O}_{24}\cdot 4\text{H}_2\text{O}$ (PDF #70-1707) and $(\text{NH}_4)_2\text{Mo}_4\text{O}_{13}$ (PDF #80-0757). For the experiment with Mo and Co, XRD peaks have been attributed to $\beta\text{-CoMoO}_4$ with space group $C2/m$ (PDF # 021-0868).

Experiments performed under a scCO_2 atmosphere have shown in both cases (with/without Co), the presence of crystalline species at the end of the reaction. When the molybdenum is the only metal impregnated on the support, crystalline species of ammonium polymolybdates have been observed. Whereas if molybdenum and cobalt are impregnated together, cobalt molybdenum species are obtained at the end of the reaction. The formation of this specie may be attributed to the formation of a CoMo oxyhydroxide specie precursor. XRD measurements have been performed after grinding several alumina pellets whereas *in situ* Raman experiments were done only on the surface of one pellet. A heterogeneity of species is therefore possible depending of the alumina's pellet analyzed.

III.3. Conclusion about experiment under air and under scCO_2

In conclusion, scCO_2 leads to species which are crystalline compared to an experiment under air. In catalysis, large particles are detrimental for the activity due to their difficulty to be activated and a low contact surface due to the large volume of particles. The use of scCO_2 for the drying of samples impregnated with AHM in water does not seem to be a promising route.

In the case of an impregnation with just AHM, a scCO_2 treatment leads to crystalline polymeric molybdate species, whereas in the case of an impregnation with AHM and cobalt nitrate, the formation of cobalt molybdate species is observed. The crystallization of species may be due to the injection of scCO_2 which leads to a fast removing of water contained inside the pores. This change

of dielectric constant between water and scCO₂ leads to the precipitation of species [40]. If the precipitation is fast, the increase of the temperature will only generate the growth of particles. Moreover, the dissolved species in water can be entrained during its removing and generate a heterogeneity of species on the support.

A fast drying of species dissolved in water by using scCO₂ is thus inefficient to obtain a well-dispersed species onto alumina support. An alternative method has thus been proposed. The use of another Mo source to introduce molybdenum, the phosphomolybdic acid.

IV. *In situ* investigation of the preparation of HDS catalyst precursors using phosphomolybdic acid (HPA)

This part describes the *in situ* investigation of the preparation of HDS catalyst precursors using phosphomolybdic acid as Mo source with the first section dedicated to the evolution of species after the ageing time. The second part presents results obtained by comparing the evolution of species under air and under supercritical CO₂ atmosphere.

IV.1. Evolution of species after ageing

First, to evaluate the influence of the impregnation solvent on species during ageing time, four samples have been prepared as presented in Table IV.1

Table IV.1: Samples studied in the evolution of species as a function of the solvent.

<i>Sample</i>	<i>Solvent</i>	<i>Solution</i>
1	H ₂ O	HPA
2	H ₂ O	HPA + cobalt nitrate
3	Ethanol	HPA
4	Ethanol	HPA + cobalt nitrate

After 24h of ageing time, Raman spectra of impregnated sample have been recorded and are presented in Figure IV.15.

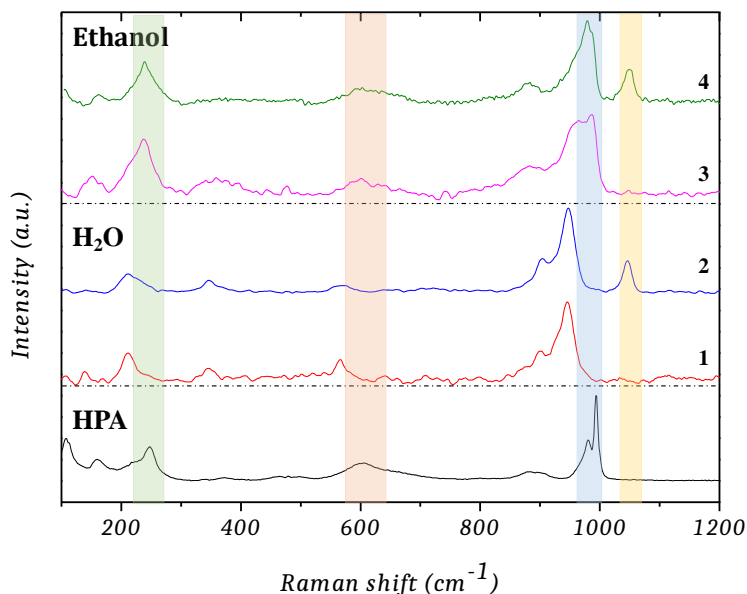


Figure IV.15: Raman spectra of Mo species after ageing: case of ethanol (green & pink curves) and case of water (blue & red curves). The black curve corresponds the Raman spectra of HPA solid.

In the case of an impregnation with ethanol (Raman spectra 3 & 4), the Raman spectra correspond to the one of HPA. In these samples, the band located at $\sim 990 \text{ cm}^{-1}$ is assigned to the symmetric stretching mode of the Mo-O_d bond (blue area), the band at $\sim 965 \text{ cm}^{-1}$ is assigned to the asymmetric stretching mode of the Mo-O_d bond, the band at $\sim 600 \text{ cm}^{-1}$ to the symmetric stretching and bending modes of the Mo-O_c-Mo bond (red area) and the band at $\sim 250 \text{ cm}^{-1}$ to the symmetric stretching mode of the Mo-O_a bond (green area). However, in the case of sample 4, a small shift towards lower

wavenumbers is observed for the $\nu_s(\text{Mo-O}_d)$ band. This may be due to a partial degradation of the HPA on alumina

Looking at the Raman spectra of samples impregnated with an aqueous solution (sample 1 & 2), Raman features corresponding to the Keggin type HPA are not observed. Raman spectra exhibit bands at 946, 902, 566, 346 and 211 cm^{-1} . These bands correspond to an Anderson heteropolyanion $\text{AlMo}_6\text{O}_{24}\text{H}_6^{3-}$ (AlMo_6). In the case of the impregnation with water, the dissolution of the support and reaction of aluminium ions with molybdate ions is observed (as in the case of the use of AHM). A decomposition of the Keggin structure during maturation is observed [41,42]. This decomposition of the Keggin unit over alumina has already been reported during an impregnation with aqueous solutions [43].

The use of ethanol does not decompose the Keggin structure because it may stabilize this structure. Rives et al. [44] have observed the conservation of this Keggin structure over alumina when they used dimethylformamide (DMF) as solvent. We can therefore postulate the same stabilization effect induced by ethanol.

By using water to impregnate molybdenum from HPA, the same species are observed after ageing than with an impregnation using AHM. It has been observed after ageing the formation of an Anderson type HPA AlMo_6 . This specie being detrimental to the dispersion of molybdenum our work has thus been focused on the use of ethanol as solvent for impregnation. Before performing *in situ* Raman experiments by using ethanol as solvent and HPA as Mo source, Raman spectra of impregnated and aged samples with HPA and cobalt nitrate were carried out.

In both solvents, the addition of cobalt nitrate has no major effect on the resulting species after ageing. Indeed, during the impregnation with ethanol, Raman bands can be assigned to a heteropolyanion having a Keggin structure. Whereas for an impregnation with water, Raman spectrum exhibits features of an Anderson heteropolyanion.

The use of water leads to the decomposition of the Keggin-type heteropolyanion and to the formation of an Anderson-type heteropolyanion AlMo_6 . The formation of an Anderson-type heteropolyanion could lead to the presence of cobalt aluminate (CoAl_2O_4), a surface phase of the aluminium molybdate $\text{Al}_2(\text{MoO}_4)_3$ type and/or MoO_3 oxides. Molybdenum species ($\text{Al}_2(\text{MoO}_4)_3$ and MoO_3 oxides) are resistant to the sulfidation and incapable of generating the active phase. Whereas cobalt aluminate will inhibit the promotion of MoS_2 slabs by the cobalt which remained “fixed” in this phase. All these species are detrimental for the HDS activity of the catalyst.

Based on the aforementioned results, *in situ* Raman experiments were performed on $\delta\text{-Al}_2\text{O}_3$ supports impregnated using ethanol as solvent. Figure IV. 16 summarizes the different experiments performed with HPA as molybdenum source.

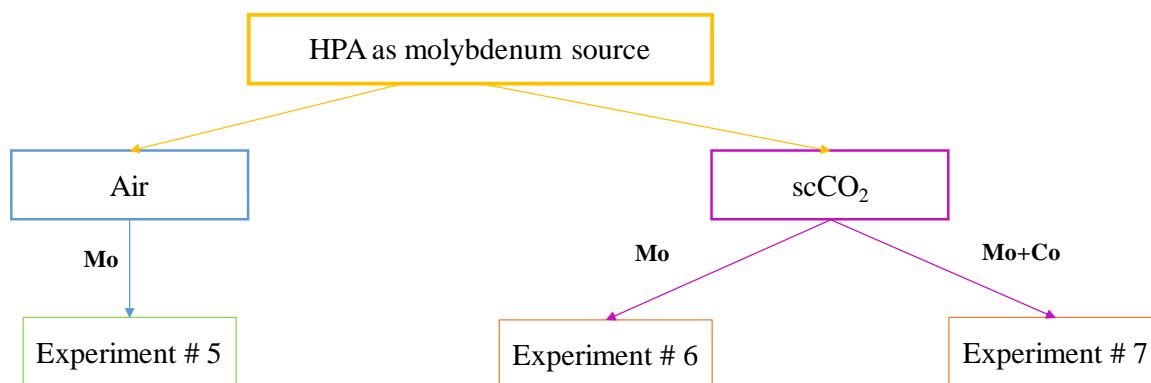


Figure IV.16: Summary of experiments carried out using HPA as Mo source.

IV.2. *In situ* investigation of impregnation of alumina with HPA

IV.2.1. Evolution of species under air drying

One experiment has been conducted under air to compare it with an experiment under scCO_2 . Figure IV.17 presents the evolution of Raman spectra under air as a function of temperature.

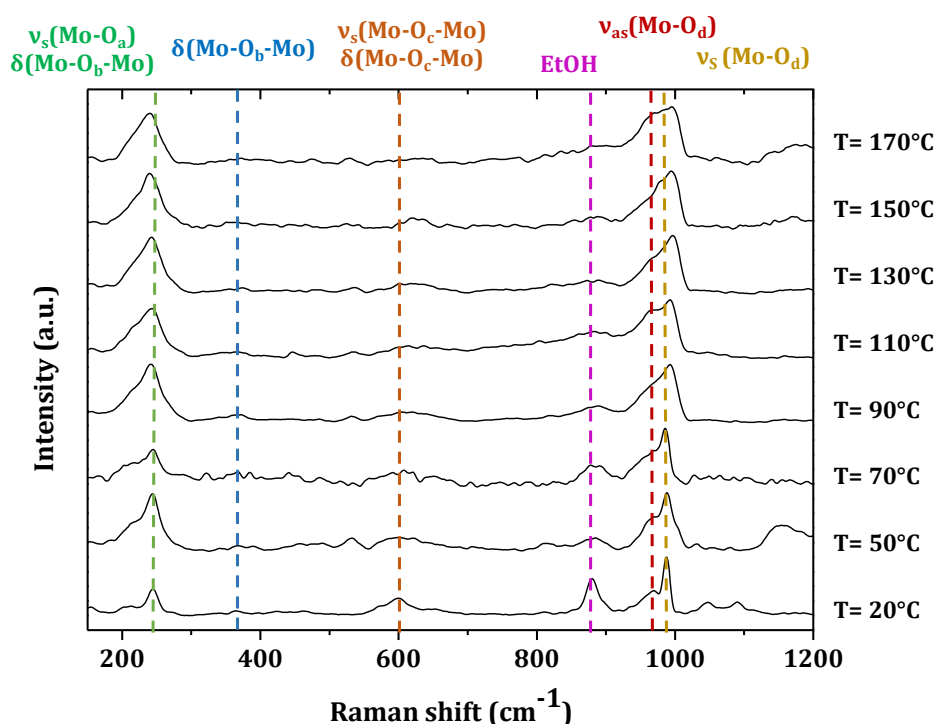


Figure IV.17: Raman spectra showing the evolution of Mo species under air when increasing temperature.

Bands assigned to HPA are still observed at 170°C but are broader than at room temperature. The band assigned to the stretching mode of Mo-O_d has been shifted from 988 to 995 cm^{-1} at the end of the reaction. This broadening of Raman bands may indicate an increase of the dispersion of the Keggin-type heteropolyanion compounds. The band corresponding to ethanol is increasingly reduced with the increase of temperature and almost disappears at 70 - 90°C . This observation is in accordance with the boiling temperature of ethanol ($T_b = 78.4^\circ\text{C}$) at atmospheric pressure. After having analyzed the sample by XRD, no diffraction peaks were observed. This suggests the presence of an amorphous phase and/or the presence of very small crystallites amorphous to XRD.

IV.2.2. Evolution of Mo species under scCO₂ drying

In the case of the use of scCO₂ to induce precipitation of species, two experiments were carried out. The first sample has been impregnated with HPA and the second with HPA and cobalt nitrate. Figure IV.18 shows the evolution of Raman spectra as a function of temperature under scCO₂. At the end of the reaction, Raman bands correspond to a Keggin-type heteropolyanion with the symmetric stretching of Mo-O_d located at 991 cm⁻¹. A broadening of Raman bands is also observed which is attributed to an increase of the dispersion of molybdenum species. Furthermore, the intensity of the band corresponding to ethanol decreases when scCO₂ is injected. It can be proposed that scCO₂ leads to the expansion and extraction of ethanol and thus to the precipitation of species.

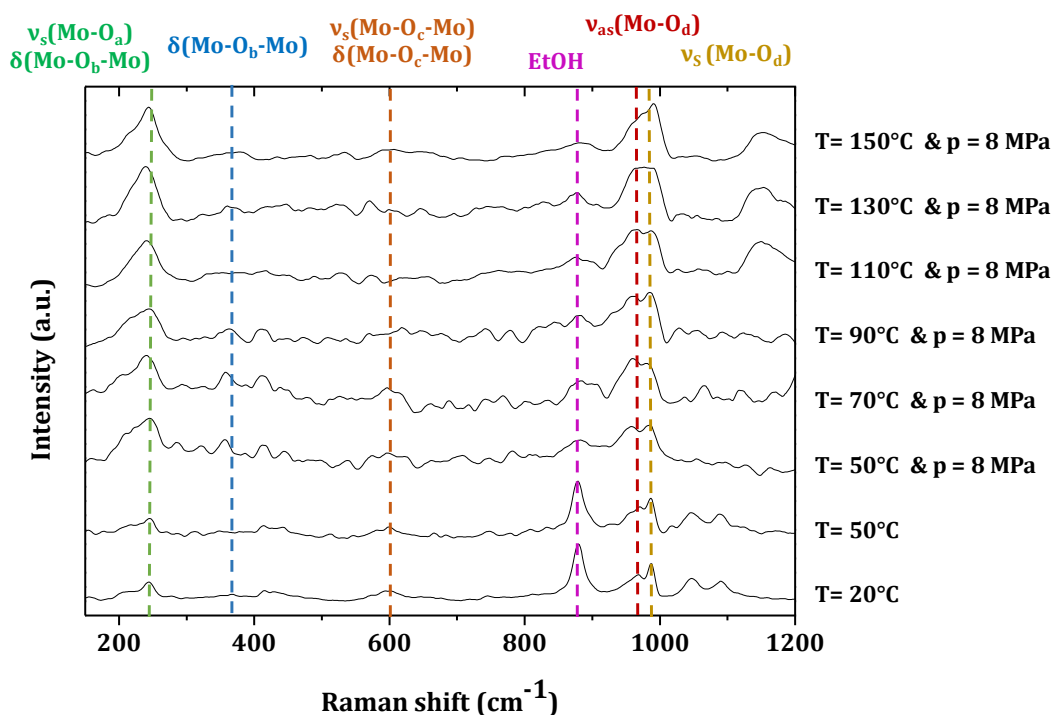


Figure IV.18: Raman spectra showing the evolution of Mo species in presence of scCO₂ as a function of the temperature.

Then, we performed XRD measurements to complete Raman investigations. Except the support signature, no peaks concerning Mo based species are observed.

These results suggest the presence of Keggin type entities on the surface of the support which are too small to be detected by XRD measurements. The use of scCO₂ expanded ethanol process appears thus to be an interesting option for the dispersion of HPA onto the alumina support

However, this process should be tested in the case of a sample impregnated with HPA and cobalt nitrate. For that, two experiments were carried out in these conditions to check the reproducibility of the obtained results, concerning the evolution of species under scCO₂. Results obtained from these experiments are presented in Figure IV.19 and Figure IV.20.

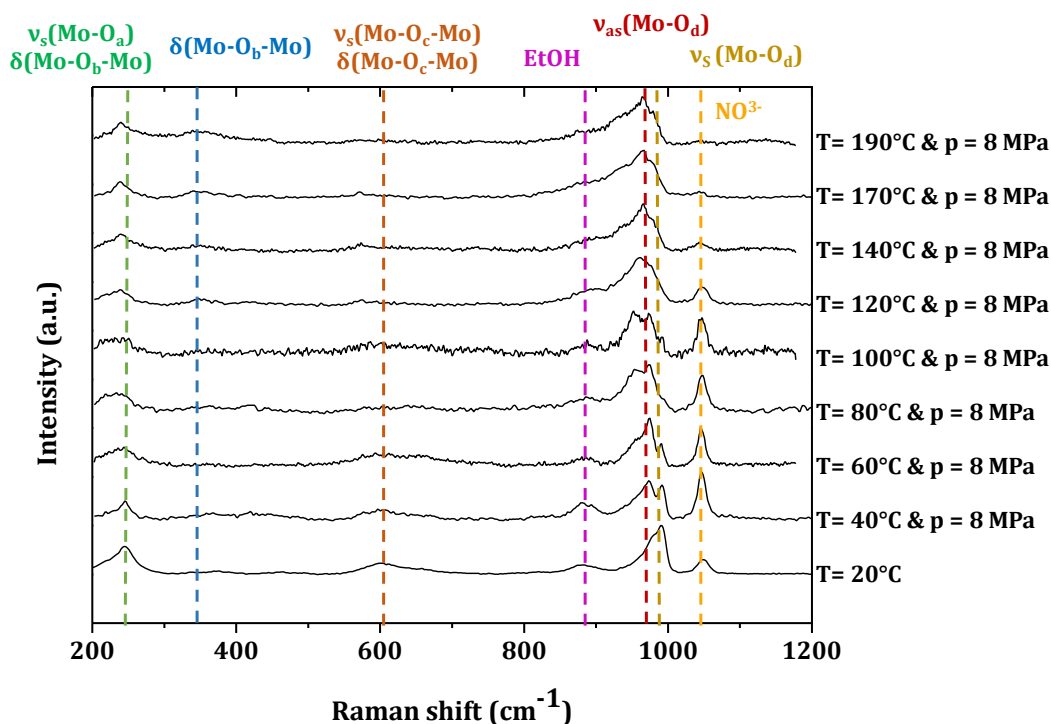


Figure IV.19: Raman spectra showing the evolution of Mo and Co species in scCO₂ as a function of temperature (first experiment).

From this experiment, a decrease of the intensity of the symmetric stretching of the Mo-O_d bond is first observed which became a shoulder for temperatures above 100°C. A transformation of the HPA occurs from this temperature. At the highest temperature (190°C), the main band is located at 964 cm⁻¹. Van Veen et al. have worked on the adsorption of HPA [45,46] on alumina and have proposed a depolymerisation of HPA into a mixture of [PMo₁₁O₃₉]⁶⁻ and [PMo₉O₃₁(OH)₃]⁶⁻. These compounds having their main Raman bands located between 960 cm⁻¹ and 970 cm⁻¹. We can therefore postulate the presence of these species at the end of the synthesis. These molybdenum species have not been observed in the impregnation with only HPA. It could be explained by the fact that, during previous experiments, the temperature of 190°C has not been reached. Previously a temperature of 150-170°C was reached at the end of the experiment and depolymerisation of HPA seems to occur around this range of temperature. Moreover, the addition of Co(NO₃)₂·6H₂O has increased the pH of the solution and provided water molecules.

As during the *in situ* investigation, the Raman laser is focused on only one alumina pellet, a second experiment has been performed to observe if the same evolution of Mo species occurs in another pellet. Raman spectra obtained from this second experiment are presented in Figure IV.20.

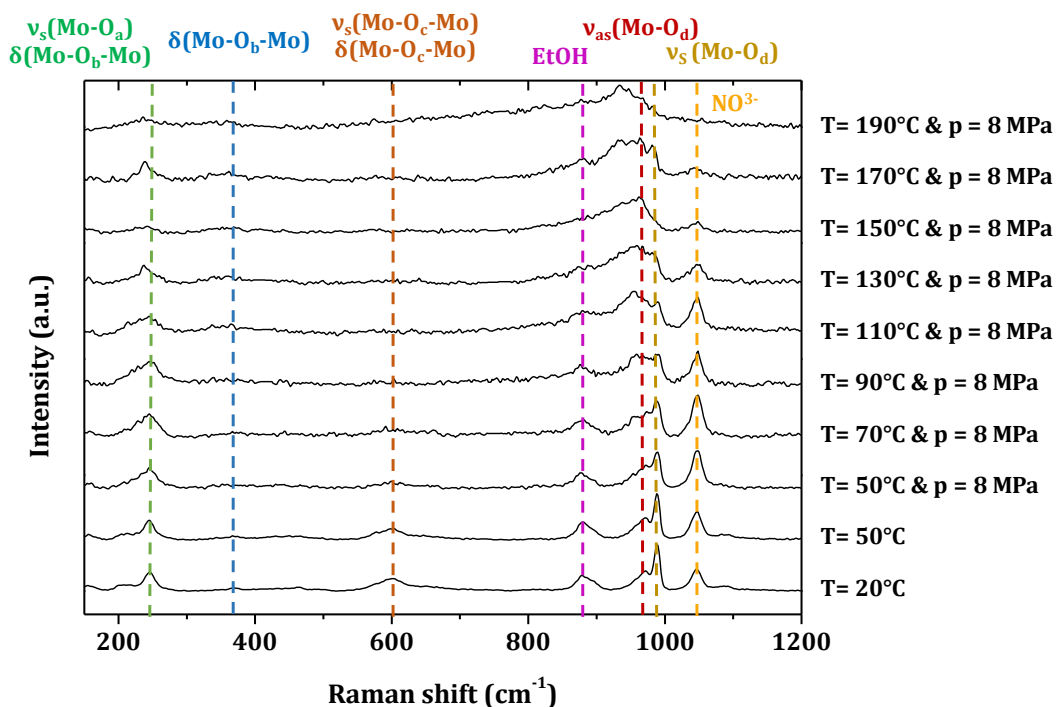


Figure IV.20: Raman spectra showing the evolution of Mo and Co species in scCO_2 as a function of temperature (second experiment).

The same trend than previously is observed. A decrease of the intensity of the symmetric stretching of the Mo-O_d bond assigned to the destruction of the HPA when the temperature is increased. Contrarily at the previous experiment, at the highest temperature (190°C), the main band is located at 933 cm^{-1} . The location of this band could indicate the presence of cobalt molybdate species, as observed previously with the use of AHM in water. The fact that this band at 933 cm^{-1} is not observed in the previous experiment could be due to a longer time of synthesis and/or to a heterogeneity for the evolution of species depending on the alumina pellet analyzed.

These two samples obtained have then been characterized by XRD. For that, several pellets were grinded to perform measurements. Raman analyses have also been carried out on several alumina pellets from the first experiment. Results from these characterizations are presented in Figure IV.21.

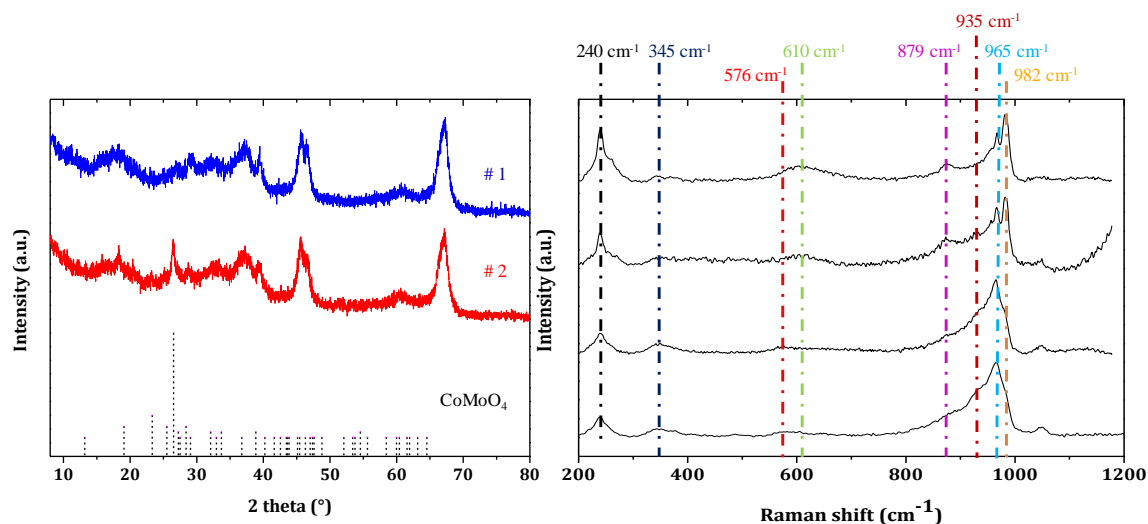


Figure IV.21: XRD patterns of samples from the two experiments and Raman spectra of different alumina pellets from #1.

XRD patterns of the two samples prepared by scCO_2 are presented in Figure IV.21 (left). From the first experiment, no diffraction peaks are observed and peaks present are assigned to the alumina support. However, in the second experiment, two additional diffraction peaks are observed and can be assigned to CoMoO_4 (PDF # 21-0868). This difference between the two samples may be explained by a longer time of synthesis in the second experiment and the formation of cobalt molybdate species. Raman spectra have been then carried out on the sample from the first experiment in order to detect the presence of other species depending on the alumina pellet analyzed. We observed that Raman spectra are different which implies a heterogeneity of species depending on the pellet analyzed. The presence of a band at 982 cm^{-1} and a band at 610 cm^{-1} which are assigned to the stretching mode of Mo-O_d bonds and to the bending mode of $\text{Mo-O}_c\text{-Mo}$ bonds respectively, suggests the presence of HPA entities. The band located at 965 cm^{-1} can be assigned to the stretching mode of Mo-O bonds of polymeric molybdenum species. While the band located at 879 cm^{-1} could suggest the presence of cobalt molybdenum species.

In the surface of the catalyst, the presence of several species has thus been detected. Some HPA entities are still present onto the surface whereas some of them are depolymerized. Monomolybdate species due to the depolymerization of HPA may have react with cobalt ions to form cobalt molybdenum species when the temperature is increased.

IV.3. Conclusion about the use of HPA as Mo source

First, it has been observed that it is possible to keep the Keggin structure intact after 24h of ageing in the case of the use of ethanol. When water is employed as solvent of impregnation, a destruction of the Keggin entities is observed as well as the formation of an Anderson HPA AlMo_6 resulting of the reaction between aluminium ions released and polymolybdate species. To avoid this AlMo_6 specie, the use of ethanol appears as a good option.

Using HPA as source of molybdenum permits to avoid the presence of ammonium ions as in the case of the use of AHM. This counterion being detrimental for the catalyst activity because it can form precipitate molybdenum ions and leads to bulk species of molybdenum onto the surface of alumina (as observed in the experiment performed with molybdenum from AHM in scCO_2). Moreover, the HPA contains in its Keggin structure a phosphorus atom and it has been shown that

the addition of phosphorus enhances the activity of alumina-supported catalysts. Ferdous et al. [47] have shown that the stacking of MoS₂ layers is increased as well as the activity of the catalyst when phosphorus is added to the solution of impregnation. Atanasova et al. [48] have shown that the addition of phosphorus leads to more reducible polymolybdate species and that phosphorus modifies the structure of Co²⁺ cations from tetra-coordinated to octahedrally coordinated cations. These ones are more likely to be sulfided and a better promotion effect is thus observed. Van Veen and coworkers [46,49] have also shown that a simultaneous impregnation of phosphorus and molybdenum increases molybdenum dispersion whereas impregnation of phosphorus before molybdenum leads to less-dispersed molybdenum species.

In our *in situ* investigations using HPA in ethanol under scCO₂, we have observed the presence of different species depending of the pellet analyzed. However, it has been show the possibility of obtaining an amorphous phase and/or the presence of very small crystallites amorphous to XRD, which is important for the future activation of catalysts. The presence of crystalline cobalt molybdates has also been observed at temperatures around 150-200°C, this is elucidated in the next chapter dedicated to the influence of experimental parameters on the oxometallic phase. The use of scCO₂ with ethanol can also bring formation of metal complexes, as observed by Ming et al [50], and detailed in the next chapter.

V. Conclusion

This chapter has presented the monitoring of the preparation of HDS catalyst precursors. For that, a home-made cell which permits the recording of Raman spectra through a sapphire window has been used. A reactor placed before the *in situ* cell have played the role of preheater in order to allow the injection of carbon dioxide under its supercritical conditions into the *in situ* cell.

In order to compare our results with a common synthesis of oxide catalyst precursors, *in situ* Raman measurements were also carried out under air. We have then tested two different systems, ammonium heptamolybdate in water with or without a cobalt promoter and phosphomolybdic acid in ethanol with and without cobalt promoter.

For the system AHM in water without addition of a promoter, we have observed that a treatment under supercritical carbon dioxide leads to the presence of crystallized ammonium polymolybdate species while in the case of a classical drying under air, an amorphous phase and/or the presence of too small crystallites to be detected by XRD is observed. This difference can be explained by the fact that scCO_2 removes water present in the pores very quickly, but water carries with it dissolved species. The formation of poor and rich metals containing areas are then observed on the support.

The same trend has been observed with the addition of the cobalt promoter. For a synthesis under air, a well-dispersed phase of polymeric molybdate species has been observed while for a synthesis under scCO_2 , the presence of crystallized cobalt molybdate species has been reported. The presence of $\beta\text{-CoMoO}_4$ onto the support is surprising due to the temperature of formation of this β -phase which is known to be the high temperature phase. More detailed are given in the next chapter with the influence of the synthesis temperature on the resulting species.

In conclusion, the use of AHM dissolved in water as solution of impregnation followed by a scCO_2 treatment does not seem to be an efficient way to disperse oxide species onto the surface of alumina support. A physical removing of water by scCO_2 for the precipitation of species is not the most efficient method. For that, we have chosen to use another solvent for the impregnation of metals, ethanol. As AHM is not soluble in ethanol, we have chosen the use of HPA to impregnate molybdenum onto the surface of alumina. This also permits us to avoid the presence of undesirable counterions and to have the presence of phosphorus in the Mo precursor.

Experiments using HPA dissolved in ethanol with or without the addition of a cobalt promoter have been performed. For the preparation of HDS catalyst precursors without addition of cobalt promoter, we found that for a treatment under air or under scCO_2 leads to the presence of a well-dispersed polymolybdate phase (phase could be slightly different depending on the atmosphere but we cannot afford this by using XRD and Raman analyses). The use of ethanol to obtain small crystallites is thus better than the use of water.

Regarding the preparation of HDS catalyst precursors with a cobalt promoter, after a treatment under scCO_2 , the presence of a wide range of different species is observed. This includes the presence of polymolybdate and/or cobalt molybdate compounds. Depending on the experiment (and hence of the alumina's pellet analyzed), crystallized species have been found in one case and not in the other one.

A work with ethanol as solvent of impregnation permits to enhance dispersion of species compared to the use of water as solvent of impregnation. For that, it has been chosen to focus our study on the use of scCO_2 with ethanol as solvent of impregnation. The influence of several experiment

parameters on the resulting oxometallic phases has been investigated. These results are discussed in the next chapter.

VI. Bibliography

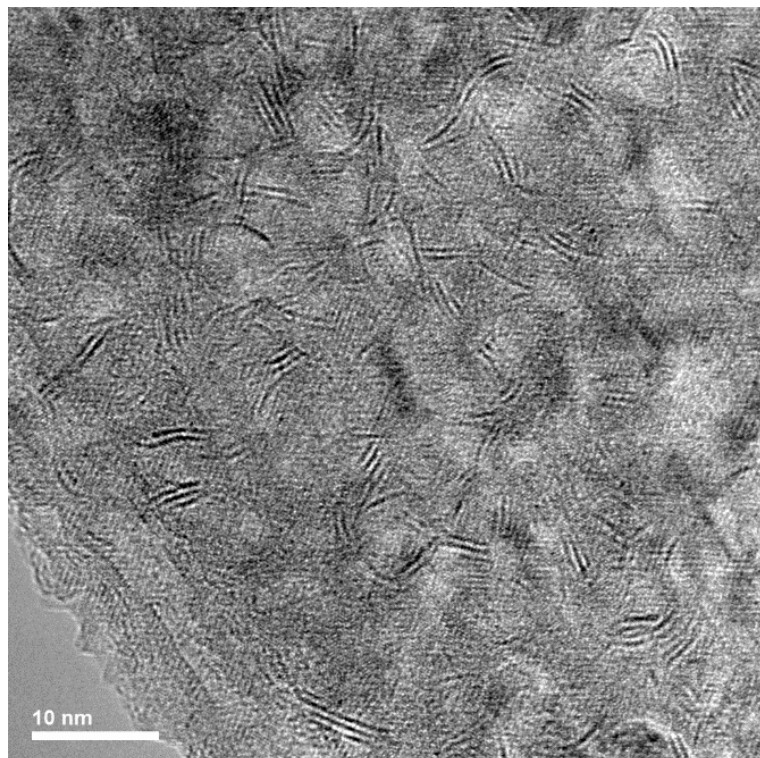
- [1] I.E. Wachs, In situ Raman spectroscopy studies of catalysts, *Top. Catal.* 8 (1999) 57–63.
- [2] M. Digne, K. Marchand, P. Bourges, Monitoring hydrotreating catalysts synthesis and deactivation using Raman spectrometry, *Oil Gas Sci. Technol. - Rev. l'IFP.* 62 (2007) 91–99.
- [3] H. Jeziorowski, H. Knozinger, Raman and ultraviolet spectroscopic characterization of molybdena on alumina catalysts, *J. Phys. Chem.* 83 (1979) 1166–1173.
- [4] H. Jeziorowski, H. Knözinger, Laser induced electronic excitation of surface hydroxide ions and scattering background in laser raman spectra of oxide surfaces, *Chem. Phys. Lett.* 51 (1977) 519–522.
- [5] E. Payen, J. Grimblot, S. Kasztelan, Study of oxidic and reduced alumina-supported molybdate and heptamolybdate species by *in situ* laser Raman spectroscopy, *J. Phys. Chem.* 91 (1987) 6642–6648.
- [6] H. Knozinger, H. Jeziorowski, Raman spectra of molybdenum oxide supported on the surface of aluminas, *J. Phys. Chem.* 82 (1978) 2002–2005.
- [7] I.E. Wachs, C. A Roberts, Monitoring surface metal oxide catalytic active sites with Raman spectroscopy., *Chem. Soc. Rev.* 39 (2010) 5002–17.
- [8] H. Hu, I.E. Wachs, S.R. Bare, surface structures of supported molybdenum oxide catalysts : characterization by Raman and Mo L3-Edge XANES, *J. Phys. Chem.* 99 (1995) 10897–10910.
- [9] D.S. Kim, K. Segawa, T. Soeya, I.E. Wachs, Surface structures of supported molybdenum oxide catalysts under ambient conditions, *J. Catal.* 136 (1992) 539–553.
- [10] I. Lindqvist, Crystal-structure investigation of the paramolybdate ion, *Ark. Foer Kemi.* 2 (1950) 325–341.
- [11] H.T. Evans, B.M. Gatehouse, P. Leverett, Crystal structure of the heptamolybdate(vi) (paramolybdate) ion, $[\text{Mo}_7\text{O}_{24}]^{6-}$, in the ammonium and potassium tetrahydrate salts, *J.C.S Dalt.* (1975) 505–514.
- [12] J.F. Keggin, *Proc. R. Soc. London, Ser. A.* 144 (1934) 75–100.
- [13] J.M. Poblet, X. Lopez, C. Bo, Ab initio and DFT modelling of complex materials: towards the understanding of electronic and magnetic properties of polyoxometalates, *Chem. Soc. Rev.* 32 (2003) 297.
- [14] A.J. Bridgeman, Density functional study of the vibrational frequencies of a -Keggin heteropolyanions, *287 (2003) 55–69.*
- [15] C. Rocchiccioli-Deltcheff, M. Fournier, R. Franck, R. Thouvenot, Vibrational investigations of polyoxometalates. 2. Evidence for anion-anion Interactions in molybdenum(VI) and tungsten(VI) compounds related to the Keggin structure, *Inorg. Chem.* 22 (1983) 207–216.

-
- [16] F.F. Bamoharram, Vibrational spectra study of the interactions between Keggin heteropolyanions and amino acids., *Molecules*. 14 (2009) 3214–21.
- [17] H. Tian, C.A. Roberts, I.E. Wachs, Molecular structural determination of molybdena in different environments: aqueous solutions, bulk mixed oxides, and supported MoO₃ Catalysts, *J. Phys. Chem. C*. 114 (2010) 14110–14120.
- [18] A.G. Kalampounias, G. Tsilomelekis, R.W. Berg, S. Boghosian, molybdenum(vi) oxosulfato complexes in MoO₃ –K₂S₂O₇–K₂SO₄ molten mixtures: stoichiometry, vibrational properties, and molecular structures, *J. Phys. Chem. A*. 116 (2012) 8861–8872.
- [19] A. Guevara-Lara, R. Bacaud, M. Vrinat, Highly active NiMo/TiO₂-Al₂O₃ catalysts: Influence of the preparation and the activation conditions on the catalytic activity, *Appl. Catal. A Gen.* 328 (2007) 99–108.
- [20] G. Deo, I.E. Wachs, Predicting molecular structures of surface metal oxide species on oxide supports under ambient conditions, *J. Phys. Chem.* 95 (1991) 5889–5895.
- [21] L. Le Bihan, P. Blanchard, M. Fournier, E. Payen, V. Cedex, Raman spectroscopic evidence for the existence of 6-molybdoaluminate entities on an Mo/Al₂O₃ oxidic precursor, *J. Chem. Soc., Faraday Trans.* 94 (1998) 937–940.
- [22] X. Carrier, J.F. Lambert, M. Che, Ligand-promoted alumina dissolution in the preparation of Mo/ γ -Al₂O₃ catalysts: evidence for the formation and deposition of an Anderson-type alumino heteropolymolybdate, *J. Am. Chem. Soc.* 119 (1997) 10137–10146.
- [23] J. A. Bergwerff, T. Visser, B.M. Weckhuysen, On the interaction between Co- and Mo-complexes in impregnation solutions used for the preparation of Al₂O₃-supported HDS catalysts: A combined Raman/UV–vis–NIR spectroscopy study, *Catal. Today*. 130 (2008) 117–125.
- [24] J. Bergwerff, M. Jansen, B. Leliveld, T. Visser, K. Dejong, B. Weckhuysen, Influence of the preparation method on the hydrotreating activity of MoS₂/Al₂O₃ extrudates: A Raman microspectroscopy study on the genesis of the active phase, *J. Catal.* 243 (2006) 292–302.
- [25] J.A. Bergwerff, T. Visser, B.R.G. Leliveld, B.D. Rossenaar, K.P. de Jong, B.M. Weckhuysen, Envisaging the physicochemical processes during the preparation of supported catalysts: Raman microscopy on the impregnation of Mo onto Al₂O₃ extrudates., *J. Am. Chem. Soc.* 126 (2004) 14548–56.
- [26] X. Carrier, J.-F. Lambert, S. Kuba, H. Knözinger, M. Che, Influence of ageing on MoO₃ formation in the preparation of alumina-supported Mo catalysts, *J. Mol. Struct.* 656 (2003) 231–238.
- [27] I.E. Wachs, Raman and IR studies of surface metal oxide species on oxide supports: Supported metal oxide catalysts, *Catal. Today*. 27 (1996) 437–455.
- [28] I.L. Botto, A. C. Garcia, H.J. Thomas, Spectroscopical approach to some heteropolymolybdates with the Anderson structure, *J. Phys. Chem. Solids*. 53 (1992) 1075–1080.

-
- [29] B.N. Ivanov-Emin, L.A. Filatenko, S. Ol'gin, Kin'Ones, G.Z. Kaziev, *Russ. J. Inorg. Chem.* 83 (1978) 1166–1173.
- [30] C. Papadopoulou, J. Vakros, H.K. Matralis, C. Kordulis, A. Lycourghiotis, On the relationship between the preparation method and the physicochemical and catalytic properties of the CoMo/ γ -Al₂O₃ hydrodesulfurization catalysts, *J. Colloid Interface Sci.* 261 (2003) 146–153.
- [31] J. Vakros, C. Papadopoulou, G.A. Voyiatzis, A. Lycourghiotis, C. Kordulis, Modification of the preparation procedure for increasing the hydrodesulfurisation activity of the CoMo/ γ -alumina catalysts, *Catal. Today.* 127 (2007) 85–91.
- [32] P. Blanchard, C. Lamonier, A. Griboval, E. Payen, New insight in the preparation of alumina supported hydrotreatment oxidic precursors: A molecular approach, *Appl. Catal. A-General.* 322 (2007) 33–45.
- [33] J. Bergwerff, M. Jansen, B. Leliveld, T. Visser, K. de Jong, B. Weckhuysen, Influence of the preparation method on the hydrotreating activity of MoS₂/Al₂O₃ extrudates: A Raman microspectroscopy study on the genesis of the active phase, *J. Catal.* 243 (2006) 292–302.
- [34] N.F.D. Verbruggen, G. Mestl, L.M.J. Von Hippel, B. Lengeler, H. Knozinger, Structure of K-doped molybdena-on-alumina catalysts as studied by X-ray absorption and Raman spectroscopy, *Langmuir.* 10 (1994) 3063–3072.
- [35] D.S. Kim, K. Segawa, T. Soeya, I.E. Wachs, Surface-structures of supported molybdenum oxide catalysts under ambient conditions, *J. Catal.* 136 (1992) 539–553.
- [36] P.A. Spevack, N.S. McIntyre, Raman and XPS investigation of supported molybdenum oxide thin films. 2. Reactions with hydrogen sulfide, *J. Phys. Chem.* 97 (1993) 11031–11036.
- [37] S.L. González-Cortés, T.-C. Xiao, P.M.F. Costa, B. Fontal, M.L. Green, Urea–organic matrix method: an alternative approach to prepare Co-MoS₂/ γ -Al₂O₃ HDS catalyst, *Appl. Catal. A Gen.* 270 (2004) 209–222.
- [38] T. Ono, N. Ogata, Y. Miyaryo, Characteristic features of Raman band shifts of Scheelite-type molybdate catalysts exchanged with the ¹⁸O tracer via redox reactions, *J. Catal.* 161 (1996) 78–86.
- [39] I. Kanesaka, H. Hashiba, I. Matsuura, Polarized Raman spectrum and normal coordinate analysis of α -MnMoO₄, *J. Raman Spectrosc.* 19 (1988) 213–218.
- [40] B. Motos-Pérez, D. Uzio, C. Aymonier, Preparation of nickel phosphide hydrodesulfurization catalysts assisted by supercritical carbon dioxide, *ChemCatChem.* 7 (2015) 3441–3444.
- [41] V. Costa, K. Marchand, M. Digne, C. Geantet, New insights into the role of glycol-based additives in the improvement of hydrotreatment catalyst performances, *Catal. Today.* 130 (2008) 69–74.

-
- [42] S. Damyanova, J.L.G. Fierro, I. Sobrados, J. Sanz, Surface behavior of supported 12-Heteropoly acid as revealed by Nuclear Magnetic Resonance , X-ray Photoelectron Spectroscopy , and Fourier Transform, *Langmuir*. 15 (1999) 469–476.
- [43] A. Griboval, P. Blanchard, E. Payen, M. Fournier, J.L. Dubois, Alumina supported HDS catalysts prepared by impregnation with new heteropolycompounds. Comparison with catalysts prepared by conventional Co–Mo–P coimpregnation, *Catal. Today*. 45 (1998) 277–283.
- [44] A. Rives, E. Payen, R. Hubaut, P. Vázquez, L. Pizzio, C. Cáceres, M. Blanco, Silica and alumina impregnated with dimethylformamide solutions of molybdophosphoric or tungstophosphoric acids for hydrotreatment reactions, 71 (2001) 193–201.
- [45] J.A.R. van Veen, O. Sudmeijer, C. a. Emeis, H. de Wit, On the identification of molybdophosphate complexes in aqueous solution, *J. Chem. Soc. Dalt. Trans.* (1986) 1825.
- [46] J. A. R. van Veen, P.A.J.M. Hendriks, R.R. Andréa, E.J.G.M. Romers, A.E. Wilson, Phosphomolybdate adsorption on alumina surfaces. 2. The molybdate/phosphated alumina and phosphomolybdate/alumina systems, *J. Phys. Chem.* 94 (1990) 5282–5285.
- [47] D. Ferdous, A.K. Dalai, J. Adjaye, A series of NiMo/Al₂O₃ catalysts containing boron and phosphorus Part I. Synthesis and characterization, *Appl. Catal. A-General*. 260 (2004) 137–151.
- [48] P. Atanasova, R.L. Cordero, L. Mintchev, T. Halachev, A.L. Agudo, Temperature programmed reduction of the oxide form of PNiMo/Al₂O₃ catalysts before and after water extraction, *Appl. Catal. A-General*. 159 (1997) 269–289.
- [49] J.A.R. van Veen, P.A.J.M. Hendriks, R.R. AndrCa, E.J.G.M. Romers, A.E. Wilson, Chemistry of phosphomolybdate adsorption on alumina surfaces. 1. The molybdate/alumlna system, *J. Phys. Chem.* 94 (1990) 5275–5282.
- [50] J. Ming, C. Wu, H. Cheng, Y. Yu, F. Zhao, Reaction of hydrous inorganic metal salts in CO₂ expanded ethanol: Fabrication of nanostructured materials via supercritical technology, *J. Supercrit. Fluids*. 57 (2011) 137–142.

Chapter V : Understanding of the process of precursor catalyst preparation through a parametric study



I. INTRODUCTION.....	149
II. INFLUENCES OF THE SYNTHESIS PARAMETERS ON OXOMETALLIC AND SULFIDED PHASES	151
II.1. REFERENCE CATALYST	151
II.1.1. <i>Characteristics of the oxometallic phase</i>	151
II.1.2. <i>Characteristics of the sulfided phase</i>	153
II.2. INFLUENCE OF THE TEMPERATURE OF SYNTHESIS	154
II.2.1. <i>Evolution of the oxometallic phase as a function of the synthesis temperature</i>	155
II.2.2. <i>Characteristics of sulfided catalysts as a function of the synthesis temperature</i>	157
II.3. INFLUENCE OF THE PRESSURE	162
II.3.1. <i>Evolution of the oxometallic phase with pressure</i>	162
II.3.1. <i>Characteristics of sulfided catalysts as a function of pressure</i>	164
II.4. INFLUENCE OF THE MOLAR RATIO CO ₂ /EtOH.....	165
II.4.1. <i>Evolution of the oxometallic phase as a function of the ratio CO₂/EtOH.....</i>	165
II.4.2. <i>Characteristics of the sulfide phase as a function of the ratio CO₂/EtOH.....</i>	168
II.5. INFLUENCE OF THE SOLVENT OF IMPREGNATION	170
II.5.1. <i>Evolution of the oxometallic phase as a function of alcohol nature.....</i>	171
II.5.2. <i>Characteristics of the sulfided phases as a function of the alcohol nature.....</i>	175
II.6. INFLUENCE OF THE REACTION TIME	177
II.6.1. <i>Evolution of the oxometallic phase as a function of reaction time.....</i>	178
II.6.2. <i>Characteristics of the sulfided phase</i>	180
II.7. INFLUENCE OF THE MOLYBDENUM CONTENT.....	182
II.7.1. <i>Evolution of the oxometallic phase as a function of Mo content.....</i>	182
II.7.2. <i>Characteristics of the sulfided phase</i>	184
III. CONCLUSION ABOUT THE VARIATION OF EXPERIMENTAL PARAMETERS.....	186
IV. BIBLIOGRAPHY.....	189

I. Introduction

This chapter is dedicated to the synthesis of HDS catalyst precursors using $scCO_2$ to induce the precipitation and enhance dispersion of cobalt and molybdenum species. From the previous chapter, the use of ethanol has appeared to avoid undesirable species and to enhance the dispersion of species onto the support compared to the use of water. The use of ethanol as solvent of impregnation has thus been selected to prepare the HDS catalyst precursors.

The preparation of the HDS catalysts can be divided in four main parts. i) the first being the impregnation of metal precursors in the pores of alumina by dry impregnation, ii) the second is the injection of $scCO_2$ on the impregnated and aged sample, iii) the third is the reaction at defined temperature under $scCO_2$ medium and iv) the last step is dedicated to the activation of these catalyst precursors by sulfidation.

Along the synthesis of catalyst precursors, several parameters have been tested and are reported in Figure V.1, whereas Table V.1. presents the tested values of each parameter.

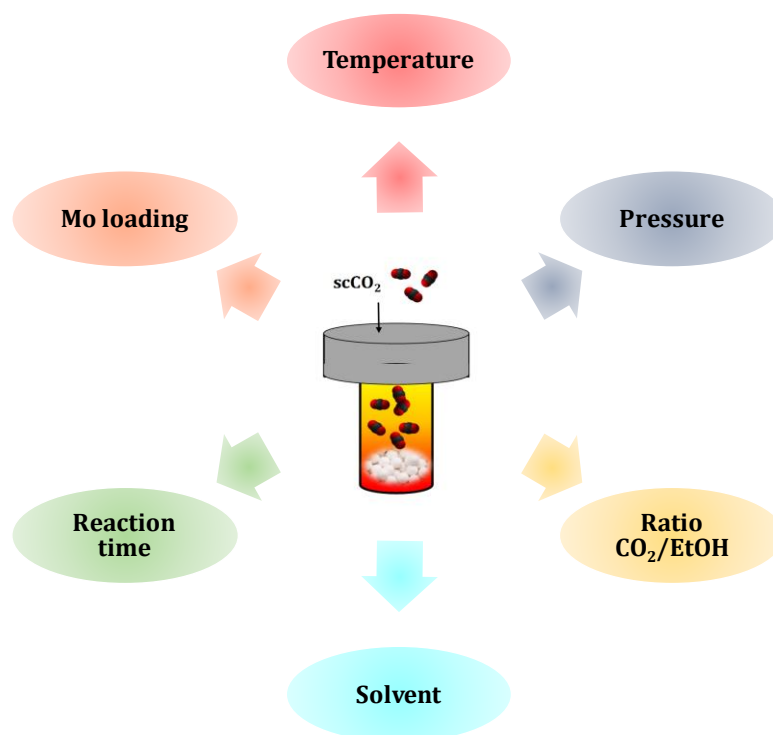


Figure V.1: Different parameters evaluated during the preparation of HDS catalyst precursors.

Table V.1: Different parameters tested for the preparation of HDS catalyst precursors.

<i>Parameter</i>	<i>Tested values</i>
Temperature (°C)	50, 100, 120, 150, 200, 250, 300, 400
Pressure (MPa)	5, 20
Ratio CO₂/solvent (mol/mol)	80/20, 95/5, 98/2
Solvent of impregnation	Methanol, ethanol, propan-1-ol
Reaction time (min)	<1, 60, 120
Loading of Mo (wt%)	10, 13

All catalyst precursors are characterized in their oxometallic phase before being activated, characterized and tested in their sulfided phase. This chapter describes the influence of each parameter on the resulting oxometallic and sulfided phases. The presentation of experimental parameters tested and their effects on resulting phases are described and compared with a reference catalyst. This reference corresponds to a synthesis performed in the same experimental conditions excepted for the atmosphere which was the air.

For the sake of clarity, it has been chosen to use this nomenclature: C-T-S-R-t, with T corresponding to the temperature of reaction, S to the solvent of impregnation, R to the ratio CO₂/solvent and t to the time of reaction. For example, a sample synthesized at 100°C, using a molar ratio between scCO₂/EtOH of 95/5 and for a reaction time of 60 minutes will be denoted: C-100-EtOH-95/5-60. When parameters are constant in a same section, they are given at the beginning of the paragraph and do not appear in the nomenclature.

II. Influences of the synthesis parameters on oxometallic and sulfided phases

This part presents the effects induced by the variation of experimental parameters, presented in Table V.1, on the oxometallic phase obtained after synthesis, as well as on the sulfided phases. All samples investigated have been characterized using XRD, Raman, elementary analysis, XPS and TEM techniques. First of all, the description of a reference catalyst is given before investigations on other experimental parameters.

II.1. Reference catalyst

A reference catalyst has been prepared using the same reactor than for the preparation of samples using supercritical carbon dioxide. Typically, after impregnation and ageing for 1 hour, the impregnated sample was placed into the reactor. The temperature was then increased to 100°C and reaction was performed for 1 hour without adding CO₂ into the reactor. This sample has been noted C-100-EtOH-Air. After 1 hour of experiment, the sample was recovered and analyzed before and after sulfidation step.

II.1.1. Characteristics of the oxometallic phase

Metals loadings obtained by ICP analyses are presented in Table V.2.

Table V.2: Metals contents of reference catalyst.

<i>Reference</i>	<i>Experimental loading</i>			<i>Theoretical loading</i>		
	<i>wt. % Mo</i>	<i>wt. % Co</i>	<i>Molar ratio Co/(Co+Mo)</i>	<i>wt. % Mo</i>	<i>wt. % Co</i>	<i>Molar ratio Co/(Co+Mo)</i>
C-100- EtOH-Air	8.3	1.9	0.3	10	2.6	0.3

The differences obtained between experimental and theoretical contents of metals are due to the transfer of the impregnated samples from the beaker to the reactor (small quantity of solution stays on the walls of the beaker). This has been observed in all experiments carried out but the ratio between promoter and molybdenum has been kept fixed.

XRD characterizations of this reference catalyst is shown in Figure V.2 as well as the assignments of XRD peaks. First, peaks located above $2\theta = 35^\circ$ are assigned to the support: δ -Al₂O₃ (PDF # 046-1215) as presented in Chapter III. In the reference sample synthesized, XRD peaks have been assigned to the presence of a hydrated heteropolyanion which corresponds to H₃PMo₁₂O₄₀.6H₂O (PDF # 070-0059).

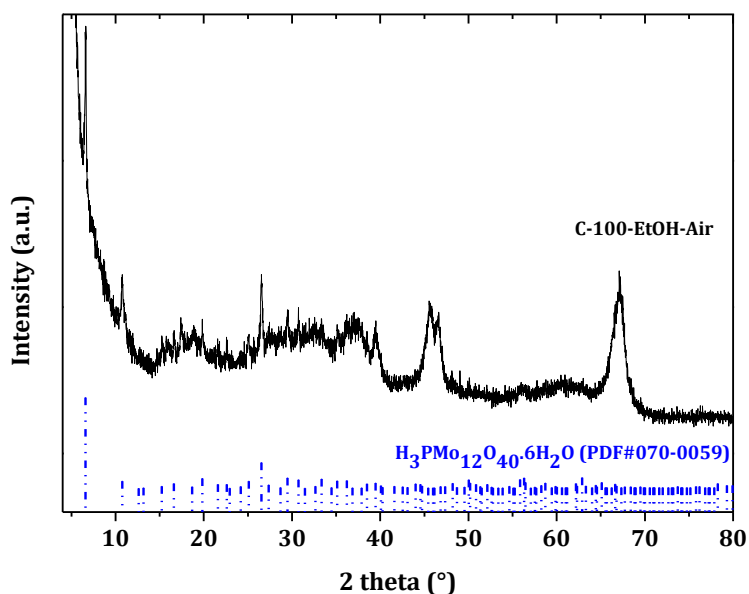


Figure V.2: XRD patterns of the reference catalyst and $\text{H}_3\text{PMo}_{12}\text{O}_{40}\cdot 6\text{H}_2\text{O}$ (PDF #070-0059).

Crystallites size of HPA onto the support has been estimated at 30 nm. By performing Raman measurements, the presence of a heteropolyanion has been attested as shown in Figure V.3. The blue line represents Raman spectrum of the solid HPA.

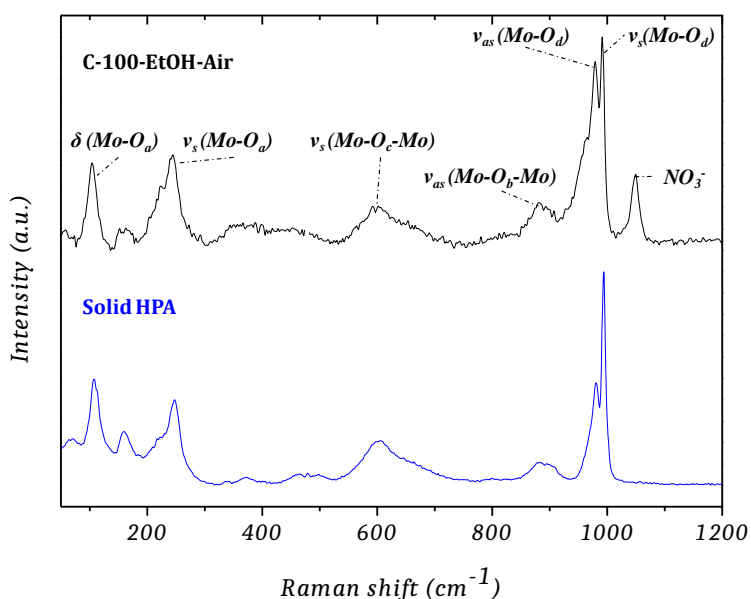


Figure V.3: Raman spectra recorded on the surface of the reference catalyst and the solid HPA.

The presence of bands located at $\sim 990\text{ cm}^{-1}$ and at $\sim 600\text{ cm}^{-1}$ are representative of a Keggin-type heteropolyanion [1–3]. The presence of crystallized heteropolyanions onto the surface of the alumina support of the reference catalyst is thus confirmed. However, repartition of these species onto the surface of alumina has to be checked. For that, electron microprobe characterization has been carried out onto the surface of cut in two alumina pellets.

From this analysis, a coefficient of repartition (R) can be given and values obtained correspond to the following conclusions. A R equal to 1 means that element detected is properly dispersed onto the surface of the alumina pellet cut in two, if $R < 1$ element concentration has a bowl profile (the

concentration is higher in the shell of the pellet than in the core) and if $R > 1$ element concentration has a domed profile (higher concentration in the core of the pellet than in the shell). Figure V.4 depicts the average profiles in concentration of elements contained in sample C-100-EtOH-Air.

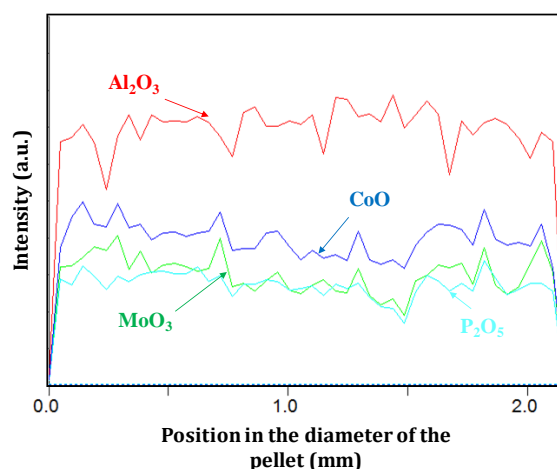


Figure V.4: Average profiles in concentration of Al_2O_3 , MoO_3 , CoO and P_2O_5 obtained by electron microprobe for sample C-100-EtOH-Air.

Probed elements have shown good distribution profiles with coefficients of repartition close to 1. However, it has been observed a slight heterogeneous concentration of elements depending on the alumina pellet analyzed.

Characterizations carried out on reference sample permit to assess the presence of crystalline Keggin heteropolyanions, having a crystallites size about 30 nm, onto the surface of alumina. A good distribution of elements has been observed along the diameter of alumina pellets. However, a slight heterogeneity of concentrations between alumina pellets analyzed is observed. This reference catalyst has then been sulfided in our laboratory (see Chapter III for detailed information) and characterized in its sulfided phase.

II.1.2. Characteristics of the sulfided phase

The lengths of MoS_2 slabs as well as their stacking have been estimated using TEM measurements. XPS measurements and deconvolutions of different species allowed us to determine the concentration of each phase present in sulfided catalysts. The equations used to determine the concentration of each phase have been detailed in the experimental part (see Chapter III). Table V.3 presents results obtained for atomic concentrations of phases present in the catalysts by XPS analysis.

Table V.3: Atomic concentrations of phases present in reference catalyst.

C-100-EtOH-Air	Atomic concentration (%)								
	MoS_2	MoO_xS_y	Mo^{6+}	CoMoS	Co_9S_8	Co^{2+}	$\text{S}_{\text{sulfide}}^{2-}$	$\text{S}_{\text{oxysulf}}^{2-}$	$\text{S}_{\text{sulfate}}$
	67	6	27	54	21	25	94	6	0

For molybdenum species, a content of around 65 % of MoS_2 phase is observed. A low content (~ 5 %) of the transition molybdenum oxysulfides MoO_xS_y has been detected whereas a large part of molybdenum remains in its oxide phase (~ 30 %). Concerning the degree of promotion of the active phase by Co atoms, it has been estimated to 54%. No sulfates species have been observed.

In order to estimate the lengths and stacking numbers of MoS₂ slabs, the count of 200 particles has been carried out on sample C-100-EtOH-Air and results are shown in Figure V.5 and Table V.4.

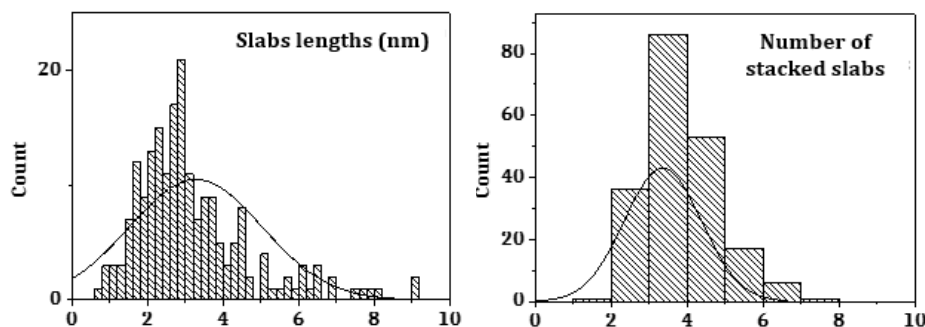


Figure V.5: Slabs lengths and numbers of stacked slabs for C-100-EtOH-Air.

Table V.4: Averages length and stacking with their associated standard deviation (STD).

	<i>Average length L (nm)</i>	<i>Average stacking (N)</i>
C-100-EtOH-Air	3.3 ± 1.8	3.4 ± 1

Crystallites of MoS₂ have been observed and no presence of segregated Co₉S₈ were revealed. MoS₂ particles and have an average length of 3.3 nm and an associated standard deviation of 1.8 nm. Concerning the degree of stacking, it has been calculated to be of 3.4 layers with an associated standard deviation of 1. These results are in agreement with literature for catalyst prepared by impregnation (water as solvent of impregnation), drying and calcination [4,5] where usually for MoS₂ slabs supported on alumina are about 2-3 nm and 3 slabs are stacked together.

The synthesis and characterizations of the reference catalyst under air will allow to compare it with catalysts prepared using supercritical carbon dioxide. From characterizations, it has been first observed the presence of Keggin-type heteropolyanions dispersed onto alumina.

After sulfidation, catalyst showed the presence ~ 65 % of MoS₂ phase, ~ 5 % of intermediate Mo_xS_y phase whereas ~ 30 % of Mo is remained in its oxide state. An average of 3.4 stacked slabs of MoS₂ having an average length of 3.3 nm has been determined.

After the presentation of the catalyst chosen as reference, the evaluation of some experimental parameters during preparation of catalysts using scCO₂ has been made by characterizations of catalysts before and after sulfidation.

II.2. Influence of the temperature of synthesis

The previous chapter has examined the evolution of species under a scCO₂ atmosphere. It has been shown that a temperature increase has a major effect on the final species present on the support. To study this effect on materials, several samples were prepared at different temperatures keeping fixed other parameters. The solvent of impregnation was ethanol and the volume of CO₂ introduced into the reactor was calculated to obtain a molar ratio of CO₂/EtOH= 95/5. The reaction time was 60 min and the temperature of injection of scCO₂ was 120°C. For two temperatures (50 and 100°C), experiments were carried out two times and obtained results are similar in terms of characterizations and testing results. Samples are denoted C-T-EtOH-95/5-60. However, for clarity and temperature being the only studied parameter, they are denoted C-T

II.2.1. Evolution of the oxometallic phase as a function of the synthesis temperature

Elementary analyses have been carried out to check if the desired molybdenum content was obtained. Table V.5 summarizes metals contents obtained by ICP analyses.

Table V.5: Metals contents of synthesized catalyst precursors.

Reference	Experimental loading			Theoretical loading		
	wt.% Mo	wt.% Co	Molar ratio Co/(Co+Mo)	wt.% Mo	wt.% Co	Molar ratio Co/(Co+Mo)
C-50	9.0	2.2	0.3	10	2.6	0.3
C-100	9.2	2.3	0.3	10	2.6	0.3
C-120	8.2	2.3	0.3	10	2.6	0.3
C-150	9.0	2.2	0.3	10	2.6	0.3
C-200	8.2	1.8	0.3	10	2.6	0.3
C-250	8.3	1.9	0.3	10	2.6	0.3
C-300	8.1	1.8	0.3	10	2.6	0.3

Theoretical quantity of molybdenum was 10 wt.%. These lower contents are due to same reasons as explained previously and the difference of contents between samples is due to the use of different batches of HPA (which possess different contents of crystallization molecules). The quantity of metals lost during the scCO₂ treatment is almost negligible. All catalysts synthesized have the same molar ratio of promoter on molybdenum. XRD characterizations performed on these materials are presented in Figure V.6.

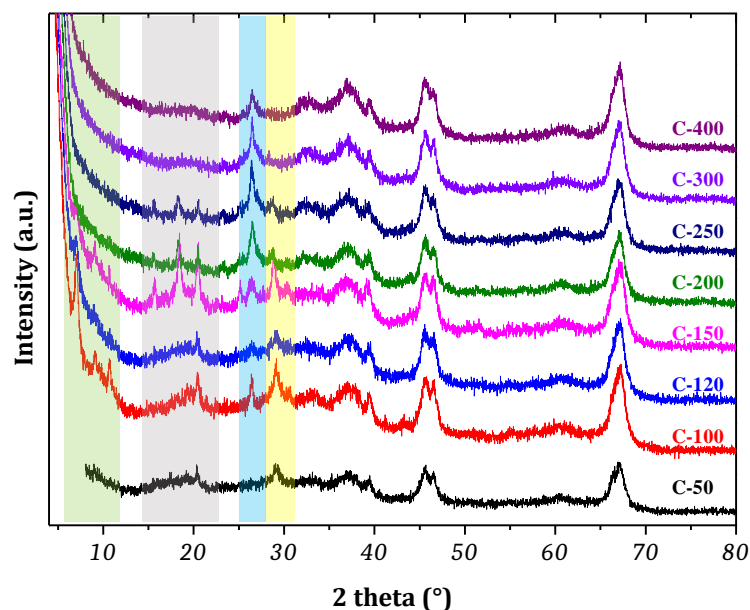


Figure V.6: XRD patterns of the materials synthesized at different temperatures.

An evolution of XRD patterns with the increase of temperature is observed. First, for synthesis temperatures lower than 200°C, the presence of a peak located at 28.8° (yellow area) as well as peaks located at 7.1°, 9.0° and 10.7° (green area) are observed. Secondly, for synthesis temperatures between 150 and 250°C, the presence of three peaks located at 15.7°, 18.4° and 20.4° (grey area) is observed. And starting from 200°C, the presence of a peak at 26.4° (blue area) is detected.

To support our XRD observations, Raman measurements have been carried out on samples synthesized at different temperatures. Raman spectra have been recorded on the surface of the synthesized samples directly after synthesis and spectra are presented in Figure V.7.

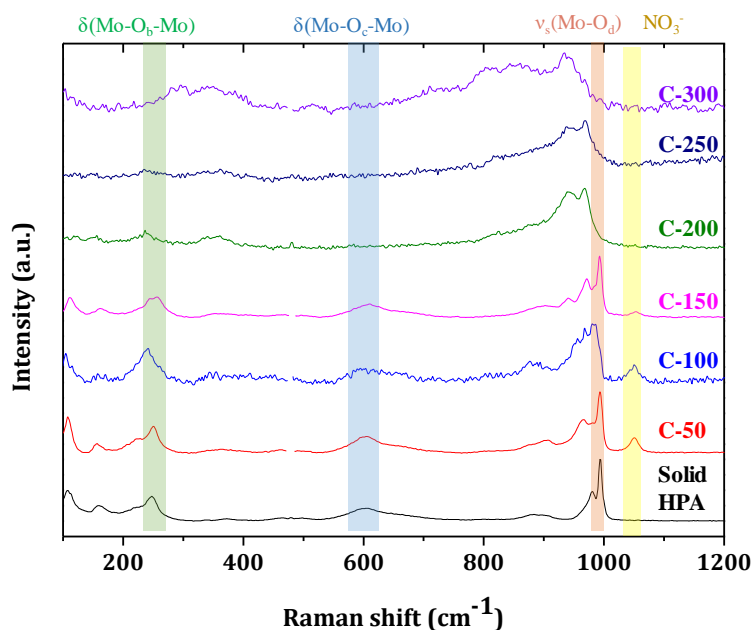


Figure V.7: Raman spectra of materials synthesized at different temperatures.

From Raman characterizations, the presence of Keggin-type heteropolyanion structure is observed until a temperature of 150°C. Indeed, the presence of the main band at 990 cm⁻¹, the band at ~ 600 cm⁻¹ and the band at 245 cm⁻¹ which are assigned to $\nu_s(\text{Mo-O}_d)$ (red area), $\delta(\text{Mo-O}_c\text{-Mo})$ (blue area) and $\delta(\text{Mo-O}_b\text{-Mo})$ (green area) respectively, confirms the presence of this type of structure onto the surface of alumina.

For synthesis temperatures between 50°C and 150°C, XRD peaks located in yellow and green areas could be assigned to hydrated heteropolymolybdate species which are decomposed for temperatures higher than 150°C. No viable PDF file has been found to assign these XRD peaks. By using Scherrer's equation, particle sizes of these species have been estimated to 10-15 nm.

When the temperature is increased, the band corresponding to the bending mode of Mo-O_c-Mo bonds (blue area) disappears and the most intense band is shifted to lower wavenumbers. The presence of polymeric molybdate species is suggested as well as the presence of cobalt molybdate species. For a synthesis at 300°C, the bands at 810 and 870 cm⁻¹ can be assigned to the Mo-O bond stretching mode of two crystallographically inequivalent MoO₄ tetrahedra present in the $\beta\text{-CoMoO}_4$ structure [6–9].

Looking at XRD patterns, at synthesis temperatures of 200°C and higher, peak at 26.4° is attributed to the presence of crystalline $\beta\text{-CoMoO}_4$ species (PDF # 021-0868). CoMoO_4 can exist under two different polymorphs (α and β), stable at room temperature, and under a hydrate phase. $\alpha\text{-CoMoO}_4$ corresponding to the low temperature isomorph whereas $\beta\text{-CoMoO}_4$ is generally synthesized at high temperature and corresponds to the high temperature modification isomorph [10,11]. However, the synthesis of the β -phase has already been reported by using ultrasonic synthesis at moderate temperature (60°C) [12]. The formation of $\beta\text{-CoMoO}_4$ at temperature of 200°C using our process is therefore possible. Moreover, the presence of crystallized cobalt molybdates, at these synthesis

temperatures, is in agreement with conclusions made after *in situ* Raman characterizations presented in Chapter IV.

For synthesis temperatures between 150°C and 250°C, disappearance of XRD peaks located at 15-21° could suggest the presence of precursors for the formation of cobalt molybdate species. These XRD peaks could not be assigned using ICDS database. However, by working in conditions close to these employed in this work, Ming et al. [13] have made reacted hydrous inorganic metal salts in CO₂ expanded ethanol and observed the formation of a cobalt hydroxide coordinated with nitrate and carbonate ions and having a formula type Co_x(OH)_y(NO₃)_z(CO₃)_m.nH₂O.

The band corresponding to the symmetric stretching mode of nitrate ions located at ~ 1050 cm⁻¹ (yellow area) decreases with the temperature to disappear at 200°C, which suggests a departure of nitrate ions around this temperature. Raman characterizations are in accordance with XRD results which suggest a change of species for temperature around 150°C with the nitrate departure and decomposition of the crystalline heteropolyanion compounds to form polymeric molybdate species as well as cobalt molybdenum species.

To check the dispersion of molybdenum, cobalt and phosphorus onto the surface of alumina, microprobe measurements were carried out on the surface of cut in two alumina beads. All samples show a good dispersion of molybdenum, cobalt and phosphorus species with a repartition coefficient between 0.95 and 1. Even for a temperature of synthesis of 200°C, where the presence of CoMoO₄ is confirmed, a good dispersion of molybdenum species is found with a repartition coefficient of 0.9. Figure V.8 is an example of a microprobe analysis for material C-50.

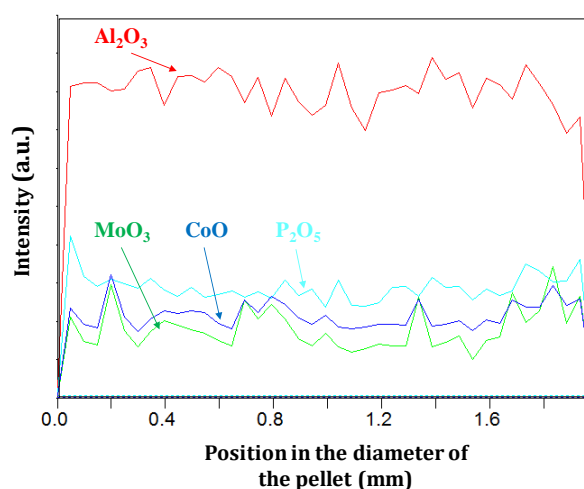


Figure V.8: Average profiles in concentration of Al₂O₃, MoO₃, CoO and P₂O₅ obtained by electron microprobe for sample C-50.

After characterizations of the oxometallic phases obtained as a function of the temperature, catalysts were sulfided and characterized in their sulfided phase.

II.2.2. Characteristics of sulfided catalysts as a function of the synthesis temperature

This part summarizes results obtained from characterizations of sulfided phases. Table V.6 presents the different chemical compositions in elements for samples synthesized at different temperatures. Samples synthesized at temperatures higher than 200°C have not been characterized due to the

presence of large crystallites of cobalt molybdates (see Figure V.6), which are known to be refractory to sulfidation [14,15].

Table V.6: Binding energies and % atomic of elements determined by XPS for catalysts as a function of the synthesis temperature.

<i>Temperature of synthesis</i>	<i>C-50</i>		<i>C-100</i>		<i>C-120</i>		<i>C-200</i>	
	<i>BE (eV)</i>	<i>% at.</i>	<i>BE (eV)</i>	<i>% at.</i>	<i>BE (eV)</i>	<i>% at.</i>	<i>BE (eV)</i>	<i>% at.</i>
C 1s-Ref.	284.6	14.4	284.6	14	284.6	15.3	284.6	12.1
O 1s	531.6	46	531.2	45.4	531.4	45.4	531.1	46.4
Al 2p	74.7	32.9	74.4	33.4	74.6	32.7	74.2	33.8
Mo 3d	228.75	1.7	228.65	1.7	228.75	1.7	228.55	2.3
Co 2p	778.8	0.6	778.6	0.6	778.7	0.5	778.6	0.5
S 2p	162.25	4.2	161.7	4.6	161.7	4.2	161.6	4.7
P 2p	135	0.2	134.8	0.3	135.6	0.1	134.9	0.2

Looking at atomic concentrations of molybdenum and cobalt, it is observed that a similar concentration has been found in all catalysts with a slightly higher content for C-200 compared to others. As ICP analyses have shown similar Mo contents for all samples and electron microprobe has shown a good distribution of elements, this difference is assigned to the error rate of XPS measurements.

Table V.7 summarizes the different concentrations of each phase determined from XPS measurements.

Table V.7: Atomic concentrations of phases present in sulfided catalysts

	<i>Atomic concentration (%)</i>								
	<i>MoS₂</i>	<i>MoO_xS_y</i>	<i>Mo⁶⁺</i>	<i>CoMoS</i>	<i>Co₉S₈</i>	<i>Co²⁺</i>	<i>S_{sulfide}²⁻</i>	<i>S_{oxysulf}²⁻</i>	<i>S_{sulfate}</i>
C-50	74	14	16	56	12	32	72	12	16
C-100	73	6	21	56	18	26	68	24	8
C-120	69	9	22	54	15	31	75	19	6
C-200	53	29	18	47	27	26	69	21	10

First observation is the decrease of MoS₂ content with the temperature of synthesis of the oxometallic phase. For samples synthesized at temperature of 120°C and less, the sulfidation of molybdenum is around 70 % whereas for a sample synthesized at 200°C, the sulfidation of molybdenum is around 50 %. This lower degree of sulfidation of molybdenum can be attributed to the presence of crystallized cobalt molybdate species before sulfidation, the latter being resistant to the sulfidation.

For C-200, a larger part of molybdenum oxysulfide species has been detected compared to other samples. The presence of such a large part of intermediate MoO_xS_y may also be related to the presence of crystalline CoMoO₄ in its oxometallic phase. This specie being more difficult to sulfide, the sulfidation has led to the intermediate molybdenum oxysulfides. In comparison with reference catalyst, samples prepared by scCO₂ route present a similar amount of MoS₂ phase. The presence of polymolybdates and/or heteropolyanions onto the surface of alumina prepared by supercritical

carbon dioxide allows thus to obtain a similar sulfidation than a sample synthesized via a conventional method. Compared to the reference sample, it has been observed a slightly higher degree of sulfidation for molybdenum, certainly due to the presence of larger crystallites in the reference catalyst. The use of scCO₂ seems thus to increase the dispersion of oxometallic species compared to a treatment under air.

Concerning the promotion of MoS₂ by Co atoms (active phase CoMoS), a similar content (around ~ 55 %) has been observed in the different materials with a slightly lower content for C-200. This sample possesses also a larger amount of Co₉S₈ phase than other samples. This may also be attributed to the presence of CoMoO₄ in C-200 before sulfidation. The materials prepared by scCO₂ route show a similar degree of promotion than the reference catalyst.

An important observation is the presence of around 10 % of sulfates in the samples prepared in scCO₂. Their concentrations are linked to the concentrations of MoO_xS_y detected in each sample. However, the presence of sulfates has not been observed in the reference catalyst C-100-EtOH-Air. As XPS measurements have been performed in the same experimental conditions, the presence of sulfates in samples synthesized in scCO₂, may be explained by the presence of CO₂ adsorbed on the surface of the support which could generate sulfates during sulfidation. Usually CO₂ is considered as an inert molecule but in presence of catalyst it can act as a soft oxidant [16] and can react according to Eq. V.1.



Moreover, Liu et al. [17] have observed that carbonyl sulfide can be oxidized on alumina to form sulfate and surface hydrogen carbonate. However, our high reducing conditions during sulfidation suggest more investigations about this presence of sulfates for sample prepared in carbon dioxide and on the genesis of the active phase for this type of catalyst. A treatment under H₂ before sulfidation could have been appropriated to reduce the amount of sulfates formed during sulfidation.

TEM measurements have then been performed on samples C-50 and C-100 as well as calculation of the averages lengths of MoS₂ particles and number of stacked slabs in each particle. Figure V.8 shows an example of TEM micrographs for these samples. Average lengths of layers as well as average degree of stacking of MoS₂ are presented in Table V.8 with their associated standard deviation.

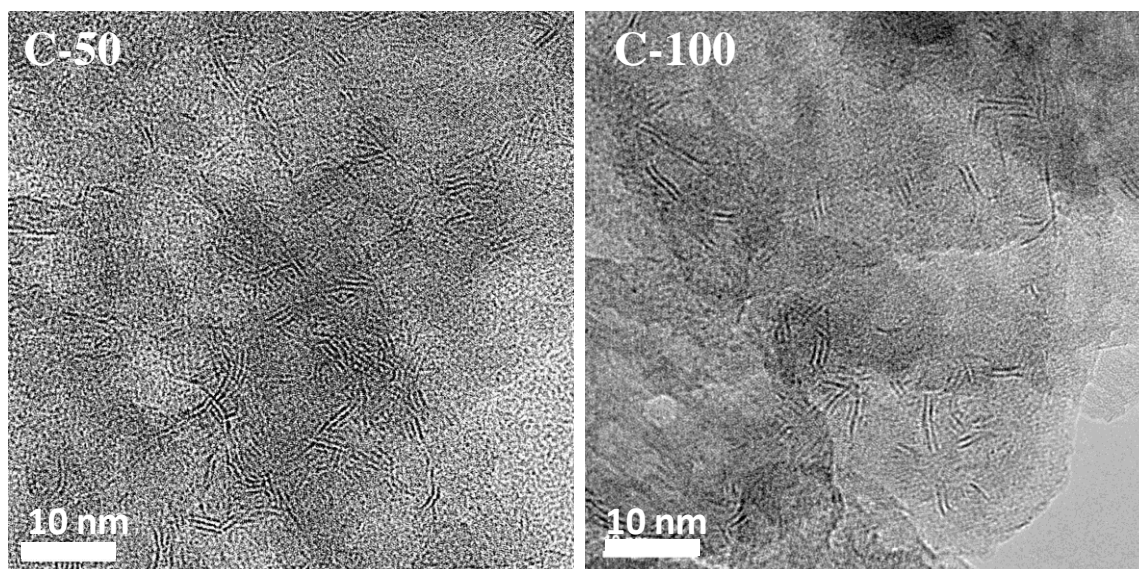


Figure V.8: TEM micrographs of samples C-50 (left) and C-100 (right).

On micrographs presented in Figure V.8, a large number of MoS_2 particles dispersed onto the surface of alumina is observed. No Co_9S_8 segregates and no major differences between the two samples have been observed during analyses. These particles consist of a stacking of several MoS_2 layers linked by Van der Waals forces. However, it has been pointed out that in the case of C-50, some areas contain only a small number of particles and other ones a large content of particles. In the case of C-100, the particles seem to be better distributed onto the support.

Table V.9: Average lengths and average degrees of stacking and their associated standard deviations for samples C-50 and C-100 (counting on 200 particles).

	<i>Average length L (nm)</i>	<i>Average stacking (N)</i>
C50	3.1 ± 1.6	3.2 ± 0.9
C100	2.7 ± 1.3	3.3 ± 1

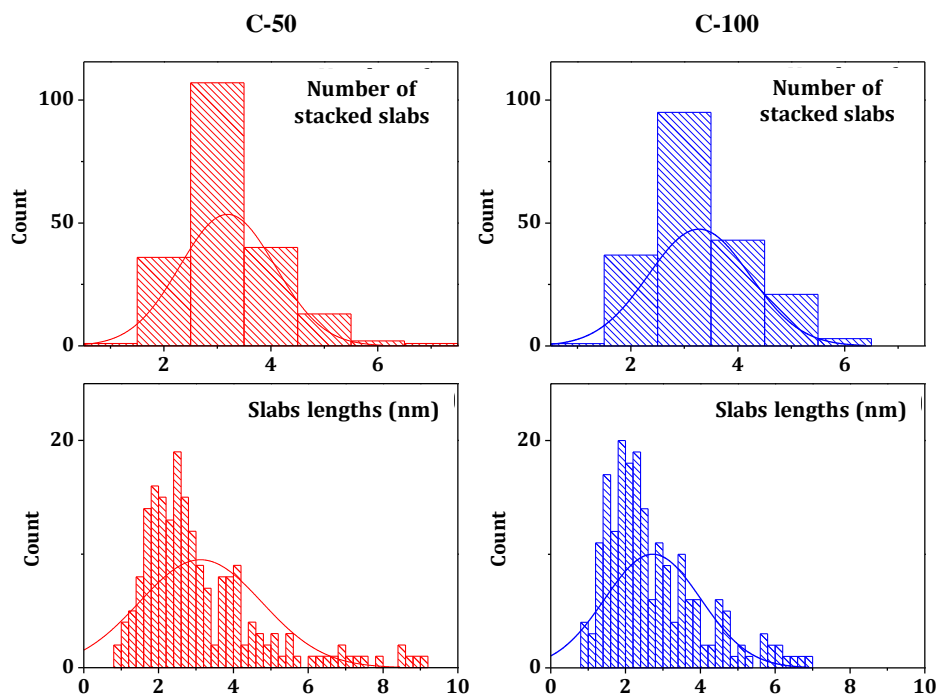


Figure V.9: Slabs lengths and numbers of stacked slabs for samples C50 and C100

Average lengths of MoS₂ slabs are in agreement with literature where layers have usually an average length of 3 to 4 nm and an average degree of stacking of 2 to 3 [4]. Figure V.9 presents the distribution of slabs lengths and stacking numbers of samples C-50 and C-100. Looking at standard deviation data obtained, sample C-100 possesses a narrower distribution than C-50.

The temperature of synthesis has an important effect on the resulting species present onto the surface of alumina. For temperatures between 50°C and 150°C, crystallized species have been detected onto the surface of alumina and have been assimilated to heteropolyanions more or less hydrated having crystallites sizes about 10-15 nm. For temperatures between 150°C and 250°C, the presence of a compound Co_x(OH)_y(NO₃)_z(CO₃)_m.nH₂O has been suggested due to its observation by other research group working in similar conditions. For temperature of 200°C and higher, the presence of crystalline cobalt molybdate species has been detected and the concentration of this phase increases with temperature of synthesis.

The sulfidation of samples synthesized at temperatures lower than 200°C has given a degree of sulfidation of molybdenum around 70% with MoS₂ slabs having an average length of ~ 3 nm and a stacking degree of slabs of ~ 3. Then, for samples synthesized at higher temperatures and containing crystallized CoMoO₄, a lower sulfidation degree of molybdenum has been detected as well as a larger part of MoO_xS_y species. A similar degree of promotion has been detected in all samples with a slightly lower for C-200. Moreover, this sample contains a larger part of Co₉S₈ than others.

Samples prepared via scCO₂ route have shown smaller MoS₂ crystallites having a narrower distribution compared to C-100-EtOH-Air, a slightly lower content of MoS₂ phase and but similar content of CoMoS phases. Compared to C-100-EtOH-Air, materials prepared via scCO₂ have shown the presence of sulfate species, which may due to adsorbed CO₂ on alumina's surface. Smaller crystallites of heteropolyanion are thus easily sulfided than larger crystallites as in the case of C-100-EtOH-Air.

Due to the effect of synthesis temperature on the formation of cobalt molybdate species, we have chosen to avoid them by working at low temperature (between 50°C and 100°C). Moreover, the antisolvent effect of CO₂ which induces precipitation of species has been reported to be more pronounced at higher pressures or lower temperatures [18]. The precipitation of particles occurs when the supersaturation is reached. A supersaturation reached rapidly facilitates uniform nucleation and almost instantaneous crystallization. This limits the growth of the particles and permits to obtain particles with a narrow distribution.

The second experimental parameter tested was the pressure of synthesis and results obtained in terms of characterizations of the oxometallic and sulfided phases are presented hereafter.

II.3. Influence of the pressure

The previous section has investigated the influence of the temperature synthesis and this one presents the influence of the pressure. Two samples were prepared at two different pressure (5 MPa and 22 MPa) keeping fixed other parameters (except ratio CO₂/EtOH which is linked to the pressure). The solvent of impregnation was ethanol and the mass of sample introduced into the reactor was calculated to have 3 mL of ethanol impregnated in the support. The temperature of synthesis was 100°C and reaction time was 60 min. Samples are denoted C-100-EtOH-P. However, for clarity and pressure being the only studied parameter, they are denoted C-P.

II.3.1. Evolution of the oxometallic phase with pressure

The first characterization was the check of the content in metals in synthesized samples. Results obtained are presented in Table V.10 and are those expected.

Table V.10: Metals contents as a function of the pressure.

<i>Reference</i>	<i>Experimental loading</i>			<i>Theoretical loading</i>		
	<i>wt. % Mo</i>	<i>wt. % Co</i>	<i>Molar ratio Co/(Co+Mo)</i>	<i>wt. % Mo</i>	<i>wt. % Co</i>	<i>Molar ratio Co/(Co+Mo)</i>
C-22	9.2	2.3	0.3	10	2.6	0.3
C-5	8.7	2.0	0.3	10	2.6	0.3

XRD characterizations are presented in Figure V.10 as well as the assignments of XRD peaks.

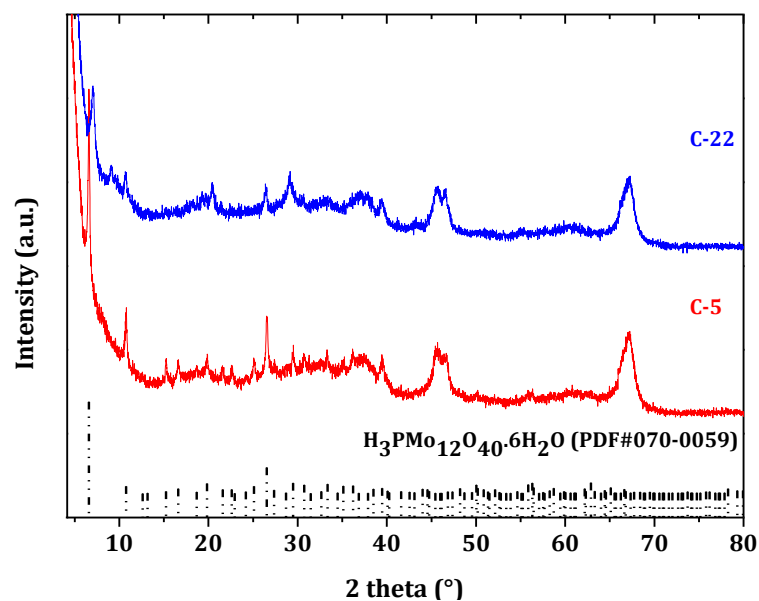


Figure V.10: XRD patterns of the materials synthesized at different pressures.

In both samples, the presence of a crystalline phase is detected but they are not equivalent. For the sample C-5, this phase has been assigned to $\text{H}_3\text{PMo}_{12}\text{O}_{40}\cdot 6\text{H}_2\text{O}$ (PDF #70-0059) and crystallite sizes have been estimated to be around 30-35 nm. In the sample C-22, the XRD pattern obtained is equivalent to those obtained at low temperatures and previously presented. This pattern has been assigned to a Keggin phase with several number of crystallization water. Crystallite sizes of this phase has been estimated to be around 10-15 nm. The pressure of CO_2 has thus an effect on the size of particles.

The presence of a heteropolyanion has been attested by performing Raman measurements. Results are presented in Figure V.11.

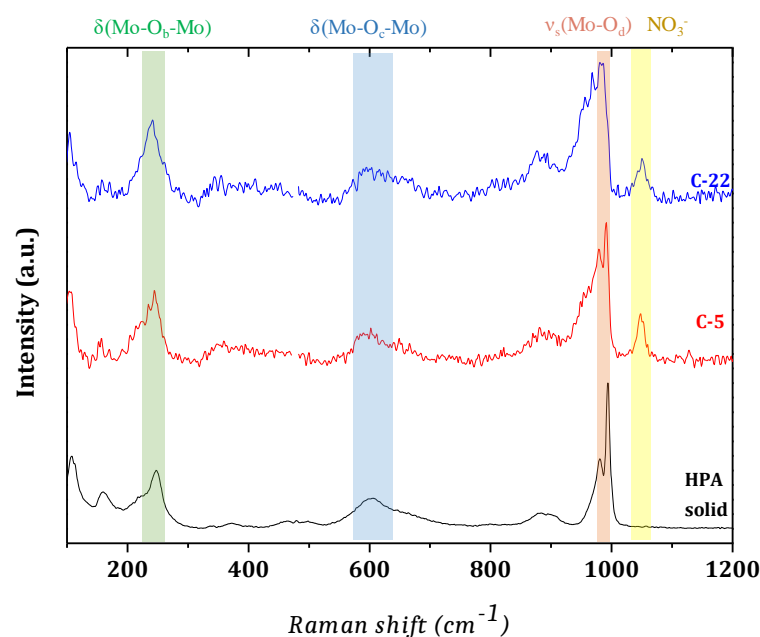


Figure V.11: Raman spectra of materials synthesized at different pressures.

The presence of bands located at $\sim 990\text{ cm}^{-1}$ and at $\sim 600\text{ cm}^{-1}$ are representative of a Keggin-type heteropolyanion. The presence of crystallized heteropolyanions onto the surface of the alumina support is thus confirmed. Moreover, a band located at $\sim 965\text{ cm}^{-1}$ with a low intensity may be attributed to the presence of a small part of polymolybdates. To verify the profiles in concentration of elements onto the surface of alumina, electron microprobe characterizations have been carried out onto the surface of cut in two alumina pellets. Figure V.12 presents the average profiles in concentration of elements contained in samples C-5 (a) and C-22 (b).

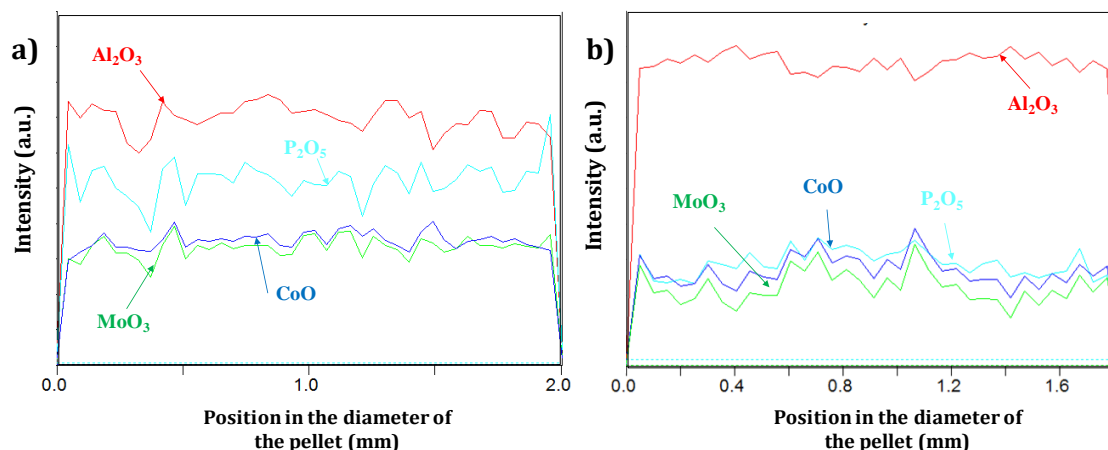


Figure V.12: Average profiles in concentration of Al₂O₃, MoO₃, CoO and P₂O₅ of C-5 (a) and C-22 (b).

Both samples have shown coefficients of repartition close to 1 for elements analyzed and thus confirm similar concentration of elements in the whole surface of alumina pellets.

The presence of different Keggin HPA as well as polymolybdates has been obtained in both samples. For a synthesis under a low pressure, the six times hydrated Keggin HPA has been obtained with crystallite sizes of around 30-35 nm. In the case of a synthesis at higher pressure, a phase of Keggin HPA and a phase of polymolybdates have also been observed and crystallite sizes have been estimated to be around 10-15 nm. The pressure has thus an effect on the size of crystallites of the HPA. This difference in crystallite sizes may be explained by a higher supersaturation in the case of a synthesis at high pressure. In both cases, a good repartition of elements has been obtained. These samples have then been characterized after sulfidation by XPS and TEM.

II.3.1. Characteristics of sulfided catalysts as a function of pressure

Degree of sulfidation of molybdenum as well as promotion of MoS₂ by cobalt atoms have been determined by XPS and results are presented in Table V.11.

Table V.11: Atomic concentrations of phases present in sulfided catalysts (case of the variation of pressure of reaction).

	<i>Atomic concentration (%)</i>								
	<i>MoS₂</i>	<i>MoO_xS_y</i>	<i>Mo⁶⁺</i>	<i>CoMoS</i>	<i>Co₉S₈</i>	<i>Co²⁺</i>	<i>S_{sulfide}²⁻</i>	<i>S_{oxysulf}²⁻</i>	<i>S_{sulfate}</i>
C-22	73	6	21	56	18	26	68	24	8
C-5	69	18	13	50	17	33	72	14	14

Concerning molybdenum species, both samples have shown a similar degree of sulfidation for molybdenum. A larger part of molybdenum oxysulfides has been observed in C-5 compared to C-22. Concerning cobalt species, samples contain similar amounts of each phases. The presence of sulfates is also detected and same hypothesis as previously can be formulated.

TEM measurements have only been performed on sample C-22. From these measurements, it has been determined an average length of MoS₂ slabs of 2.7 nm (± 1.3) and an average stacking of 3.3 (± 1).

It has been shown that the pressure influences the oxometallic phase obtained. At low pressure six times hydrated Keggin HPA has been observed whereas another HPA was found at higher pressure. Moreover, a work at high pressure permits to obtain smaller crystallites. After sulfidation, these catalysts have shown similar amounts of different phases.

As the precipitation occurs via ethanol expansion by scCO₂ to reach supersaturation, the ratio CO₂/EtOH is an important parameter to be considered.

II.4. Influence of the molar ratio CO₂/EtOH

To investigate the effect of the ratio CO₂/EtOH, three samples have been prepared wherein the weight of the impregnated support was varied and the pressure of CO₂ was kept fixed. For that, three different weights of support have been impregnated and permit to play on the molar ratio CO₂/EtOH. They are presented in Table V.12.

Table V.12: Different molar ratios tested and their respective mass of impregnated support

<i>Ratio CO₂/EtOH</i>	<i>Weight of impregnated support (g)</i>
C-98/2	1
C-95/5	3
C-80/20	10

Experiments were carried out for 60 min at 50°C using ethanol as solvent of impregnation. The scCO₂ was injected into the reactor at a temperature of 120°C. Samples are denoted C-50-EtOH-R-60. However, the ratio being the only variable parameter, samples are denoted C-R in this part.

The difference of molar ratio CO₂/EtOH modifies critical coordinates of mixtures. These critical coordinates have been found in the literature [19,20] and interpolated to obtain values for molar ratio employed. Critical coordinates interpolated are presented in Table V.13.

Table V.13: Interpolated critical coordinates for different mixtures CO₂/EtOH.

<i>Molar ratio CO₂/EtOH</i>	<i>T_c (°C)</i>	<i>p_c (MPa)</i>
C-98/2	34.8	7.6
C-95/5	39.5	8.1
C-80/20	71.5	12.0

As syntheses, have been carried out at a temperature of 50°C and a pressure of 22 MPa, in the case of the sample C-80/20, the mixture CO₂/EtOH was not under supercritical conditions during the reaction. These samples have then been characterized after synthesis and after sulfidation.

II.4.1. Evolution of the oxometallic phase as a function of the ratio CO₂/EtOH

First, loadings of molybdenum and cobalt obtained by ICP analyses are presented in Table V.14 and show for all samples similar contents in molybdenum and cobalt as previously obtained.

Table V.14: Metals contents as a function of the molar ratio CO₂/EtOH.

<i>Molar ratio of CO₂/ethanol</i>	<i>Experimental loading</i>			<i>Theoretical loading</i>		
	<i>wt. % Mo</i>	<i>wt. % Co</i>	<i>Molar ratio Co/(Co+Mo)</i>	<i>wt. % Mo</i>	<i>wt. % Co</i>	<i>Molar ratio Co/(Co+Mo)</i>
C-98/2	8.6	2.2	0.3	10	2.6	0.3
C-95/5	9	2.2	0.3	10	2.6	0.3
C-80/20	8.3	1.9	0.3	10	2.6	0.3

Figure V.13 represents XRD patterns obtained for samples C-98/2, C-95/5, C-80/20 as well as reference XRD pattern of a hydrated Keggin-type heteropolyanion H₃PMo₁₂O₄₀.6H₂O (PDF #70-0059).

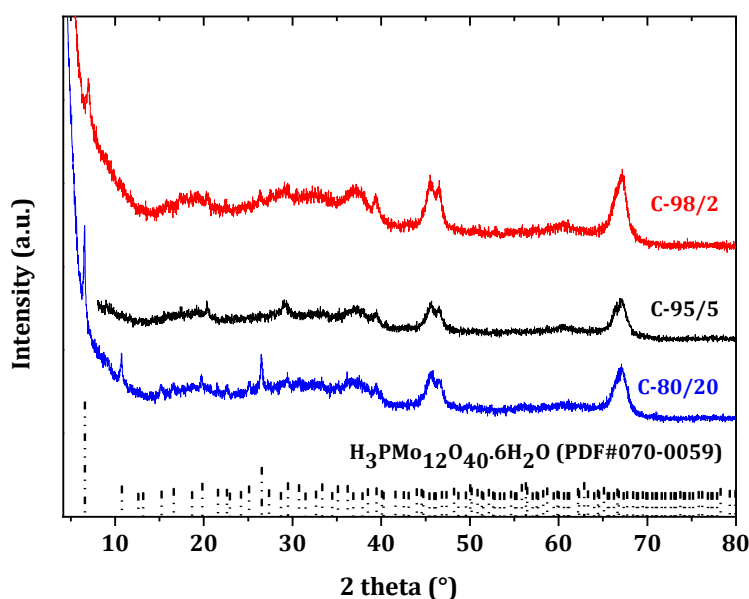


Figure V.13: XRD patterns of samples C-80/20, C-95/5 and C-98/2 as well as XRD pattern of H₃PMo₁₂O₄₀.6H₂O (PDF # 70-0059).

First, XRD patterns of samples synthesized with a high content of CO₂ (C-98/2 and C-95/5) are equivalent and consistent with those obtained at low synthesis temperatures in the previous part and may be attributed to a Keggin heteropolyanion with a different degree of hydration and having crystallites size around 10 nm. While the XRD pattern of the sample C-80/20 is different. XRD peaks present in this pattern can be assigned to a Keggin-type heteropolyanion H₃PMo₁₂O₄₀.6H₂O (PDF # 70-0059). Crystallites size of HPA phase present in this sample have been estimated to 35 nm. It has been presented in section III.3.1 that for sample C-80/20, the synthesis has not been performed under supercritical conditions due to a higher concentration of ethanol in the mixture. Yet, crystalline phase observed is equivalent to this obtained in reference catalyst C-100-EtOH-Air.

Working at low molar ratio CO₂/EtOH leads to larger crystallites of Keggin-type heteropolyanion.

Raman analyses have been carried out to attest our observations made from XRD characterization and recorded spectra are presented in Figure V.14.

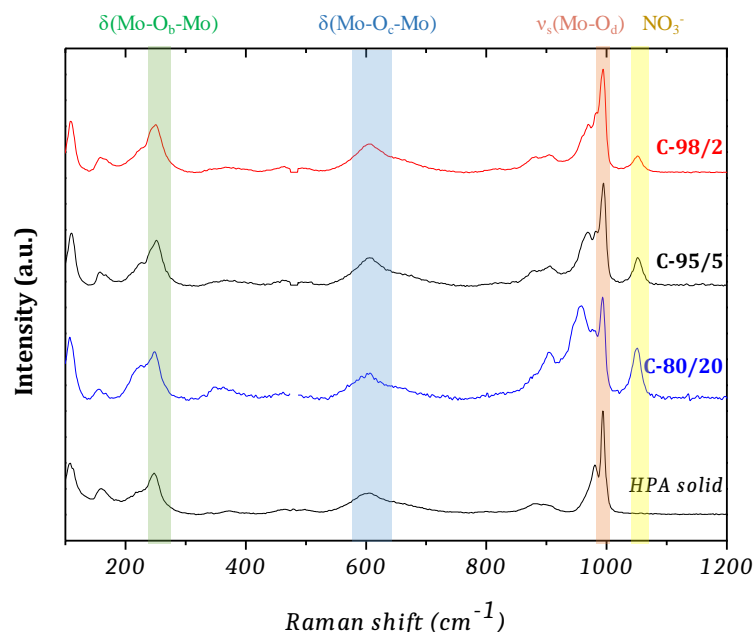


Figure V.14: Raman spectra of samples C-80/20, C-95/5, C-98/2 and solid HPA.

For all samples, Raman spectra exhibit features of a Keggin-type heteropolyanion. The symmetric stretching mode of $M-O_d$ bonds located at 994 cm^{-1} and the stretching and bending modes of $Mo-O_c-Mo$ bonds located at 605 cm^{-1} are characteristic of this type of structure. For samples synthesized with a molar ratio $CO_2/EtOH = 95/5$ & $98/2$, all bands are similar and the presence of the same structure onto the surface of alumina is probable. However, sample synthesized with a $CO_2/EtOH$ molar ratio of $80/20$ possesses an intense band located at 958 cm^{-1} while this band is only present as a shoulder in other samples. This band could correspond to polymeric molybdenum species due to the partial degradation of some Keggin units.

All catalysts show a repartition coefficient higher than 0.9 which attest of a good repartition of species on the surface of pellets. Figure V.15 represents an example of a microprobe analysis of C-98/2.

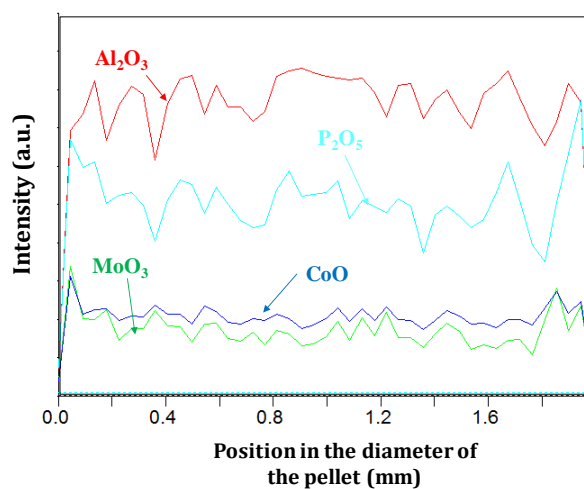


Figure V.15: Microprobe results for the sample synthesized with a molar ratio $CO_2/EtOH$ of $98/2$.

The ratio $CO_2/EtOH$ used to perform the synthesis plays a role on the obtained materials. First, when a synthesis is carried out with a mixture $CO_2/EtOH$ of $80/20$, a crystalline phase of six times

hydrated Keggin heteropolyanions is observed. This observation has also been made in the reference catalyst C-100-EtOH-Air. Raman bands have shown the presence of this Keggin heteropolyanion as well as the presence of polymeric molybdates species. The resulting crystallites have been estimated to be around 35 nm.

Secondly, when the synthesis is performed with larger quantity of CO₂, a crystalline phase is also observed and has been attributed to a Keggin heteropolyanion phase having a different degree of hydration where crystallite sizes have been estimated to be around 10 nm.

The ratio CO₂/EtOH is an important parameter impacting the crystallite sizes, as pressure. When the volume of ethanol to expand is low, the supersaturation is important and many nuclei are formed which implies few growth of the particles [21–23].

A second explanation may be the presence of a larger volume of ethanol for the synthesis of C-80/20 than for other samples. HPA compounds are known to be acidic and oxidative catalysts [24]. HPA compounds possess a discrete ionic structure, comprising fairly mobile basic structural units and exhibit a high affinity for the polar molecules such as ethanol. These polar molecules are easily absorbed in the bulk of HPA without affecting the Keggin units to form a so called “pseudo-liquid phase” [25]. This allows to these compounds to catalyse reactions at moderate temperatures. Okuhara et al. [26] have studied the thermal desorption of ethanol over H₃PW₁₂O₄₀, previously absorbed at 25°C. They have observed a dehydration of ethanol, and thus the formation of water, during desorption of ethanol for temperatures lower than 100°C. Alharbi et al. [27] have shown that ethanol can be dehydrated at temperatures around 100°C on supported HPA catalysts. One can consider the same reaction during the preparation of our catalysts, but it should be noted that our synthesis temperature was lower (50°C).

Alumina is also known to be a catalyst for the dehydration of alcohols. into ethers and alkenes. However this reaction occurs at higher temperatures [28–30] than our temperature of synthesis.

The larger amount of formed water in the case of the preparation of C-80/20 may explained these difference of crystallite sizes with other samples. HPA entities aggregate around water molecules and lead to large HPA crystallites. To obtain well distributed small crystallites, a synthesis with a high CO₂/EtOH ratio is recommended.

The presence of polymolybdates in the case of C-80/20 may be explained by the instability of the HPA entities in water (formed by dehydration of ethanol).

To estimate and investigate the effect of the ratio employed during synthesis, these samples have also been characterized after sulfidation.

II.4.2. Characteristics of the sulfide phase as a function of the ratio CO₂/EtOH

After sulfidation, these catalysts have been characterized and Table V.15 presents the atomic concentrations of phases determined by XPS.

Table V.15: Atomic concentrations of phases present in sulfided catalysts.

<i>Atomic concentration (%)</i>									
	<i>MoS₂</i>	<i>MoO_xS_y</i>	<i>Mo⁶⁺</i>	<i>CoMoS</i>	<i>Co₉S₈</i>	<i>Co²⁺</i>	<i>S_{sulfide}²⁻</i>	<i>S_{oxysulf}²⁻</i>	<i>S_{sulfate}</i>
C-80/20	69	18	13	57	20	23	72	12	16
C-95/5	74	14	16	56	12	32	72	12	16
C-98/2	76	7	17	61	16	23	87	8	5

For all samples a concentration of MoS₂ phase around 70-75% has been observed. Sample C-98/2 possesses a slightly lower content of MoO_xS_y phase compared to other samples where similar Mo⁶⁺ content is observed. Concerning the promotion of MoS₂ by cobalt atoms (CoMoS phase) it has been determined to be around 55-60 %. In all samples, the presence of sulfates has been detected with a lower concentration for the sample C-98/2. To explain the presence of these sulfates and their absence in the reference catalyst C-100-EtOH-Air, the same hypothesis, as previously discussed, can be advanced.

Each sample has shown a good degree of sulfidation of molybdenum as well as a good promotion. The difference of crystallite sizes between samples has not shown major effects on the sulfidation of molybdenum and promotion of MoS₂ by Co atoms.

The measurements of the lengths of slabs as well as stacking numbers have been calculated for these three samples and results are presented in Table V.16. Figure V.16 represents TEM pictures of samples synthesized with a different CO₂/EtOH ratio whereas Figure V.17 depicts statistics in terms of slabs lengths and stacking numbers of slabs.

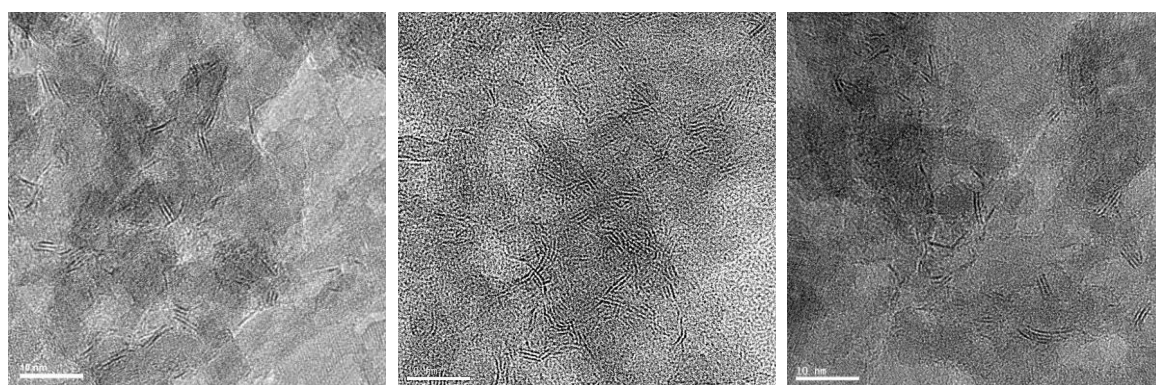


Figure V.16: TEM micrographs of samples C-80/20, C-95/5 and C-98/2.

In all cases, a large number of slabs and a homogeneity of layers onto the support have been observed. Looking at the average lengths of layers, we found a slightly higher average length for sample C-95/5 compared to C-80/20 and C-98/2. Concerning the average of degree of stacking, an average of 3 layers has been found in the case of each sample. In all cases, no presence of crystallized Co₉S₈ was observed.

Table V.16: Average lengths and degrees of stacking for samples C-80/20, C-95/5 and C-98/2.

	<i>Average length L (nm)</i>	<i>Average stacking (N)</i>
C-80/20	2.8 ± 1.4	3.0 ± 1.0
C-95/5	3.1 ± 1.6	3.2 ± 0.9
C-98/2	2.8 ± 1.3	3.3 ± 0.9

The difference of slabs lengths between samples is low as well as associated standard deviations. C-80/20 has shown larger particles (~ 35 nm) before sulfidation compared to others samples (~ 10 nm) but average MoS₂ lengths estimated have found to be similar. The presence of large particles of crystallized hydrated heteropolyanions seems not to be non-detrimental to obtain short MoS₂ slabs. By comparison with reference catalyst C-100-EtOH-Air, in all samples average of slabs lengths are smaller. The use of scCO₂ seems more efficient to obtain small MoS₂ slabs after sulfidation compared to air.

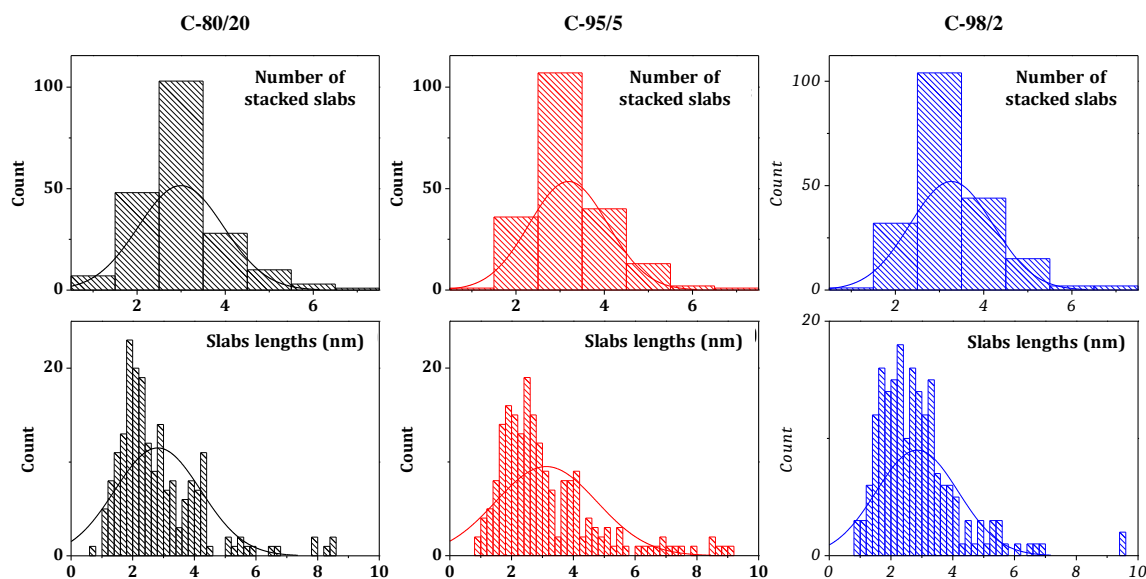


Figure V.17: Crystallite sizes and numbers of stacked layers for samples C-80/20, C-95/5 and C-98/2.

In the three samples, the presence of Keggin-type heteropolyanion structure has been identified by Raman and XRD. The presence of crystallized six times hydrated Keggin-type heteropolyanion has been observed in sample C-80/20 as well as the presence of polymeric molybdates, whereas another crystallized heteropolyanions have been found in other samples. A synthesis with lower CO_2 quantity leads to the presence of $\text{H}_3\text{PMo}_{12}\text{O}_{40}\cdot 6\text{H}_2\text{O}$ as observed in samples C-80/20. Same crystalline phase has been observed for the reference catalyst C-100-EtOH-Air.

Estimated crystallites sizes have been found to be larger in the case of C-80/20 compared to others. However, no major differences of MoS_2 slabs lengths have been observed after the sulfidation of the samples.

This difference of crystallites sizes before sulfidation may be attributed to several reasons; a volume of ethanol to be expanded/extracted larger in the case of C-80/20 and thus a lower supersaturation compared to C-95/5 or C-98/2. Less nuclei are formed and the growth of particles is more important [21,31]. The second possible explanation being the formation of water, due to the dehydration ethanol, and agglomeration of Keggin entities around these water molecules. Moreover, the difference of weight of alumina present in the reactor may have also impacted the temperature profile inside it.

After the variation of the temperature, pressure of reaction and the ratio CO_2/EtOH , the study of the influence of the solvent of impregnation appeared to be interesting. Results associated to this investigation are presented in the following part.

II.5. Influence of the solvent of impregnation

As seen in the previous chapter, the solvent already plays an effect during impregnation and maturation. Using ethanol as solvent instead of water permits to keep the Keggin structure intact. It has been shown that the precipitation of species occurs when the supersaturation is reached by expansion/extraction of the solvent. For this work, it has been decided to test two other alcohols besides ethanol: methanol and propan-1-ol.

Experiments for the study of the solvent of impregnation were carried out at 100°C and at a pressure of 22 MPa. The reaction time was 60 min and the temperature of scCO₂ injection was 120°C. The ratio CO₂/alcohol employed was 95/5. Depending of the alcohol employed, critical coordinates will differ as well as those of mixtures of CO₂/alcohols (see Chapter III). These coordinates have been taken from the literature [20] and are presented in Table V.16. Samples will be denoted C-100-S-95/5-60-12 during their comparison with other samples. However, in this part the only variable being the solvent, they are denoted C-S (C-MeOH in the case of methanol as solvent).

Table V.16: Interpolated critical coordinates for CO₂/alcohol mixtures with a molar ratio 95/5

<i>Solvent of impregnation</i>	<i>T_c (°C)</i>	<i>p_c (MPa)</i>
Methanol	35.8	7.6
Ethanol	39.5	8.1
Propan-1-ol	45.1	8.9

The critical temperature and pressure increase with the chain length of alcohol for a mixture of CO₂/alcohol with a molar ratio of 95/5. In our reaction conditions, the supercritical regime is reached just several seconds after beginning of experiment for methanol and ethanol and several minutes in the case of the propan-1-ol.

II.5.1. Evolution of the oxometallic phase as a function of alcohol nature

The same characterizations than previously have been carried out to check the loadings of metals and the dispersion of molybdenum and cobalt species onto the surface of the alumina support. In this part, Raman mapping of alumina beads cut in two are also presented.

ICP analyses have been carried out on synthesized samples with different alcohols and results are presented in Table V.17.

Table V.17: Metals contents of synthesized samples with different solvents of impregnation.

<i>Solvent of impregnation</i>	<i>Experimental loading</i>			<i>Theoretical loading</i>		
	<i>wt. % Mo</i>	<i>wt. % Co</i>	<i>Molar ratio Co/(Co+Mo)</i>	<i>wt. % Mo</i>	<i>wt. % Co</i>	<i>Molar ratio Co/(Co+Mo)</i>
C-MeOH	8.7	2.2	0.3	10	2.6	0.3
C-EtOH	9.2	2.3	0.3	10	2.6	0.3
C-PrOH	9.0	2.3	0.3	10	2.6	0.3

A loading of about 9 wt.% of Mo has been reached for all samples keeping a molar ratio of promoter on molybdenum constant.

XRD patterns of synthesized samples using different solvents of impregnation are presented in Figure V.18.

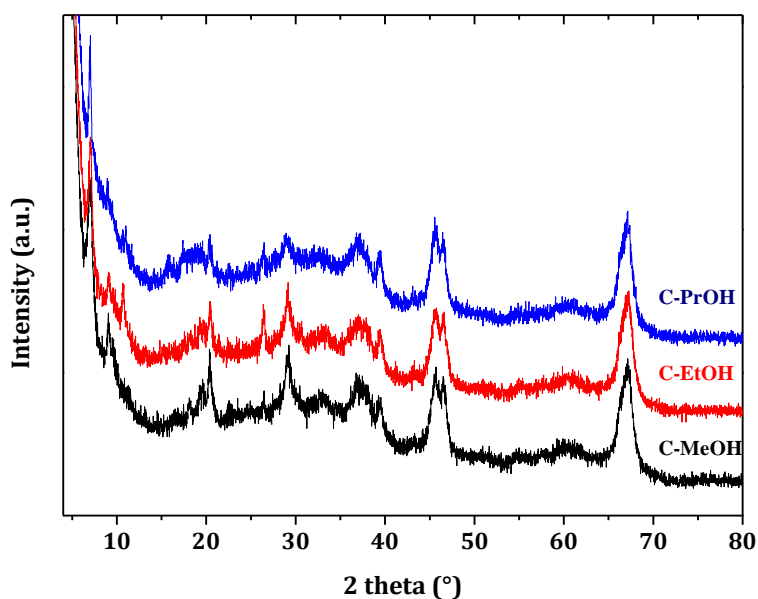


Figure V.18: XRD patterns of samples synthesized with different solvents of impregnation.

XRD patterns of these samples show crystalline species onto the surface of alumina in all cases. The same XRD peaks which corresponding to those observed at low temperatures of synthesis. These XRD peaks are assigned to a crystallized hydrated Keggin-type heteropolyanion. Crystallite sizes have been estimated to be around 10-15 nm in all cases.

Raman measurements have been carried out on the surface as well as on the surface of cut in two alumina pellets. Raman spectra recorded at the surface of pellets are presented in Figure V.19.

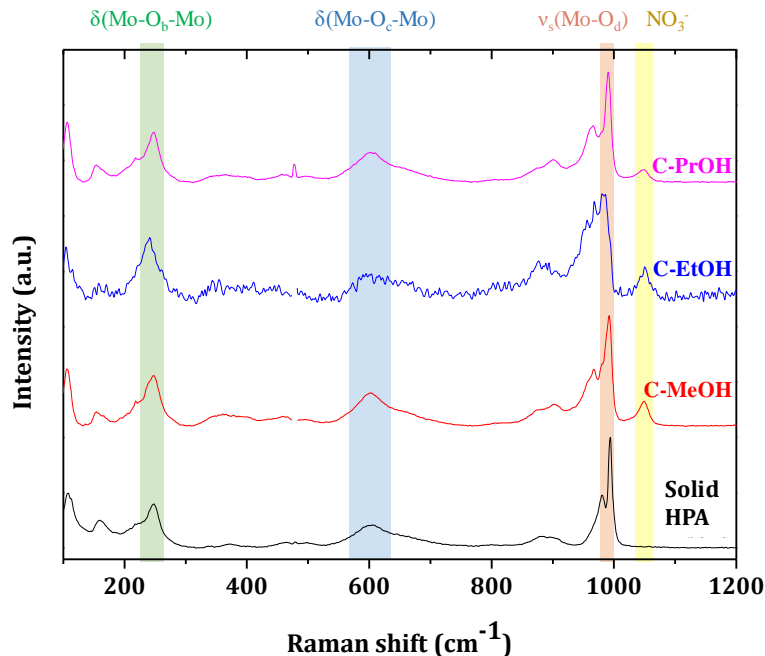


Figure V.19: Raman spectra of samples synthesized using different solvents of impregnation and of the solid HPA.

Each sample exhibits the same Raman spectra. The band located at $\sim 990 \text{ cm}^{-1}$ is assigned to the symmetric stretching mode of the Mo-O_d bonds, whereas the band located at 605 cm^{-1} is assigned to the symmetric stretching and bending modes of $\text{Mo-O}_c\text{-Mo}$ bonds. The presence of a Keggin-type heteropolyanion on the surface of the support is thus attested.

For these samples, a Raman mapping has also been recorded on the surface of an alumina bead cut in two. This mapping permits us to qualitatively determine if species present along the surface of the half bead are equivalent.

Figure V.20 represents the Raman mappings performed on alumina beads cut in two. Raman mappings show position in extrudate as a function of the Raman shift. Most intense Raman bands are depicted in red whereas low intensities Raman bands are depicted in blue.

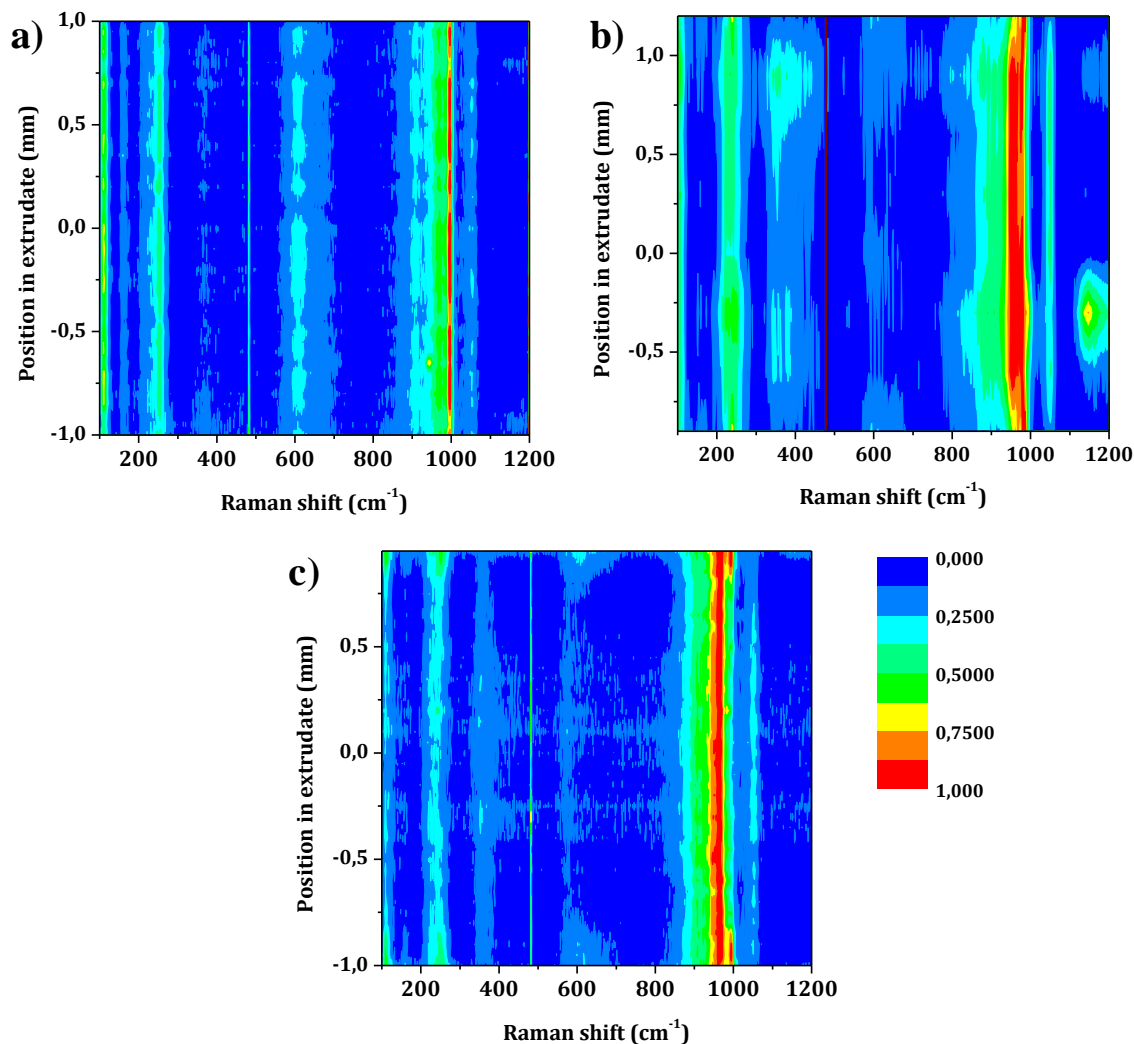


Figure V.20: Raman mappings of samples: a) C-MeOH, b) C-EtOH and c) C-PrOH.

First, the conservation of the Keggin structure along the extrudate is observed for the case of a synthesis with methanol. This can be affirmed by the presence of the symmetric and bending modes of Mo-O_c-Mo bonds located around 600 cm^{-1} . Moreover, the symmetric stretching mode of Mo-O_d bonds is observed at 990 cm^{-1} for each position in the extrudate.

In the case of a sample synthesized with ethanol as solution of impregnation, the presence of Keggin heteropolyanion is observed along the position of the extrudate and more pronounced on the edges of the extrudate. Inside the core of the pellet, the presence of polymeric molybdate species is also detected (symmetric stretching mode of Mo=O bonds). A depolymerisation of the Keggin heteropolyanion is thus observed for species present into the core of the pellet.

The same trend as for a synthesis in ethanol has been observed in the case of a synthesis with propan-1-ol. But in this case, the presence of Keggin heteropolyanion has only been observed at the edges of the extrudate (the surface of the bead). Inside the core of the pellet, polymeric molybdate species are present with their symmetric stretching band located around 960 cm^{-1} .

The solvent of impregnation has thus an effect on the resulting species present onto the surface of alumina. It seems that in the case of a synthesis in methanol, Keggin-type heteropolyanion is conserved in all positions of the pellet. For a synthesis in ethanol, this compound is also observed onto the whole surface of the support but the presence of polymolybdates is also detected inside the pellet. In the case of propan-1-ol, the presence of heteropolyanions is only detected on the exterior of the pellets and species present inside are assigned to polymeric species. Figure V.21 is a schematic representation of different species present onto the support as a function of the solvent of impregnation.

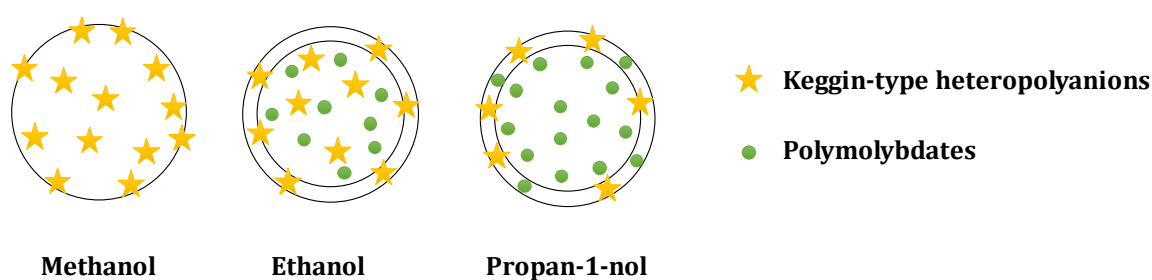


Figure V.21: Schematic representation of species present onto the support as a function of the solvent of impregnation.

Raman mapping allowed us to determinate qualitatively species present onto the surface of the support. To determine quantitatively the content of metals, microprobe analyses have been carried out.

For samples synthesized using methanol or ethanol, microprobe analyses have shown a good repartition for molybdenum, cobalt and phosphorus with repartition coefficient between 0.95 and 1.05. On the other hand, for the sample C-PROH, molybdenum and cobalt are well dispersed (repartition coefficient between 0.95 and 1.05) but phosphorus is more present on the edges of the pellet than in the core as shown in Figure V.22.

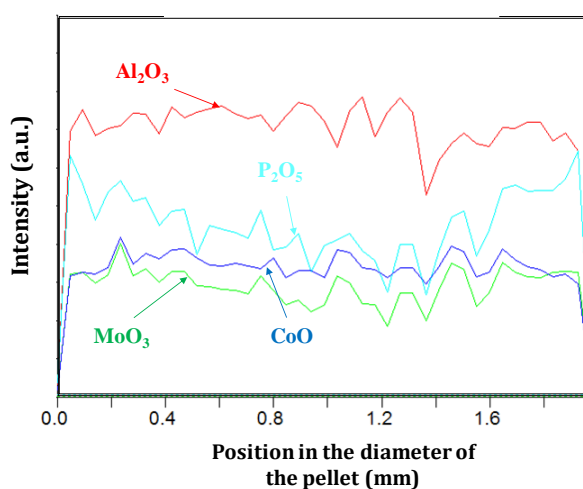


Figure V.22: Microprobe analysis of the sample synthesized using propan-1-ol as solvent of impregnation.

Observations made from Raman mapping characterization are in agreement with the profile of concentration of phosphorus along the position in the extrudate, namely the presence of Keggin compounds only on the outside of the pellet.

Several reasons could explain this difference of species which are dependant of the solvent of impregnation employed. The presence of polymolybdate species in the C-EtOH and C-PrOH system may be explained by the formation of water from dehydration of alcohols due to the instability of Keggin-type heteropolyanions in water as seen in Chapter IV. An alcohol with a longer carbon chain is easier to be dehydrated than an alcohol with a smaller carbon chain length. The amount of water formed is thus more important for the following solvents: n-propanol, ethanol and methanol. It has been presented previously that HPA can dehydrate small alcohols. Moreover, alumina is therefore known to be a catalyst for the dehydration of alcohols. into ethers and alkenes at higher temperatures [28–30].

Almost no differences of crystallite sizes have been observed with XRD. However, the expansion of solvent is not identical for each alcohol. Methanol is less viscous and possesses a higher affinity with CO₂ than ethanol and propanol. Its expansion is easier than for other alcohols, more nuclei will thus be formed and less growth observed compared to a synthesis using ethanol or propanol. In theory, crystallite sizes increase in the following order: methanol < ethanol < n-propanol. But this was not observed in our case and may be more visible for lower CO₂/ROH ratios.

After characterizations of the catalysts after synthesis, their characterizations after sulfidation are presented in the following part.

II.5.2. Characteristics of the sulfided phases as a function of the alcohol nature

Atomic concentrations of phases present onto the surface of catalysts after sulfidation are presented in Table V.18.

Table V.18: Atomic concentration of phases present in sulfided catalysts.

	<i>Atomic concentration (%)</i>								
	<i>MoS₂</i>	<i>MoO_xS_y</i>	<i>Mo⁶⁺</i>	<i>CoMoS</i>	<i>Co₉S₈</i>	<i>Co²⁺</i>	<i>S_{sulfide}²⁻</i>	<i>S_{oxysulf}²⁻</i>	<i>S_{sulfate}</i>
C-MeOH	76	8	16	60	14	26	83	11	6
C-EtOH	73	6	21	56	18	26	68	24	8
C-PrOH	61	25	14	55	23	22	73	18	9

Atomic concentrations of MoS₂ is around 75 % for sample C-MeOH and C-EtOH whereas is 61 % for the sample C-PrOH. Moreover, sample C-PrOH possesses a higher content of intermediate species MoO_xS_y compared to other samples. This difference of degree of sulfidation of molybdenum may be due to the presence of a larger part of polymolybdates in C-PrOH compared to other samples.

For the promotion of MoS₂ by cobalt, we have found a high degree of promotion in each case (~ 55-60 %). The solvent of impregnation has almost a negligible effect on the promotion of the active phase. In this case also, the presence of sulfates is reported and can be due to the presence of adsorbed CO₂ onto the surface of alumina.

Estimations of MoS₂ lengths as well as degree of stacking of each catalyst are presented in Table V.19 and Figure V.23.

Table V.19: Average lengths and degrees of stacking as well as associated standard deviations for samples C-MeOH, C-EtOH and C-PrOH

	<i>Average length L (nm)</i>	<i>Average stacking (N)</i>
C-MeOH	3.0 ± 1.9	3.0 ± 0.9
C-EtOH	2.7 ± 1.3	3.3 ± 1.0
C-PrOH	3.2 ± 2.0	3.2 ± 1.1

For all samples, three stacked slabs of MoS₂ in average have been obtained. Average lengths of MoS₂ layers increase in the following order C-EtOH < C-MeOH < C-PrOH. Looking at Figure V.21 and to standard deviations, a broader distribution in particles sizes is observed for sample C-PrOH compared to others.

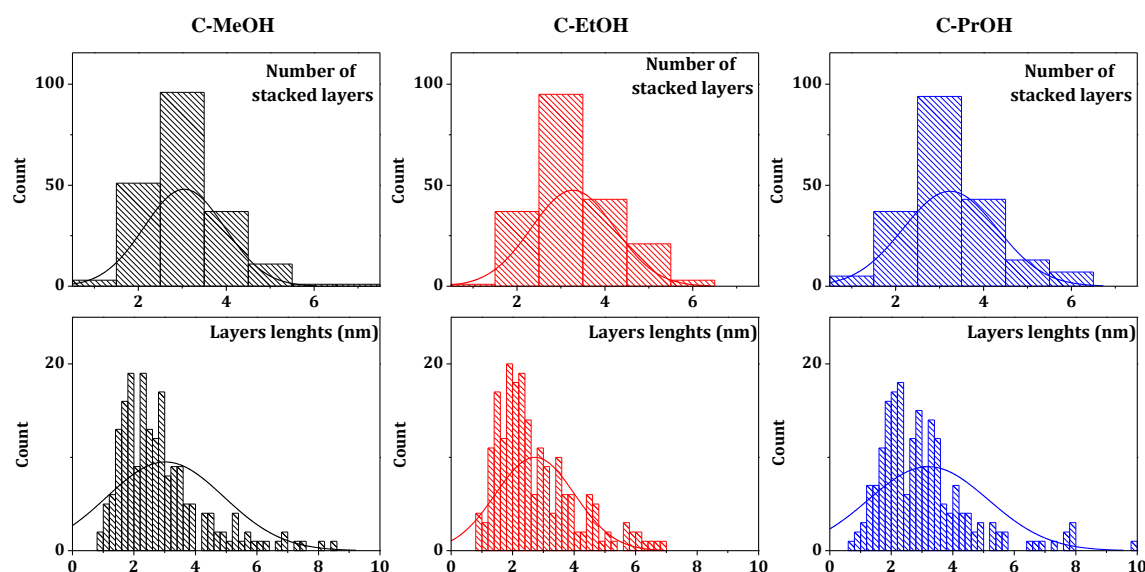


Figure V.23: Crystallite sizes and numbers of stacked layers for samples C-MeOH, C-EtOH and C-PrOH

The solvent of impregnation has an effect of the resulting species present onto the surface of alumina after synthesis. First observation was that, for all solvents of impregnation, the structure of the Keggin-type heteropolyanion is retained at the surface of the support after synthesis. Nevertheless, having performed Raman mapping experiments, it has been observed that in the case of methanol the structure was retained along the core of alumina pellets. In the case of ethanol, we have observed that Keggin units were present along the core of alumina beads and polymolybdate species were present only inside of pellets. In the case of using propan-1-ol as solvent of impregnation, polymeric molybdenum species at all places of pellets have been observed while the structure of the heteropolyanion was only detected onto the surface of pellets.

Several explanations can be proposed to clarify these differences. The first possible explanation may be due to the dehydration of alcohols as mentioned in the previous intermediate conclusion. The formed water from this dehydration could then decompose Keggin entities and this could explain the formation of polymolybdates in the case of a synthesis using ethanol or n-propanol. Dehydration rates for n-alcohols are the following: n-propanol > ethanol > methanol [28]. More water molecules are formed in the case of C-PrOH compared to others. Over alumina, the formation of ethers from alcohols by intermolecular dehydration starts around 130-140°C [29] and the formation of alkenes by monomolecular dehydration occurs at higher temperatures. However, our conditions of temperature synthesis are lower to these generally observed for the dehydration of

alcohols over alumina. This let us think that dehydration of alcohols can be catalyzed by the HPA entities, as proposed during the study of the influence of CO₂/EtOH ratio.

The second explanation could be related to the volume expansion of the alcohols which decreases with increasing molecular weight of the co-solvent molecule [32,33], as presented in Figure V.24.

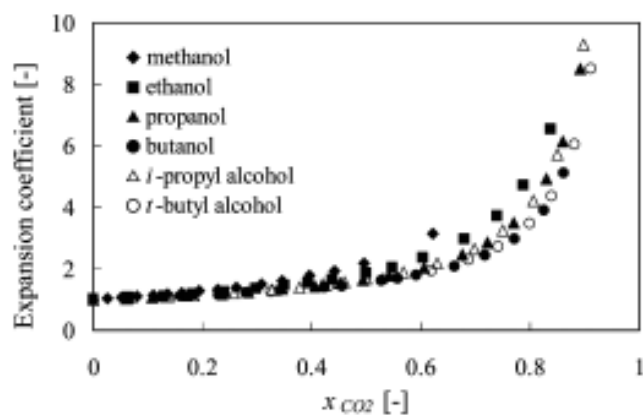


Figure V.24: Expansion coefficient versus pressure for CO₂-alcohol mixtures at 40°C (from [33])

The CO₂-*n*-PrOH mixture is less expanded than the CO₂-MeOH and CO₂-EtOH mixtures. The fact that precipitation occurs in a longer period of time, due to a lower expansion coefficient, in the case of CO₂-*n*-PrOH system can be explained by the presence of polymolybdate species in the core of alumina pellets.

The third explanation could be the difference of binary diffusion coefficients (D_{12}) of alcohols. Yi Kong et al. [34] have determined binary diffusion coefficients for polar compounds in supercritical carbon dioxide and found a decrease of D_{12} when the carbon chain of the alcohol increases. Working with *n*-propanol allows less diffusion than a work with methanol.

Concerning characteristics of the sulfided phase, it has been determined that samples C-MeOH and C-EtOH possess equivalent amounts of each phase. However, it has been found in the case of C-PrOH, a lower concentration of MoS₂ and a higher concentration of MoO_{*x*}S_{*y*}. A larger part of Co₉S₈ has also been detected in this sample. The solvent of impregnation has thus an indirect influence on the resulting sulfided phase.

After having studied the effects of the reaction temperature, the pressure, the ratio CO₂/solvent and the solvent of impregnation, one major effect to investigate is the reaction time. This process could permit a work with a very short reaction if the supersaturation of the solvent is reached rapidly. The next part is thus dedicated to the investigation of this experimental parameter.

II.6. Influence of the reaction time

This part deals with the influence of the reaction time on the catalyst precursor formation. To investigate the effect of the reaction time, three experiments were carried out for 120 min, 60 min and less than one minute. Figure V.25 represents the flow scheme of the experiments performed at different times.

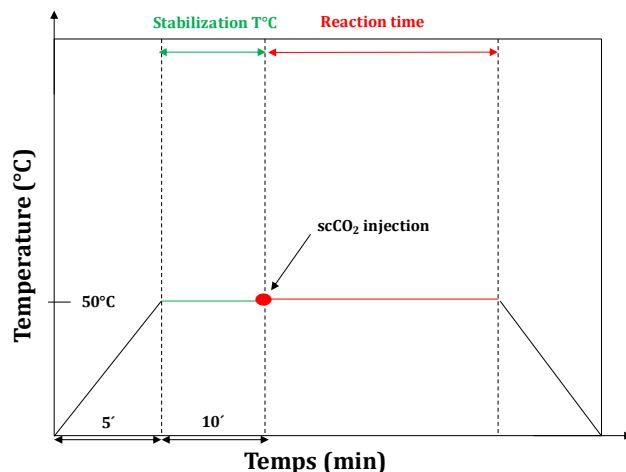


Figure V.25: Flow scheme of an experiment.

The reaction time beginning when the desired temperature and pressure are reached and stabilized. In the case of these syntheses, the reaction temperature was 50°C and the pressure was 22 MPa. The temperature of supercritical carbon dioxide during its injection in the reactor was about 120°C. Experiments were carried out using ethanol as solvent of impregnation and a molar ratio CO₂/ethanol of 95/5. For comparison, these catalysts will be denoted C-50-EtOH-95/5-t-120. However, the reaction being the only variable, they are denoted C-t in this section.

II.6.1. Evolution of the oxometallic phase as a function of reaction time

As previously, expected contents have been checked by ICP analyses and results are presented in Table V.20.

Table V.20: Metals contents of synthesized samples with different reaction times.

<i>Reaction time (min)</i>	<i>Experimental loading</i>			<i>Theoretical loading</i>		
	<i>wt. % Mo</i>	<i>wt. % Co</i>	<i>Molar ratio Co/(Co+Mo)</i>	<i>wt. % Mo</i>	<i>wt. % Co</i>	<i>Molar ratio Co/(Co+Mo)</i>
C-120	8.5	2.1	0.3	10	2.6	0.3
C-60	9	2.2	0.3	10	2.6	0.3
C-<1	7.6	1.8	0.3	10	2.6	0.3

Molar ratio between promoter and molybdenum have been kept fixed. Difference of metal contents are also due to reasons previously mentioned.

Figure V.26 shows the XRD patterns performed on these materials.

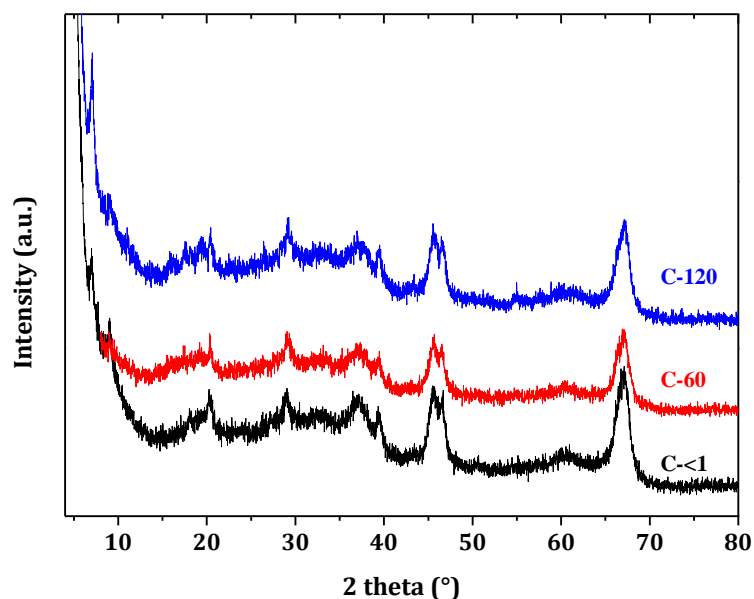


Figure V.26: XRD patterns of samples synthesized with different reaction times.

XRD patterns obtained for samples synthesized with different reaction times possess similar diffraction peaks. As in the studies of other parameters, the presence of Keggin-type heteropolyanion species is envisaged. Estimations of crystallite sizes are about 10 nm and are identical for all samples.

The time of reaction leads to identical crystalline species which possess equivalent crystallite sizes. As expected, it can be proposed that supersaturation becomes quickly high and precipitation occurs directly after the injection of scCO_2 .

To confirm the presence of Keggin species onto the support, Raman characterizations have been performed on the surface of alumina pellets and spectra are depicted in Figure V.27.

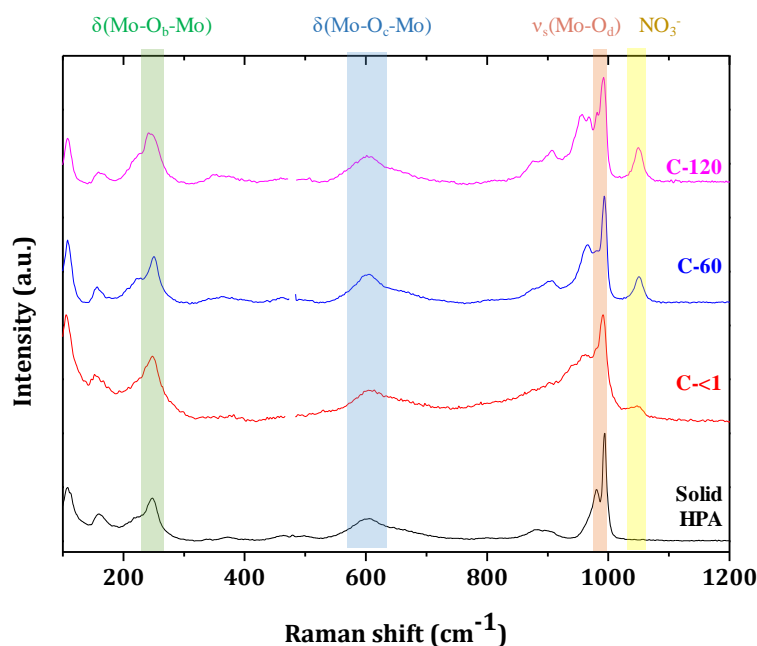


Figure V.27: Raman spectra of samples synthesized with different reaction times and of the solid HPA.

Several species have been identified using Raman spectroscopy. First, the heteropolyanion with a Keggin structure has been identified in both samples. Even after two hours of reaction the Keggin structure is still present for a reaction at low temperature. In the case of the sample synthesized with a longer time, a more intense band assigned to polymolybdates species is also detected. The reaction time has so an effect on the depolymerization of the Keggin structure even for low temperature reaction. The formation of water during synthesis can support the presence of polymolybdates for a long synthesis time. In the sample C-< 1, the presence of polymolybdates is not observed due to a direct precipitation of species. Dehydration of ethanol has not had time to occur due to its kinetic and no water has been formed.

It has been determined through microprobe analyses that phosphorus, cobalt and molybdenum were well distributed onto the support with repartition coefficients between 0.95 and 1 for all samples except for the sample synthesized for 2 h where molybdenum has been found to have a higher concentration in the edges of beads.

It has appeared that for a synthesis at low temperature (50°C) and with a molar ratio CO₂/EtOH of 95/5, the reaction time has no major effects on the species obtained before sulfidation. Only for sample C-120, a more intense Raman band associated polymolybdate has been detected. The main result being the possibility to obtain well distributed elements with a reaction time inferior to one minute. This is a real advantage for a scale up to industry. To verify the possibility of obtaining a catalyst precursor in a short time, these samples have been sulfided and characterized in their sulfide phase.

II.6.2. Characteristics of the sulfided phase

Looking at Table V.21, the samples C - < 1 and C-60 possess similar atomic concentrations of different molybdenum phases whereas the sample C-120 has a slightly lower atomic concentration of MoS₂ and slightly higher concentration of molybdenum oxysulfides.

Table V.21: Atomic concentration of phases present in sulfided catalysts.

<i>Atomic concentration (%)</i>									
	<i>MoS₂</i>	<i>MoO_xS_y</i>	<i>Mo⁶⁺</i>	<i>CoMoS</i>	<i>Co₉S₈</i>	<i>Co²⁺</i>	<i>S_{sulfide}²⁻</i>	<i>S_{oxysulf}²⁻</i>	<i>S_{sulfate}</i>
C-< 1	70	14	16	64	7	29	78	15	7
C-60	74	14	16	56	12	32	72	12	16
C-120	65	19	16	50	26	23	58	36	6

For promotion of the active phase, we have determined that C-<1 possesses a higher CoMoS content than the other samples. In the case of the sample C-120, a larger concentration of Co₉S₈ has been detected as well as a lower concentration of sulfide phase than for other samples. A longer synthesis time may conduct to the segregation of a part of Co atoms leading to a higher amount of Co₉S₈ during sulfidation.

As observed previously, the presence of sulfates onto the support has been observed and same hypothesis concerning adsorbed CO₂ can be made. A larger part of oxysulfides species has also been detected in sample C-PrOH.

TEM analyses have then been performed on samples C-< 1 and C-60 and results of average length and average degree of stacking are presented in Table V.22. Figure V.28 shows distribution in sizes and stacked slabs with their associated standard deviations.

Table V.22: Average lengths and degrees of stacking as well as associated standard deviations for samples C-<1 and C-60.

	<i>Average length L (nm)</i>	<i>Average stacking (N)</i>
C-<1	3.4 ± 1.6	3.2 ± 0.9
C-60	3.1 ± 1.6	3.2 ± 0.9

Sample C-<1 possess an average of MoS₂ slabs lengths of 3.4 nm whereas C-60 has an average length of 3.1 nm. Both samples possess an average of stacking slabs of 3.2.

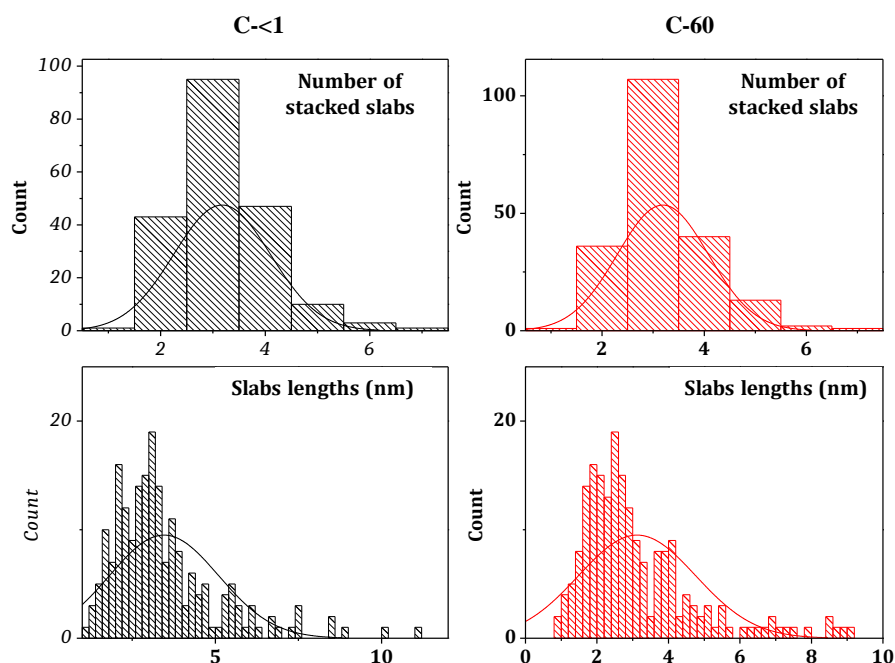


Figure V.28: Crystallite sizes and numbers of stacked layers for samples C-<1 and C-60.

Sample C-<1 possess thus MoS₂ slabs slightly higher than for C-60 but these values are similar and it can be affirmed that in terms of results obtained for sulfide characterizations, a reaction time which includes only injection of scCO₂, gives similar characteristics than a sample synthesized in one hour.

The investigation of the reaction time allowed us to determine the effect induced by the time of synthesis. Results have shown that even for a synthesis in a short time, it was possible to obtain well distributed species onto the support. A longer time of reaction leads to the presence of a larger part of polymolybdates. This presence of polymeric molybdate species may be due to the formation of a larger amount of water due to ethanol dehydration in the case of C-120. The HPA entities being decomposed in the presence of water.

The possibility to obtain similar results in terms of amount of MoS₂ and slabs layers is a key parameter in our process. By comparison with a conventional process where after ageing catalysts are dried for a long time and then calcined at high temperature, our process is time saver. This being very interesting for a possible scale up of the process into industrial scale.

The last studied parameter during this work was the effect of the loading of molybdenum. For that, the comparison between a sample containing around 10 wt.% of Mo and a sample containing around 13 wt.% of Mo has been done and results are presented in the following part.

II.7. Influence of the molybdenum content

The last studied parameter was the loading of molybdenum onto the alumina support. Indeed, to reach environmental regulations in terms of sulfur content in oil, catalysts containing a high loading of molybdenum are necessary. For that, we have prepared two samples. One containing ~ 13 wt.% of Mo (highest loading which can be obtained due to the limit of solubility of HPA in ethanol) and the other one containing ~10 wt.% of Mo. For each experiment, carbon dioxide was first preheated and pressurized into a preheater at 120°C and 22 MPa, respectively. It was then introduced into the reactor, containing the impregnated sample, to reach a pressure of 8 MPa. Both experiments were carried out for 60 min. The reaction temperature was fixed at 100°C and the pressure was adjusted to 22 MPa before the reaction. Experiments were carried out using ethanol as solvent of impregnation and a molar ratio CO₂/EtOH of 95/5. For future comparison, these catalysts will be denoted C-100-EtOH-95/5-60-X. However, in this part, the only variable being the molybdenum content, they are denoted C-X.

II.7.1. Evolution of the oxometallic phase as a function of Mo content

This part describes the different results obtained in terms of characterizations of the resulting phases obtained after the precipitation of species onto the support.

Table V.23 presents metals contents obtained by ICP analysis.

Table V.23: Metals contents of synthesized samples with different Mo loadings

<i>Mo loading</i>	<i>Experimental loading</i>			<i>Theoretical loading</i>		
	<i>wt. % Mo</i>	<i>wt. % Co</i>	<i>Molar ratio Co/(Co+Mo)</i>	<i>wt. % Mo</i>	<i>wt. % Co</i>	<i>Molar ratio Co/(Co+Mo)</i>
<i>10 wt%</i>	9.2	2.3	0.3	10	2.6	0.3
<i>13 wt%</i>	12.3	3.4	0.3	13	3.5	0.3

A higher content of metals has been obtained in one case and both samples have the same molar ratio promoter/molybdenum.

XRD patterns associated to each catalyst C-10 and C-13 are shown in Figure V.29.

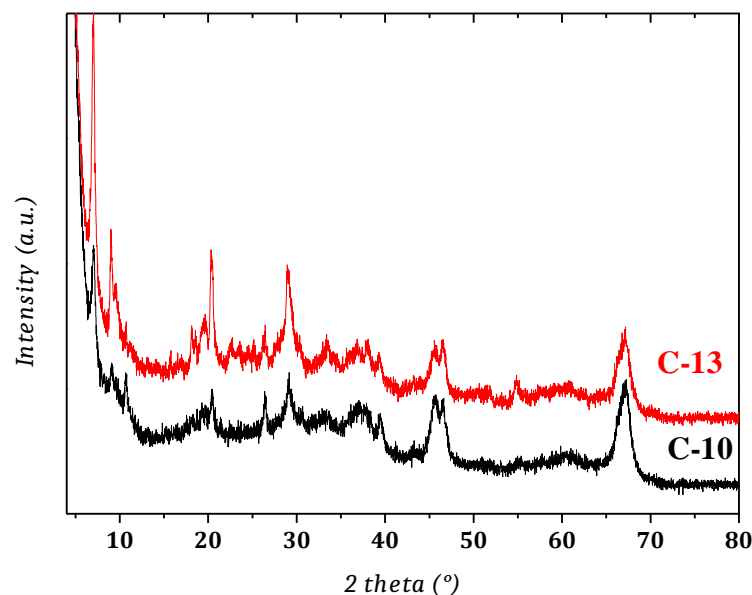


Figure V.29: XRD patterns of samples synthesized with two molybdenum loading.

XRD patterns possess same diffraction peaks than those obtained by varying other parameters and can be assigned to a hydrated phase of Keggin type heteropolyanion.

To support the presence of crystalline Keggin heteropolyanion onto the support, Raman mapping recorded along a cut in two extrudates is presented in Figure V.30. For each position on the cut in two extrudate, the same Raman spectrum is observed and is assigned to a Keggin heteropolyanion. No other species are detected onto the surface of the support.

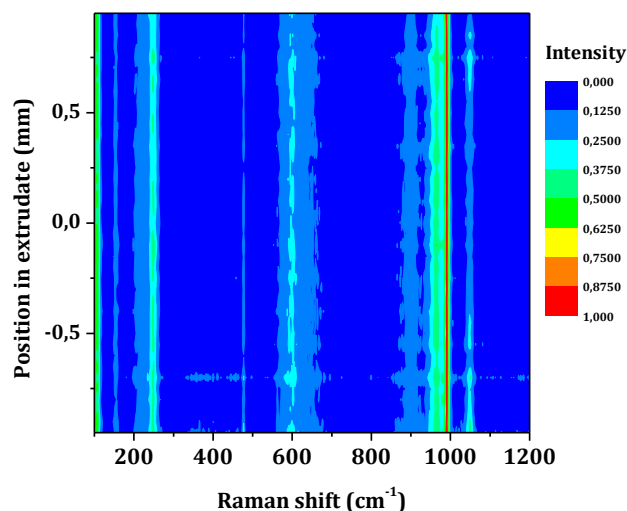


Figure V.30: Raman mapping of sample C-13

No polymolybdate species were detected on the surface of alumina in the case of C-13. This may be explained by the saturation of alumina by Keggin species and thus species are aggregated together and form a stable layer of HPA. This result is different for a lower molybdenum loading (cf Raman mapping located in the part: “Influence of the solvent of impregnation”). For a lower loading, we have observed the presence of both molybdenum entities: Keggin-type heteropolyanion and polymolybdate species. A stabilization of the Keggin structure is thus favoured at high Mo content.

From a qualitatively point of view, well-dispersed species along all positions in extrudates have been obtained. To verify quantitatively the well-dispersion of molybdenum species, microprobe analyses were performed on this sample.

Figure V.31 represents the microprobe profile obtained in the case of a catalyst synthesized with a high molybdenum loading.

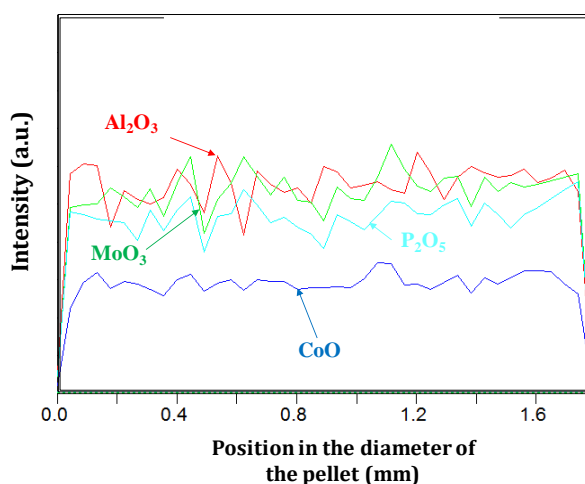


Figure V.31: Microprobe analysis of sample C-18.5

A good coefficient of repartition (R) of species has been found for all elements with $0.98 < R < 1.01$. This confirms a good dispersion of all elements onto the whole surface of alumina extrudates. By linking information obtained with Raman mapping and microprobe analyses, we can therefore affirm that at high molybdenum content, this process permits to obtain a well-dispersion of Keggin-type entities onto the whole surface of the support.

II.7.2. Characteristics of the sulfided phase

Table V.24 presents results obtained after XPS characterizations.

Table V.24: Atomic concentrations of phases present in sulfided catalysts C-10 and C-13.

	Atomic concentration (%)								
	MoS_2	MoO_xS_y	Mo^{6+}	$CoMoS$	Co_9S_8	Co^{2+}	$S_{sulfide}^{2-}$	$S_{oxysulf}^{2-}$	$S_{sulfate}$
C-10	73	6	21	56	18	26	68	24	8
C-13	65	9	26	52	24	24	70	18	12

The sample C-13 contains a slightly lower molybdenum disulfide phase compared to sample C-10. This can be explained by a larger amount of well crystallized Keggin units to sulfide. To obtain a higher content in MoS_2 , the sulfidation requires certainly a longer time of reaction compared to a sample containing less molybdenum. For cobalt species, equivalent amounts of different species have been found. As in previous studied parameters, the presence of sulfates onto the surface of the support has been detected.

The loading of molybdenum has thus an effect on the species present onto the surface of alumina after synthesis. For a high Mo content, the presence of only Keggin type units has been detected whereas for a lower loading the presence of polymolybdates has also been observed. Using this

process, it is therefore possible to obtain a well dispersed phase of Keggin type units along the whole surface of alumina pellets.

As the sulfidation of these catalysts have been performed using same experimental parameters, a lower amount of MoS₂ has been observed for sample C-13 compared to sample C-10. To obtain a higher content of MoS₂, a longer sulfidation time could be necessary.

III. Conclusion about the variation of experimental parameters

As presented through this chapter, several parameters have been studied to understand but also to optimize the synthesis of catalysts with the process developed in the frame of this PhD. It has been observed that each parameter has an influence, more or less important, on the oxometallic and sulfided phases.

Key results obtained from this parametric study are compared to the synthesis of a HDS catalyst via the conventional method and Figure V.32 depicts these comparisons.

Conventional method	scCO ₂ synthesis employed
<i>Impregnation with water</i> → destruction of HPA and formation of AlMo ₆	<i>Impregnation with ethanol</i> → conservation of HPA
<i>Maturation time</i> : between 1 to 24 h	<i>Maturation time</i> : 1 h
<p>Drying: T (°C) = ~ 100°C t (h) = 1- 12</p> <p>Calcination: T (°C) = ~ 500°C t (h) = 1 - 5</p>	<p>scCO₂ precipitation: T (°C) = 50°C < T < 120°C t (h) = < 1 min</p>

Figure V.32: Comparison between the scCO₂ process developed and the conventional method to prepare HDS catalysts.

By comparing the process developed with the conventional method to prepare HDS catalysts, several advantages favour the scCO₂ process. First, the use of ethanol as solvent of impregnation permits to avoid the formation of AlMo₆ species and time of ageing is reduced compared to an impregnation using water where generally this step lasts between 1 to 24 h. Secondly, the use of scCO₂ to precipitate species permits a synthesis at low and moderate temperatures (between 50 °C and 150 °C) and precipitation can occur in a very short period of time. By comparison, a conventional method includes a drying step at moderate temperatures (100-120°C) for generally a period of time between 1 to 12 h and includes a calcination step at high temperatures (400-500°C) for a period of time between 1 to 5 h.

The scCO₂ process developed allows thus the preparation of HDS catalyst precursors at low temperatures and in a short period of time. This process appears promising for the future and can be applied to a wide range of different metals and supports. It is an energy and time saver process compared to the traditional method employed for the preparation of catalyst precursors, and it can be tuned by experimental parameters and each one has its own influence on the resulting phase, as presented hereafter.

First, we have seen that the temperature has a large effect on the resulting species present onto the surface of the support. Indeed, for temperatures of synthesis higher than 150°C, the formation of cobalt molybdate species is observed. This result agrees with those obtained with *in situ* Raman

experiments presented in Chapter IV. The formation of cobalt molybdate species starts around 150-200°C and crystallization of these species is enhanced with the increase of the temperature. This formation of cobalt molybdate species has been proposed to be due to the presence of a cobalt hydroxide coordinated with nitrate and carbonate ions and having a formula type $\text{Co}_x(\text{OH})_y(\text{NO}_3)_z(\text{CO}_3)_m \cdot n\text{H}_2\text{O}$, which is probably a precursor for the formation of CoMoO_4 . For a synthesis temperature, lower than 150°C, it has been observed the presence of crystallized Keggin-type heteropolyanions more or less hydrated.

The study of the effect of the temperature permits us to conclude that a work at low temperature is therefore advisable to avoid the formation of cobalt molybdate species. The temperature of this process must be fixed below 150°C.

Then, the influence of the pressure of the reaction has been investigated. For that, two materials prepared at 5 MPa and 22 MPa, respectively, have been prepared and compared. It has been shown, that in the case of a synthesis under low pressure, the presence of $\text{H}_3\text{PMo}_{12}\text{O}_{40} \cdot 6\text{H}_2\text{O}$ having crystallite sizes around 35 nm. Whereas, for a synthesis performed at high pressure, the presence of a Keggin HPA has been observed, having crystallite sizes of around 15 nm. However, no major differences were observed by XPS measurements.

Thirdly, the effect of the ratio CO_2/EtOH has been investigated. As the precipitation of species occurs when the solvent of impregnation is expanded, the ratio between carbon dioxide and ethanol has a large effect. Kordokowski et al.[21] have studied expansion of various solvents with scCO_2 and measured their relative expansions. They have shown that the volume expansion of ethanol increases drastically with the increase of the carbon dioxide mole fraction present in the liquid phase. This result lets us to think that the precipitation of dissolved species in ethanol occurs faster than in the case of a high ratio CO_2/EtOH . A high CO_2/EtOH ratio will lead to smaller particles than a lower CO_2/EtOH ratio. Indeed, we have observed by varying the ratio CO_2/EtOH , that at low CO_2/EtOH ratio, the presence of large crystallized Keggin-type heteropolyanion. In the case of the synthesis performed with a ratio of 80/20, the presence of six times hydrated Keggin heteropolyanions has been observed. Same observation has been done for the reference catalyst C-100-EtOH-Air. The presence of polymolybdates has also been revealed in C-80/20 and may due to the destruction of the HPA in presence of water. The latter being formed by the dehydration of ethanol, catalysed by the HPA. After sulfidation, samples have shown similar results in terms of MoS_2 slabs lengths and stacking degree. The presence of large crystallized Keggin HPA seems not to be detrimental for the formation of small MoS_2 slabs.

The fourth effect studied was the solvent of impregnation. For that, the three smaller alcohols were used to prepare these catalyst precursors. The study of this effect leads to interesting results in terms of resulting species onto the surface. Indeed, by performing Raman mapping along cut in two alumina extrudates that depending of the solvent, the presence of Keggin-type heteropolyanions and/or polymolybdates. These differences could be explained by an easier dehydration of alcohol with a longer carbon chain. Dehydration of alcohol leads to the formation of water and heteropolyanions supported on alumina are unstable in water (see Chapter IV). Moreover, systems employed had different critical coordinates and an alcohol with a longer carbon chain will be less expanded than a short carbon chain alcohol for a same pressure (and thus fraction) of CO_2 . All these effects induced can play a role on the depolymerization of Keggin units.

The effect of the reaction time has then been investigated and the presence of polymolybdates in the sample synthesized for the longest time has been observed. This observation agrees with the

formation of water by dehydration of the alcohol. Using this process to prepare catalysts is therefore an interesting option because of the possibility, in a reduced time, to obtain species well-dispersed onto a support.

In all sulfided catalysts prepared in scCO₂, the presence of sulfates has been observed. A treatment under H₂ before sulfidation could have been appropriate to reduce the amount of sulfates formed during sulfidation.

The catalysts prepared have then been evaluated in catalysis through three different reactions.

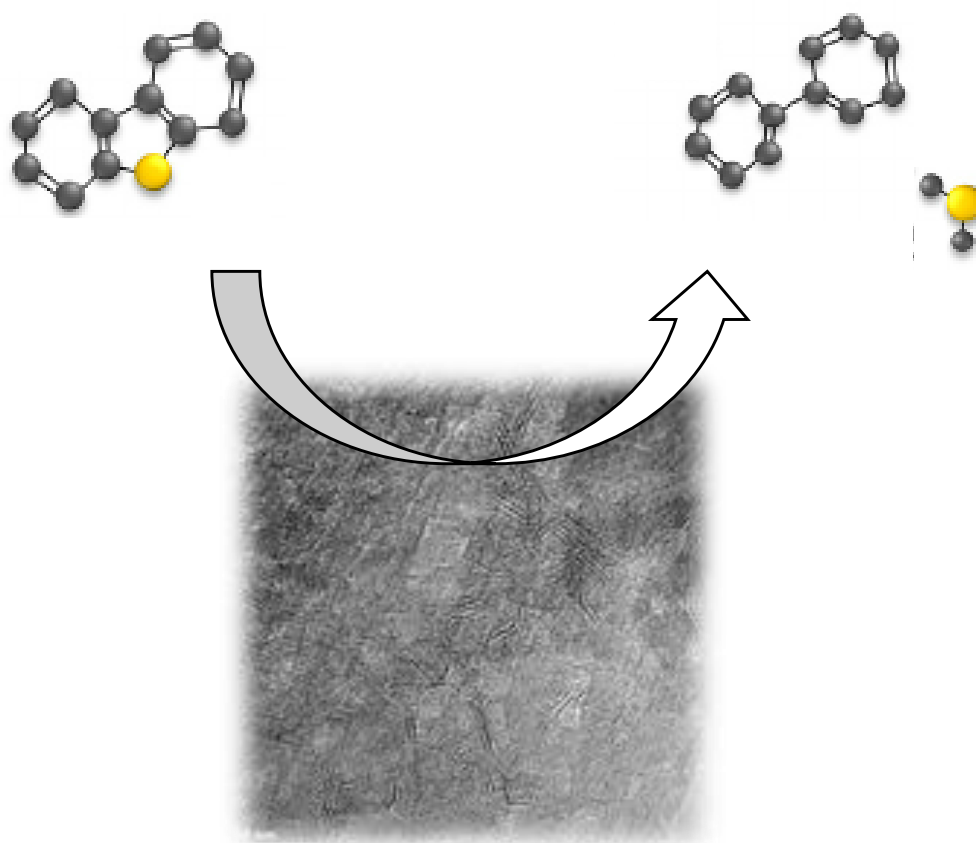
IV. Bibliography

- [1] A.J. Bridgeman, Density functional study of the vibrational frequencies of a Keggin heteropolyanions, 287 (2003) 55–69.
- [2] C. Rocchiccioli-Deltcheff, M. Fournier, R. Franck, R. Thouvenot, Vibrational investigations of polyoxometalates. 2. Evidence for anion-anion Interactions in molybdenum(VI) and tungsten(VI) compounds related to the Keggin structure, *Inorg. Chem.* 22 (1983) 207–216.
- [3] F.F. Bamoharram, Vibrational spectra study of the interactions between Keggin heteropolyanions and amino acids., *Molecules.* 14 (2009) 3214–21.
- [4] C. Roukoss, D. Laurenti, E. Devers, K. Marchand, L. Massin, M. Vrinat, Hydrodesulfurization catalysts: Promoters, promoting methods and support effect on catalytic activities, *Comptes Rendus Chim.* 12 (2009) 683–691.
- [5] M. Vrinat, M. Breysse, C. Geantet, J. Ramirez, F. Massoth, Effect of MoS₂ morphology on the HDS activity of hydrotreating catalysts, *Catal. Letters.* 26 (1994) 25–35.
- [6] H.A. Al-Megren, T. Xiao, S.L. Gonzalez-Cortes, S.H. Al-Khowaiter, M.L.H. Green, Comparison of bulk CoMo bimetallic carbide, oxide, nitride and sulfide catalysts for pyridine hydrodenitrogenation, *J. Mol. Catal. A-Chemical.* 225 (2005) 143–148.
- [7] T. Ono, N. Ogata, Y. Miyaryo, Characteristic features of Raman band shifts of Scheelite-type molybdate catalysts exchanged with the 18 O tracer via redox reactions, *J. Catal.* 161 (1996) 78–86.
- [8] I. Kaneshaka, H. Hashiba, I. Matsuura, Polarized Raman spectrum and normal coordinate analysis of α -MnMoO₄, *J. Raman Spectrosc.* 19 (1988) 213–218.
- [9] P. Blanchard, C. Lamonier, A. Griboval, E. Payen, New insight in the preparation of alumina supported hydrotreatment oxidic precursors: A molecular approach, *Appl. Catal. A Gen.* 322 (2007) 33–45.
- [10] J.L. Brito, A.L. Barbosa, Effect of phase composition of the oxidic precursor on the hds activity of the sulfided molybdates of Fe(II), Co(II), and Ni(II), *J. Catal.* 171 (1997) 467–475.
- [11] A. Calafat, F. Vivas, J.L. Brito, Effects of phase composition and of potassium promotion on cobalt molybdate catalysts for the synthesis of alcohols from CO₂ and H₂, *Appl. Catal. A Gen.* 172 (1998) 217–224.
- [12] S. Hajebi, A. Abedini, Cobalt molybdate nanoparticles: synthesis, characterization, optical and photocatalytic properties, *J. Mater. Sci. Mater. Electron.* 27 (2016) 4489–4493.
- [13] J. Ming, C. Wu, H. Cheng, Y. Yu, F. Zhao, Reaction of hydrous inorganic metal salts in CO₂ expanded ethanol: Fabrication of nanostructured materials via supercritical technology, *J. Supercrit. Fluids.* 57 (2011) 137–142.

-
- [14] J. Grimblot, Genesis, architecture and nature of sites of Co(Ni)–MoS₂ supported hydroprocessing catalysts, *Catal. Today*. 41 (1998) 111–128.
- [15] F. Colbeau-Justin, C. Boissière, A. Chaumonnot, A. Bonduelle, C. Sanchez, aerosol route to highly efficient (Co)Mo/SiO₂ mesoporous catalysts, *Adv. Funct. Mater.* 24 (2014) 233–239.
- [16] M.B. Ansari, S.-E. Park, Carbon dioxide utilization as a soft oxidant and promoter in catalysis, *Energy Environ. Sci.* 5 (2012) 9419–9437.
- [17] J. Liu, Y. Yu, Y. Mu, H. He, Mechanism of heterogeneous oxidation of carbonyl sulfide on Al₂O₃: An in situ Diffuse Reflectance Infrared Fourier Transform spectroscopy investigation, *J. Phys. Chem. B*. 110 (2006) 3225–3230.
- [18] M. Mukhopadhyay, S.V. Dalvi, Partial molar volume fraction of solvent in binary (CO₂-solvent) solution for solid solubility predictions, *J. Supercrit. Fluids*. 29 (2004) 221–230.
- [19] H. Pöhler, E. Kiran, Volumetric Properties of Carbon Dioxide + Ethanol at High Pressures, *J. Chem. Eng. Data*. 42 (1997) 384–388.
- [20] S.-D. Yeo, S.-J. Park, J.-W. Kim, J.-C. Kim, Critical Properties of Carbon Dioxide Methanol, Ethanol, 1-Propanol, and 1-Butanol, *J. Chem. Eng. Data*. 45 (2000) 932–935.
- [21] A. Kordikowski, A.P. Schenk, R.M. Van Nielen, C.J. Peters, volume expansions and vapor-liquid equilibria of binary mixtures of a variety of polar solvents and certain near-critical solvents, *J. Supercrit. Fluids*. 8 (1995) 205–216.
- [22] F.G. Denardin, S.A.B. Vieira, D. Melo, R. Mammucari, R. Foster, Phase transition and volume expansion in CO₂ - expanded liquid systems, 32 (2013) 529–534.
- [23] A. Braeuer, R. Adami, S. Dowy, M. Rossmann, A. Leipertz, Observation of liquid solution volume expansion during particle precipitation in the supercritical CO₂ antisolvent process, *J. Supercrit. Fluids*. 56 (2011) 121–124.
- [24] I. V Kozhevnikov, Catalysis by heteropoly acids and multicomponent polyoxometalates in liquid-phase reactions, *Chem. Rev.* 98 (1998).
- [25] I. V Kozhevnikov, Advances in Catalysis by Heteropolyacids, *Russ. Chem. Rev.* 56 (1987) 1417–1443.
- [26] T. Okuhara, A. Kasai, N. Hayakawa, Y. Yoneda, M. Misono, Catalysis by heteropoly compounds. VI. The role of the bulk acid sites in catalytic reactions over Na₃H^{3-x}PW₁₂O₄₀, *J. Catal.* 83 (1983) 121–130.
- [27] W. Alharbi, E. Brown, E.F. Kozhevnikova, I. V Kozhevnikov, Dehydration of ethanol over heteropoly acid catalysts in the gas phase, *J. Catal.* 319 (2014) 174–181.
- [28] H. Adkins, P.P. Perkins, Dehydration of alcohols over alumina, *J. Am. Chem. Soc.* 47 (1925) 1163–1167.
- [29] H. Knözinger, Dehydration of alcohols on alumina oxide, *Angew. Chemie Int. Ed.* 7 (1968) 791–806.

- [30] H. Knoezinger, A. Scheglila, A.M. Watson, Dehydration of alcohols over alumina. VIII. Ether formation from the deuterated methanols CH_3OH , CD_3OH , CH_3OD , and CD_3OD , *J. Phys. Chem.* 72 (1968) 2770–2774.
- [31] R. Sih, M. Armenti, R. Mammucari, F. Dehghani, N.R. Foster, Viscosity measurements on saturated gas-expanded liquid systems—Ethanol and carbon dioxide, *J. Supercrit. Fluids.* 43 (2008) 460–468.
- [32] K.D. Tilly, N.R. Foster, S.J. Macnaughton, D.L. Tomasko, Viscosity correlations for binary supercritical fluids, *Ind. Eng. Chem. Res.* 33 (1994) 681–688.
- [33] T. Aida, T. Aizawa, M. Kanakubo, H. Nanjo, Relation between volume expansion and hydrogen bond networks for CO_2 – alcohol mixtures at 40 °C, *J. Phys. Chem. B.* 114 (2010) 13628–13636.
- [34] C. Yi Kong, T. Funazukuri, S. Kagei, Binary diffusion coefficients and retention factors for polar compounds in supercritical carbon dioxide by chromatographic impulse response method, *J. Supercrit. Fluids.* 37 (2006) 359–366.

Chapter VI: Catalytic evaluation



I. INTRODUCTION.....	195
II. CATALYTIC PERFORMANCES OF THE CATALYSTS.....	195
II.1. CATALYTIC PERFORMANCES IN TOLUENE HYDROGENATION.....	195
II.1.1. <i>Effect of the synthesis temperature</i>	195
II.1.2. <i>Effect of the pressure</i>	197
II.1.3. <i>Effect of the ratio CO₂/EtOH</i>	198
II.1.4. <i>Effect of the solvent of impregnation</i>	199
II.1.5. <i>Effect of the reaction time</i>	200
II.1.6. <i>Effect of the Mo loading</i>	201
II.1.7. <i>Conclusion on catalytic performances in toluene hydrogenation</i>	201
II.2. CATALYTIC PERFORMANCES IN HYDRODESULFURIZATION OF DBT.....	203
II.2.1. <i>Effect of the temperature</i>	203
II.2.2. <i>Effect of the pressure</i>	204
II.2.3. <i>Effect of the ratio CO₂/EtOH</i>	205
II.2.4. <i>Effect of the solvent of impregnation</i>	206
II.2.5. <i>Effect of the reaction time</i>	207
II.2.6. <i>Effect of the Mo loading</i>	208
II.2.7. <i>Conclusion about the hydrodesulfurization of DBT</i>	208
II.3. CATALYTIC PERFORMANCES IN HYDRODESULFURIZATION OF 4,6-DMDBT.....	209
II.3.1. <i>Effect of the temperature during synthesis of the oxometallic phase</i>	209
II.3.2. <i>Effect of the ratio CO₂/EtOH</i>	210
III. CONCLUSION	211
IV. BIBLIOGRAPHY.....	212

I. Introduction

The previous chapter has described the influence of different experimental parameters on the resulting oxometallic and sulfided phase of the catalyst precursors. This chapter deals with the catalytic evaluation of our materials and the highlight of the structure/reactivity relationships.

This chapter has been divided as a function of the catalytic test performed and subdivided as a function of experimental parameter studied during the preparation of the catalyst before its activation. Three different model reactions have been studied: the first corresponding to the hydrogenation of toluene, which permits to evaluate the hydrogenation ability of the catalyst and allows a first screening of catalytic performances. The hydrodesulfurization of dibenzothiophene (DBT) and 4,6-dimethyldibenzothiophene (4,6-DMDBT) have been investigated to compare a selection of catalysts.

II. Catalytic performances of the catalysts

As detailed in the experimental part of this work, HDS catalyst precursors have been first sulfided *in situ* prior to perform the tests. These catalytic tests have been carried out at IFPEN Solaize. From the analysis of the recovered products after testing, it is therefore possible to obtain the reaction rate constant associated to each test and each catalyst, and allows a comparison of them to estimate the influence of each parameter during the preparation of the oxometallic phase.

The first section presents the results obtained in the hydrogenation of toluene where catalysts tested have been compared with the reference catalyst C-100-EtOH-Air. The second section is dedicated to the hydrodesulfurization of DBT and the third one to the hydrodesulfurization of 4,6-DMDBT.

II.1. Catalytic performances in toluene hydrogenation

As previously mentioned in Chapter III, toluene hydrogenation test allows a first screening of catalysts and permits to obtain a first order reaction rate constant of toluene hydrogenation normalized by moles of Mo contained in the catalyst. To estimate the reproducibility of our synthesis using $scCO_2$, several experiments have been carried out two times (not presented here) and have shown activities with 10 % of absolute difference: We will thus consider a 10 % error bar for this test.

II.1.1. Effect of the synthesis temperature

Figure VI.1 presents the catalytic results compared with the reference sample. On the left of Figure VI.1 are presented reaction rate constants associated to the hydrogenation of toluene (K_{Tol}) as a function of the sample synthesized and on the right, K_{Tol} as a function of the amount of CoMoS phase present in the catalyst, determined by XPS. On the top of the Figure VI.1 is presented a summary of sulfided phase characterizations.

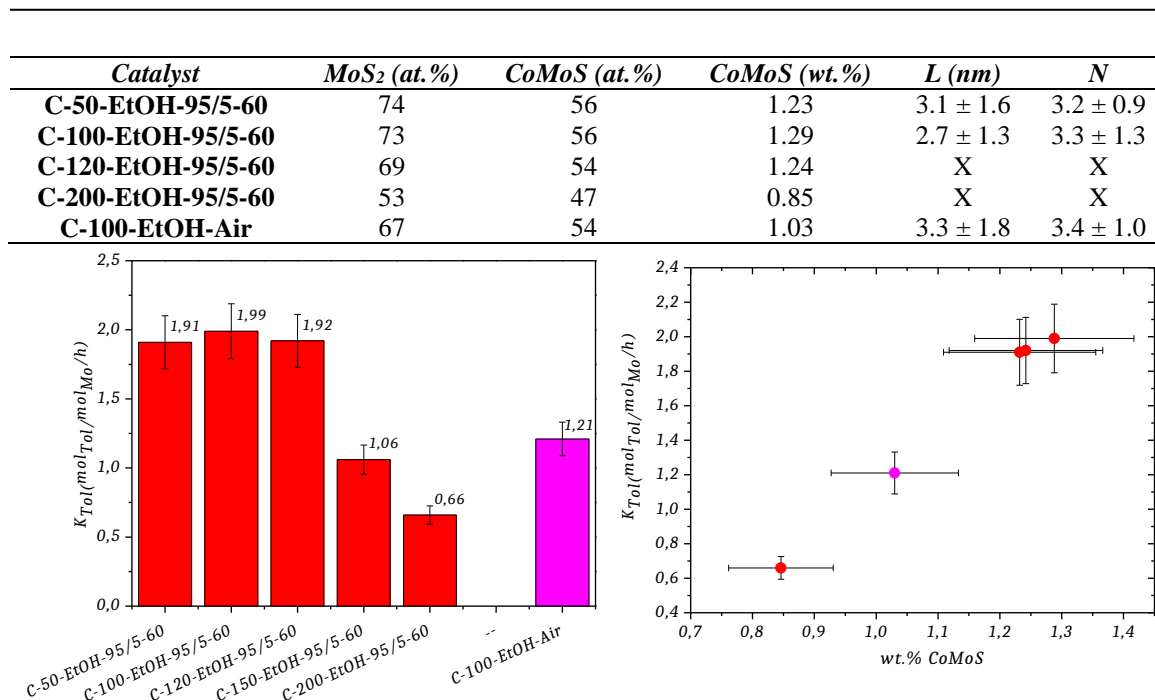


Figure VI.1: (Left) K_{Tol} of the samples synthesized at different temperatures and the reference catalyst. (Right) K_{Tol} as a function of the amount of CoMoS. (Top) Characterizations of the sulfided phases.

One can see that hydrogenation rate is the same for samples prepared at $T < 150^{\circ}\text{C}$. For catalysts prepared at higher temperatures, K_{Tol} decreases drastically with the increase of the synthesis temperature. This decrease of reaction rate constant may be due to the presence of a lower amount of active phase CoMoS (see Figure VI.1 (top)) in sample C-200-EtOH-95/5-60.

These tendency does not allow to explain the lower activity of the reference catalyst C-100-EtOH-Air which has a K_{Tol} 40 % lower than sample prepared with scCO_2 . Other factors may explain this result such as slight different electronic properties or slab stacking/assembling difficult to evaluate precisely by TEM.

Even if differences are small, one can observe that average MoS₂ length are also in agreement with the evolution of reaction rate constant K_{Tol} . A higher average MoS₂ length has been found for C-100-EtOH-Air compared to samples C-50-EtOH-95/5-60 and C-100-EtOH-95/5-60. Shorter MoS₂ slabs gives better catalytic performances in toluene hydrogenation because they expose more edges.

The presence of Keggin-type heteropolyanion onto the surface of catalysts before activation has shown better catalytic performances than the presence of bulk CoMo₄ obtained for catalysts prepared at $T > 150^{\circ}\text{C}$. The latter being undesirable for the activity of catalysts [1,2]. Catalysts synthesized at low temperatures exhibit thus better catalytic performances in toluene hydrogenation. By comparing catalysts synthesized with scCO_2 and a reference catalyst prepared at 100°C in air, it has been shown a higher K_{Tol} for samples prepared in scCO_2 at $T < 150^{\circ}\text{C}$ than the reference catalyst. The content of CoMoS and in a lesser extent the average slabs length may explain these results. A synthesis at low temperature and using scCO_2 appears to be a good option to increase efficiency of hydrogenation catalysts.

The second synthesis parameter investigated was the effect of the pressure on the resulting oxometallic phase. Catalytic performances of these catalysts in toluene hydrogenation are presented hereafter.

II.1.2. Effect of the pressure

Figure VI.2 presents K_{Tol} obtained for sample C-100-EtOH-22, prepared under 22 MPa of CO_2 and C-100-EtOH-5 prepared under 5 MPa. Both experiments were carried out at 100°C .

Catalyst	MoS_2 (at. %)	CoMoS (at. %)	CoMoS (wt. %)	L (nm)	N
C-100-EtOH-22	73	56	1.29	2.7 ± 1.3	3.3 ± 1.3
C-100-EtOH-5	69	50	1.00	X	
C-100-EtOH-Air	67	54	1.03	3.3 ± 1.8	3.4 ± 1.0

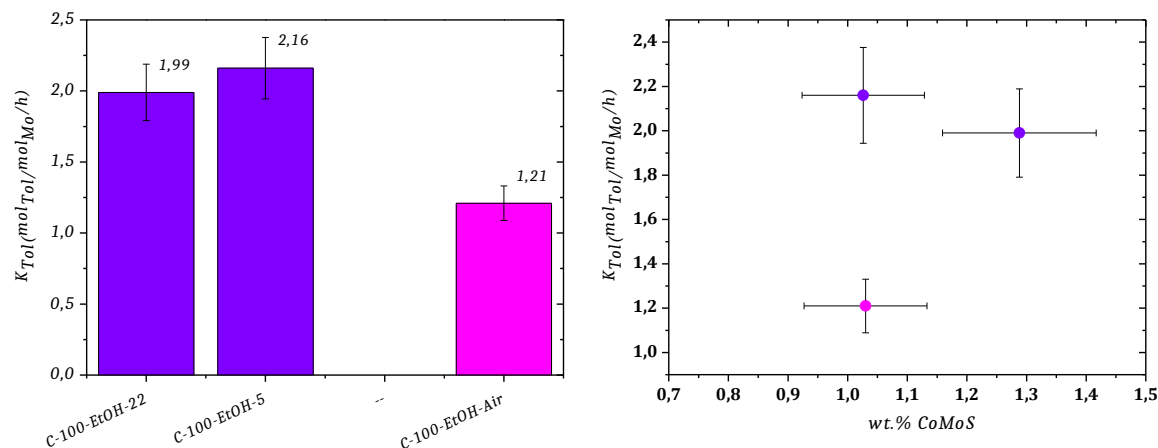


Figure VI.2: (Left) K_{Tol} of the samples synthesized at different pressures and the reference catalyst. (Right) K_{Tol} as a function of the amount of CoMoS. (top) Characterizations of the sulfided phases.

Samples, where the oxometallic phases have been synthesized at different pressures, show similar K_{Tol} of around 2 mol_{Tol}/mol_{Mo}/h. Compared to the reference sample, these catalysts show K_{Tol} largely higher. By looking at K_{Tol} as a function of the CoMoS content, it is observed that C-100-EtOH-5 possesses a slightly lower amount of CoMoS compared to C-100-EtOH-22. However, it contains a similar CoMoS content than the reference catalyst and yet has an almost two times higher K_{Tol} . By looking at Figure VI.2 (top), it is observed a similar degree of sulfidation for molybdenum and CoMoS content. The difference may be due to a difference of MoS_2 slabs lengths between these samples. Unfortunately, TEM analysis has not been carried out on sample C-100-EtOH-5.

No major differences have been observed for samples synthesized at different pressures. However, by comparing catalytic performances obtained with reference catalyst, a synthesis of the oxometallic phase under CO_2 atmosphere appears, in this case also, to be an interesting option to enhance catalytic activity in toluene hydrogenation. The difference of K_{Tol} between sample C-100-EtOH-5 and the reference catalyst may be due to a difference of MoS_2 lengths but no characterizations can prove this hypothesis.

The third influence studied during the preparation of the oxometallic phase of catalyst precursors was the ratio CO_2/EtOH employed.

II.1.3. Effect of the ratio CO₂/EtOH

Results for toluene hydrogenation of these catalysts are presented in Figure VI.3.

Catalyst	MoS ₂ (at. %)	CoMoS (at. %)	CoMoS (wt. %)	L (nm)	N
C-50-EtOH-80/20-60	69	57	1.25	2.8 ± 1.4	3.0 ± 1.0
C-50-EtOH-95/5-60	74	56	1.23	3.1 ± 1.6	3.2 ± 0.9
C-50-EtOH-98/2-60	76	61	1.16	2.8 ± 1.3	3.3 ± 0.9
C-100-EtOH-Air	67	54	1.03	3.3 ± 1.8	3.4 ± 1.0

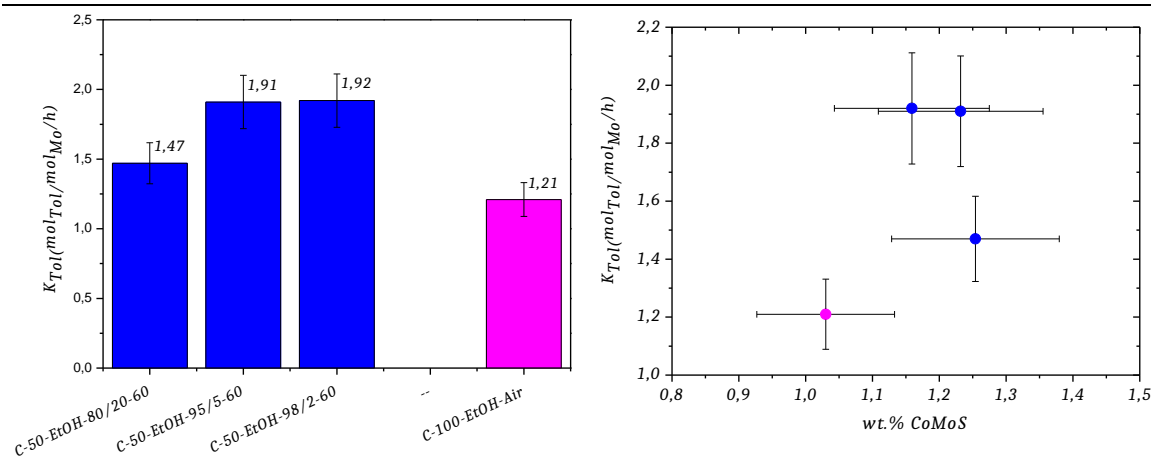


Figure VI.3: (Left) K_{Tol} for samples synthesized at different CO₂/EtOH ratios and the reference catalyst. (Right) K_{Tol} as a function of the amount of CoMoS. (Top) Characterizations of the sulfided phases.

An enhancement of K_{Tol} with the increase of the ratio CO₂/EtOH is noticed from 80/20 to 95/5. For ratios, higher than 95/5, reaction rate constants are stable. In this case also, the reference catalyst has shown a lower catalytic performance than samples synthesized with a high CO₂/EtOH ratio and a closer activity to the 80/20 ratio.

By looking at Figure VI.3 (left), it is observed an enhancement of K_{Tol} with the increase of the CoMoS content.

As presented in Figure VI.3 (top), it has been determined that in all samples sulfidation of molybdenum was about 70-75% and slabs lengths were about 3 nm. If no major differences have been highlighted in sulfided samples, differences were observed before activation of catalysts. It has been put forwards the presence of large crystallites of H₃PMo₁₂O₄₀.6H₂O and the presence of polymolybdates (detected on the surface of the support by Raman analysis) in C-50-EtOH-80/20-60. Compared to others samples where crystallites of around 10 nm of a hydrated HPA.nH₂O have been observed without the presence of polymolybdates on the surface of the alumina pellets.

The ratio employed to perform the synthesis of the oxometallic phase has an indirect influence on the catalytic performances in toluene hydrogenation. It has been put forwards that the presence of large crystallized H₃PMo₁₂O₄₀.6H₂O and polymolybdates before sulfidation leads to a lower amount of CoMoS and thus to lower catalytic performances.

Next experimental parameter studied was the effect of impregnation solvent and catalytic performances in toluene hydrogenation are presented hereafter.

II.1.4. Effect of the solvent of impregnation

This part summarizes results obtained in terms of toluene hydrogenation for samples where oxometallic phase has been synthesized using methanol, ethanol and n-propanol. Figure VI.4 shows reaction rate constants obtained in toluene hydrogenation for these samples and the reference catalyst as well as characterizations of the sulfided phases.

Catalyst	MoS ₂ (at. %)	CoMoS (at. %)	CoMoS (wt. %)	L (nm)	N
C-100-MeOH-95/5-60	76	60	1.32	3.0 ± 1.9	3.0 ± 0.9
C-100-EtOH-95/5-60	73	56	1.29	2.7 ± 1.3	3.3 ± 1.0
C-100-PrOH-95/5-60	61	55	1.27	3.2 ± 2.0	3.2 ± 1.1
C-100-EtOH-Air	67	54	1.03	3.3 ± 1.8	3.4 ± 1.0

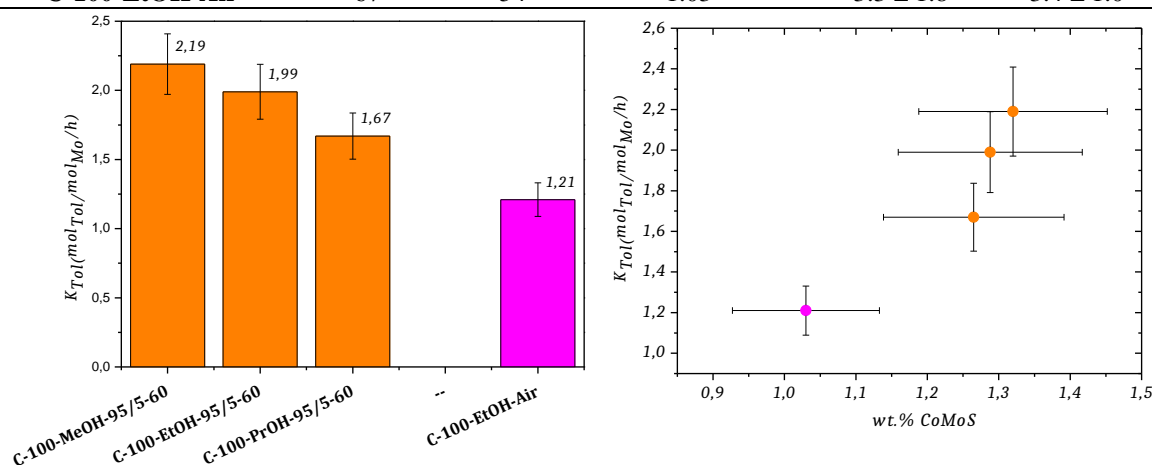


Figure VI.4: (Left) K_{Tol} for samples synthesized with different solvents and the reference catalyst. (Right) K_{Tol} as a function of the amount of CoMoS. (Top) Characterizations of sulfided phases.

First observation is the decrease of K_{Tol} as a function of the solvent employed to perform the impregnation. The evolution is the following: MeOH > EtOH > PrOH. This effect is well-observed between catalyst C-100-MeOH-95/5-60 and C-100-PrOH-95/5-60.

By looking at Figure VI.4 (right), unsurprisingly, an increase of the K_{Tol} with an increase of the CoMoS is observed. Table VI.4 recalls the results obtained in terms of characterizations of the sulfided phase.

A decrease of the CoMoS content is observed between C-100-MeOH-95/5-60 and C-100-PrOH-95/5-60. This affects the reaction rate constant of toluene hydrogenation. Moreover, it has been determined that sample C-100-PrOH-95/5-60 possesses slightly longer MoS₂ slabs, even if this observation is not striking.

The presence of Keggin entities onto the alumina support before sulfidation leads thus to better catalytic performances than samples containing partially decomposed Keggin entities (leading to polymolybdates). The nature of the solvent and its ability to dehydrate during the synthesis forming water seems to be a key parameter.

The next parameter studied was the effect of the synthesis time and results concerning toluene hydrogenation are presented in the following part.

II.1.5. Effect of the reaction time

In this part, we compare catalytic performances of a catalyst synthesized in a short time (only precipitation) with catalysts prepared in one hour and two hours of synthesis. Figure VI.5 shows reaction rate constants obtained as well as the characterizations of the sulfided phases.

Catalyst	MoS ₂ (at.%)	CoMoS (at.%)	CoMoS (wt.%)	L (nm)	N
C-50-EtOH-95/5-<1	70	64	1.15	3.4 ± 1.6	3.2 ± 0.9
C-50-EtOH-95/5-60	74	56	1.23	3.1 ± 1.6	3.2 ± 0.9
C-50-EtOH-95/5-120	65	50	1.05	X	X
C-100-EtOH-Air	67	54	1.03	3.3 ± 1.8	3.4 ± 1.0

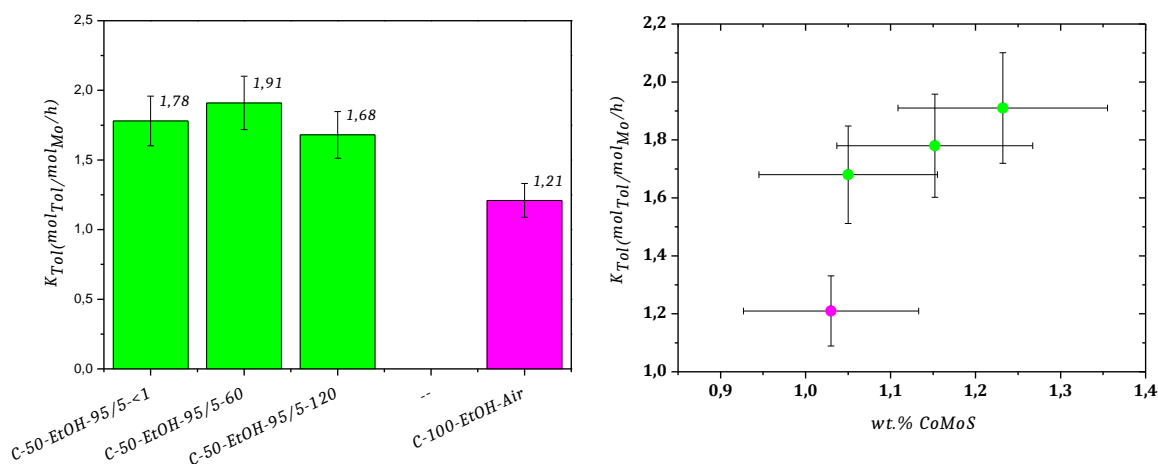


Figure VI.5: (Left) K_{Tol} for samples synthesized at different reaction times. (Right) K_{Tol} as a function of the amount of CoMoS. (Top) Characterizations of the sulfided phase.

Reaction rate constants of toluene hydrogenation have shown quasi similar values independent of the synthesis time employed for the precipitation of the oxometallic phase. It has been reported in the previous chapter that a higher part of polymolybdates was observed in the sample C-50-EtOH-95/5-120. Looking at Figure VI.5 (left), all samples contains an amount of active phase between 1.0 and 1.3 wt.%.

By looking at more precisely, we observe that the amount of CoMoS is reliable to the K_{Tol} obtained. However, the reference catalyst has shown a lower K_{Tol} compared to other samples containing the same content of active phase.

The synthesis time employed to prepare these catalysts has shown no major effect on reaction rate constants for toluene hydrogenation. However, these slight changes can be observed in Figure VI.5 and are in agreement with the characterizations of the sulfided phases. Using $scCO_2$ to precipitate species is thus an interesting option. It has indeed been shown that for a reaction time inferior at a minute, it is possible to obtain a catalyst having performances equivalent to those with longer synthesis times and higher than a drying under air.

The last parameter studied was the content of molybdenum and catalytic performances in toluene hydrogenation are presented in the following part.

II.1.6. Effect of the Mo loading

The two samples having different metal contents have been tested in toluene hydrogenation and results are presented in Figure VI.6 with a summary of characterizations of the sulfided phases.

Catalyst	MoS ₂ (at. %)	CoMoS (at. %)	CoMoS (wt. %)	L (nm)	N
C-100-EtOH-95/5-60-10 wt.% Mo	73	56	1.29	2.7 ± 1.3	3.3 ± 1.0
C-100-EtOH-95/5-60-13 wt.% Mo	65	52	1.76	X	
C-100-EtOH-Air	67	54	1.03	3.3 ± 1.8	

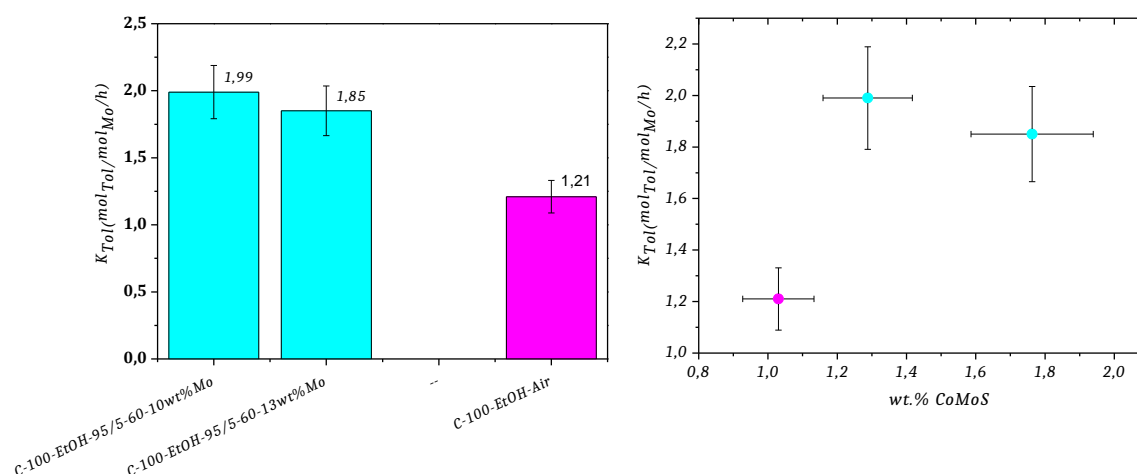


Figure VI.6: Results in terms of hydrogenation of toluene for samples synthesized with different Mo loadings and the reference catalyst. (Left) K_{Tol} as a function of the sample. (Right) K_{Tol} as a function of the amount of CoMoS. (Top) Characterizations results for samples synthesized with different synthesis time and reference catalyst.

First, it is observed that reaction constant rates associated to each sample synthesized in scCO₂ have found to be similar, with a negligible decrease at high Mo loading. This means that the quality of the active sites is not damaged which is an important issue when high activity is targeted.

The preparation of catalyst precursor with a high loading of molybdenum is therefore possible and catalyst prepared shows similar performances in toluene hydrogenation than a sample having a lower Mo loading.

II.1.7. Conclusion on catalytic performances in toluene hydrogenation

The catalysts prepared in supercritical fluids have shown good catalytic performances in toluene hydrogenation compared to the reference sample synthesized under air. In order to visualize the relationship between content of active phase and catalytic performances, a summary of K_{Tol} associated to all samples prepared as a function of the CoMoS phase in MoS₂ content is presented in Figure VI.7.

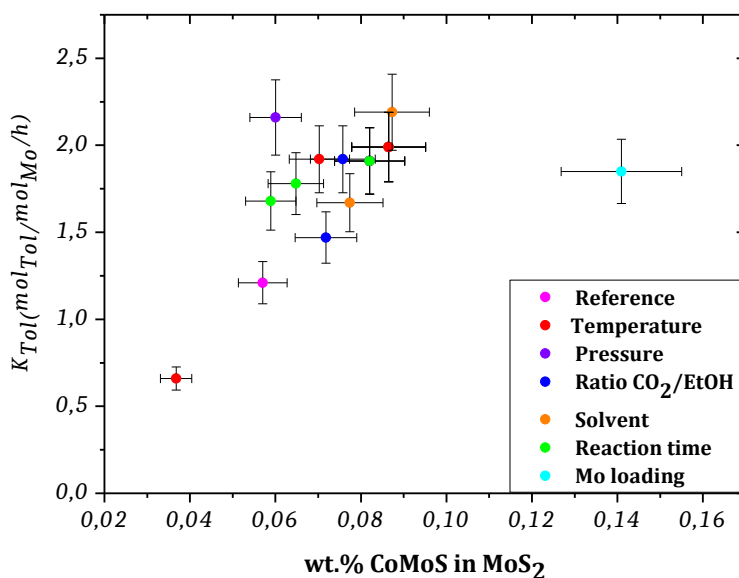


Figure VI.7: Reaction rate constants of toluene hydrogenation as a function of the CoMoS content in MoS₂ of all synthesized samples.

An increase of the reaction rate constant associated to toluene hydrogenation with the increase of CoMoS content in the catalyst is observed in all cases. Results from XPS measurements are thus in good agreement with catalytic performances obtained in toluene hydrogenation.

Through this test, it has been observed that using CO₂ to prepare HDS catalyst precursors leads to better results than those obtained for a synthesis under air. From these catalytic tests, it is therefore possible to assign the most active catalyst to each experimental parameter. For the temperature of synthesis, best catalysts are those having been synthesized at temperatures lower than 150°C. The pressure employed during the synthesis of the oxometallic phase has no major effects on the resulting catalytic performances and a work at a pressure of 5 MPa has given interesting results. By studying the effect of the ratio CO₂/EtOH, it has been found that best results in terms of toluene hydrogenation have been obtained for catalysts synthesized with a high CO₂/EtOH ratio. Using different solvents to impregnate species, it has been shown that the use of methanol appears to give a better activity compared to the use of propanol. And the study of the synthesis time has permitted to highlight that synthesis time has no major effect on the catalytic performances in toluene hydrogenation.

Combining all these observations, it is therefore possible to predict which are the most optimized experimental parameters to obtain the best catalytic performances. This catalyst should be synthesized using methanol as solvent of impregnation. The ratio CO₂/solvent should be the highest possible and the temperature of synthesis should be around 50-100°C. Moreover, only a short time of synthesis will be necessary to obtain a catalyst with good catalytic performance in toluene hydrogenation. The process developed allows to prepare catalyst precursors in several minutes.

In order to confirm the promising results in toluene hydrogenation of our catalyst prepared with this novel process, catalysts have been tested in HDS of common compounds used as model molecules. Catalysts which have shown the best catalytic performances have been thus tested in hydrodesulfurization of DBT and results are presented hereafter.

II.2. Catalytic performances in hydrodesulfurization of DBT

DBT is a model molecule widely used to evaluate performances of HDS catalyst. HDS of DBT occurs via two main routes: the direct desulfurization (DDS) route with the direct removal of sulfur through C-S cleavage which leads to the formation of the biphenyls compounds. And the hydrogenation route (HYD) with the hydrogenation of a thiophenic ring to destabilize the molecule followed by elimination of sulfur and to the formation of cyclohexylbenzenes, dicyclohexyls and other hydrogenated compounds. Generally, it is considered that the main reaction pathway for HDS of DBT is the DDS route [3,4] with a contribution of 80% of the overall reaction [5]. Catalysts have been tested in HDS of DBT at various temperatures and reaction rate constants have been calculated using equations presented in Chapter III. Catalytic performances are presented as a function of the experimental parameter investigated for the study of toluene hydrogenation.

In our calculations of reaction rates constants, we have chosen to merge all hydrogenated products (described in Chapter III) to obtain the HYD route whereas biphenyls products were the only product obtained via DDS route. We also consider that biphenyl is not hydrogenated to cyclohexylbenzene since Prins et al. [6] have observed that the HYD of biphenyls products to cyclohexylbenzene was not observed over CoMo catalyst and our experimental conditions are similar to these used in their work.

As for toluene hydrogenation, the first studied parameter presented is the influence of the temperature of synthesis.

II.2.1. Effect of the temperature

Catalysts tested in the case of the study of the temperature of synthesis were C-50-EtOH-95/5-60 and C-100-EtOH-95/5-60. Their reaction rate constant in DBT HDS are presented in Figure VI.8 as well as the one of reference catalyst.

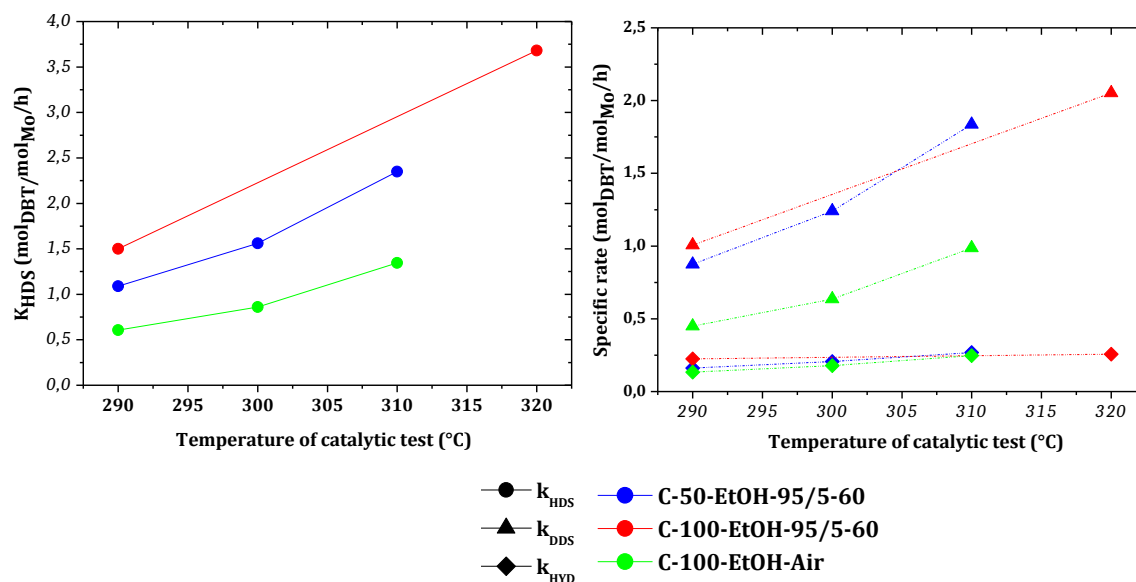


Figure VI.8: Specific rates of DBT HDS (left) and specific rates of DDS and HYD pathways (right) for samples C-50-EtOH-95/5-60 and C-100-EtOH-95/5-60 as well as reference catalyst as a function of the temperature of catalytic test.

For the overall reaction, an increase of the temperature of the catalytic test leads to an increase of reaction rates constants (K_{HDS}). This observation is also made for the reaction rates constants of the

DDS pathway (K_{DDS}) whereas reaction rates constants of the HYD pathway (K_{HYD}) shows almost no change with the temperature. This indicates an increase of the selectivity towards biphenyl with the increase of the temperature as already reported [7].

Reaction rate constants increase in the following order: C-100-EtOH-Air < C-50-EtOH-95/5-60 < C-100-EtOH-95/5-60. The same trend as for toluene hydrogenation is then observed. Catalysts synthesized in scCO_2 possess therefore much more active sites dedicated to the DDS route than the sample C-100-EtOH-Air.

By plotting the logarithm of reaction rate constants obtained in the case of the HDS of DBT with the inverse of the temperature and applying the Arrhenius law, this allows us to estimate the activation energy (E_A) of the overall reaction. Activation energies for the HDS reaction have been calculated to be in the range 80-105 $\text{kJ}\cdot\text{mol}^{-1}$. These values are in good agreement with published data concerning CoMo catalysts [8].

The next presents catalytic performances in DBT HDS of catalysts prepared at different CO_2 pressures.

II.2.2. Effect of the pressure

Catalysts synthesized at different pressures have then been tested in DBT HDS and results obtained are presented in Figure VI.9.

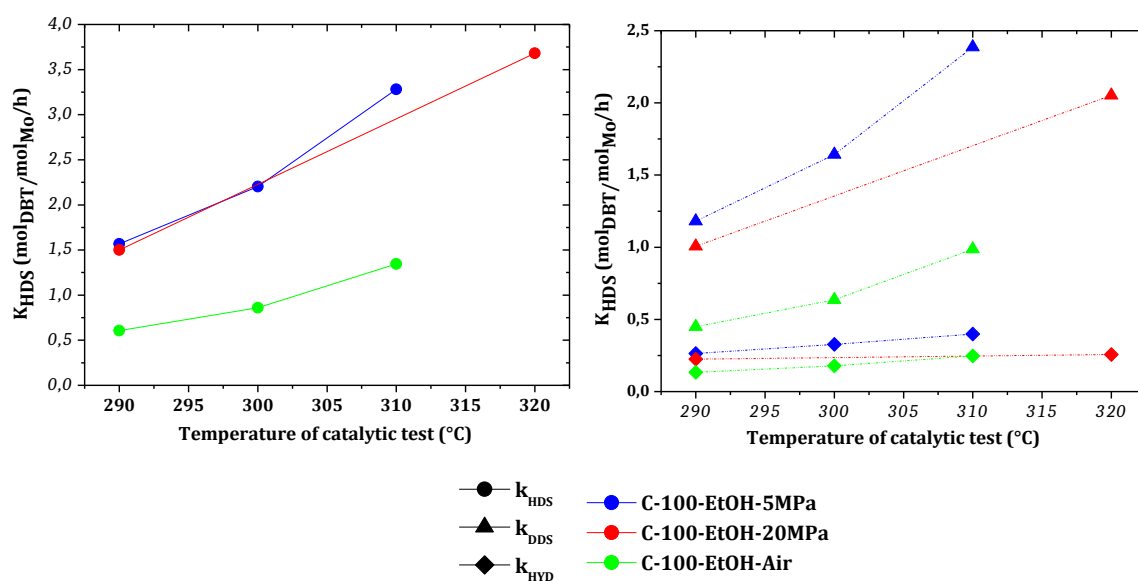


Figure VI.9: Specific rates of DBT HDS (left) and specific rates of DDS and HYD pathways (right) for samples C-100-EtOH-5MPa and C-100-EtOH-20MPa as well as reference catalyst as a function of the temperature of catalytic test.

Compared to reference catalyst C-100-EtOH-Air, catalysts prepared with CO_2 at different pressures show a higher reaction rate constants K_{HDS} . Indeed, a K_{Tot} three times higher is observed for C-100-EtOH-5MPa and C-100-EtOH-20MPa compared to the reference catalyst. This observation is more striking for the K_{DDS} than for the K_{HYD} . Here also the selectivity towards DDS route is increased with the increase of the temperature of the catalytic test. Looking at the sample C-100-EtOH-5MPa, it is observed a slightly higher K_{DDS} and K_{HYD} compared to the sample C-100-EtOH-20MPa. This observation is in agreement with previous results obtained in terms of hydrogenation of toluene.

The pressure of CO₂ employed during synthesis of the oxometallic phase has thus no major effect on the catalytic performances in DBT HDS.

The influence of the ratio used during synthesis of the oxometallic phase on the catalytic performances in DBT HDS is now presented.

II.2.3. Effect of the ratio CO₂/EtOH

Catalysts synthesized with different ratios CO₂/EtOH have then been tested in DBT HDS and results obtained are presented in Figure VI.10.

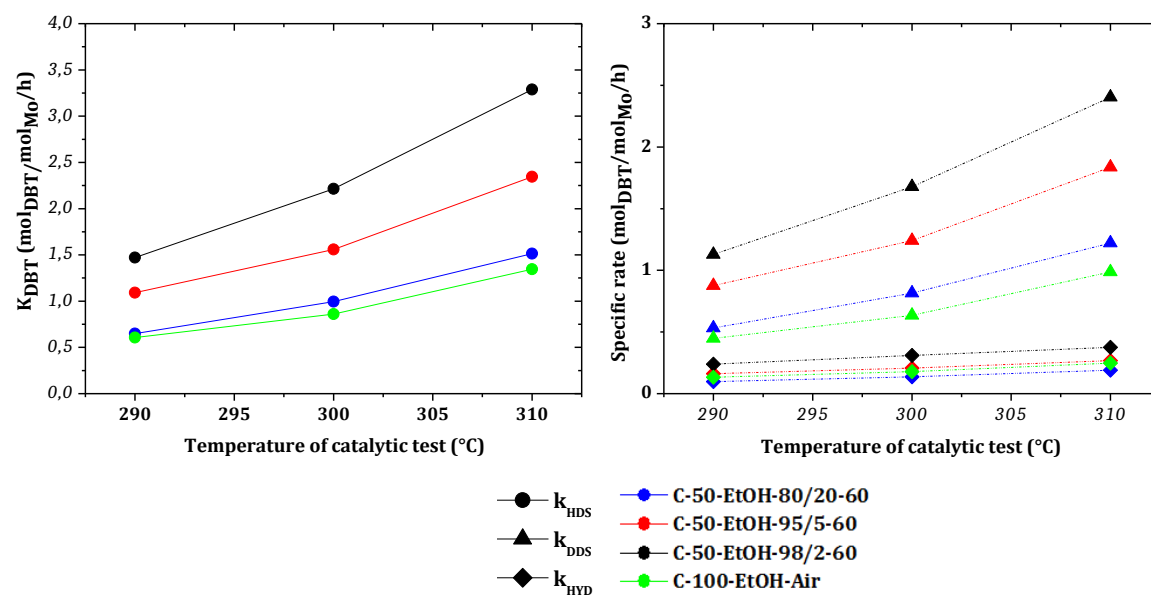


Figure VI.10: Specific rates of DBT HDS (left) and specific rates of DDS and HYD pathways (right) for samples C-50-EtOH-80/20-60, C-50-EtOH-95/5-60 and C-50-EtOH-98/2-60 as well as reference catalyst as a function of the temperature of catalytic test.

Same trends than for toluene hydrogenation have been observed, namely an increase of the catalytic activity for samples synthesized with a smaller volume of solution of impregnation. For all samples, specific rates associated to DDS and HYD routes evolve in the same manner. A larger increase between them is observed for an increase of the temperature of the catalytic test. This is more visible in the case of K_{DDS} than K_{HYD} . Reaction rate constants associated to the DDS route increase in the following order: C-50-EtOH-80/20-60 < C-50-EtOH-95/5-60 < C-50-EtOH-98/2-60. Catalyst C-50-EtOH-98/2-60 possesses thus more active sites responsible of the DBT HDS via DDS route. The catalyst C-50-EtOH-80/20-60 shows similar reaction rate constant than reference catalyst C-100-EtOH-Air. The presence of the same oxometallic phase before sulfidation independently of the atmosphere employed leads thus to the same catalytic performances in DBT HDS. Results obtained are in accordance with the content of the active phase.

Then, the effect of the solvent of impregnation and its influence on catalytic performances in DBT HDS is presented hereafter.

II.2.4. Effect of the solvent of impregnation

Results concerning DBT HDS for samples synthesized with different solvents of impregnation are presented in Figure VI.11.

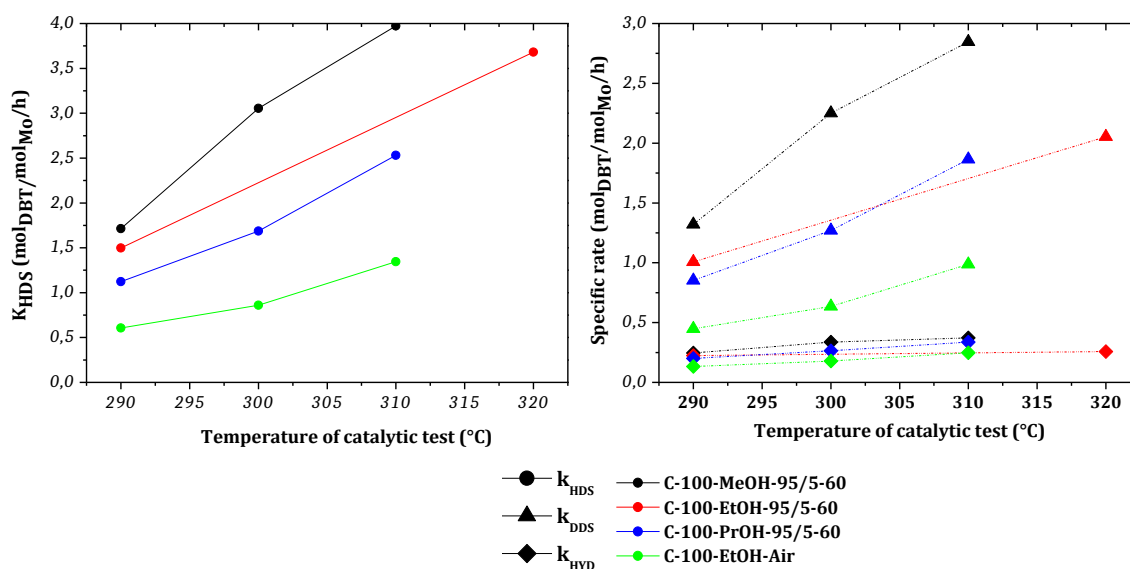


Figure VI.11: Specific rates of DBT HDS (left) and specific rates of DDS and HYD pathways (right) for samples C-100-MeOH-95/5-60, C-100-EtOH-95/5-60 and C-100-PrOH-95/5-60 as well as reference catalyst as a function of the temperature of catalytic test.

For all temperatures of the catalytic test, the sample C-100-MeOH-95/5-60 was the one with the highest reaction rate constants for the overall HDS reaction. This difference is increased with the increase of the temperature of the catalytic test. Looking at reaction rate constants associated at each route, it is observed that the solvent has a negligible effect on the hydrogenation route whereas this effect is much larger in the case of the DDS route. This effect is also promoted with the temperature of the catalytic test where k_{DDS} associated to C-100-MeOH-95/5-60 is much more increased than in other cases. The good performances of C-100-MeOH-95/5-60 are related to its high content of CoMoS in MoS₂ phase.

Concerning samples C-100-EtOH-95/5-60 and C-100-PrOH-95/5-60, it is observed an almost similar k_{DDS} , suggesting a comparable number of active sites related to DDS route involved in the catalytic reaction. It has been estimated by TEM analyses, that these samples possess, indeed, a similar average degree of stacking slabs (~ 3.3). However, sample C-100-EtOH-95/5-60 has shown MoS₂ slabs shorter than C-100-PrOH-95/5-60. Activation energies have been determined to be around ~ 100 kJ.mol⁻¹ for all samples.

The influence of the reaction time during synthesis of the oxometallic precursors is the next parameter studied in DBT HDS.

II.2.5. Effect of the reaction time

For that, catalysts C-50-EtOH-95/5-<1 and C-50-EtOH-95/5-60 have been tested in DBT HDS and results are presented in Figure VI.12.

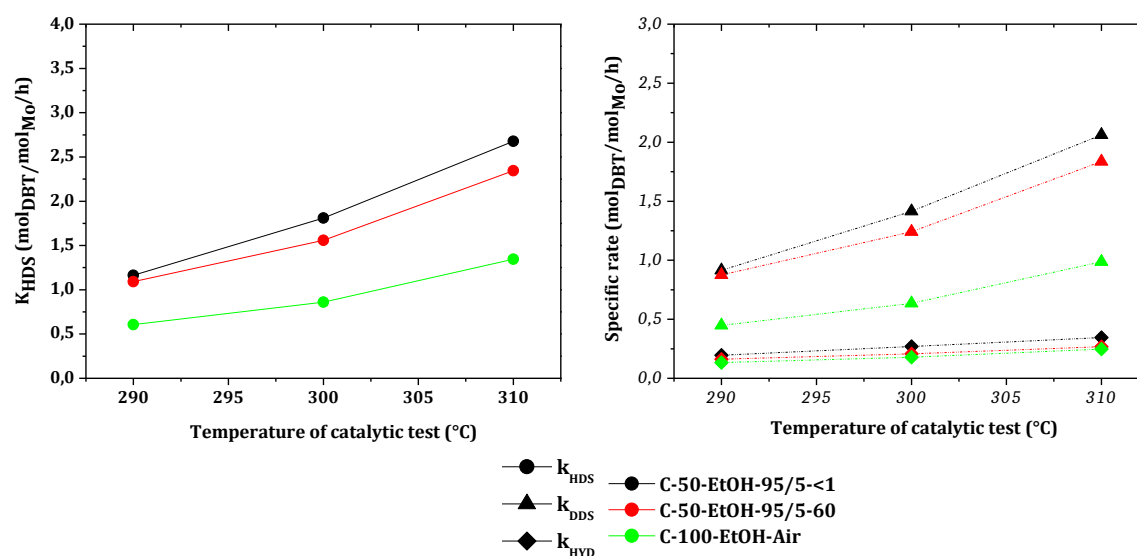


Figure VI.12: Specific rates of DBT HDS (left) and specific rates of DDS and HYD pathways (right) for samples C-50-EtOH-95/5-<1 and C-50-EtOH-95/5-60 as well as reference catalyst as a function of the temperature of catalytic test

Reaction rate constants associated to the overall HDS reaction (k_{HDS}) are similar in both cases with a k_{HDS} slightly higher at high temperature of the catalytic test for C-50-EtOH-95/5-<1. For reaction rate constants associated to each pathway, they evolve in the same manner in the two samples. The effect of the reaction time has thus almost no effect on catalytic performances in DBT HDS and catalysts possess a similar number of active sites involves in the catalytic reaction. By estimating kinetics parameters for each catalyst, we found similar results in terms of activation energies (around 100-110 kJ.mol⁻¹).

The last experimental parameter studied was the loading of Mo. Results in terms of DBT HDS are presented in the following part.

II.2.6. Effect of the Mo loading

Results obtained in DBT HDS for catalysts containing 10 wt.% Mo (14 wt.% MoO₃) and 13 wt.% Mo (18.5 wt.% MoO₃) are presented in Figure VI.13.

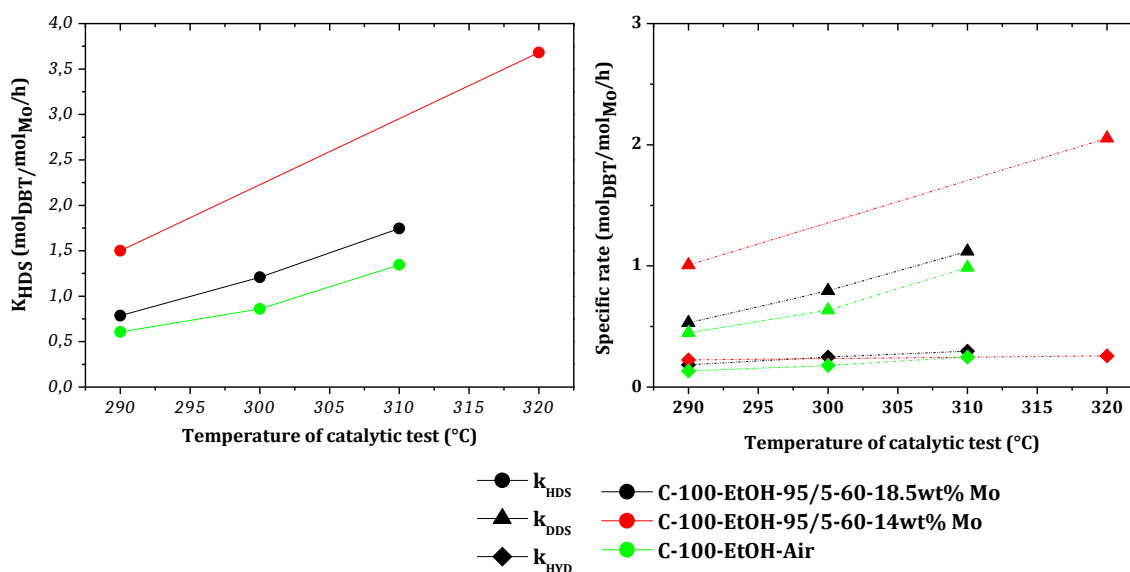


Figure VI.13: Specific rates of DBT HDS (left) and specific rates of DDS and HYD pathways (right) for samples C-100-EtOH-95/5-60-18.5 and C-100-EtOH-95/5-60-14 as well as reference catalyst as a function of the temperature of catalytic test.

Reaction rate constants calculated for DBT HDS have found to be 2 times higher in the case of the catalyst containing the lowest Mo content. However, looking at reaction rate constants associated to each route, we observe that the main difference is related to the DDS route. Whereas k_{HYD} calculated are similar for both samples. This result may agree with the catalytic performance in toluene hydrogenation where samples have shown similar reaction rate constants. Numbers of catalytic sites associated to HYD route are thus equivalent independently of the molybdenum content, whereas a higher number of active sites related to the DDS route are present in the sample synthesized with a lower Mo content.

II.2.7. Conclusion about the hydrodesulfurization of DBT

From toluene hydrogenation, it has been observed some differences between samples synthesized depending on the preparation conditions. These differences were less visible in the case of DBT HDS because this reaction occurs mainly via the DDS route. However, the same trends were observed for the DDS route than those found during toluene hydrogenation. Indeed, same catalysts have shown the best performances in DBT HDS and differences between them were enhanced.

From the variation of the temperature of synthesis of the oxometallic phase, it has been observed that a synthesis at 100°C leads to better catalytic performances. The study of the ratio CO₂/ethanol has shown catalysts with better performances for catalysts synthesized with a high CO₂/ethanol ratio. In the case of the solvent of impregnation, catalyst synthesized with methanol has shown the best catalytic performances compared to all others tested. The loading of molybdenum which has almost no effect on the reaction rate constant for the hydrogenation of toluene has shown to be less active in DBT HDS at high Mo loading. Finally, the time of reaction does not have shown difference in HDS DBT.

To evaluate the influence of these experimental conditions employed for the synthesis of the oxometallic phase, some catalysts have been tested in hydrodesulfurization of 4,6-DMDBT, the most refractory molecule in HDS.

II.3. Catalytic performances in hydrodesulfurization of 4,6-DMDBT

In the case of 4,6-DMDBT HDS, the removal of sulfur occurs also via two pathways. The hydrogenation (HYD) pathway with the formation of methylcyclohexyltoluene (MCHT) through a hexahydrodimethyldibenzothiophene (6H-DMDBT) intermediate. Whereas, through the DDS pathway, the product formed is 3,3'-dimethylbiphenyl (3,3'-DMBP). The main route to remove sulfur from 4,6-DMDBT is the HYD route [10]. This is mainly due to the presence of methyl groups in β -position of the sulfur atom which induce a steric hindrance [11]. The HDS of 4,6-DMDBT occurs thus more easily after the hydrogenation of aromatics groups before the C-S scission.

This catalytic test has only been performed on four catalysts due to technical issues related to this test. The samples tested were those synthesized at two different temperatures and two different ratios CO₂/EtOH. Results are presented in the following part.

II.3.1. Effect of the temperature during synthesis of the oxometallic phase

Figure VI.12 presents results obtained in 4,6-DMDBT HDS for catalysts C-50-EtOH-95/5-60 and C-100-EtOH-95/5-60.

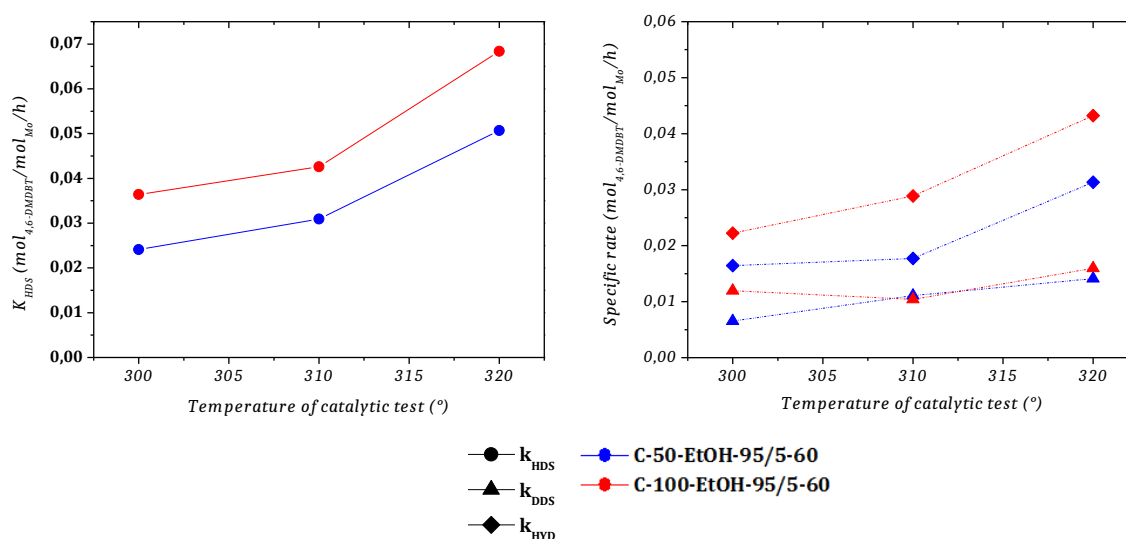


Figure VI.12: Specific rates of 4,6-DMDBT HDS (left) and specific rates of DDS and HYD pathways (right) for samples C-50-EtOH-95/5-60 and C-100-EtOH-95/5-60 as a function of the temperature of catalytic test

First observation is the refractory character of the 4,6-DMDBT compared to the DBT with reaction rate constants 100 times lower than for DBT HDS.

Then it is observed better k_{HDS} for the sample synthesized at 100°C than sample synthesized at 50°C. This observation has also been made for DBT HDS. Looking at Figure VI.12 (right), it is observed that 4,6-DMDBT occurs mainly via the HYD route which is in accordance with the literature reports [12–14]. These catalysts have a similar k_{DDS} which was also the case for DBT HDS. For these catalysts, activation energies have been calculated to be in the range of 90-105 kJ.mol⁻¹. A synthesis of the oxometallic phase at temperature of 100°C is therefore benefit for the catalytic performances in HDS.

The second experimental parameter studied was the influence of the ratio CO_2/EtOH .

II.3.2. Effect of the ratio CO_2/EtOH

The second effect studied and where catalysts have been tested concerns the ratio employed during the synthesis of catalysts and results of 4,6-DMDBT HDS are presented in Figure VI.13.

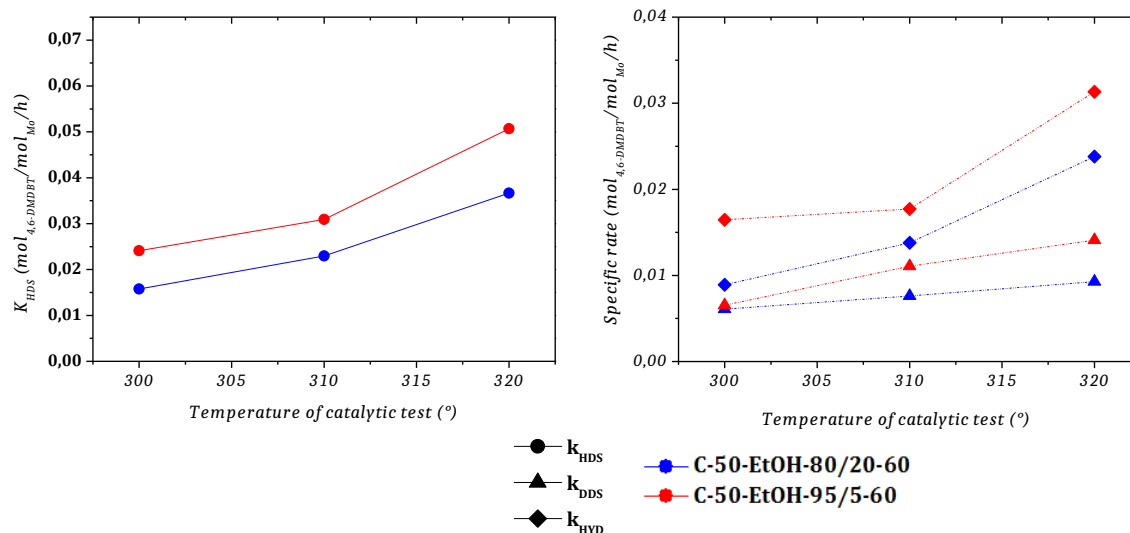


Figure VI.13: Specific rates of 4,6-DMDBT HDS (left) and specific rates of DDS and HYD pathways (right) for samples C-50-EtOH-80/20-60 and C-50-EtOH-95/5-60 as a function of the temperature of catalytic test

Sample C-50-EtOH-95/5-60 possess a K_{HDS} higher than C-50-EtOH-80/20-60 at each temperature of the catalytic test. This observation is also true for reaction rate constants associated to each route. The catalyst C-50-EtOH-95/5-60 has already shown a better catalytic performance in toluene hydrogenation compared to the other. This was also the case for the DBT HDS. However, this higher K_{HYD} for C-50-EtOH-95/5-60 was less pronounced in DBT HDS than in 4,6-DMDBT HDS. The activation energy associated to the 4,6-DMDBT HDS has been calculated to be of $105 \text{ kJ}\cdot\text{mol}^{-1}$ for C-50-EtOH-95/5-60 and to be of $120 \text{ kJ}\cdot\text{mol}^{-1}$ for sample C-50-EtOH-80/20-60.

In summary, a sample synthesized with a higher CO_2/EtOH ratio gives better catalytic performances than a sample synthesized at lower ratio.

III. Conclusion

This chapter was dedicated to the catalytic performances of activated catalysts prepared by supercritical carbon dioxide and the influence of the parameter employed during the synthesis of the oxometallic phase.

It has been shown that results obtained in terms of characterizations of the sulfided phase are in agreement with catalytic results obtained. This being valid for the three catalytic reactions studied. By comparing the catalysts synthesized using carbon dioxide with the reference sample synthesized under air, it has been shown that for all samples tested (except the one synthesized at 200°C), catalysts have shown better catalytic performances than the reference.

A trend in each effect studied has been observed and is in agreement with the conditions of synthesis.

The temperature of synthesis during the preparation of catalyst is important due to the formation of undesirable species at temperatures higher than 150°C which inhibits catalyst activity, as shown in toluene hydrogenation. It has been found, for DBT and 4,6-DMDBT HDS, that the catalyst synthesized at 100°C temperatures gives the best catalytic results.

By varying the ratio carbon dioxide/ethanol during synthesis, it has been demonstrated that a high ratio CO₂/EtOH gives the best performances. This is observed in each catalytic reaction studied. This difference may be attributed to a higher supersaturation in the case of a synthesis with a high CO₂/EtOH ratio, leading to the presence of smaller crystallites.

By testing different solvents, to perform impregnation of the support, we have determined that working with methanol gives catalyst with better performances than working with ethanol and propanol. The solvent of impregnation has thus an important effect on the catalyst activity. This difference may be attributed to the difference of volume expansion which is link to the properties of the solvent.

One of the main interest of our process, was the possibility of obtaining an active catalyst in a short synthesis time. This has been proven by comparing different synthesis times which have shown same performances in catalysis independent of the time of synthesis. It can be postulated from these results that during synthesis of the oxometallic phase, all molybdenum species precipitate directly after scCO₂ injection and no growth of particles is observed after a longer time of synthesis.

It has also been shown that it is possible to obtain a high loading of molybdenum in the support employed, keeping the toluene hydrogenation activity constant. A loss of activity with DBT was observed may be due to diffusion hindrance.

With the variation of all these experimental parameters, we can suppose that to obtain the most active catalyst, the synthesis will consist of using methanol as solvent of impregnation, having the highest ratio CO₂/MeOH and on working at moderate temperatures (100-120°C). Moreover, it will be possible to prepare it in a short time.

This process, consisting to expand the solvent of impregnation to precipitate species onto a support, has led to interesting results in terms of hydrodesulfurization of DBT and 4,6-DMDBT and combines advantages in terms of time and energy efficiency to be scaled up at an industrial level.

IV. Bibliography

- [1] M. Daage, Structure-function relations in molybdenum sulfide catalysts: The “Rim-Edge” Model, *J. Catal.* 149 (1994) 414–427.
- [2] J. Grimblot, Genesis, architecture and nature of sites of Co(Ni)–MoS₂ supported hydroprocessing catalysts, *Catal. Today.* 41 (1998) 111–128.
- [3] F. Colbeau-Justin, C. Boissière, A. Chaumonnot, A. Bonduelle, C. Sanchez, Aerosol route to highly efficient (Co)Mo/SiO₂ Mesoporous Catalysts, *Adv. Funct. Mater.* 24 (2014) 233–239.
- [4] M. Houalla, N.K. Nag, A. V Sapre, D.H. Broderick, B.C. Gates, Hydrodesulfurization of dibenzothiophene catalyzed by sulfided CoO–MoO₃–Al₂O₃: The reaction network, *AIChE J.* 24 (1978) 1015–1021.
- [5] R.Z. Lee, F.T.T. Ng, Effect of water on HDS of DBT over a dispersed Mo catalyst using in situ generated hydrogen, *Catal. Today.* 116 (2006) 505–511.
- [6] F. Bataille, J.-L. Lemberon, P. Michaud, G. Pérot, M. Vrinat, M. Lemaire, E. Schulz, M. Breyse, S. Kasztelan, Alkyldibenzothiophenes hydrodesulfurization-promoter effect, reactivity, and reaction mechanism, *J. Catal.* 191 (2000) 409–422.
- [7] M. Egorova, Hydrodesulfurization of dibenzothiophene and 4,6-dimethyldibenzothiophene over sulfided NiMo/Al₂O₃, CoMo/Al₂O₃, and Mo/Al₂O₃ catalysts, *J. Catal.* 225 (2004) 417–427.
- [8] C. Song, X. Ma, New design approaches to ultra-clean diesel fuels by deep desulfurization and deep dearomatization, *Appl. Catal. B-Environmental.* 41 (2003) 207–238.
- [9] T. Kabe, K. Akamatsu, A. Ishihara, S. Otsuki, M. Godo, Q. Zhang, W. Qian, Deep hydrodesulfurization of light gas oil. 1. Kinetics and mechanisms of dibenzothiophene hydrodesulfurization, *Ind. Eng. Chem. Res.* 36 (1997) 5146–5152.
- [10] M. Houalla, D.H. Broderick, A. V. Sapre, N.K. Nag, V.H.J. de Beer, B.C. Gates, H. Kwart, Hydrodesulfurization of methyl-substituted dibenzothiophenes catalyzed by sulfided Co–Mo/Al₂O₃, *J. Catal.* 61 (1980) 523–527.
- [11] D.H. Broderick, B.C. Gates, M. Houalla, N.K. Nag, A. V. Sapre, Hydrodesulfurization of dibenzothiophene catalyzed by sulfided CoO–MoO₃– γ -Al₂O₃: The reaction network, *AIChE J.* 24 (1980) 1015–1021.
- [12] H. Topsøe, B.S. Clausen, F.E. Massoth, *Hydrotreating Catalysis*, in: J.R. Anderson, M. Boudart (Eds.), *Catalysis*, Springer Berlin Heidelberg, Berlin, Heidelberg, 1996: pp. 1–269.
- [13] M. Egorova, R. Prins, Competitive hydrodesulfurization of 4,6-dimethyldibenzothiophene, hydrodenitrogenation of 2-methylpyridine, and hydrogenation of naphthalene over sulfided NiMo/ γ -Al₂O₃, *J. Catal.* 224 (2004) 278–287.

- [14] M.J. GIRGIS, B.C. GATES, Reactivities, reaction networks, and kinetics in high-pressure catalytic hydroprocessing, *Ind. Eng. Chem. Res.* 30 (1991) 2021–2058.

General Conclusion

In the context of producing and using clean fuels to meet regulations about sulfur content, the development of catalysts with a higher activity and lifetime is thus mandatory. In order to increase catalytic activity, new synthesis methods are put forwards to obtain catalyst with a well-dispersed active phase onto the support where maximum of atoms participates to the catalytic reaction. Hydrodesulfurization (HDS) is a well studied topic and many researches have been carried out during the last decades. However, the use of supercritical fluids to synthesize this kind of catalysts based on molybdenum disulfides slabs promoted at their edges by cobalt atoms, has only been reported by a few research groups. In the case of supported HDS catalysts, the use of supercritical carbon dioxide was to impregnate metallic species onto a support by dissolving precursors into scCO₂. Although, this technique has been shown to be efficient in terms of resulting catalytic activity, the use of harmful and difficult to store molybdenum precursors, such as molybdenum hexacarbonyl, as well as its long time of synthesis made this process complexly to be scaled up to industrial level. The coupling of a dry impregnation with the use of scCO₂ to precipitate species has been proposed in this PhD as an alternative process for the preparation of catalyst precursors.

First of all, the study of elements contained in HDS catalysts through assessments of their criticality has been done in collaboration with the University of Augsburg and the Fraunhofer Institute. This work has been fruitful and has permit to obtain a wider vision on elements employed during these three years of PhD. From this chapter, we have put forward that cobalt is an element which can become critical for the European industry. In fact, cobalt is an element difficulty substitutable and necessary for the development of greener energies. Moreover, a major part of its reserves is located in a geopolitically instable and poor country, the Democratic Republic of Congo. For molybdenum, ours researches have shown that reserves are more dispersed onto the Earth crust and located in developed countries which implies less disruptions in supply.

Secondly, the major part of this work was focused on the synthesis of HDS catalyst using scCO₂. For that, we first studied chemical reactions occurring during the preparation of catalysts and have compared them to a conventional synthesis of these catalytic materials. The use of *in situ* Raman experiments has appeared to be one of the best option for this study which implies measurements in temperature and under pressure. Moreover, thanks to this investigation, we have put forwards best experimental conditions in terms of molybdenum precursors and solvent of impregnation to avoid undesirable species and to obtain a good dispersion of species. Majors results were the following. In the case of the use of ammonium heptamolybdate (AHM) dissolved in water for solution of impregnation, we observe that a work with scCO₂ for the precipitation of species was detrimental for the dispersion. We detect the presence of cobalt molybdate species for a work under scCO₂ which was not observe for a thermal treatment under air. The usage of scCO₂ has led to crystalline particles onto the support. Moreover, the acidity brought by the solution of impregnation (AHM dissolved in water), has released some aluminium ions present in the alumina support and led to the presence of Anderson-type heteropolyanion which can form large unsupported precipitates onto the surface of alumina. We have proposed that scCO₂ acts as a flash dryer for the precipitation of species by replacing water into the pores of alumina and water can entrain dissolved metals species during its removal which leads to a heterogeneity of species onto the support.

As the use of water as solvent of impregnation has led to crystalline species and to the formation of undesirable Anderson heteropolyanions, a work with ethanol as solvent of impregnation has been preferred. Due to insolubility of AHM precursor in alcohol, we have employed phosphomolybdic acid (HPA) to introduce molybdenum onto the surface of our support. The first observation was that a treatment under scCO₂ leads to the presence of an amorphous phase consisting of dispersed

polymolybdate and/or heteropolyanion phases. However, it has been shown the presence of different species as a function of the alumina pellet analyzed. The scCO₂ permits to expand/extract ethanol and to precipitate species when the supersaturation is reached. A work in ethanol as solvent of impregnation has given better results in terms of dispersion of the oxometallic phases formed than a work with water. This system scCO₂/EtOH has thus been chosen in the study of the influence of experimental parameters.

In order to study effects induced by varying experimental parameters for a better understanding of our process, several catalyst precursors were synthesized using a batch reactor. From characterizations of the oxometallic phases obtained several conclusions have been highlighted:

- The temperature of reaction has a major effect on resulting species. The presence of cobalt molybdates for temperature of synthesis higher than 150°C has been observed. To avoid them, a work at low temperature is therefore mandatory. Working at temperatures of 50 - 120°C, permits us to obtain Keggin-type heteropolyanions and/or polymolybdates with crystallites sizes around 10 nm dispersed onto the alumina.
- The second parameter studied was related to the pressure of CO₂ employed during the synthesis where crystalline entities of Keggin HPA were found in both cases. However, these Keggin units were not identical and differ by their hydration degree and also by the size of their crystallites,
- The ratio between CO₂ and solvent of impregnation employed has also an important effect. It has been put forward that a work with a high ratio CO₂/EtOH is thus recommended to obtain smaller crystallites. This result may be explained by the fact that a higher supersaturation of ethanol is obtained when the amount of scCO₂ is high and the volume of ethanol to expand is low. The formation of more nuclei permits to limit the growth of particles,
- The fourth experimental parameter studied was the solvent of impregnation. For that, three alcohols having between one and three carbon atoms have been employed to perform impregnation of the support. By Raman mapping experiments, it has been observed that in the case of methanol, the presence of Keggin-type heteropolyanions was found along the whole surface of alumina pellets. For ethanol, the presence of Keggin-type heteropolyanions has been detected along all the surface of pellets as well as the presence of polymolybdates only in the core of alumina pellets. For a synthesis with propan-1-ol, the presence of polymolybdates has been observed along the pellets whereas Keggin-type heteropolyanions were present only on the core of pellets. These differences may be explained in several ways as for example the easier dehydration of propan-1-ol compared to ethanol and methanol coupled with the instability of Keggin entities in water,
- The fifth main parameter which has been found to be very important is the reaction time. We observed that the precipitation of species occurs almost directly after injection of scCO₂. By performing a synthesis in one hour after temperature stabilization, the same species were obtained than performing an experiment in less than one minute. This time saver compared to a conventional drying and calcination steps, appears thus to be a main advantage to a future scale up of the process to industry.

All samples synthesized have then been sulfided and characterized in their sulfided phase. It has been observed that on average, a degree of sulfidation of around 70 % of molybdenum and a promotion of MoS₂ slabs by cobalt atoms of around 50 % were obtained in all cases. Only slight differences in terms of sulfidation degree and lengths of MoS₂ slabs were observed between each parameter studied but these differences were in agreement with catalytic performances obtained.

The last part of this PhD work has been dedicated to the evaluation of catalytic performances of our HDS catalyst precursors. For that all catalysts synthesized have been first tested in toluene. This test allowed us to determine catalysts with best activities to test them in hydrodesulfurization of model molecules (DBT and 4,6-DMDBT). From these catalytic tests, the influence of each experimental parameter studied has been highlighted and several conclusions have been made with the first important observation being that all samples synthesized using our process have shown better catalytic performances than the reference catalyst chosen.

It has been observed that samples synthesized at temperatures lower than 150°C shown better catalytic performances. This was the case for the three studied reactions. The low activity of samples synthesized at higher temperatures has been assigned to the presence of bulk cobalt molybdate species in these samples. The pressure employed for the synthesis of the oxometallic phase has, for its part, almost no effect on catalytic performances. Catalytic tests have put forward that samples synthesized with a high ratio carbon dioxide/ethanol show the best performances. This has been linked to the presence of smaller crystallites in the oxometallic phase for high CO₂/EtOH ratios. It has then been highlighted that catalytic performances were indirectly linked to the solvent employed during the impregnation. Methanol has shown better performances than ethanol and propan-1-ol. The last striking result was the possibility of obtaining a catalyst with a good activity in a short time of synthesis. It has indeed been shown same catalytic performances than a catalyst prepared in one hour of synthesis.

From the assessment of the criticality of metals contained in HDS catalysts to the important catalytic performances of these catalysts prepared by using this scCO₂ process passing by *in situ* characterizations of the catalyst preparation and the influence of several parameters, this PhD work has covered a wide range of domains. The most important result is probably the saving of time and of energy made using such process for the synthesis of HDS catalysts. These advantages coupled with the use of a “green solvent” makes it a good candidate to implement it in an industrial scale tomorrow.

Appendices

Appendix I: An overview of sulfur

This work was the subject of an article being published.

Introduction

The aim of this paper is to give an outlook about one of the most known element, the sulfur, by trying to cover its entire life cycle, from cradle to grave. Reserves and resources, production, uses, trade and recycling of sulfur will be addressed through this paper. Sulfur is a chemical element essential for human kind. Its abundance made it one of the most used element during the human history. It is the thirteenth most abundant element, present at 2.92 wt% in the Earth's crust. Sulfur is a word of latin origin and the root has been traced to reconstruct proto-Indo-European *swel* or *swel* which means "to burn"¹. The sulfur was already mentioned in the Torah and the Bible, and also in texts from ancient Egypt, India, China and preclassical Greece for its uses as fumigants, balms and anti-parasitics². In 1777, Antoine Lavoisier succeeded to convince the scientific community that it was an integral part. Uses of sulfur are multiple, a major part being dedicated to the production of sulfuric acid, one of the most produced chemical compound worldwide and necessary in the production of fertilizers. As the population will continue to grow in the next decades, sulfur is important and it is necessary to keep an eye on it.

Reserves and Resources of sulfur

Reserves

Reserves of sulfur, which is present in fossils resources (crude oil, natural gas, coal and sulfides ores), are important³⁻⁵. Most of its production comes from the processing and refining of the fossil resources and reserves seems sufficient for a foreseeable future⁶. As the processing and refining of fossil resources are not necessarily realized in the country where fossil resources are recovered, the production of sulfur may be located everywhere a refinery process is present^{3,4}.

Resources

Sulfur is present in evaporite and volcanic deposits as its elemental form and the sulfur presence in natural gas, petroleum, tar sands and metal sulfides is estimated about 5 billion tons^{3,5,7,8}. Moreover, resources of sulfur in gypsum and anhydrite are almost limitless and resources present in coal, oil shale and shale rich in organic matter are estimated about 600 billion tons⁷. Sulfur is abundant in the Earth's crust even if processes to recover all resources types are economically unviable at the moment.

Production of sulfur

Production of sulfur (all forms) by country

Data were compiled from USGS Mineral Commodity Summaries in the last five years^{3-5,7,9}. The Table 1 shows the major producing countries of sulfur as a function of the year. Data are given in 1000 metric tons.

Table 1 : Major producing countries of sulfur for these 5 past years.

Major producing countries of sulfur (all forms)

Country	2010	2011	2012	2013	2014
	1000 metr. t	1000 metr. t	1000 metr. t	1000 metr. t	1000 metr. t
United States	9070	8930	9000	9210	9770
Australia	940	940	860	860	900
Brazil	480	480	480	545	550
Canada	7255	6520	5910	6370	6000
Chile	1676	1720	1680	1700	1700
China	9600	9700	9900	10500	12000
Finland	590	590	1350	740	740
France	1305	1310	650	650	650
Germany	3905	3910	3820	3880	3900
India	1171	1190	1190	2430	2430
Iran	1780	1780	1880	1890	1900
Italy	740	740	740	740	740
Japan	3292	3300	3250	3300	3300
Kazakhstan	2000	2700	2700	2850	2850
Republic of Korea	660	1200	1200	1300	1300
Kuwait	830	830	800	820	820
Mexico	1810	1660	1740	1810	1810
Netherlands	530	530	515	515	515
Poland	732	1140	1160	1080	1100
Qatar	1124	1200	820	850	850
Russia, Europe	7070	7280	7270	7250	7300
Saudi Arabia	3300	4600	4090	3900	4000
South Africa	465	370	310	270	290
Spain	637	637	680	270	270
United Arab Emirates	1763	1800	1900	2000	2000
Uzbekistan	520	520	540	560	560
Venezuela	800	800	800	800	800
Other countries	4020	4080	2900	3360	3360
World total (rounded)	68100	70500	68100	70400	72400

The production of sulfur has not slightly evolved over the past few years with a total stable world production about 70 million metric tons per year. The major production of sulfur comes from China, United States, Russia, Canada and Saudi Arabia. These countries are also the largest producers of oil and gas, indicating that recovered sulfur represents the main part of the sulfur production. An increase of production is expected from sulfur recovery at liquefied natural gas operations in the Middle East and expanded oil sands operations in Canada^{3,5,7,8}.

Evolution of the world production and price of sulfur over the last century¹⁰

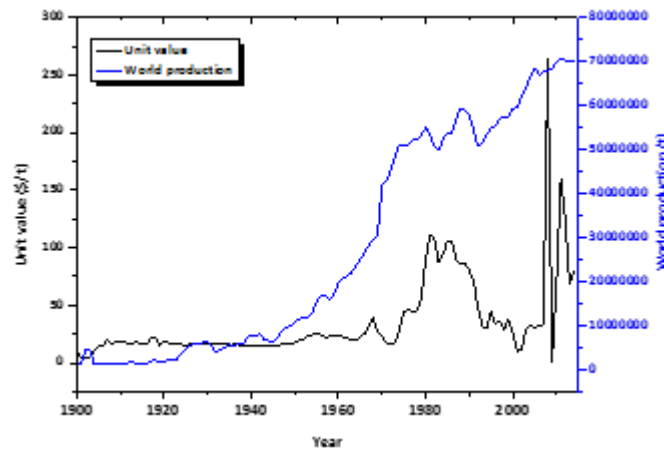


Figure 1: Evolution of the sulfur production and price over the last century

Figure 1 represents the evolution of the price and the production of sulfur over the last century. The sulfur production has constantly increased during the last century, with a major drop during the 1950-1980 period. The price of sulfur has known a large increase in the 80's to reach 100\$/t. This drop was mainly due to the energy crisis. A second large increase of sulfur price was observed after 2005 due to this time to the economy crisis where the price has reached 250\$/t. As sulfur roots can come of many sources but mainly of fossil resources, energy and economy have a large impact on its price and production.

Sources of sulfur

As previously mentioned, sulfur can be recovered from different sources: it can be mined in its elemental form (minor part), can be recovered as co-product from oil and gas production (major part) or can be produced as a by-product of ferrous and non-ferrous metal smelting under its sulfuric acid form⁶. Nowadays, the extraction of sulfur from underground deposits is very low (less than 2 wt% of the world production) but during the 20th century, most of the sulfur was obtained from the soil using the Frasch process. The amount of sulfur recovered from different sources is presented in Figure 2.

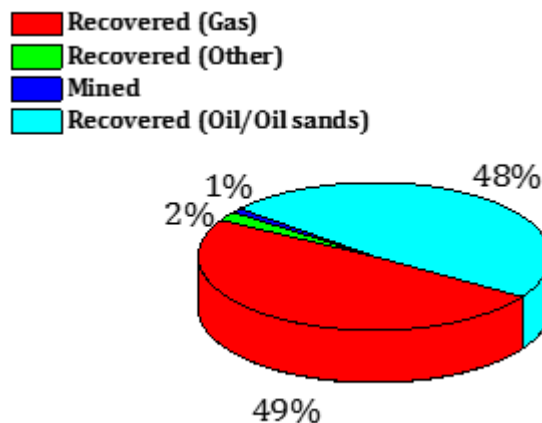


Figure 2: Elemental sulfur production in 2012 by sources adapted from [11].

Mined sulfur

The Frasch process, named after Herman Frasch (1851-1914), was the only economic method of recovering sulfur from the underground deposits¹². In this process, hot water (about 170°C) is introduced into sulfur deposits, the sulfur melts (melting point: 115.2°C) and is lifted to the surface by means of compressed air¹²⁻¹⁴. High purity sulfur (up to 99%) can then be solidified. A graphical scheme of the process is presented in Figure 3.

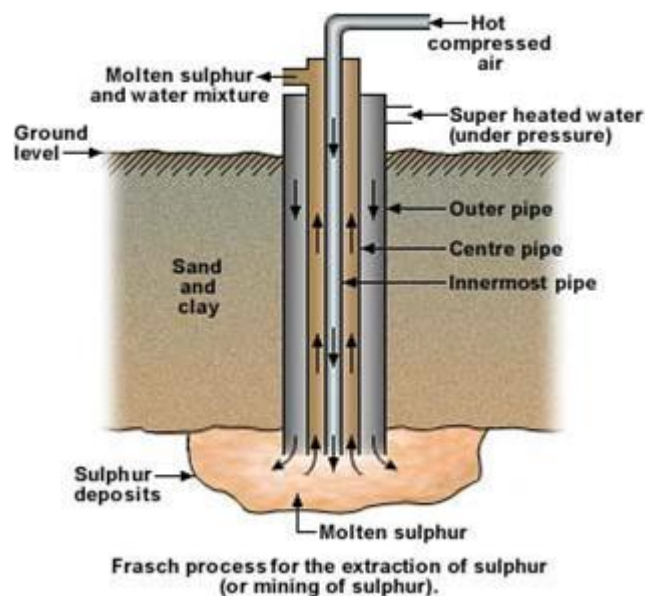


Figure 3: The Frasch process showing the extraction of elemental sulfur from underground deposits (scheme from [15])

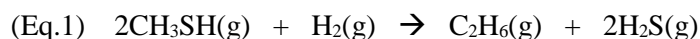
The second main source of sulfur is its recovery from fossil resources, which is nowadays the major source of sulfur. It has been previously mentioned that sulfur is naturally present in crude oil, natural gas and coke. It was recovered primarily to comply the environmental regulations that were applicable directly to emissions from the processing facilities or indirectly by restricting the sulfur content of the fuels sold or used by the facilities¹⁶.

Recovered sulfur

Natural gas and oil contain hydrogen sulfide (H_2S) and a wide variety of organo-sulfur compounds (R-SH). Nowadays, environmental regulations are very stringent concerning the level of sulfur present in feedstocks. It is now mandatory to remove more than 99.9 wt% of sulfur compounds present in fossil resources to meet a level of 10 ppm of sulfur in diesel and gasoline in Europa¹⁷. Sulfur compounds are responsible of environmental pollution when they are burned (formation of sulfur dioxide and reaction of it in the upper atmosphere to form sulfuric acid which is responsible of acid rains). They are also a poison for catalysts used in the chemical manufacturing and for catalysts present in automotive parts when gas or oil are used as fuels. Several steps are necessary to obtain the elemental sulfur from the organo-sulfur compounds present in the natural gas or oil¹⁸.

Hydrodesulfurization

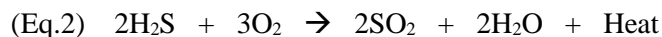
The first step, called hydrodesulfurization, consists in the sulfur removing from fossil resources. In this process natural gas or oil pass through a fixed bed reactor filled with a catalyst and has an addition of hydrogen in order to have the following reaction (example with the methanethiol molecule)¹⁹:



During this step the reactor works at 300-450°C with a H₂ pressure up to 200 bar²⁰. Then the hydrogen sulfide formed is separated by dissolution in an aqueous solution of organic base. When the solution is heated, pure hydrogen sulfide is released¹⁸. A second step is necessary to recover the elemental sulfur from hydrogen sulfide. This step is called the Claus process.

Claus process

In this process, the hydrogen sulfide is transformed into elemental sulfur, sulfur dioxide and hydrogen sulfide which has not reacted and will be treated a second time. First, the sour gas is enriched with oxygen in order to convert some hydrogen sulfide to SO₂ according to the reaction:

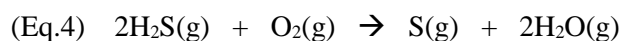


Then, the mixture formed reacts according the Claus reaction to elemental sulfur and water as described in the equation below:



About 70% of sulfur is recovered at this time of the process, and the remaining gas is introduced into a tail gas unit to remove the remaining sulfur²¹.

The overall reaction can be written as this:



Production of sulfur depending of its origin

The different sources of sulfur with their different origins are presented hereafter. These data have been compiled using information found on CRU Fertilizers¹¹ and The Sulphur Institute²² websites.

Over the past decades, the origin of sulfur comes from three main types of production. Elemental sulfur can be recovered from gas, oil and others fossil resources. But it can also be recovered from smelter acids where the sulfur is recovered from ores, and from pyrites when it is obtained as sulfur dioxide.

The sulfur coming from recovered sources and from acid smelters is considered as an involuntary production. These involuntary productions represent more than 90 wt.% of the total production. In another case, from pyrites, sulfur is the desired product and corresponds to a light part of the total production.

Due to the actual environmental restrictions concerning the sulfur content in gas emission and thus in fossil feedstocks, the production of elemental sulfur is mainly driven by the production of gas and oil (see Figure 2). The second main part of elemental sulfur comes from acid smelters which is also an involuntary production due to the fact that extraction of metals is mainly from sulfide ores.

The actual markets and uses of non-ferrous metals lead to an increase of the production of elemental sulfur from acid smelters. The third origin of sulfur is from pyrites. A decrease of the production of sulfur from this source due to a large involuntary production which obsoletes this way of obtaining sulfur. The major producing country of sulfur from pyrites is China, with about 92% of the total world production²². It could be explained by less restricting regulations in terms of sulfur content in fuels and also by a growing constant population. The sulfur is mainly used as sulfuric acid and the latter being mainly used in fertilizers.

Uses of sulfur

The largest sulfur use is for the production of sulfuric acid (H₂SO₄), which is the most abundantly made industrial chemical and is a good indicator of the industrial strength of a nation^{23,24}. About 90 wt% of produced or recovered sulfur is as sulfuric acid^{18,22}. Sulfur is also used to synthesize carbon disulfide in the case of the manufacture of cellophane and for the vulcanization of rubber, where polysulfides chains crosslink organic polymers. Sulfites are used to bleach paper and as preservatives in many food products. Sulfur, under its sulfate, is found in surfactants and detergents. Many other sulfur containing compounds are found in a wide range of applications such as Li-ion batteries, semiconductors, pigments, optoelectronic, pharmaceutical and numerous others^{1,6,25–27}.

Sulfuric acid

Main uses of sulfuric acid

As 90 wt% of the elemental sulfur is used to produce sulfuric acid, a large part of this report is focused on it. Figure 4 presents the main different uses of sulfuric acid. Half of the production of sulfuric acid is used in the case of the production of phosphate fertilizers. More precisely, the sulfuric acid is employed to obtain phosphoric acid, the latter being used for the production of phosphate fertilizers (calcium dihydrogenophosphates and ammonium phosphates). Sulfuric acid is also used to synthesize ammonium sulfate, which is an important fertilizer for sulfur-deficient soils²⁸.

Although the major use of sulfuric acid being for the fertilizing industry, it has many other fields of applications. Almost 10 wt.% of the production is employed in metal processing, where large amounts of sulfuric acid are involved during the leaching step. It is also used in the synthesis of fibres, hydrofluoric acid but also as catalyst and dehydrating agent in many chemical reactions²⁹. Minor uses of this molecule are in paints and pigments and many others.

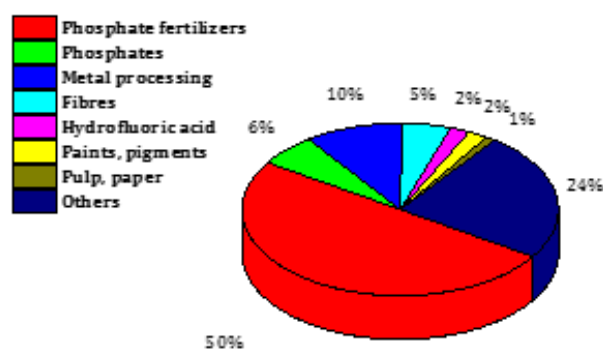
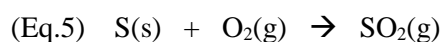


Figure 4: Main uses of sulfuric acid.

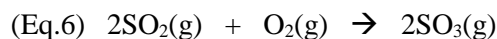
The world production of sulfuric acid has been estimated to 200 million tonnes around the world in 2011, with a major part coming from elemental sulfur (122 million tonnes). Most of the remainder is produced at non-ferrous metals smelters (64 million tonnes) and pyrites mines (16 million tonnes). The largest producer of sulfuric acid is East Asia, led by China, followed by North America, Africa and Latin America. The rapid growth of China is the reason of its monopoly in the sulfuric acid production^{6,25}.

Process to produce sulfuric acid

If the sulfur comes from metals smelters, sulfur dioxide is directly obtained during the roasting of sulfide ores (example of pyrites). If it comes from emissions of non-ferrous smelters, it is also in its sulfur dioxide form. But when the sulfur comes from elemental sulfur, a first step is required to convert it into sulfur dioxide. For that, molten sulfur is sprayed into a high temperature furnace and is burnt in a blast of dry air at about 1030°C²⁸, according to the following reaction:



Then, the sulfur dioxide is converted into sulfur trioxide by The Contact Process³⁰. For that, sulfur dioxide is introduced in a fixed bed reactor ($T = 400\text{-}450^\circ\text{C}$, $P = 0.1\text{-}0.2\text{MPa}$) with oxygen and the mixture pass through a catalyst (generally V_2O_5 supported on silica) in order to obtain the sulfur trioxide:



The hot sulfur trioxide is then cooled down and dissolved in concentrated H_2SO_4 to form an oleum, which after reacting with water forms concentrated sulfuric acid:



Sulfur in fertilizers

This part deals with the importance of sulfur in fertilizers and their production.

Why sulfur is so important in the case of fertilizers?^{6,22,25}

In 2050, they will be around 10 billion of people on Earth and we will have to double the food production compared to nowadays. Intensive agriculture is already in action and soils needs in nutrients are more and more important. The use of fertilizers, in order to avoid a lack of resources, is mandatory, especially in sulfur which has become to be less abundant in soils. This sulfur deficiency is due to several factors.

More sulfur is removed from the soil due to intensive agriculture and less sulfur is added to the soil due to the increasing proportions of sulfur-free fertilizers. Furthermore lower sulfur dioxide emissions leads to a depletion of sulfur in soil.

Sulfur can be considered as one of the most important element on Earth. That is why we have to keep an eye on it due to its action at several levels, whether to produce fertilizers or to be used as nutriment. Indeed, sulfuric acid is first required to produce phosphate fertilizers and sulfur is also

one of the essential plant nutrients with nitrogen, phosphorus and potassium. Sulfur contributes to an increase in crop yields by three different manners:

- It provides a direct nutritive value to the plant,
- It provides an indirect nutritive value as soil amendments,
- It improves the efficiency of the other nutrients.

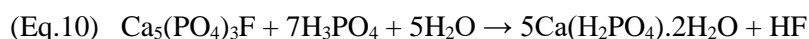
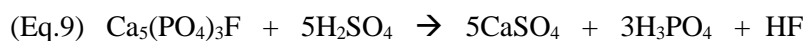
The use of sulfur in fertilizer increases crop yields and quality, which means an increase in food production, feed and fibres to feed the growing population, and also higher economic returns to farmers.

Some studies report the effect of sulfur on crop yields. In Africa for example, it has been showed that a sulfur fertilization of groundnut, maize and other crops leads to increase by 6 to 45% per hectare yields³¹. Researchers have also demonstrated that in India, where the population is growing fast and rice is the major source of food, that sulfur fertilization can increase by 20% the supply per capita and thus gives an economic return for farmers of US\$37 for every US\$1 invested on a basis of the utilization of 15kg S/ha³². These increases of crop yields have also been observed in North America³³ and in China³².

Production of phosphate fertilizers³⁴⁻³⁶

As it has been described previously, the major use of sulfuric acid is to produce phosphate fertilizers, where salts of phosphoric acid and phosphates are widely used in agriculture.

First, phosphate rocks (apatite, $\text{Ca}_5(\text{PO}_4)_3(\text{F}, \text{Cl}, \text{OH})$) are mined and then treated with sulfuric acid in order to produce phosphoric acid (H_3PO_4) and phosphogypsum ($\text{CaSO}_4 \cdot 2\text{H}_2\text{O}$). Several reactions occurred during the production of phosphates and are summarised as follows, with for example the fluoroapatite:



Many other reactions take place during this step due to the different elements contained in the phosphate rocks. After this step, an addition of limestone, potassium chloride (potash) and ammonium sulphate may be done depending on the wanted product.

A flow chart representing the main steps for the production of fertilizers is shown on Figure 5.

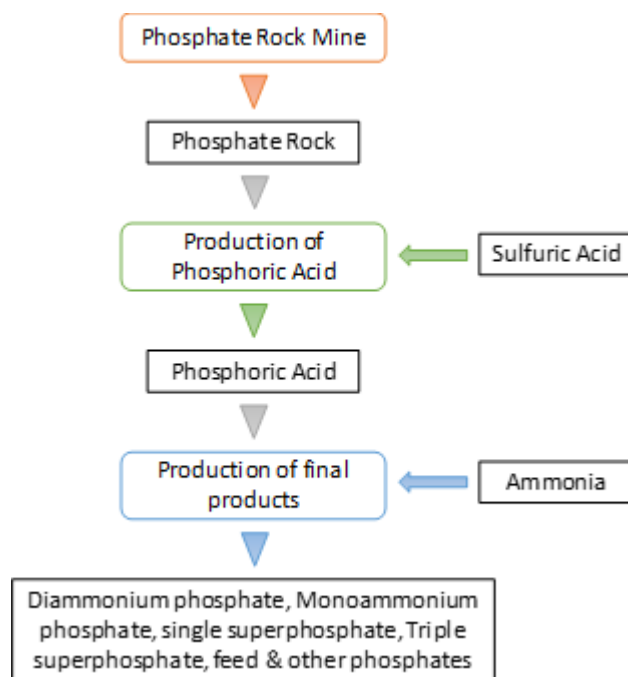


Figure 5: Flow chart of the production of phosphates fertilizers³⁵.

Sulfur used as soil amendments

Sulfur is also used as soil amendment in several regions around the world, particularly in arid regions where soils suffer of a high pH. This alkalinity leads to a deterioration of soil health and suppresses plant intake of essential elements, which lead to a poor crop yield. The use of sulfur to acidify the soil is thus necessary in order to enhance the crop productivity^{6,37}. The absorption of elemental nutrients is function of the soil's pH with a target pH of 6.5³⁸.

Other uses of elemental sulfur

Elemental sulfur has also other fields of use. For example, sulfur can bring profits in terms of ecology in the domain of construction and urban development. Indeed, concrete is one of the most used synthetic material in the world but its manufacture is very polluting in terms of carbon dioxide emission³⁹. The use of sulfur concrete could, in the future, replace the use of Portland cement as the binder and thus reduce CO₂ emissions, thus due to the fact that it needs lower heat to be synthesized. Furthermore, this type of sulfur based concrete can give better properties in terms of corrosion resistance, durability, impermeability and longer life service⁴⁰.

Sulfur can also be incorporate in asphalt in order to replace a part of the binder which then can be used for other applications. Moreover, the use of sulfur asphalt roads enable the laying of roads at lower temperature, which mean less consumption of energy and it has a high corrosion resistance, mechanical strength and fast hardening⁴¹.

Sulfur trade

Sulfur is an element which is trade internationally and its market is mainly due to its large application as sulfuric acid which is subsequently used to produce, in a major part, phosphate fertilizers. The consumption of sulfur is then indirectly affected by the demand of phosphate fertilizers. Figure 6 illustrates major needs in sulfur. Demand is dominated by fertilizer production (phosphoric acid, ammonium sulphate, single superphosphate) with more than 50% of the total

demand in sulfur. The second large demand of sulfur is for its use in metals production and chemical processing, where sulfuric acid is widely present.

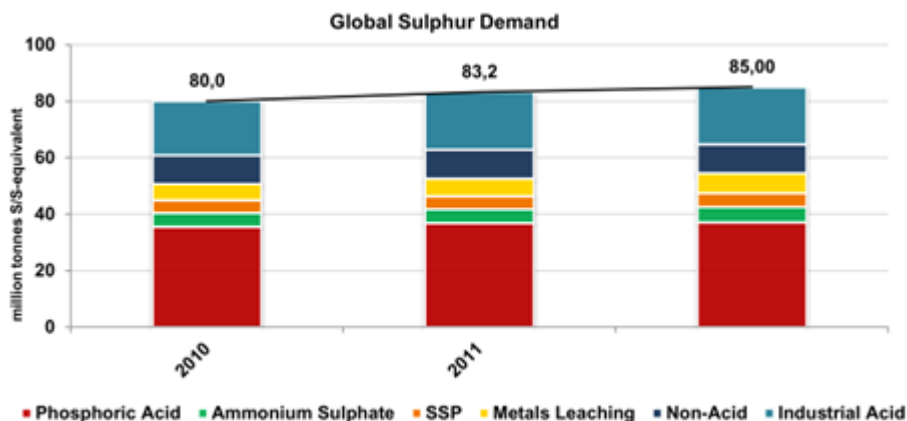


Figure 6: Global sulfur demand¹¹.

Several countries are major actors in the sulfur trading. The main routes for its export and import are summarized in Figure 7.

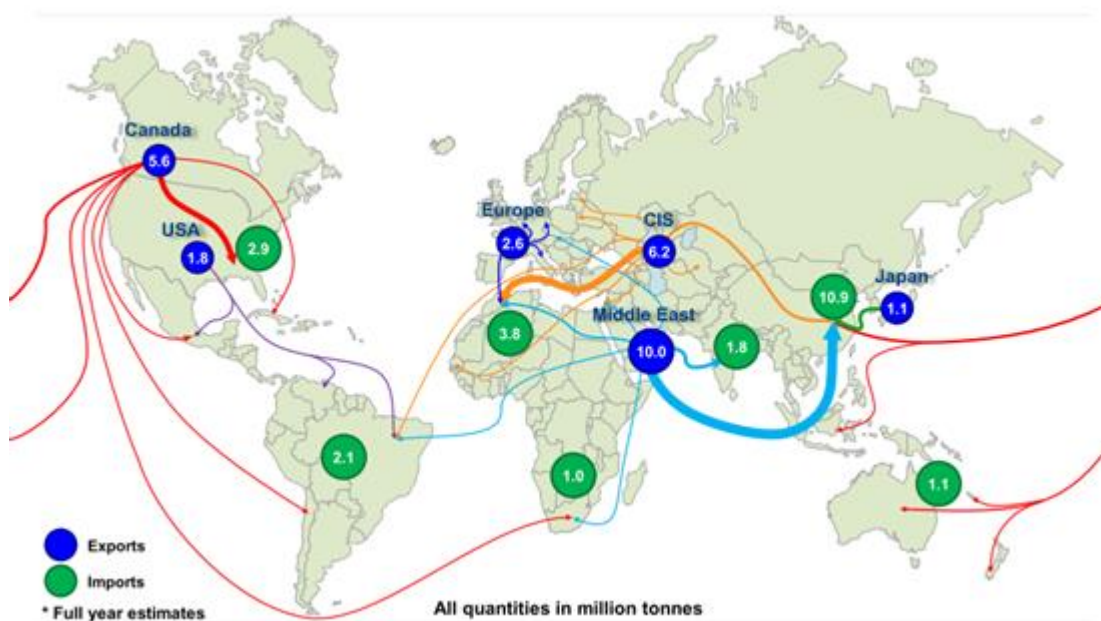


Figure 7: Key sulfur trade routes¹¹.

The major exporters of sulfur are Middle East, CIS (Commonwealth of Independent States) and Canada. These countries possess large reserves of gas and oil and so are the main exporters of recovered sulfur. The main importers of sulfur are China, Morocco, United States and South America (principally Chile). China is a growing country which needs large sulfur quantities either for fertilizers as for mineral processing. Morocco is one of the largest phosphates producers and so their needs in sulfuric acid are very important to produce fertilizers. In the case of South America and especially Chile, the need of sulfuric acid is more related to the mining operations in these

regions, principally for copper processing operations⁴². For Brazil, consumption of sulfuric acid increases for its use in fertilizers which are used to increase crop's yields in the development of biofuels⁴³.

Sulfuric acid prices are dictated by phosphate fertilizer prices. As the major changes in fertilizers would come from India and China, in order to stimulate their agriculture productivity for both food and biofuel production purposes, prices of sulfuric acid and so of sulfur will be mainly driven by the demand of these countries. This is one point that market's analysts have to keep in mind.

The other important factor influencing the sulfur value is the low price of oil's barrel at this moment, due to intensive production of oil from oil sands by the United-States and the large production of Middle Eastern producers which dictate the oil price. A low barrel price, which means large production of recovered sulfur, should help keep low the sulfur prices⁴².

Phosphate outlook to 2018^{11,44,45}

Global demand for phosphate fertilizers will rise in the few years (short-term forecast) (+2.4% per year), with the largest demand coming from East Asia, South Asia and Latin America. In a medium-term forecast, the demand for phosphate fertilizers will rise with a lower growth (+1.9% per year), with the highest growth rates in demand from Latin America and Africa. The demand for phosphate fertilizers by China will reach a plateau and demand will be weak in the rest of the world.

Table 2: World phosphoric acid potential supply/demand balance⁴⁵.

<i>World Phosphoric Acid Potential Supply/Demand Balance</i>					
<i>(million metric tonnes P₂O₅)</i>					
	<i>2014</i>	<i>2015</i>	<i>2016</i>	<i>2017</i>	<i>2018</i>
<i>Supply</i>					
<i>Capacity</i>	55.60	57.67	58.62	60.41	61.51
<i>Potential Supply</i>	46.71	48.14	49.33	50.80	52.03
<i>Demand</i>					
<i>Fertilizer Demand</i>	37.33	38.18	38.98	39.74	40.49
<i>Non-fertilizer Use</i>	5.59	5.88	5.95	6.15	6.28
<i>Distribution Losses</i>	0.86	0.88	0.90	0.92	0.94
<i>Total Demand</i>	43.77	44.94	45.83	46.81	47.71
<i>Potential Balance</i>	2.93	3.20	3.50	3.99	4.32

A large supply of phosphate rock located in Africa and West Asia will emerge where Morocco, China and Saudi Arabia will account for almost 60% of the growth in the supply demand as it is shown on Figure 8.

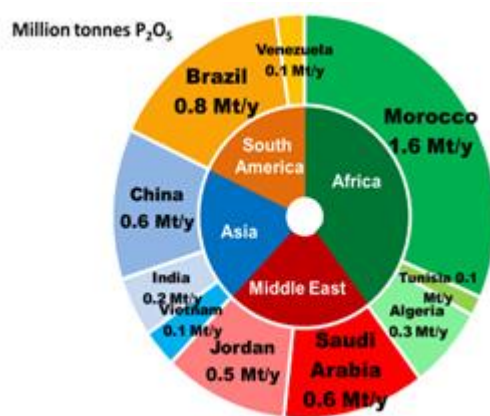


Figure 8: Phosphoric acid capacity growth (2011-2017)¹¹.

These moderate demand growth and new supply will lead to a surplus of phosphoric acid in a near term. As sulfuric acid demand is largely related to phosphoric acid demand, the next part will present the evolution of sulfur market.

Sulfur outlook to 2018¹¹

The supply of sulfur is estimated to increase during these next years due to new supply from Middle East and lower import demand in China and the United States. The production will increase in China, in Saudi Arabia and in UAE (United Arab Emirates) for the next years. This growth of supply can be attributed to the increase of sulfur recovery from shale oil and gas from North America and the increase of the oil production in Saudi Arabia and UAE. Moreover, the growth of new producers of gas from CUS (especially Russia, Kazakhstan and Turkmenistan) will also play a major impact on the sulfur production. Furthermore, the supply of sulfur will also come from mining processing (by e.g. from Norilsk Nickel mine). The operation of Sichuan gas fields will allow China to reduce its sulfur imports and thus increase the global supply of sulfur.

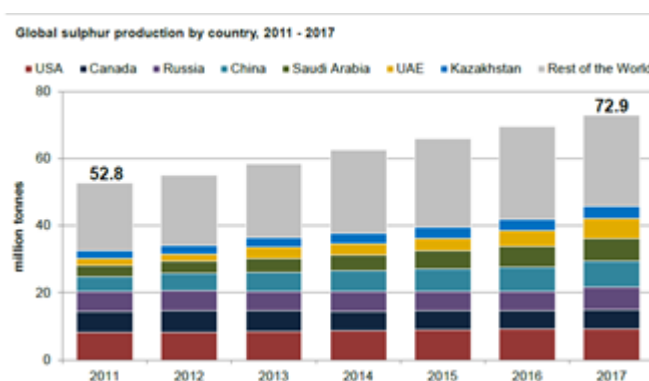


Figure 9: Global sulfur production by country from 2011 to 2017¹¹.

The demand of sulfur will increase for mainly two markets: phosphate fertilizers and metal processing. The demand in sulfur is estimated to grow about 0.4 Mt/year in the case of nickel leaching for example. But this demand is too low compared to the annual sulfur supply growth of ~ 4.0Mt/year.

Table 3: World elemental sulfur potential supply/demand balance⁴⁵

World Elemental Sulfur Potential Supply/Demand Balance (million metric tonnes S)					
	2014	2015	2016	2017	2018
Sulfur Demand					
S for sulfuric acid	53.44	55.36	57.48	59.83	62.04
Non-sulfuric acid uses	7.99	8.11	8.18	8.25	8.34
Total Demand	61.44	63.47	65.65	68.08	70.38
Sulfur Supply					
Oil recovered	27.56	28.70	29.76	30.76	32.11
Gas recovered	28.05	31.52	33.96	35.84	36.38
Others, including Frasch	3.72	3.9	4.31	4.83	4.80
Total Supply	59.33	64.12	68.02	71.42	73.29
Potential Balance	-2.11	0.65	2.37	3.35	2.91
% Supply	-4%	1%	3%	5%	4%

Table 3 summarizes the potential supply/demand balance for elemental sulfur from 2014 till 2018. The potential balance is estimated to be positive for the next few years.

Recycling of sulfuric acid

Sulfuric acid is often contaminated by organic materials and/or metal when he is used as a catalyst or drying agent. In this case, the acid may be recovered, cleaned and concentrated in order to reproduce sulfuric acid. Figure 10 shows the process to regenerate spent sulfuric acid.

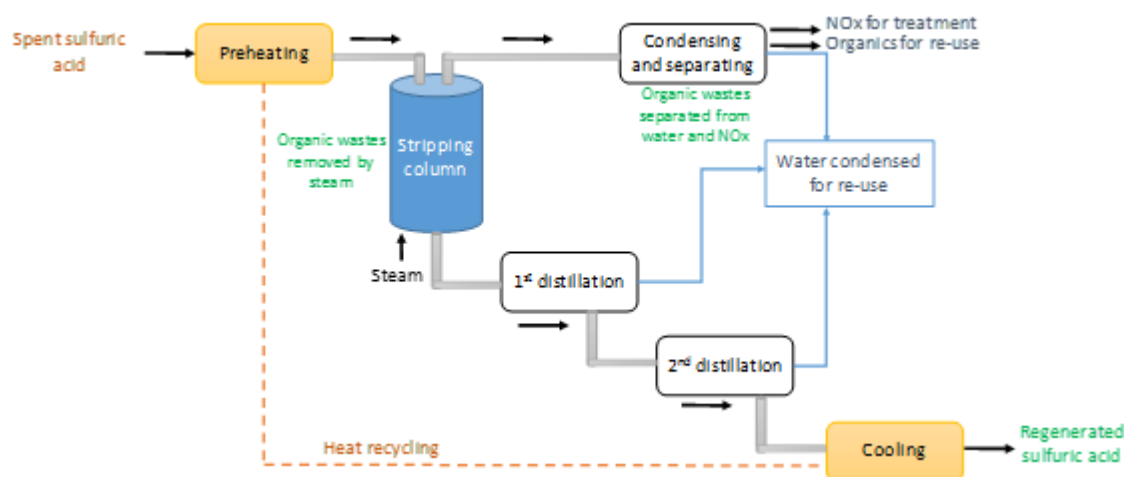


Figure 10: Process for regeneration of sulfuric acid (adapted from [46])

First, the spend acid is preheated in order to remove water, and then fed in a stripping column in order to remove organic materials using steam. Secondly, the sulfuric acid is distilled in order to concentrate it.

It is also possible to crack it in order to recycle it. In this case, the spent sulfuric acid is first concentrated to remove its volume by removing water contains inside. Then, the concentrated spent sulfuric acid is mixed with compressed air and injected in a high temperature furnace (1000-1200°C) in order to crack it into sulfur dioxide and steam⁴⁶.

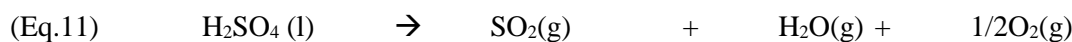


Figure 11 presents the SATCO process (Sulfuric Acid by Thermal Cracking Oxidation) used to regenerate sulfuric acid by thermal cracking.

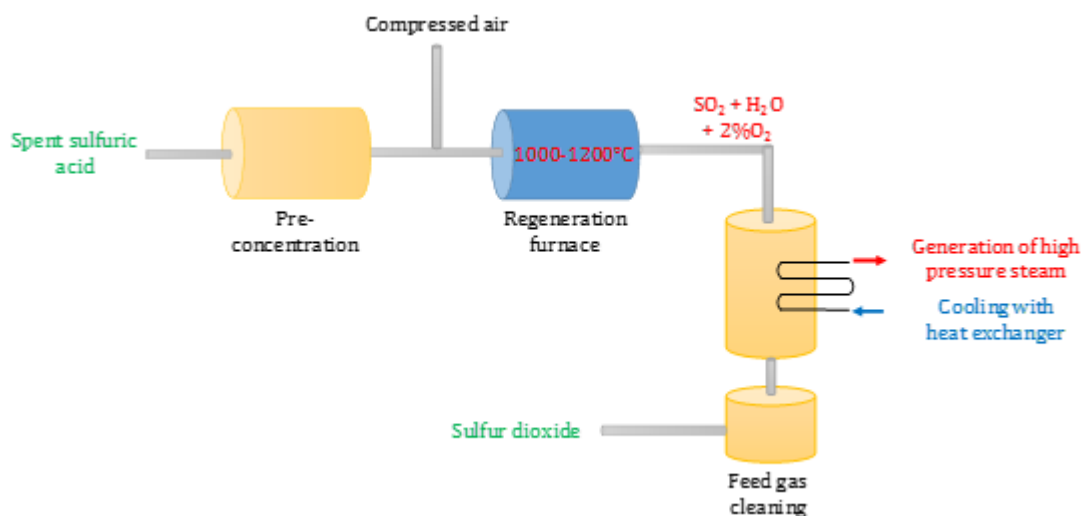


Figure 11: Process for the regeneration of sulfuric acid by thermal treatment (adapted from [46])

The recycling part focuses only on the recycling of this chemical, because of the main sulfur use for the sulfuric acid production.

Conclusion

It has been shown through this review that sulfur is an element essential for humans and plants, and that it can be found in a wide range of process and uses. Its large occurrence on Earth and its different sources of production made it difficult to quantify. Nowadays, the sulfur production is mainly involuntary and thus dependent of the extraction and production of fossil resources. And so on for its demand, which is principally driven by the market of fertilizers. Reserves of sulfur on the Earth crust are very large but it is not recovered from deep underwater reserves for technical reasons at this time. A deficit of sulfur for industry is not envisaged in a foreseeable future as the sulfur is becoming more and more important in the remaining gas and oil reserves. But as sulfur is essential for the development of a population either to feed the world population as to the development of economy, people has to keep an eye on it.

Acknowledgements

Authors acknowledge the University of Bordeaux and the IFPEN for their financial support for the PhD grant of Cyril Quilfen.

Bibliography

1. American Elements. Sulphur (S). Available at: <http://www.americanelements.com/sulfur.html>. (Accessed: 4th February 2015)
2. Davis, D. W. & Detro, R. Fire and brimstone: the history of melting Louisiana's sulphur. (Louisiana Geological Survey, 1992).
3. Apodaca, L. E. & Survey, U. S. G. Sulfur - Mineral Commodity Summaries. (2015).
4. Apodaca, L. E. & Survey, U. S. G. Sulfur - Mineral Commodity Summaries. (2014).
5. Apodaca, L. E. & U.S. Geological Survey. Sulfur - Mineral Commodity Summaries. (2013).
6. The Sulphur Institute. Learn more about sulfur. (2015). Available at: <http://www.sulphurinstitute.org/learnmore/faq.cfm#where>. (Accessed: 4th February 2015)
7. U.S. Geological Survey & U.S. Department of the Interior. Mineral Commodity Summaries 2016. Kim B., Shedd U.S. Geological Survey (2016). doi:<http://dx.doi.org/10.3133/70140094>
8. Apodaca, L. E., Survey, U. S. G., U.S. Geological Survey, Survey, U. S. G. & U.S. Geological Survey. Sulfur - Mineral Commodity Summaries. (2014).
9. Apodaca, L. E. & U.S. Geological Survey. Sulfur - Mineral Commodity Summaries. (2012).
10. Kelly, T. D. & Matos, G. R. Sulfur statistics [through 2014, last modified January 28, 2016]. (2016).
11. Harrison, P. & CRU Fertilizers. Global Sulphur Market Outlook.
12. Nehb, W. & Vydra, K. Sulfur. Ullmann's Encycl. Ind. Chem. 34, 431–505 (2012).
13. Britannica Encyclopaedia, Hustrulid, W. A. & Wikipedia. Frasch process. (2014). Available at: http://en.wikipedia.org/wiki/Frasch_process. (Accessed: 4th February 2015)
14. Nehb, W. & Vydra, K. Ullmann's Encyclopedia of Industrial Chemistry. (2006).
15. Nuroil. Sulphur Production & Uses. Available at: <http://www.nuroil.com/sulphur-production-and-uses.aspx>. (Accessed: 31st August 2016)
16. Ober, J. A. & U.S. Geological Survey. Sulfur. (2003).
17. The European Parliament & The Council of the European Union. DIRECTIVE 2009/30/EC OF THE EUROPEAN PARLIAMENT AND OF THE COUNCIL of 23 April 2009. (2009).
18. The University of York. Sulfur. The Essential Chemical Industry online (2014). Available at: www.essentialchemicalindustry.org/chemicals/sulfur.html. (Accessed: 2nd May 2015)
19. Topsøe, H., Clausen, B. S. & Massoth, F. E. in Catalysis (eds. Anderson, J. R. & Boudart, M.) 1–269 (Springer Berlin Heidelberg, 1996). doi:10.1007/978-3-642-61040-0_1
20. Yoshimura, Y., Toba, M. & Technology, V. Development of highly-active hydrodesulfurization catalyst for sulfur-free diesel production. 1, 161–168 (2009).
21. Claus unit Tail gas treatment catalysts.
22. Messick, D. L. & The Sulphur Institute. World Sulphur Outlook.
23. Kotz, J., Treichel, P., Townsend, J. & Treichel, D. in Chemistry & Chemical Reactivity 122 (Cengage Learning, 2014).
24. Chenier, P. J. Survey of Industrial Chemistry. (1987).
25. The Sulphur Institute. FAQ About Sulphur. Available at: <http://www.sulphurinstitute.org/learnmore/faq.cfm#used>. (Accessed: 5th February 2015)
26. Nehb, W. & Vydra, K. in Ullmann's Encyclopedia of Industrial Chemistry (Wiley-VCH Verlag GmbH & Co. KGaA, 2000). doi:10.1002/14356007.a25_507.pub2

27. Royal Society of Chemistry. Sulfur. Available at: <http://www.rsc.org/periodic-table/element/16/sulfur>.
28. The University of York. Sulfuric acid. The Essential Chemical Industry online (2013). Available at: <http://www.essentialchemicalindustry.org/chemicals/sulfuric-acid.html>. (Accessed: 5th February 2015)
29. Greener Industry. Sulphuric Acid. Available at: <http://www.greener-industry.org.uk/>. (Accessed: 5th February 2015)
30. The Contact Process. Available at: <http://www.chemguide.co.uk/physical/equilibria/contact.html>. (Accessed: 5th February 2015)
31. Amberger, A. & International Fertilizer Industry Association & International Potash Association. Soil Fertility and Plant Nutrition in the Tropics and Subtropics. (2006).
32. Fan, M. X. & The Sulphur Institute. IFA Crossroads Asia-Pacific. (2007).
33. Sawyer, J. & Iowa State University. Evaluation of Corn Response to Sulfur Fertilization in Central to Northeast Iowa.
34. Simpsons, J., Petherick, J. & Donaldson, L. in Chemical Processes in New Zealand (ed. Wansbrough, H.) 1–9
35. Resources Sunkar. How phosphate fertilizers are produced. (2009). Available at: http://www.sunkarresources.com/en/pages/How_phosphate_fertilizers_are_produced. (Accessed: 6th February 2015)
36. Wikipedia. Phosphogypsum. (2014). Available at: <http://en.wikipedia.org/wiki/Phosphogypsum>. (Accessed: 2nd June 2015)
37. National Iranian Gas Company. Soil amendments_Sulfur Information Service. (2012). Available at: <http://sulfur.nigc.ir/en/sulfuruses/agricultural/sulfuramendments/soilamendments>. (Accessed: 2nd June 2015)
38. Sulfur Information Services & National Iranian Gas Company. Sulfur Bentonite. (2012). Available at: <http://sulfur.nigc.ir/en/sulfuruses/agricultural/sulfurfertilizers/elementalsulfurfertilizers/sulfurbentonite>. (Accessed: 2nd November 2015)
39. The Sulphur Institute. Sulphur – an advantaged element ® in more sustainable value chains.
40. Okumura, H. A. & Cominco LTD. Sulfurcrete_Sulfur Concrete.
41. Al-Mehthel, M., Wahhab, H. I. A., Al-idi, S. H. & Baig, M. G. Sulfur extended asphalt as a major outlet for sulfur that outperformed other asphalt mixes in the Gulf. in Sulphur World Symposium 1–16 (2010).
42. Chilean Copper Commission Research Department. The Chilean Sulfuric Acid Market Estimations Through 2015. (2009).
43. Fan, Z. Chinese fertilizer market affect the international price of sulfur Interview with British senior analyst at CRU International Ltd. - Kimberly Gustin. China Agri-production news (2013).
44. Heffer, P. & Prud'homme, M. Fertilizer Outlook 2013-2017. in International Fertilizer Industry Association (IFA) Annual Conference 1–8 (2013).
45. Heffer, P., Prud'homme, M. & International Fertilizer Industry Association & International Potash Association. Fertilizer Outlook 2014-2018. in 82nd IFA Annual Conference (2014).
46. Greener Industry. Sulfuric acid Recycling. Available at: http://www.greener-industry.org.uk/pages/sulphuric_acid/8SulphuricAcidRecycling.htm.

Appendix II: Characterizations of commercial phosphomolybdic acid

The precursor employed for the synthesis of HDS catalyst precursors using supercritical CO₂ is phosphomolybdic acid (HPA). This commercial compound has been characterized using by TGA and XRD in temperature to determine its hydration degree and follow the evolution of the crystalline phases.

Thermogravimetric analysis

The evolution of the mass of H₃PMo₁₂O₄₀.xH₂O permits us to determine the content of crystallization molecules of water (number x) [1–4]. This allowed to introduce the right mass of molybdenum precursor into the support. Figure 1 represents the mass loss and the heat flow of the TGA performed on commercial HPA.

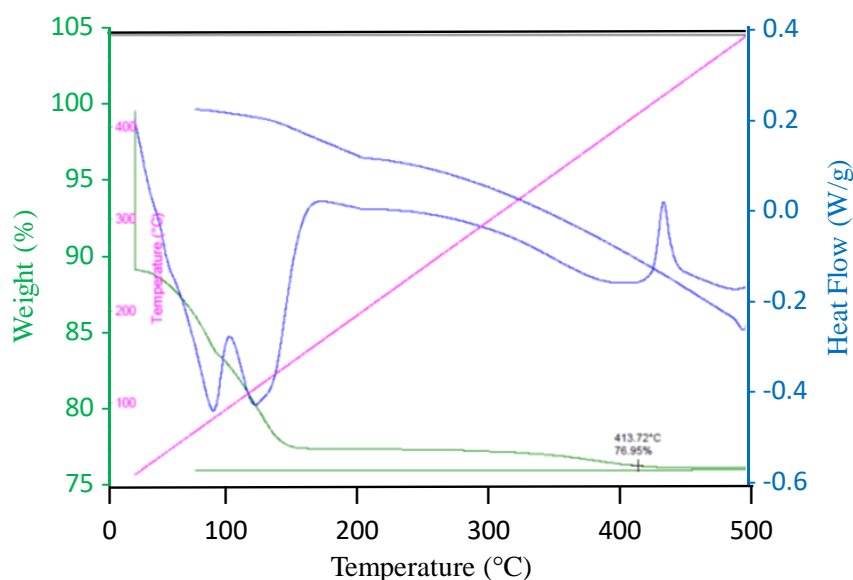
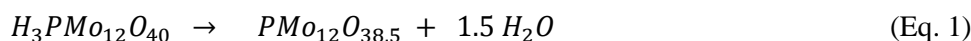


Figure 1: TGA analysis of the commercial phosphomolybdic acid hydrate.

From RT to 150°C, the mass loss is due to the former water. It has been found that the former water is 28,5 water molecules. The commercial HPA formula is thus H₃PMo₁₂O₄₀.28,5H₂O. Between 150°C and 270°C, a plateau ascribed to the anhydrous heteropolyanion (H₃PMo₁₂O₄₀) is observed. Above 270°C, the “constitutional” water (the protons bound to the external oxygen atoms) is lost. 1,5 H₂O is found for homonuclear Keggin structure and the reaction is represented in Eq. 1



An exothermic peak is observed at 450°C and is related to the crystallization of oxides.

Evolution of crystalline species with temperature

The commercial HPA has been characterized in XRD at different temperatures. This permits to follow the evolution of the crystalline structure along the temperature. Figure 2 shows diffraction patterns recorded at different temperatures.

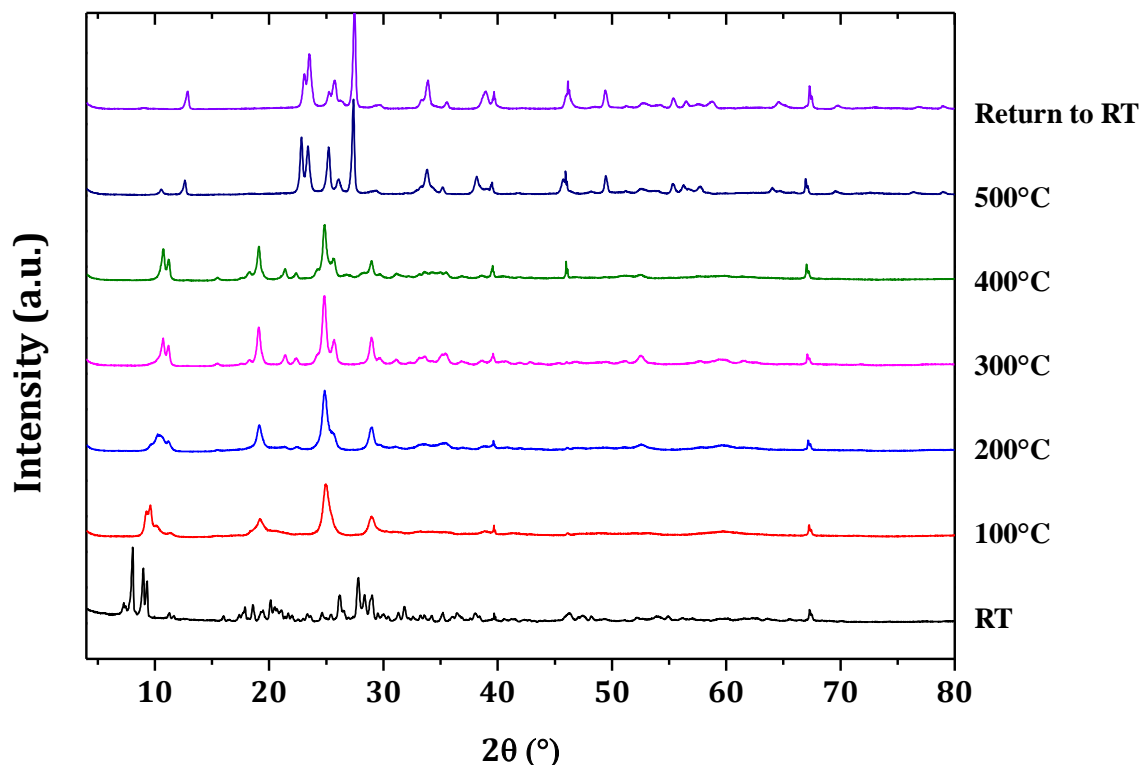


Figure 2: XRD patterns showing the evolution of crystalline phases of the commercial HPA as a function of the temperature.

At room temperature, XRD pattern is assigned to a hydrated HPA (PDF # 43-0317, # 01-0032 and # 75-1588). For temperatures between 100°C and 300°C, crystalline phase is assigned to a HPA containing less water molecules than at room temperature (PDF # 46-0482). At 400°C, the presence of a small part of MoO₃ (PDF # 05-0508) together with the previous phase is observed. For a temperature of 500°C, only the presence of respective oxides: MoO₃ and P₂O₅ are observed.

XRD observations are in agreement with TGA analysis, with the presence of a dehydrated HPA between 100 and 400°C and the appearance of oxides at higher temperatures.

These characterizations allowed us to determine the exact content of water molecules contain in the HPA and thus to weight the right mass to obtain the expected loading of Mo in our catalyst precursors. In addition, XRD patterns recorded along the temperature permit to follow the evolution of crystalline phases in order to have information for the assignments of XRD peaks in the materials prepared.

Appendix III: Raman characterization

Principle of Raman spectroscopy

When a monochromatic radiation having a frequency of ν_0 interacts with the matter, the radiation scattered is dispersed and do not contain only the original frequency ν_0 (Rayleigh scattering) but also pairs of new frequencies ($\nu_0 \pm \nu_M$) [5]. This change of frequency is called Raman scattering. These new frequencies constitute the Raman bands and constitute the Raman spectrum and are characterized by the frequency shift $|\nu - \nu_0| = \nu_M$.

When, the incident radiation excites the scattering matter from its electronic ground state into a virtual state, from which it relaxes under the emission of a Raman scattered photon of smaller or higher energy, known as respectively Stokes or anti-Stokes scattering.

Figure 1 is a schematic illustration of the infrared absorption and the Rayleigh and Raman scattering. In the case of the infrared absorption, the incident photon has the same frequency as the molecular vibration. In Rayleigh and Raman scattering, the incident photon has higher frequency. In the case of Rayleigh scattering, the scattered photon has the same frequency as the indent photon. But in the case of Raman scattering, the scattered photon has a lower or higher frequency. This difference in photon frequencies is the same as the molecular vibrational frequency [6].

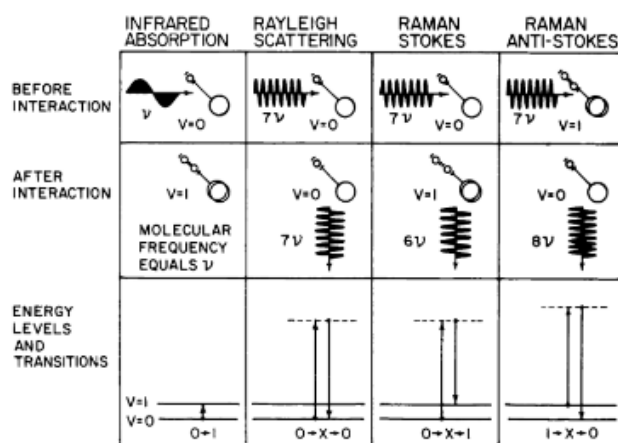


Figure 1: Illustration of Raman and Rayleigh scattering and infrared absorption (from [6])

Scheme of a Raman spectrometer

Figure 2 represents a scheme of a Raman spectrometer. A laser consisting of a monochromatic light is directed on the sample through an objective lens. The excitation light is then absorbed, transmitted or scattered by the sample. The elastic scattered light is blocked by a notch filter in order to have only the inelastic scattered light which goes to a mirror and a grating to arrive in a CCD detector. The signal obtain is then proceeded by a computer and a spectra containing Raman bands intensities as a function of the Raman shift is obtained.

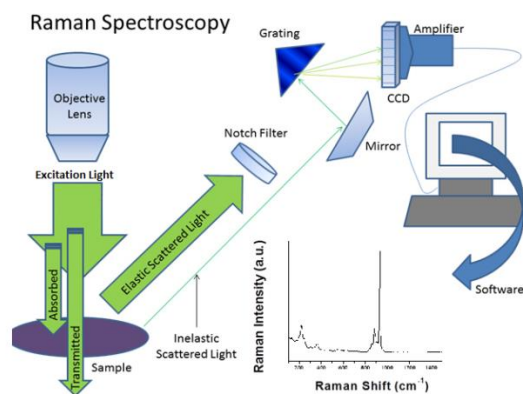


Figure 2: Scheme of a Raman spectrometer (adapted from [7])

For the *in situ* Raman studies, a Raman spectrometer, “XploRA One” from Horiba Jobin-Yvon has been employed. A laser having wavelength of 532 nm and operating at a power between 1 and 10 mW has been used. At the exit of the laser, an 10x objective is located horizontally thanks to a 45° mirror and is directed towards the sample. Raman spectra were recorded from 100 cm⁻¹ to 1600 cm⁻¹ with an acquisition time of 10*10s times. These operating conditions have been adapted depend of the sample studied and its Raman response.

Bibliography

- [1] M. Mo, M.F.C. Feumi-jantou, C. Rabia, G. Herve, S. Launay, Polyoxometalates Catalyst Materials : X-Ray Thermal Stability Study of Phosphorus-containing Heteropolyacids, *J. Mater. Chem.* 2 (1992) 971–978.
- [2] C. Rocchiccioli-Deltcheff, M. Fournier, R. Franck, R. Thouvenot, Vibrational Investigations of Polyoxometalates. 2. Evidence for Anion-Anion Interactions in Molybdenum(VI) and Tungsten(VI) Compounds Related to the Keggin Structure, *Inorg. Chem.* 22 (1983) 207–216.
- [3] K. Pandey, N. Lakshmi, S. Chandra, Transport and thermal behaviour of composite $\text{XH}_3\text{PMo}_{12}\text{O}_{40} \cdot n\text{H}_2\text{O} + (1-x)\text{Al}_2\text{O}_3$, *Indian J. Pure Appl. Phys.* 37 (1999) 242–244.
- [4] S.F. West, L.F. Audrieth, Differential thermal analysis of some heteropoly acids of Mo and W, *J. Phys. Chem.* 59 (1955) 1069–1072.
- [5] G. Mestl, In situ Raman spectroscopy — a valuable tool to understand operating catalysts, *J. Mol. Catal. A Chem.* 158 (2000) 45–65. doi:10.1016/S1381-1169(00)00042-X.
- [6] N.B. Colthup, L.H. Daly, S.E. Wiberley, Introduction to infrared and Raman spectroscopy, 2nd Editio, Academic Press. Inc., n.d.
- [7] Spectroscopy Facilities || The Prashant Kamat lab at the University of Notre Dame, (n.d.). https://www3.nd.edu/~kamatlab/facilities_spectroscopy.html.

Titre : Synthèse en milieux supercritiques, caractérisation et tests de catalyseurs d'hydrodésulfuration (HDS). Evaluation de la criticité des éléments contenus dans les catalyseurs HDS.

Résumé : Dans un contexte environnemental où les législations concernant la teneur en soufre présent dans les coupes pétrolières sont de plus en plus drastiques, le développement de nouveaux catalyseurs toujours plus actifs est donc nécessaire. Cette augmentation de l'activité catalytique est possible à plusieurs niveaux dont, par exemple, par l'utilisation de nouveaux procédés de synthèse tel que l'emploi de la voie fluides supercritiques. Dans un premier temps, l'objectif est d'étudier les éléments utilisés pour préparer ces catalyseurs afin d'avoir une vision plus large des réserves, des utilisations, des possibilités de substitutions... La criticité de ces éléments a donc été évaluée par le biais de plusieurs indicateurs. Dans un second temps, la compréhension de la synthèse de catalyseurs d'hydrodésulfuration (HDS) a été étudiée. Pour cela des expériences utilisant différents solvants et précurseurs métalliques ont été suivies via des analyses *in situ* Raman. Après avoir défini les résultats les plus probants, le procédé de préparation de catalyseurs HDS assisté par le CO₂ supercritique (scCO₂) a été optimisé à travers une étude paramétrique. Pour cela, la température, la pression, le solvant d'imprégnation, le ratio entre CO₂ et solvant d'imprégnation, le temps de réaction et le chargement en métaux ont été variés. Les matériaux obtenus ont ensuite été finement caractérisés (microscopie, DRX, Raman, ICP, microsonde) avant d'être activés par sulfuration et testés dans différentes réactions catalytiques (hydrogénation du toluène, hydrodésulfuration du dibenzothiophène et du 4,6-diméthylthiophène).

Mots clés : Fluides supercritiques, Hydrodésulfuration, *In situ* Raman, Criticité, Catalyse.

Title : Supercritical fluids synthesis, characterization and tests of hydrodesulfurization (HDS) catalysts. Assessment of the criticality of metals contained in HDS catalysts.

Abstract : In an environmental context where legislations concerning the sulfur content in oil are increasingly drastic, the research for new and ever more active catalysts is necessary. This increase of the catalytic activity is possible at several levels, for example, with the use of novel synthetic processes such as the use of the supercritical fluids route. In a first stage, the objective is to study the elements used to prepare these catalysts in order to have a broader view of the reserves, the uses, the possibility of substitutions ... The criticality of these elements has therefore been evaluated by means of several indicators. In a second stage, the understanding of the synthesis of hydrodesulfurization catalysts (HDS) was studied. For this purpose, experiments using different solvents and metallic precursors were followed by *in situ* Raman analyses. After defining the most convincing results, the process for preparing HDS catalysts assisted by supercritical CO₂ medium (scCO₂) was optimized through a parametric study. For this, temperature, pressure, impregnation solvent, ratio of CO₂ to impregnation solvent, reaction time and metal loading were varied. The materials obtained were then characterized (microscopy, DRX, Raman, ICP, microprobe) before being activated by sulfidation and tested in various catalytic reactions (hydrogenation of toluene, hydrodesulfurization of dibenzothiophene and 4,6-dimethyldibenzothiophene).

Keywords: Supercritical fluids, Hydrodesulfurization, *In situ* Raman, Criticality, Catalysis.

Unité de recherche

ICMCB-CNRS, UPR9048, 87 Av. du Dr. Schweitzer, 33608 Pessac cedex (France)